An ultra scale-down tool set for the predictive design of a membrane separation procedure for preparation of human cell therapies

A thesis submitted to University College London for the degree of Doctor of Philosophy in Biochemical Engineering

By

María Fernanda Masri

The Advanced Centre of Biochemical Engineering
Department of Biochemical Engineering
University College London

September 2014

To my grandfather and my family.

Gracias.

Abstract

Tools that allow cost-effective screening of the susceptibility of cell lines to operating conditions which may apply during full-scale processing are central to the rapid development of robust processes for cell-based therapies. In this study, an ultra scale-down (USD) device has been developed for the characterization of the response of human cell lines to membrane-based processing, using just a small quantity of cells that is often all that is available at the early discovery stage. Key operating conditions investigated were cross-membrane flow rate, cell age prior to processing and cell concentration (viscosity). The impact was evaluated by cell damage on completion of membrane processing as assessed by trypan blue exclusion and release of intracellular lactate dehydrogenase (LDH). Similar insight was gained from both methods and this allowed the extension of the use of the LDH measurements to examine cell damage as it occurs during processing by a combination of LDH appearance in the permeate and mass balancing of the overall operation.

The main cell line studied was a clinically relevant human fibroblast. As expected, increased shear rates led to significant increases in rate and extent of cell damage. Cells aged (21°C hold for 24 hours) before processing led to a doubling of the extent of damage. Increased cell concentration from $1x10^6$ to $100x10^6$ cells mL^{-1} gave no change in the proportion of cells damaged. Preliminary studies showed that increased shear stress also led to morphological changes and the appearance of apoptotic cells post-processing.

Two other human cell lines were also tested briefly for cell damage; a neural stem cell line and a prostate cancer cell line. These appear to be less robust than the fibroblasts with, for example ~0%, ~18% and ~42% damage being observed at the lowest shear stress (~44 Pa) conditions for fibroblasts, prostate cells and neural stem cells respectively. The effects of increasing shear rate, age of cells or concentration varied for each of the cell lines studied.

Overall, this work suggests how membrane processing may be used for the recovery of human cells for therapy and how USD studies can speed the route to manufacture.

Declaration

I hereby declare that the work presented in this thesis is solely my own work and that to the best of my knowledge the work is original except where otherwise indicated by reference to other authors.

Fernanda Masri

August 2014

Acknowledgements

This project was funded by the Biotechnology and Biological Sciences Research Council (BBSRC) and encompassed the collaboration of several industrial and academic groups around the UK; University College London and Onyvax Ltd and ReNeuron through the supply of cells for investigation.

First and foremost, I would like to express my gratitude towards Prof. Mike Hoare. Your continual guidance and input over the years have been invaluable throughout my master and doctoral studies. I have learned incredible amounts from you and it really has been a true honour and a privilege to work under your supervision. You have provided me with so many opportunities and given me endless support that went beyond your obligations. For all of that Mike, I am eternally grateful.

I would also like to thank Dr Ivan Wall, my co-supervisor at UCL, for providing direction and support when needed and sharing his knowledge with me. Thank you to Dr Kate Lawrence, my unofficial co-supervisor at UCL, you have been paramount to the success of this research. You have shared your wealth of knowledge and expertise always with a smile on your face (and most of the times with a cup of tea in your hand). I wish you both all the best for your future endeavours.

A special thanks to my lab friends who really have made this an unforgettable 4 years: Chris Longster (aka Ginge karaoke king) for the periodic update on the Daily News; Kate Lawrence (aka Cake) for the endless supply of sweets to the office; Mike Delahaye (aka Yoda) for “training” me to face USD research during my masters and

beyond; JP Acosta (aka Mexi-CAN) for introducing me to cell-bioprocessing; Alex Chatel (aka Camaron de la playa) for (rather infrequent!) baking amazingness; and Jen Man (aka karaoke queen) for sharing my passion for musicals. Thank you to many other UCL members who make the department a special place, to name few Helmi, Sara, Bettsy, Hughson, Lourdes, Kate Pinto, Vish, Jayan, Rhys, Rooney, Doug, Daria, Matt, Asma, recent addition "Daaaave"… I could go on. Also thank you to my friends outside UCL who have accompanied me during this whole journey and have helped me define myself as a person; the original Poly water polo girls and coaches (all of them), the all of the Goodenough College crowd (but especially Z-dawg), my friends in Spain (Bacabarden) and the G-club.

And Subhi, thanks to you, this thesis is a whole lot better! I know you have loved and enjoyed every minute of proof-reading. I truly thank you for your support, for your love and for your patience. صدبحي يد ا أحد بك أذ ا

No sería un agradecimiento sin reconocer a mi familia; papá, mamá y Marce. A ustedes les quiero agradecer por tantas cosas que no sé ni por dónde empezar. Gracias por dedicar tiempo para escucharme, ayudarme a resolver los problemas y demostrar su preocupación por mí. Gracias por brindarme apoyo incondicional y por estar dispuestos a darlo todo para asegurar mi felicidad. En definitiva, gracias por ser como son. Mamá, Papá: Una buena familia comienza con un buen ejemplo de los padres y ustedes son el ejemplo más claro de amor y de que el esfuerzo y el trabajo duro nunca son en vano. Los amo a los tres, gracias por todo.

Contents

List of figures

Chapter 1:

Chapter 2:

Chapter 3:

Chapter 4:

Chapter 5:

List of tables

Abbreviations

4-OHT - 4-hydroxy-tamoxifen

APC – antigen-presenting cell

AR – androgen receptor

bFGF – basic fibroblast growth factor

BSA – bovine serum albumin

CFD – computational fluid dynamics

cGMP – current good manufacturing practice

CIP – clean in place

CGM – complete growth medium

CMO – contract manufacturing operations

CoG – cost of goods

CQA – cell quality attribute

CTL – cytotoxic T-lymphocytes

DAPI – 4', 6-diamidino-2-phenylindole

DMEM – Dulbecco's Modified Eagles Medium

DMSO – dimethyl sulfoxide

DoE – design of experiments

DPBS – Dulbecco's phosphate buffer saline

DTI – defined trypsin inhibitor

EGF – epidermal growth factor

FCS – foetal calf serum

FDA – Food and Drug Administration

FLICA® – Fluorescent labelled inhibitor of caspases

HAS – human serum albumin

HBSS – Hanks balanced salt solution

hESC – human embryonic stem cells

HLA – human leukocyte antigen

HPV – human papilloma virus

HSA – human serum albumin

INT – tetrazolium salt

iPS – induced pluripotent stem cells

KSFM – keratinocyte serum free medium

LDH – lactate dehydrogenase

NK – natural killer

PAP – prostatic acid phosphatase

PI – propidium iodide

PSA – prostate specific antigen

PVDF – polyvinylidene fluoride

QbD – Quality by Design

QC – quality control

RDFF – Rapid Design and Fabrication Facility

RMM – reduced modified medium

STR – stirred tank reactor

TFF – tangential flow filtration

TMP – transmembrane pressure

TPP – target product profile

UCL – University College London

USD - ultra scale-down

Nomenclature

A	soluble LDH present
C	control
F	feed
i	interval number
j	number of runs
mV	millivolts

n number of measurements

N disc speed (rpm)

p pressure (bar)

P permeate

Q flow rate (mL min^{-1} or LMH)

R retentate

t time (s)

T transmission

V_P volume of permeate (mL)

V_R volume of retentate (mL)

Symbols

° degrees

| such that

[ ] concentration (cells mL^{-1} or μU mL^{-1})

Δ change

∑ sum

Ø volume fraction

ω proportion of intracellular LDH remaining

γ shear rate (s^{-1})

λ shear stress (Pa)

μ fluid viscosity (mPa s)

$\mathbb{Z}^+$ positive integer

Subscripts and superscripts

AV average

EXT external

F	final
IC	intact cells
INT	internal
LDH	lactate dehydrogenase
TB	trypan blue
TC	total cells
TOT	total

Chapter 1. Introduction

1.1 Thesis overview

This thesis will have the following structure:

Chapter 1 presents a review of the literature of the cell-based therapy bioprocessing sector. It covers the advantages and hurdles identified for a range of topics such as types of cell-based therapies and bioprocessing steps. It also highlights the importance of understanding the biological characterization of the product.

Chapter 2 provides a detailed outline of the experimental techniques developed and adopted throughout this body of work. Standard operating procedures as well as equipment and materials used will be presented to allow future execution of these tests if required.

Chapter 3 aims to characterize the physical impact of USD membrane separation parameters such as disc speed, cell ageing and cell concentration upon a model human fibroblast cell line.

Chapter 4 describes the translation of a selection of the techniques developed for the original cell line for the evaluation of a second and a third cell line (a neuronal stem cell line and a prostate carcinoma cell line).

Chapter 5 presents the evaluation of the effect of cell concentration on recovery of cells post-processing using once again the fibroblast cell line.

Chapter 6 provides some final concluding remarks and proposes ways forward for the project.

1.2 Introduction to therapeutics

Historically, therapeutic drugs have played a major role in increasing life expectancy as well as improving quality of life around the world. Various types of drug therapies have been developed to prevent, eradicate or mask symptoms and diseases.

Traditional therapies such as insulin hormone for the absorption of glucose in diabetic patients or the antibiotic penicillin commonly used for prevention or treatment of some bacterial infections, have been available since the 1920s. More contemporary therapies include a modern recombinant vaccine to prevent Human Papillomavirus (HPV) types 16 and 18 under the commercial names of Gardasil® and Cervarix® (Bayas et al. 2008); successful clinical transplantation of bioengineered airway with the patient's own cells (Macchiarini et al. 2008); or, even more recently, an upcoming cellular regeneration therapy, currently in phase II of clinical trials, that aims to reverse the functional deficits in stroke patients (Pollock et al. 2006).

These examples not only target very different diseases but were derived in completely different ways: microorganisms (penicillin and recombinant insulin), virus (HPV vaccine) and human cells (trachea transplant and stroke therapy), and may vary greatly in their method of production and administration.

1.3 Cell-based therapies

Contrary to the term ‘regenerative medicine’ which incorporates any methods and/or molecules to regenerate cells or tissues, ‘cell-based therapies’ involve the direct application of cells. Traditionally, cells would act as a host or production vector (producers) for proteins and often undergo total disruption to obtain these products. Now the cells themselves have become the product (effectors) and their applications vary greatly.

The U.S. Food and Drug Administration (FDA) defines cell therapy as “the prevention, treatment, cure or mitigation of disease or injuries in humans by the administration of autologous, allogeneic or xenogeneic cells that have been manipulated or altered ex-vivo” (U.S. Food and Drug Administration 1993). The first cell-based therapy was a successfully performed bone marrow transplant between twins in the 1950s and since then, different cell therapies have been widely used in modern medicine. More recently, in the last quarter of a century, these have experienced a rapid boost, creating a new emerging healthcare sector (Kemp 2006; Mason et al. 2011; Nerem 2010). For example, ChondroCelet® is a cartilage regeneration cell therapy where the patient’s own cartilage cells are biopsied, grown and expanded in the laboratory and then used to treat cartilage defects in knees (Saris et al. 2008). It is one of the first examples of a cell-therapy to be widely available after completion of the entire development, from research to clinical approval, all the way to commercialization.

Another example is Provenge®. Provenge® is a cellular immunotherapy indicated for the treatment of asymptomatic or minimally symptomatic castrate-resistant hormone

refractory prostate cancer (Kantoff et al. 2010). Immune antigen-presenting cells (APCs) are retrieved from the patient, cultured ex-vivo with a recombinant antigen and become fully matured APCs. Once re-injected into the patient, the fully matured APCs induce T cell proliferation. Activated T cells are able to then recognize and attack prostatic acid phosphatase (PAP) antigen expressed in prostate cancer cells, resulting in an immune response against them (Ward et al. 2002).

These two examples show just how wide the ranges of methods of action, as well as types of cells are encompassed by the term 'cell-based therapies'. There are four main categories of cell-based therapies; 1) cell replacement, such as blood transfusion from one or multiple donors into the circulatory system of a patient; 2) tissue engineering such as previously mentioned ChondroCelet®, skin grafts grown from skin stem cells to treat patients who suffered extensive burn damage or the previously mentioned transplants of fully engineered tracheas with the patient's own cells (Macchiarini et al. 2008); 3) stem cell based therapies, such as adult blood stem cells and bone marrow transplants (Thomas et al. 1977) or more recently post-stroke rehabilitation therapy ReN001 (Pollock et al. 2006); to 4) fully differentiated cell-based therapies, such as whole-cell cancer vaccines including, amongst others, immunotherapy Provenge® (Kantoff et al. 2010; Ward et al. 2002).

The different nature of each cell-based therapeutic application can determine the source, classifying all therapies into two broader categories; allogeneic (cells from a donor) and autologous (patient's own cells).

1.3.1 Allogeneic versus autologous therapies

An allogeneic cell therapy is where a patient receives cells from a donor, i.e. not the patient's own cells. Human leukocyte antigens (HLAs) are found on the surface of all types of cells and identify whether an object is foreign or known to the body. If the object is foreign, then the immune system is alerted to neutralize the perceived threat. For this reason, for an allogeneic therapy to be successful, it needs a degree of genetic match or similarity and immunosuppressants unless the immune response is what is needed.

On the other hand, autologous refers to cells or tissues that are re-implanted back into the individual from which the original tissue or cell type was sourced; in effect being one's own 'donor'. This this type of treatment is therefore preferred in certain cases for various reasons, for example, the fact that there is no need to provide immunosuppression products because the therapy is immune compatible. A common example of autologous choice for a therapy is when dealing with solid tumors as is the case with whole-cell cancer vaccines (Provenge® and OncoVAX®).

Both types of therapies have several advantages and drawbacks that make them more or less suitable for specific applications. For example, for autologous therapies, the amount of cells required and the high economic costs incurred by the patient specific bioprocessing are great challenges yet to be addressed (Mason and Hoare 2006). With allogeneic therapies however, the main issue lies on the fact that the donor used in the transplant has to present a close genetic match to the patient and as a result the number of potential donors is limited.

Over the past few decades both autologous and allogeneic cell therapies have become rapidly evolving fields. As life expectancy in developed countries increases, the need for replacement body tissues as well as the search for disease eradication is ever-growing. Currently, much of these forms of therapies are under investigation either in the laboratory or in clinical trials. Several treatments are being put into practice such as the previously mentioned clinical transplantation of tissue-engineered airways with the patient's own cells (Macchiarini et al. 2008) and autologous serum for treatment of ocular disorders (Liu et al. 2005). The potential of cell-based therapies is slowly being unmasked, but to fully understand the different therapies, it is important to first understand the hierarchy of cells and their characteristics.

1.3.1 Cell hierarchy

There are hundreds of different types of fully differentiated cells (such as skin, blood or brain) which have specific functions and characteristics that make them suitable for their specific roles. For example, skin, blood or brain cells all have very different morphologies (i.e. elongated without spikes, round, and elongated with spikes respectively).

The different types of fully differentiated cells arise through cellular differentiation of less specialized adult stem cells. Adult stem cells are themselves the product of cellular differentiation of embryonic stem cells. Embryonic stem cells are the product of cellular differentiation of the zygote and blastocysts. This "hierarchy" of development is based on the cell's ability to differentiate into different cell types; from totipotent (cells that

can differentiate into all cell types that make an organism) to unipotent cellular organisms (those that can only give rise to one specific cell lineage).

Figure 1.1 was adapted from Quante and Wang (2009) and shows the different stem cell hierarchies and differentiation potential of various types of cells - including those cell lines used in this study. Cells removed from the embryo up to (and including) the eight cell stage are known as totipotent cells, as they hold the capacity to develop into any form of human tissue including the trophectoderm. The trophectoderm comprises the placenta and umbilical cord. Cells removed from the inner cell mass of the blastocyst, i.e. past this eight cell stage, are known as pluripotent as they can differentiate into any of the three main germ layers (mesoderm, ectoderm and endoderm). Mesoderm comprises muscle, blood and bone lineages; ectoderm includes skin, ocular and neural lineages and the endoderm comprises internal and reproductive organs. Adult stem cells found within the tissue of these three germ layers hold potential to differentiate into cells of that specific germ layer only. Finally, in the past decade, induced pluripotent stem cells (iPS cells) have emerged as an alternative renewable supply from reprogrammed somatic cells (Takahashi et al. 2007).

The vast number of cell types and stages of differentiation means the mode of action and types of cell-based therapies will vary greatly on the cells used. The next few sections explain the mode of action of cell-based therapies based on the three main categories previously outlined; whole-cell cancer vaccines, stem cell based therapies and tissue engineering.

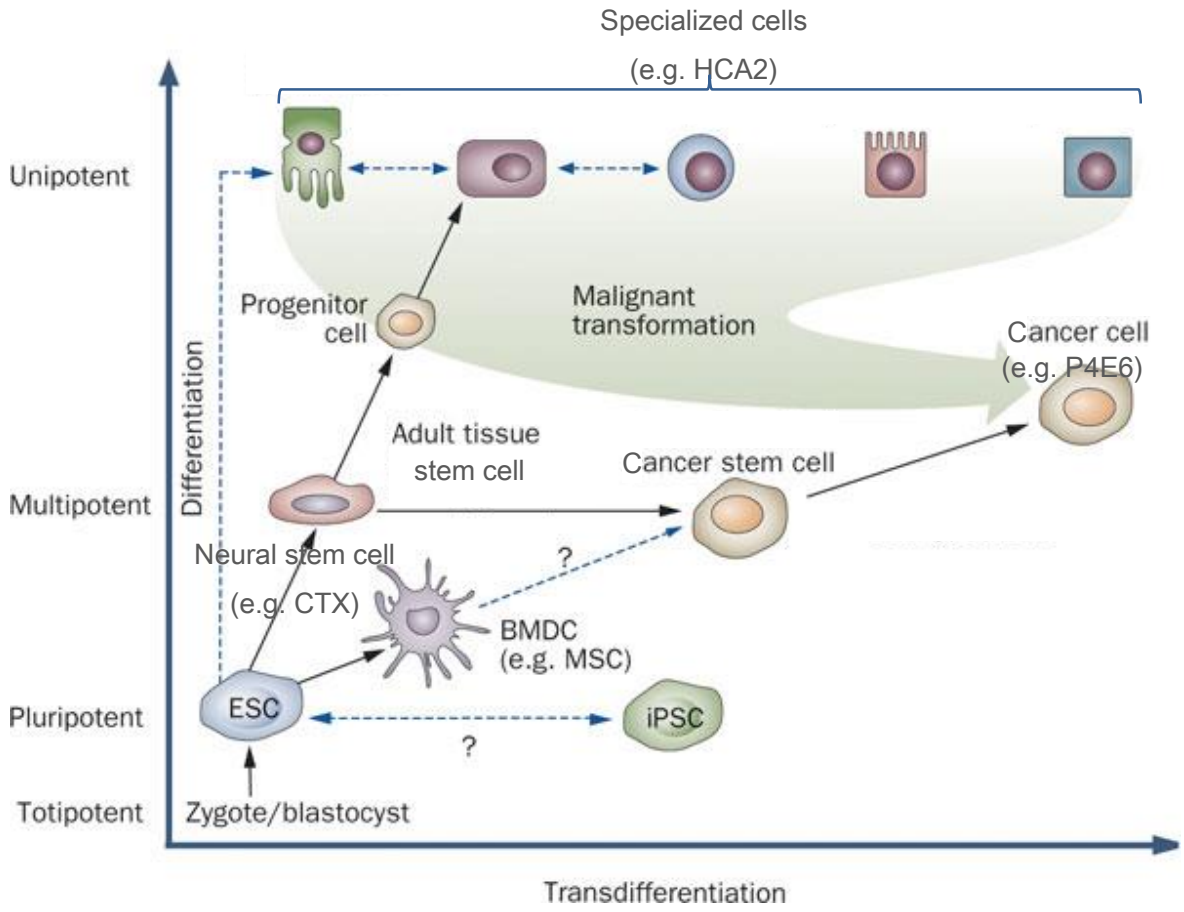

Figure 1.1: Potency hierarchies and differentiation potential of various types of cells including those cell lines used in this study. Adapted from Quante and Wang (2009).

1.3.2 Whole-cell cancer vaccines

Tumours may harbour many hundreds of different mutations which may be specific to tumour type or to an individual tumour (Haber and Settleman 2007). In light of the emergence of this data, the mechanisms used by the immune system to fight tumour cells are being understood. Therapies targeting a single antigen are slowly being replaced with multi-valent therapeutic strategies (Copier et al. 2007). For example, whole tumour cells could act as potent vehicles to target many antigens at once and therefore may offer a potential solution. Many vaccines focused on treating existing cancer have started to emerge, such as melanoma, colorectal, ovarian (Copier et al. 2007; Gruijl et al. 2008) and prostate carcinoma, as is the case of Onyvax-P vaccine (Onyvax Ltd) which includes one of the cell lines used in this study.

The increased potential shown by whole-cell cancer vaccines is due to the fact that these are made from actual cancer cells which act by enhancing the anti-tumor immunity over an extended period of time, by continuously secreting target antigens for the immune system to respond to (Ward et al. 2002). Whether an allogeneic or autologous approach is preferred, the method of action of the vaccine is essentially the same.

The immune system has two lines of defense that work in a highly cooperative manner; innate and adaptive immune system. The innate immune system is a non-specific set of disease-resistance mechanisms that act as the first line of defense and generally eradicates most of the microorganisms encountered by an individual. The adaptive (specific) immune response is triggered by the innate immune system if a microorganism is not cleared by the non-specific mechanisms. Both lines of defense are

composed of several types of cells and proteins that will trigger reactions to deal with foreign threats (Goldsby et al. 2007).

Potentially, the immune system can therefore be triggered by "mimicking" threat signals. For instance, Natural Killer (NK) cells are a type of lymphocyte of the innate system that if activated with specific ligands found in tumour cells, can generate potent immunity that could be used for whole cell vaccination (Diefenbach et al. 2001). Therefore, adjuvants administered or actions of NKs, act as a "danger" trigger signal (for example in the form of inflammatory cytokines) that is perceived by antigen-presenting cells (APCs). APCs incorporate the antigen and migrate to the lymphoid tissue, where thanks to the conditioning and cross priming of T helper cells, anti-tumour cytotoxic T-lymphocytes (CTL) are created. An attack on the specific antigen from tumour cells by CTLs is triggered after the latter have been released from the lymphoid tissue.

The key element of these vaccines is therefore the potency. The vaccine can present an array of antigens, in the case of Onyvax-P, provided by a combination of tumour cell lines at different stages. The production challenges therefore lie on maintaining the quality of the cells that comprise the vaccines to ensure the potency is not compromised.

1.3.3 Stem cell therapies

The unique regenerative capabilities of stem cells offer a promising alternative for the treatment of genetic and immunological diseases. Their capacity for self-renewal, immortality and ability to differentiate into the entire range of lineages means stem cells

can provide an endless and renewable source of cells for therapies (Ameen et al. 2008; Choumerianou et al. 2008). As was described in section 1.3.1, stem cells include adult, hESCs' and iPS cells.

Fetal and adult stem cells are used in treatments in which they may be induced to differentiate into the specific cell types required to repair damaged or destroyed cells or tissues. This is the case of the previously mentioned post-stroke rehabilitation therapy ReN001, currently in Phase II of the clinical development. It is the first fetal neural stem cell-based treatment that consists of the transplantation of a conditionally immortalized clonal neural stem cell line derived from human somatic stem cells, CTX0E03, (ReNeuron Group plc.) and administered into the patient's brain (Pollock et al. 2006). Other examples of stem cells as potential sources for therapies include hematopoietic transplantation and reconstitution (Farge et al. 2010; Passweg et al. 2013), mesenchymal stem cells for bone repair (e.g. Oeteocel® from NuVasive® Inc.) and autologous ocular (limbal epithelial) stem cell expansion and transplantation (O'Callaghan and Daniels 2011).

hESCs' longevity and the capacity to produce a wide range of cells make them a promising source of cells for therapies for the future. Several biological challenges are yet to be addressed with hESCs', such as tightly controlling the differentiation of the cells, the need to develop adequate methods for separating differentiated from non-differentiated cells whilst ensuring they are genetically stable or the need to ensure pluripotency is maintained.

The iPS cells provide a potential alternative for a renewable supply of stem cells from reprogrammed somatic cells (Takahashi et al. 2007). Ethically and morally, these present a much better alternative to the destruction of an embryo. However, their derivation efficiency remains very low and tight control of the differentiation is also an issue. On the other hand, Geron has treated 5 patients with their spinal cord trial regeneration and they displayed no adverse effects.

However, many challenges still need to be addressed before stem cell-based therapies are feasible and safe to use in patients. For example, the pluripotency characteristic that makes stem cells ideal candidates for therapies, also proposes a major challenge. The unlimited differentiation has a carcinogenic propensity which is a major concern. From a more practical point of view, fully differentiated cells present several advantages to stem cells. With stem cells, the culture complexity increases, the cells grow in colonies and the growth rates are slower than for fully differentiated cells. For instance, a 1 into 8 split of fully differentiated human fibroblasts takes the same time and yields 5 times more cells as a 1 into 2 split of hESCs'. Nevertheless, recent development of techniques to grow hESCs' in culture are aiding scientists to expand the understanding of the pathways of cell differentiation and thus the horizon of likely therapeutic uses (Halme and Kessler 2006).

1.3.4 Tissue engineering

Tissue engineering refers to the field that uses a combination of cellular material, biocompatible resources to build a scaffold and biochemical (e.g. growth factors) and physical (e.g. mechanical loading) factors to create tissue-like structures (Bell et al.

1981). The cellular material may either be an autograft (redistribution of patient's own tissue) or an allograft (implantation of tissue from another source). The scaffold (or matrix) replicates the biological and mechanical properties as well as the functions of human body tissues. In most cases, the ultimate goal of tissue-like structures is implantation of the tissue construct into the body to repair an injury or replace the function (e.g. structural, biochemical or barrier and transport related functions) of a failing organ.

The first cell-based tissue-engineered product marketed was Epicel (Genzyme, Cambrige, MA). Epicel consists of sheets of autologous keratinocytes that are used to cover patients suffering from severe cutaneous burn injuries who do not have enough viable skin remaining to be treated with traditional autografting techniques. Other similar skin graft products approved by the U.S. FDA include Integra Dermal Regeneration Template (Burke et al. 1981), Apligraft® (Organogenesis, Canton, MA) and TransCyte (Smith & Nephew). However, tissue-engineering has not only focused on skin graft products. In the last decade, the first tissue-engineered whole trachea organ was successfully transplanted into a patient (Macchiarini et al. 2008). This led to increased efforts and rapid advancements with other organs such as heart, liver and lung tissues (Farge et al. 2010; Saris et al. 2008; Uygun et al. 2010). Efforts have also focused on cartilage regeneration (TruFit, Smith & Nephew Endoscopy, San Antonio, TX).

However, despite the advancements in the field major hurdles still prevail. The complexity of tissue-engineering means deep understanding of the effect of myriad

factors on the development as well as the sustainability of the tissues and organs is needed (Berthiaume et al. 2011). Issues still to overcome include provision of functional vascular supply, control of the complex arrangement of different cell types in 3D structures, identification of reliable cell sources and scalability of the manufacturing process.

1.4 Cell bioprocessing at full scale

Bioprocessing refers to the translation from a life-science discovery into a practical product. It is the critical link between discovery stages (including research and development) and commercialization (manufacturing) (Zaborsky 1995). Depending on the nature of the cells, different therapies will require different bioprocessing techniques. However, all cell-based products have a similar process as shown in Figure 1.2.A. It shows a simplified generic bioprocess flowsheet for a whole-cell therapy. It begins with the production of the cellular material (upstream) and continues with the recovery, purification and formulation (all downstream) of the final product. Figure 1.2.B shows an example of a manufacturing process used by Onyvax Ltd for production of the cell line constituents of the Ony-P whole cell prostate cancer vaccine. For each batch produced, three 40-layer cell factories were harvested at ~70% confluency, enzymatically detached, washed, concentrated and formulated following the process flow stream shown in Figure 1.2.B.

The ability to provide cell-based therapies to a wide range of patients ultimately relies on the capacity of large scale bioprocessing to yield high number of cells of acceptable quality (Rowley et al. 2012c). However, the inherently complex nature of the biological

A.

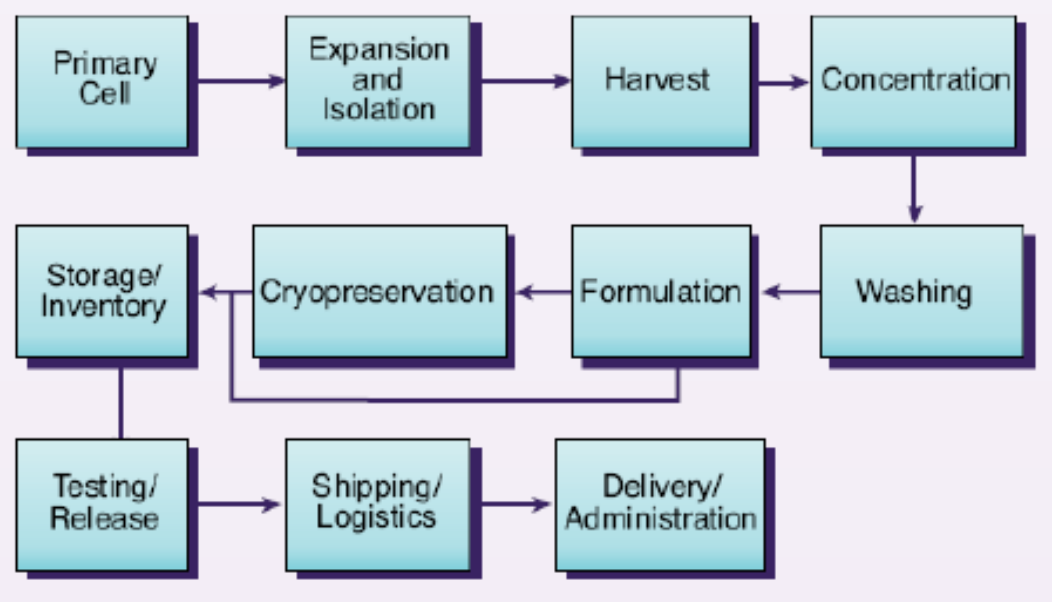

B.

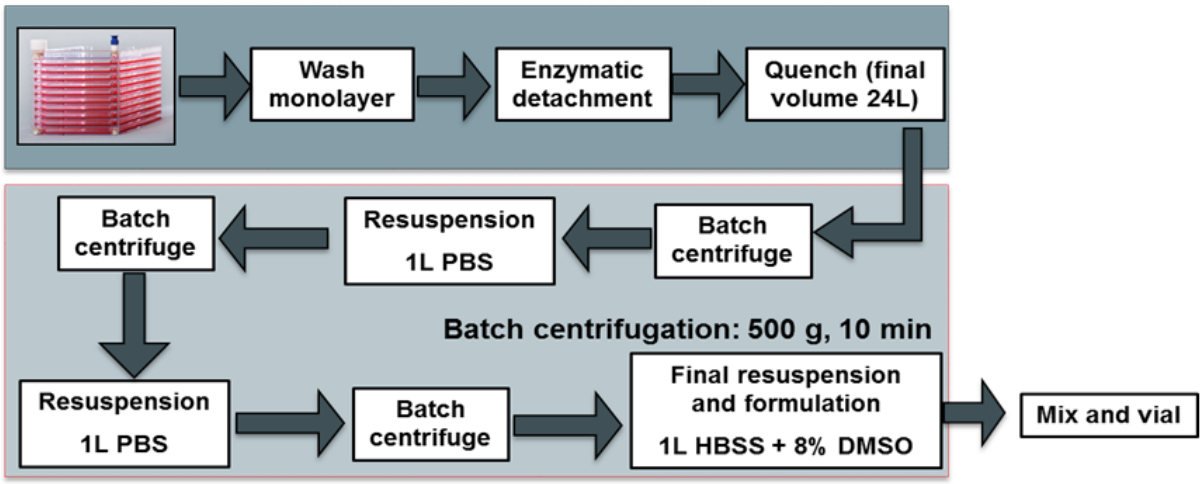

Figure 1.2: Process flowhseet for (A) a generic bioprocess for a whole-cell therapy (Lapinskas 2010) and (B) therapy specific manufacturing process used by Onyvax Ltd for production of cell line constituents of the Ony-P prostate cancer vaccine.

material makes applying current Good Manufacturing Practice's (cGMP) to the bioprocess a challenging task. Cells, as living organisms, can trigger responses to physical and chemical changes in the processing environment (Agashi et al. 2009; Al-Rubeai et al. 1995; Kretzmer and Schügerl 1991). Therefore bioprocessing will impact the quality of the end product, rendering the process and product inseparable (Mason and Hoare 2007).

Ideally, to facilitate cGMP-compliant manufacturing of cell-based therapies for clinical-scale expansion, the entire process from cell culture to post-culture processing would be completely closed and automated (Rowley et al. 2012a). Moreover, if the automated and closed system delivers a product suitable for storage and ready for use or administration in a clinical setting, the risk of variability and microbial contamination would be reduced significantly (Rowley et al. 2012a). For this reason, adopting a Quality by Design (QbD) approach has become essential for cell-based products that are in the development process. A critical component of QbD is to understand what the product needs to do in order to create a Target Product Profile (TPP) as well as to identify the needs of the patient. TPP characteristics may include composition and dose (such as cell types and formulation), function (for example immunomodulary, surgical implementation or targeting) and logistics (shell life and cold chain supply). Therapy specific cell quality attributes (CQAs) to do with clinical safety and efficacy are established in order to easily identify potential areas of significant change in cell quality (Arora et al. 2009). QbD approach can be maintained throughout the lifecycle of the product to ease innovation and encourage continuous improvement.

1.4.1 Upstream processing

The production of the cellular material (upstream processing) depends on the nature of the therapy. Various techniques are currently used and some of the issues will be addressed in this section.

1.4.1.1 Cell line selection

Cell line selection will vary according to the type of therapy. Immunogenicity, cell function, availability, proliferation potential and whether the therapy will be autologous or allogeneic are some of the factors to consider during cell line selection. If a specific cell line demonstrates suitability for a therapy but its fragility during processing compromises its ability to function, it may be deemed as unusable.

The cell source can vary greatly depending on location of the biopsy, cell type (stem cells, fully differentiated, tumour cells, etc) and even surgical practitioner. The characteristics of different sources of cells will impact on their susceptibility and adaptability to processing. In this study, three different cell lines were used; human neonatal foreskin fibroblasts for skin graft translational purposes (HCA2), an immortalized clonal neural stem cell line (CTX0E03, ReNeuron Group plc) derived from human somatic stem cells and a fully differentiated early stage prostate carcinoma cell line (P4E6, Onyvax Ltd.). Factors such as ease of culture (assessed on criteria such as colony formation and need for a feeder layer), concentration of viable cells at harvest, robustness during processing and relevance to the cell-based therapy industry were considered when choosing the cell lines for this study (Table 1.1).

	P4E6	HCA2	MSC	CTX0E03	hESC
Therapeutic relevance	Cancer vaccine	Tissue engineering	Autologous therapies	Post-stroke repair	Allogeneic therapies
Mean cell diameter in suspension	15µm	15µm	15µm	15µm	15µm
Culture complexity	***	***	****	****	*****
Surface attached	Yes	Yes	Yes	Yes	Yes
Ability to differentiate	No	No	Multipotent	Multipotent	Pluripotent
Control of differentiation	N/A	N/A	√	√√	√√√
Purify differentiated from non-differentiated?	N/A	N/A	Yes	No	Yes
QC analysis: • Cell viability • Cytokine expression • Surface markers	 √ √ √	 √ √ √	 √ √ √	 √ √ √	 √ √ √
Susceptibility to stress	***	***	TBD	TBD	TBD
Telomere activity	Finite	Finite	Indefinite	Indefinite**	Indefinite

Table 1.1: Comparison of cell lines used in this thesis (HCA2, P4E6 and CTX0E03) and other relevant cell types used in the industry (MSCs and hESCs). The information for this table was gathered from various sources in collaboration with Dr. Lawrence and Longster, UCL (Acosta-Martinez et al. 2010; Delahaye 2013; McCoy et al. 2010).

1.4.1.2 Cell culture and growth methods

Anchorage dependent or adherent cells are those cells that require a surface to attach in order to grow and proliferate. These cells are usually derived from organ tissues and therefore are immobile and embedded in connective tissue. The following sections will review some of the platforms available for adherent cell culture

1.4.1.2.1 Two-dimensional platforms

Traditional two-dimensional manufacturing platforms refer to planar tissue-culture-treated surfaces (such as plates or flasks). Tissue-culture flasks (T-flasks) surface areas range from approximatedly 5 to 175 cm^2, yielding different number of cells depending on the cell line used. Generally, for a surface area of 175 cm^2, around $20x10^6$ cells will be harvested at 80% confluency for cell lines such as the HCA2 and P4E6. For the neural stem cells, CTX0E03, approximately $10x10^6$ will be harvested for the same surface area and confluency. Multilayered flasks or cell factories have been used for larger-scale expansion of adherent cells to progress allogeneic cell therapy products into mid to late clinical development (Rowley et al. 2012c). Good examples of these include Cell Cube and the CellSTACK (Corning, New York, USA) as well as the Cell Factory (Nunc, Thermo, Strasbourg, France). These platforms increase the number of growth surfaces available by stacking layers on top of each other, offering surface growth areas up to 25,000 cm^2 (Brandenberger et al. 2011). However, commercial lot sizes for allogeneic "off-the-shelf" therapies based would require ~10^{10} – 10^{12} cells (Brandenberger et al. 2011). This means large clean rooms or even entire clean

buildings would be needed as well as a large number of operators or robotic platforms (Rowley et al. 2012c).

Cell culture in these two-dimensional platforms is labour intensive, not contained and operator dependant. On top of this, due to the inherent variability of cells, fluctuations in the culture medium, materials or operating conditions can have an effect on the quality of the cells harvested. Automation of cell culture decreases the number of operators needed, removes the operator variability and allows for cell cuclture to happen in a closed environment. Several autoamted cell culture platforms are commercially available such as Cellmate^{TM} and SelecT (The Automation Partnership, Sartorius Stedim, UK). Cellmate^{TM} was developed in the late 1980's to work with 20 up to 1,000 flasks and roller bottles with 10 different cell lines in parallel (Kempner and Felder 2002). SelecT system is a more recent version of a fully automated cell culture system which includes a robotic arm which can access an incubator of a capacity of 90 T-175 flasks. The system can also incorporate an automated cell counting machine within the laminar flow safety cabinet (Thomas et al. 2009). However, automated cell culture platforms have not been extensively used due to the high capital investment and their complexity with respect to cell line adaptation.

Attempts have been made to culture anchorage dependant cells in more contained three-dimensional platforms which would yield higher numbers of clinically viable cells, such as bioreactors with suspension microcarries and hollow fibre perfusion cultures.

1.4.1.2.2 Three-dimensional platforms

Stirred tank bioreactors (STRs) are generally associated with traditional industrial processes such as fermentation (Wendt et al. 2009). However, over the last decade, the importance to shift two-dimensional cell culture into three-dimensional platforms has gained increased recognition. Conventional STRs are well defined and characterized systems with highly effective monitoring and performance control (Want et al. 2012). However, cell culture within three-dimensional platforms introduce an array of new scientific and technical challenges associated with the complex nature of human cells (Wendt et al. 2009). Want et al. (2012) presents a review of the efforts to grow human pluripotent stem cells in three-dimensional platforms compared to two-dimensional traditional culture. He also gives an overview of the hurdles that these technologies face in order to provide standardized, scalable and efficient processes in terms of number of clinically relevant cells produced (i.e. cells that maintain critical biological functionality).

Unlike some selected cell lines such as hESCs, most adherent cells do not form agglomerates (embryoid boides) when in culture. Most therapeutic cell lines in fact, require a growth substrate such as microcarriers. Microcarriers are small particles, usually spherical, made of either natural (e.g. collagen or gelatin) or synthetic (such as polyethylene or glass) matrices that offer an increased surface-area-to-volume ratio over traditional static cultures, increasing the cell density at harvest and reducing the overall footprint (Rowley et al. 2012c). Microcarriers can present a solid or porous structure (such as Cytodex^{TM} and Cultispher® S respectively) to which the cells attach to in order to grow. The use of bioreactors with suspension microcarries for cell culture also allows increased online control and automation of the culture's environment. Kehoe et al.

(2010) described various modes in which scalable STRs can be employed to cultivate hESCs, human iPSCs and various stem cell applications to date which have shown promising results (Serra et al. 2010).

However, major concerns for cell culture in STRs still prevail. These include cell damage due to the stress induced, wether the stress is from the energy released as bubbles burst or the high levels of agitation resulting in intense hydrodynamic forces (Al-Rubeai et al. 1995; Hu et al. 2011), due to bead to bead collisions (Fernandes et al. 2007), harvesting issues (Varani et al. 1985) and seeding consistency from bead to bead (Ng et al. 1996).

Commercially available and attractive closed systems alternative to microcarrier STRs include wave bag technology (Sartorius BIOSTAT® Cultibag), perfusion reactors (Aastrom Replicell, Bartel et al. 2012) and hollow fibre perfusion culture (QUANTUM® Cell expansion system). Small scale research tools are also available for three-dimensional cultures including ambr^{TM} micro bioreator (Glen et al. 2013).

1.4.2 Downstream processing

Following cell culture, the harvested cells require downstream processing to become a suitable therapeutic product for delivery. Downstream processing includes a wash step for removing unwanted residual culture components, a volume reduction step and a buffer exchange step to formulate cells ready for direct administration or storage (Rowley et al. 2012b). Ideally, all these steps are performed within an aseptically closed system that it is simple to automate and scale, that minimizes mechanical disruption of

the cells and ensures high cell quality and unperturbed function (Brandenberger et al. 2011; Pattasseril et al. 2013).

The following sections will address the major techniques traditionally used for downstream processing (centrifugation and filtration), and a most recent technique known as continuous centrifugation (KSep®, KBI Biopharma, Durham, North Carolina, USA).

1.4.2.1 Centrifugation

Centrifugation is a crucial and widely applied technique both in research as well as industrially for the processing of biologicals and biopharmaceuticals. In cell-based therapies from pilot to industrial scale, it is commonly used batchwise in several stages of the bioprocess for the separation of cells from solution. For instance, during harvest, the cells are separated from media or detachment enzyme or further downstream from cryopreservants or buffers. Due to its popularity within the industrial sector, efforts have focused on providing small scale tools to predict the impact of key processing conditions (Delahaye 2013; Hutchinson et al. 2006; Tait et al. 2009; Zoro et al. 2009). Centrifugation has remained popular mainly due to its low running costs, straightforward process development and desired operating robustness (Axelsson 2002). However, it presents several downfalls, especially for the cell-based therapy industry. It is a poorly contained processing step, heavily operator dependent and prone to contamination. In fact, in view of the literature, centrifugation has proven to be a difficult step to automate while maintaining sterility (Mason and Hoare et al., 2006).

When dealing with cell-based therapies, it is not uncommon to expect concentration factors in the region of 25 fold, ideally with the least possible number of purification steps to decrease the mechanical manipulation. As volumes and lot sizes increase, going from lab to clinical trials and commercial scale, tens of litres of cellular suspensions will need to be handled downstream (Pattasseril et al. 2013). For the traditional batch centrifuge, this would require an increased number of iterations with several operators to process larger volumes (Pattasseril et al. 2013). To accommodate the demands of the industry and hoping to provide a suitable alternative, several technologies combining principles from centrifugation and filtration have emerged.

1.4.2.2 Continuous centrifugation

Continuous centrifugation techniques for the downstream processing of whole cells for therapy, potentially offer a low shear and contained alternative to batch centrifugation. These alternatives include systems such as Elutra® Cell Separation System (Gambro BCT, Lakewood CO, USA), CARR UniFuge® (PneumaticScaleAngelus, Barry-Wehmiller, St Louis, Missouri, USA) and kSep® (KBI Biopharma, Durham, North Carolina, USA).

KSep® in particular offers a low shear, closed, scalable and continuous system capable of processing high volumes of cell harvest while maintaining critical quality parameters (Pattasseril et al. 2013). The capital expense to place a system like kSEP® for cGMP operation can range from US$200,000 to US$700,000. High capital cost, coupled with high costs for process development due to the large number of cells required for

meaningful development runs (Pattasseril et al. 2013), mean that the success of this development even though promising, is still under scrutiny (James 2011).

1.4.2.3 Filtration

Filtration offers an alternative away from centrifugation altogether. It has been widely used in many industries and forms an integral part of the biopharmaceutical sector. Its uses range from the separation of whole cells (and fragments of cells) from the target protein within the liquid phase to viral clearance for mammalian cell processes viral clearance step (Wang 2001). Filtration works on the principle of physical separation of solid particles from a fluid-solid mixture according to size, by forcing the fluid through a filter-medium (Doran 1995). If the driving pressure differential is held constant, then the rate of filtration will decrease with time as the resistance to flow through the membrane increases with progressive fouling (Perry and Green 2008). If the flux is kept constant then the transmembrane pressure (TMP) will increase as a result of progressive fouling (Perry and Green 2008). Therefore, the performance of a filtration process is governed by the fouling of the membrane. Fouling occurs when solids are deposited on the filter (i.e. cake formation) or due to adsorption and clogging within the pore structure (i.e. pore blocking, Doran 1995) and is largely dependent on the type of operation of the filtration. Filtration is separated into two principal modes; normal flow filtration (NFF) and tangential flow filtration (TFF).

NFF, also known as dead end filtration, operates with the slurry flowing into the membrane (i.e. flow is perpendicular to the membrane, Figure 1.3.A). Particles and components which are smaller than the pores of the membrane will permeate through,

whereas those larger than the pores will be retained. NFF is typically used for suspensions with very low solid concentrations due to fouling of the filter. In the last decade, some studies have focused on the application of NFF to cell-based therapies. For instance, Sowemimo-Coker et al. (2009) described a NFF process for achieving volume reduction and red blood cell depletion in a closed and sterile manner. The investigation focused on reducing the loss of haematopoietic stem and progenitor cells to a minimum.

The second mode of operation is TFF, also known as cross-flow filtration. In TFF the fluid flow travels tangentially across the surface of the membrane (Figure 1.3.B) rather than into the filter. This can reduce the extent of surface fouling as the filter cake is constantly washed away during the process, increasing the length of time that a filter unit can be operational. Unlike NFF, TFF can be also operated in a continuous manner which can be of great advantage when dealing with large volumes of filtrate material (Pattasseril et al. 2013). With respect to the cell bioprocessing industry, TFF is becoming increasingly popular. Wash phases can be incorporated, with diafiltration using volumes of wash buffer relative to the initial feedstock volume to remove contaminants carried through from upstream (cell expansion and harvest phases). Moreover, TFF can also incorporate the concentration of cellular material and buffer exchange, all into one enclosed step without the need of resuspension. Certain obstacles remain such as how to achieve high cell recovery, viability and functionality throughout this phase (Brandenberger et al. 2011). Successful and efficient TFF operation relies on finding a balance between increased feed flow rates to maintain performance by reducing fouling and the creation of a high shear environment which can induce

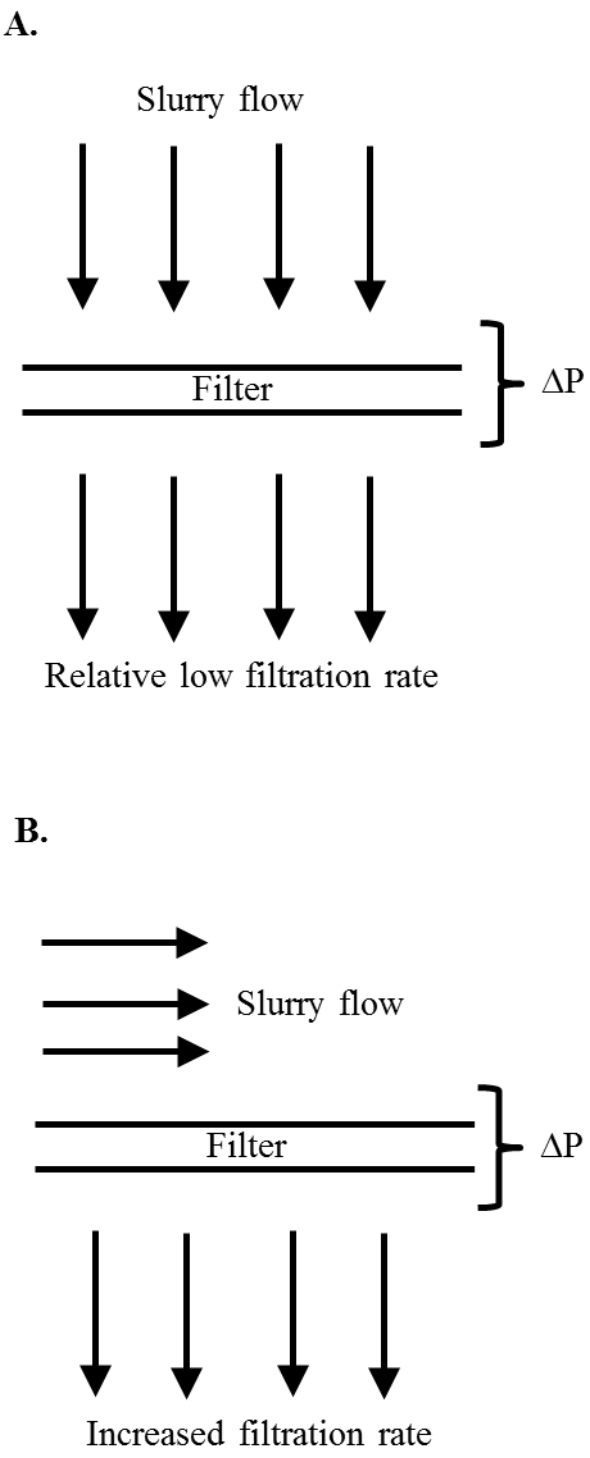

Figure 1.3: Schematic diagram of (A) normal flow filtration (NFF) and (B) tangential flow filtration (TFF) arrangements (Perry and Green 2008).

secondary flow patterns that can lead to considerable cell damage (Maiorella et al. 1991). Rowley et al. (2012a) presented a method for aseptically processing live mammalian cells in aqueous medium to yield a cellular suspension of a final concentration of $5x10^6$ cells mL^{-1} with at least 90% cell viability and 90% yield of starting cells. The method includes volume reduction using TFF whilst maintaining the TMP at less than about 5 psi, shear rate at less than 4,000 s^{-1} and transmembrane flux rates in between 50 and 100 LMH (Rowley et al. 2012a).

Membrane selection will also play a vital role during filtration. Chemical interactions (such as electrical charge or hydrophobicity repulsion) and pore size of the membrane are some of the characteristics to take into account. The membranes are typically flat discs or bundles of porous hollow fibres within a cartridge (Chang and Fane 2002) and are usually made from materials such as polyethersulfone, polysulfone or polypropylene (van Reis and Zydney 2001). However, filtration has evolved mainly as a practical exercise rather than strictly from theory (Perry and Green 2008). Therefore, unless exact data is available, small-scale tests must be performed to aid in the selection of filter material and to determine the size needed. Established systems (such as GE Healthcare's ÄKTAcrossflow™ unit) facilitate the lab-scale development of these techniques.

1.4.2.3.1 Theory of flow through filters and transmission

At any given point during filtration, the rate of filtration is mathematically described by:

$$\boldsymbol{v} = \frac{\boldsymbol{dV}}{\boldsymbol{a\,dt}} = \frac{\boldsymbol{\Delta p}}{\boldsymbol{\mu\left[\alpha\left(\frac{W}{a}\right)+r\right]}} \qquad \text{Equation 1.1}$$

where 'v' is the velocity of flow through the filter, 'a' is the filter area, 'Δp' is the pressure drop across the filter, 'μ' is the dynamic viscosity of the filtrate, 'α' is the average specific cake resistance, 'W' is the total mass of solids in the cake and 'r' is the filter medium resistance. From this equation a basic understanding of the instantaneous mass transfer across the filter (rate of filtration per unit area) as a function of the driving force and the combined resistances can be obtained (Doran 1995; Perry and Green 2008).

For cell-based products, the cells themselves are the end product which means the filtration step often focuses on the removal of contaminants. For this study in particular, the release of a specific intracellular protein will be measured to assess cell damage. Therefore, understanding the transmission of this protein through the membrane into the permeate will be crucial. Transmission at any given time 't' is given by:

$$T(t) = \frac{[P](t)}{[R](t)} \qquad \text{Equation 1.2}$$

where '$T(t)$' is the transmission of the protein investigated at time 't' and '$[P](t)$' and '$[R](t)$' are the concentrations of the protein in question at time 't' in the permeate and the retentate respectively. Therefore, 100% transmission means equal concentrations of the protein in both the retentate and the permeate, i.e. all the protein is permeating through and none is being rejected or retained by the membrane. Equation 1.2 will be of particular interest as transmission can vary depending on the operating conditions. For example, lower shear rates can lead to higher deposition of solids on the membrane which can lower transmission.

1.4.2.3.2 Bioprocessing stresses during TFF

At this stage, the basic theory of TFF and its applicability to cell-based therapies has been presented and reviewed. In this section, the nature of the most common stresses encountered during processing are presented and reviewed with a focus on how these can impact critical cell quality attributes (CQAs). Careful identification, understanding and control of these factors must be put in place to ensure successful delivery of safe and efficient therapeutic products.

A recurring topic in the cell bioprocessing industry is the importance of preserving cell quality, functionality, viability and yield throughout the production of a cell-based therapy (Brandenberger et al. 2011). Hydrodynamic stresses experienced by the cellular material throughout the various processing steps may destroy cells completely or induce physiological responses such as programmed cell death without any obvious physical damage (Chisti 2001; Veraitch et al. 2008; Zoro et al. 2008). Parameters such as shear rate, critical shear stress (Acosta-Martinez et al. 2010), average wall shear rate (Ma et al. 2010) and specific power dissipation have been used to predict and understand the nature of the forces affecting cell quality. Flow behavior is what will ultimately define the stresses encountered by the cellular material and flow behavior is governed by the viscosity of the fluid.

Viscosity is defined as the fluid's resistance to flow (Doran 1995) and it is a parameter of particular relevance to TFF. This is because as the concentration of the cellular suspension increases, the viscosity of the fluid also increases, constantly changing the shear stress experienced by the cells. To further understand this concept, consider the

development of laminar flow between two parallel plates not far from each other. When the lower plate is moved steadily whilst the upper one remains stationary, a steady Couette flow profile is attained (Doran 1995). The force applied to move the plate divided by the area of the plate is defined as shear stress:

$$\tau = \frac{F}{a} \qquad \text{Equation 1.3}$$

where 'τ' is the shear stress (Pa), 'F' is the shear force (kg m s^{-2}) responsible for the motion of the plate and 'a' is the area of the plate. Shear stress is therefore the gradient described by:

$$\tau \propto F \propto \frac{dv}{dy} \qquad \text{Equation 1.4}$$

where '$\frac{dv}{dy}$' is called the shear rate, usually denoted as 'γ' (s^{-1}). Therefore, the proportionality given in equation 1.4 is represented by *Newton's law of viscosity*:

$$\tau = -\mu \frac{dv}{dy} \qquad \text{Equation 1.5}$$

where 'μ' is the proportionality constant or dynamic viscosity (Pa s). Specific equations derived for the device used in this study derived using computational fluid analysis will be presented and reviewed in Section 1.5.1 to assess the hydrodynamic forces experienced at the various different operating conditions during membrane separation.

1.4.3 Storage and delivery

After formulation into the appropriate storage or delivery buffer, the final stage in the processing of cell-based therapies requires a scalable and reproducible technique for

freezing and storing of cells. Like with any other processing step, cell quality attributes and functionality of the cells must be maintained during storage and during transportation to the site of administration.

Depending on the nature of the therapy, storage will vary. Traditionally, mechanical freezers (-80˚C) are acceptable for short term storage (-80˚C) whereas for longer periods, liquid nitrogen (-196˚C) or vapour nitrogen (-135˚C) are preferred. However, some therapies such as tissue engineered scaffolds (e.g. Epicel) cannot be stored in the frozen state as they are part of a complex structure. These types of therapies usually have a short shelf life and are stored in special medium (e.g. Aedesta^{TM}).

Cryopreservation of cells remains a challenging task for the cell-based industry. This has led to many efforts focusing on the effect of concentration, volume, rate of freezing and buffer composition (De Loecker et al. 1998; Fuller and Devireddy 2008; Pegg 1981) in the hope of improving and understanding this crucial stage post-processing. Traditionally, to minimize the damage caused by freezing and thawing, the industry has used controlled cryoprocedures. These include protective agents such as dimethyl sulfoxide (DMSO) or glycerol as well as controlled freezing rates (Fuller and Devireddy 2008). However, toxicity has commonly been attributed to products containing DMSO and therefore its use has become a matter of concern. Commercially available storage buffers, such as Hypothermosol® (BioLife Solutions) for 2-8˚C storage and CryoStor® 2%, 5% and 10% DMSO (BioLife Solutions) for -70˚C to -196˚C storage, have attempted to reduce the level of DMSO into a safe limit.

Other aspects that need special consideration but are beyond the scope of this thesis are the logistical operations related to cold chain supply and adequate product labelling (crucial for autologous therapies, Woods 2010).

1.4.4 Scalability of cell-based therapies

For any cell therapy, the manufacturing process has to be scaled from lab to clinic whilst maintaining at all stages critical cell quality attributes (CQAs) specific to the therapy in question (such as potency, yield, purity and cell viability). The production challenges for cell-based therapies differ depending on the source (allogeneic or autologous), method of administration to the patient (injection, surgical or other), scale (number of cells needed, volume of cells to process) and the type of cells used (i.e. some will be more susceptible to processing environments than others). Gaining in-depth knowledge of cell-process interactions will help understand how scalability of the processing steps will impact cellular material both physically and biologically (Delahaye 2013; McCoy et al. 2009).

There are two main strategies for scaling cell-based therapies and both aim to increase the level of production; scale-out and scale-up. Scale-out refers to an addition of small-scale operations carried out in parallel to each other increasing the manufacturing output by increasing the number of batches. Scale-up refers to increasing the manufacturing output by increasing the volume or number of cells processed for each batch (Hourd et al. 2014a).

Both strategies have their advantages and disadvantages. For example, on the one hand, in scaling-out, there are no connections between one reactor and another (with the exception for the control systems - Mason and Hoare 2006) and there is no need for re-validation because the manufacturing process stays the same. However, the costs associated with scale-out are considerably larger due to the number of operators, equipment and working space required. On the other hand, with scaled-up products, manual labor is reduced and more material can be produced per batch reducing utilities costs and the process footprint. However, the processing steps are not always easily scalable and there is usually a limit to the size of the equipment. Moreover, changing processing platforms will require re-validation and a processing failure will incur a higher economic loss (Hourd et al. 2014b).

Currently, many companies choose to scale-out instead of developing new technologies to scale-up as their small-scale processes are already validated. However, the nature of scalability of the process will inevitably depend on the type of therapy. A therapy that is patient-specific will require production on an individual basis and ideally at the point of care (Kirouac and Zandstra 2008). This type of therapy will need a smaller volume of cellular material than a therapy that is "off-the-shelf" and targets a larger number of patients with every batch produced. Therefore, scale-out is more suited for patient-specific therapies whereas scale-up is beneficial for "off-the-shelf" solutions.

Irrespective of the strategy used for scaling a cell-based therapy, the need to understand and characterize the processing environment remains of utmost importance to facilitate scalability of the manufacturing process.

1.5 Ultra-scale down (USD) technologies

Efforts have been made to develop early stage, low cost process development predictive tools that can accurately mimic the performance of large-scale equipment using small amounts of material (Titchener-Hooker et al. 2008). Historically, scaling down any process meant using a pilot plant or few litres scale. However these options remain costly because of the need for large amounts of biological material (Tait et al. 2009). More recently, ultra-scale down (USD) tools have been developed to cover an array of techniques within cell bioprocessing and Titchener-Hooker et al. (2008) presents an overview of these techniques.

USD devices have been investigated as predictive tools for several different large-scale bioprocessing steps such as chromatography columns (Hutchinson et al. 2006; Titchener-Hooker et al. 2008), centrifugation (Delahaye 2013; Hutchinson et al. 2006; McCoy et al. 2009) and membrane separation (Ma 2009; Ma et al. 2010). For example, Hutchinson et al. (2006) combined the use of a rotating disc device and a laboratory-scale test tube centrifuge to successfully predict the separation characteristics of industrial scale disc stack centrifuges and investigated the effect of operating with different feed zones using milliliter quantities of biological material.

Due to the small volumes of material needed, high throughput experimentation is possible when using USD devices and therefore the scope for investigation is large. This feature is of particular importance for the cell-based industry, where the cellular material is expensive to produce. Therefore, identifying and understanding both mechanical and biological responses of candidate cells to processing stimuli at an early

stage will allow the design of robust bioprocesses to deliver reproducible and efficient therapies and to reject inappropriate candidates at early stages, prior to clinical manufacturing. Recent studies have used USD tools to investigate the impact on surface markers, growth rates and retention of membrane integrity of varying processing conditions during downstream operations for cell-based therapies (Acosta-Martinez et al. 2010; Delahaye 2013; McCoy et al. 2010). In this thesis, the interest is in the effect of processing conditions on cell quality during membrane separation.

1.5.1 USD membrane separation device

Several attempts to mimic the processing environment during filtration have been reported by various authors. Chandler and Zydney (2004) published work on membrane screening using a small scale high-throughput multi-well filtration plate that allows to simultaneously test 96 different conditions. Ghosh and Cui (2000) proposed for the first time an ultrafiltration rotating disc device of ~15 mL capacity. This device consisted of a magnetically driven flat impeller which constantly stirs the retentate chamber. Based on this model, Ma et al. (2010) designed a USD device with a rotating disc to mimic cross-flow microfiltration with ~10-fold less working volume than what Ghosh and Cui (2000) had presented (volume of the retentate is ~1.7 mL).

An optimized version of the latter USD device (fabricated at the Rapid Design and Fabrication Facility, RDFF, in the Department of Biochemical Engineering at University College London, UCL) will be used in this study. The most important parameter of this device is the shear rate at the membrane surface, parameter which is normally responsible for the rate of fouling of the membrane. The device is designed

such that it can be run in dead end mode but mimicking shearing conditions from a cross-flow model. This feature allows the decoupling of shear rate and pressure drop.

Ma et al. (2010) used powerful computational fluid dynamics (CFD) software as an additional design tool for the analysis of shear forces in the USD membrane separation chamber. Dr. Spyridon Gerontas kindly adapted the CFD simulations to show the minor design changes that the device has undergone through the various optimization cycles. Figures 1.4.A and 1.4.B show the magnitude of the shear rate experienced by the material present in the retentate chamber at various different locations as three-dimensional and two-dimensional heat maps (assuming a viscosity of water of 0.99 g cm^{-3} at 21±1°C). From this figure it is evident that the highest shear experienced is at the edges of the rotating disc (red areas in Figures 1.4.A and 1.4.B).

Figure 1.5 shows shear rate as a function of viscosity. By keeping the disc speed constant, and increasing the viscosity of the fluid, the shear rate experienced by the material in the retentate chamber decreases. Table below Figure 1.5 shows the maximum shear rates experiences at the two disc speeds and viscosities reported in this study.

1.6 Disruption of cell homeostasis: identification and assessment of cell quality attributes (CQAs) of the target cell population

Cells maintain a steady state or internal equilibrium by adjusting their physiological processes. They require exchanges with their surrounding environment and dynamic adjustments in order to maintain the status quo (Kumar et al. 2007; Kuo et al. 2010).

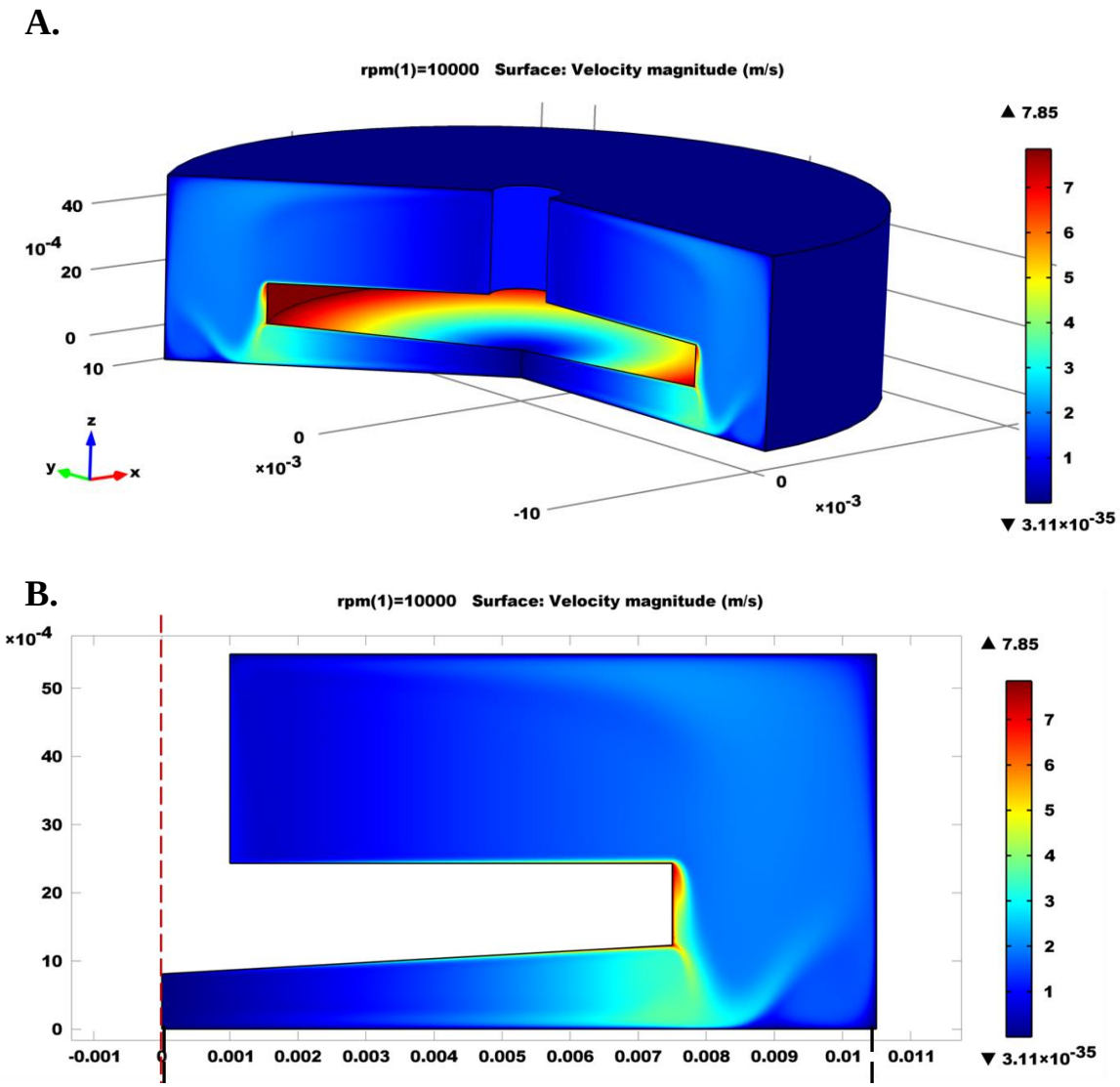

Figure 1.4: A computational fluid dynamic (CFD) simulation displaying the shear rate experienced at various locations of the USD membrane device (kindly provided by Dr Spyron Gerontas). (A) Three-dimensional and (B) two-dimensional heat maps showing the increase in magnitude of shear rate by color change (from blue to red).

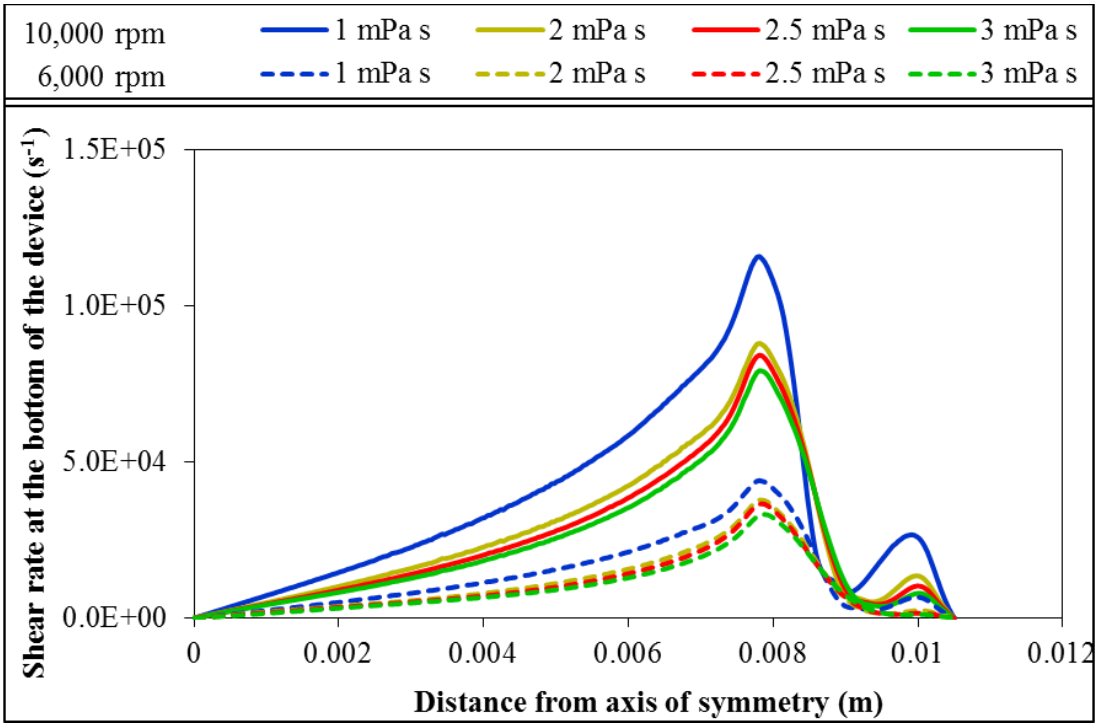

Figure 1.5: Shear rate at the bottom of the USD membrane separation device as a function of rotational speeds of 6,000 (dashed lines) and 10,000 (continuous lines) rpm for varying viscosity values. Kindly provided by Dr Spyron Gerontas.

		Average		Maximum	
Disc speed (rpm)	**Viscosity (mPa s)**	**Shear rate (s^{-1})**	**Shear stress (Pa)**	**Shear rate (s^{-1})**	**Shear stress (Pa)**
10,000	1	37,000	37	116,000	116
	1.5	31,000	46	98,000	147
	2	27,000	55	88,000	176
	2.5	25,000	63	84,000	210
	3	23,000	70	79,000	237
6,000	1	14,000	14	44,000	44
	1.5	12,000	18	40,000	59
	2	11,000	21	38,000	76
	2.5	10,000	25	36,000	91
	3	9,000	28	33,000	99

When the equilibrium of a parameter or component is disturbed there is a readjustment giving rise to a stimulus. This homeostasis or equilibrium keeps the cell functioning properly and in a constant state of balance between waste products excreted and the nutrients received. The plasma membrane and membrane proteins are the main structures which help maintain this state and therefore the disruption of the membrane or mal-regulation of proteins can serve as indicators of cell health (Kumar et al. 2007).

Exposed to a range of mechanical and physiochemical stresses during processing, living organisms such as cells intended for therapies are in a continual strive to adjust to the changes in the surrounding environment (Figure 1.6). Therefore a major challenge to successful commercializing of cell-based therapies is the development of scalable manufacturing processes while maintaining CQAs (such as potency, purity, viability) of the final live cell product (Carmen et al. 2012). However, each individual therapy will have its own unique criteria that lead to assays that can be used to characterize the cells. Each product will require a customized procedure that measures potency (or as the FDA defines it, "appropriate biological activity"). More often than not, it is not straightforward to determine what this should encompass, incurring high development costs and lengthy assays. Moreover, it remains the responsibility of the manufacturer to guarantee product safety and efficacy throughout bioprocessing of the cells as well as post-administration to the patients. For this reason, the best practices in process development will rely strongly on cell characterization and a thorough understanding of the cell-based product (Carmen et al. 2012).

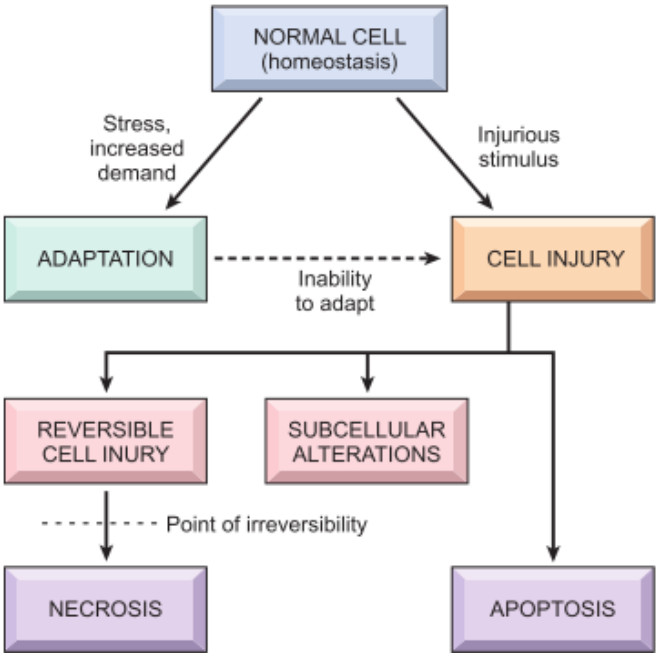

Figure 1.6: Stages in the cellular response to stress and injurious stimuli. Adapted from Kumar et al. (2007).

This section aims to provide an understanding of what defines CQAs for a generic cell-based therapy and provide an insight into some of the methods used to analyze the specific biological requirements.

1.6.1 Membrane integrity

The word integrity is derived from the Latin word "integer" which translates to "intact". Integrity is defined as "the state of being whole and undivided" (Oxford Dictionaries). The integrity of a cell membrane is said to be compromised when there is a breakage of the lipid bilayer and intracellular components are released or extracellular components can enter the cell without being appropriately regulated. Should the integrity of the plasma membrane be disrupted, cell quality is immediately affected; cell death may occur if there is no rapid restoration of the membrane (McNeil and Steinhardt 2003) as it compromises its functional role as a barrier (Kumar et al. 2007).

Therefore, membrane integrity is used as an initial analysis of cell quality (also referred to as cell viability). Viability assays can be based on one of two characteristic parameters; metabolic activity (achieved by measuring an indicator for healthy cells in cell populations) or cell membrane integrity of intact cells (accomplished by directly counting the number of cells that do not have a compromised or broken membrane). The latter, viability as measured by exclusion dyes or release of intracellular components, is by far the most common assessment criteria used due to its ease in measurement and the fact that it does not need large quantities of material (Acosta-Martinez 2011; McCoy et al. 2010; Wlodkowic et al. 2011). In this thesis, trypan blue

exclusion and release of intracellular lactate dehydrogenase (LDH) enzyme are the two measurements presented to assess cell viability and death.

1.6.1.1 Trypan blue exclusion dye as a measure of cell viability

Exclusion dye techniques are normally excluded from the inside of a healthy cell due to a functioning intact plasma membrane. Several different dyes are available, such as trypan blue and propidium iodide, and all have slightly different measuring techniques and characteristics. However, the principle is the same for all dye exclusion measurements. If the cell membrane has been disrupted, the dye can freely cross the membrane staining the intracellular components of the cell. The dead cells distinctively appear colored in blue (trypan blue) or red (propidium iodide) under a microscope and thus the distinction can be made.

For the purpose of this study, the term cell viability will therefore be a quantitative assessment of "intact" cells in a sample as measured by trypan blue exclusion dye. However, with trypan blue staining, it is possible that the cell viability has been compromised in a way that the dye might not detect (such as its capacity to grow or expression of programmed cell death proteins) due to retention of membrane integrity. Research suggests that fluorometric dyes, such as propidium iodide, are more accurate indicators as even small amounts of dye taken-up by injured cells will show under fluorescent microscopes whereas it might be hard to see with trypan blue dye. Nevertheless, trypan blue remains more commonly used due to its rapidity and ease of use (Altman et al. 1993).

1.6.1.2 Lactate dehydrogenase (LDH) release as a measure of cell death

Several standard assays have been developed in order to provide sensitive, quantitative, reliable and accurate methods for the quantification of cellular death. These assays measure intracellular proteins which are only released when membrane integrity is lost or cells are completely lysed. For example, lactate dehydrogenase (LDH) is a stable cytoplasmic enzyme widely reported to measure cell death. Its rapid release into the cell culture supernatant upon damage of the plasma membrane makes it an ideal candidate to measure cell number and viability (Markert 1984). It has been used in various systems, ranging from microwell plates (Wolterbeek and van der Meer 2005) to flask cultures (Racher et al. 1990) to perfusion reactors (Goergen et al. 1993; Herold et al. 2009; Wagner et al. 1992).

LDH has also been studied for filtration systems (Nema and Avis 1993). Nema and Avis (1993) investigated the loss of LDH activity during membrane filtration by looking at the transmission of the protein using different membrane materials and pore sizes. Their investigation concluded polycarbonate and polyvinylidene fluoride (PVDF) filters showed low loss of protein with the exception of 5 µm PVDF filters. Even though this study did not use cells as a source of LDH, the observations are relevant to membrane selection. The biggest pore size investigated by Nema and Avis (1993) with low loss of LDH activity was 0.65 µm PVDF membrane and this will be the membrane used in this study.

Like trypan blue exclusion, LDH release does not differentiate between non-viable cells and completely lysed cells or between different cell death pathways (necrosis or

apoptosis). Therefore, once it is determined whether integrity has been compromised, further studies can be made to look at attributes such as changes in protein expression, morphology and size.

1.6.2 Protein expression for cell death

Analysis that focuses on the function and biological state of the cell population is an added measure of cell quality that may not be evident from the physical measurement of cell damage. For example, harsh processing conditions can trigger cells to produce unwanted proteins or impede the creation of necessary ones (Agashi et al. 2009). Therefore, an indication of the quality and state of cellular products is the level of expression of specific proteins.

This is the case for programmed cell death protein expression (Darzynkiewicz and Pozarowski 2007). Cell death biological assays will identify the two primary types of death; apoptosis and necrosis. These two categories are different in their morphology, mechanisms and roles in the programmed cell death pathways (Dive et al. 1992). The biological assays used to measure programmed cell death are based on the detection of caspase – a key molecule in the apoptotic mechanism and induction of apoptosis (Darzynkiewicz and Pozarowski 2007; Smolewski et al. 2002). Even though the caspase sub-type involved may vary from one tissue to another, caspase-3 is known as a universal caspase which functions in almost all tissues and is an indicator that the cell is committed to irreversible cell death processes and therefore most assays work on the activation of caspase-3 (Darzynkiewicz and Pozarowski 2007; Smolewski et al. 2002). These assays recognize four populations within a cellular suspension; cells which are

live; early apoptotic cells which show apoptotic related activity but no loss of membrane integrity; late apoptotic cells which show both apoptotic related activity as well as loss of membrane integrity; and necrotic cells which did not undergo an apoptotic pathway prior to loss of membrane integrity.

Therefore, expression of caspase-3 is a widely used and reliable way of measuring apoptosis. In addition, by inspection of the morphology of cells, some preliminary observations can be made in order to assess cell health.

1.6.3 Cell morphology post-processing

Cell physical classification and identity can serve as an indication of cell health. Cells can change shape, size or physical appearance after being exposed to stresses (Al-Rubeai et al. 1995; Kretzmer and Schügerl 1991) and this can be an indication of underlying changes in structural remodelling (membrane channels changing conformation) or metabolic pathways. Size change can be a sign of the leaking of internal components into the extracellular environment (if size is reduced) or swelling if extracellular fluids are permeating into the cell (Al-Rubeai et al. 1995; Kumar et al. 2007).

Morphological changes can serve as indicators of specific cell death pathways. For instance, necrosis often leads to inflammation of the cell as a host reaction to leakage of internal components due to a damaged membrane. On the other hand, apoptosis is often characterized by shrinkage of the cell with an intact cell membrane and membrane protrusions known as blebbing (Kumar et al. 2007). Even though the most reliable way

of measuring programmed cell death is by measuring changes in protein expression, as was previously described, morphological changes can act as an indicator of programmed cell death. The clear advantage of morphological analysis is that it can be retrospectively performed from the images obtained by the automated haemocytometer.

1.6.4 Cell growth rate post-processing

The use of processed cell populations to inoculate further cultures can help assess the impact of specific processing steps or conditions upon a cell population. For successful cell division, a chain of events must be completed in an orderly and unidirectional manner. Changes in the rate of cell growth and doubling times can de-regulate this crucial chain of events (Kumar et al. 2007) and can serve as indicators of the state of cell health and its suitability for use as a whole cell product (Agashi et al. 2009; Kretzmer and Schügerl 1991). However, for growth rate studies, it is essential that numerous influential factors for cell growth (media composition, dissolved oxygen, pH, surface material for attachment, seeding density, etc) are kept constant.

1.7 Thesis aims and objectives

The successful processing of adherent cells requires a deep understanding of time-dependent relationship of cell-cell interactions and cell-surface interactions such that processing environments are not destructive of the cells themselves. Understanding how operating conditions impact cell recovery, cell integrity and cell quality is crucial for the successful processing of human cells. However, as important is having tools that will monitor and indicate key CQAs.

This study aims to develop and explore the use of a novel USD membrane separation technique to help understand the relationship between operating conditions, cell line selection and membrane (material) selection required for the successful recovery of human adherent cells for therapeutic use. The aim within this investigation is to quantify the impact of processing upon cell-based therapies, identifying mainly cell damage by loss of membrane integrity and lysis (as measured by both trypan blue exclusion and LDH release). It also provides a glance into other key cell quality attributes such as cell morphology, programmed cell death and growth post-processing.

The focus in this study lies on providing a consistent and reproducible tool to assess cell damage in response to the bioprocessing environment without intervening with the actual cell suspension. Human fibroblasts were utilized to develop the measurements of cell damage as assessed by both trypan blue and LDH. By selecting extreme processing conditions, it is hoped that mechanistic hypotheses can be established as to the source of cell responses.

Its reproducibility and suitability for cell damage assessment was subsequently tested under different operating conditions and then used to translate the impact of the same processing conditions to more expensive cell therapy candidate cell lines (tumour cells and neural stem cells). The method provides a way to assess cell damage that will be adaptable to any other filtration study and cell line as long as minimum transmission studies are carried out to ensure the underlying assumptions of the method apply with the new filtration characteristics.

Lastly, the research also aims to create a fundamental understanding of how cell-cell interactions occur in concentrated suspensions in shear conditions and how these affect cell integrity (membrane integrity) and cell-related loss (cell damage by lysis). The ability to work with microscale quantities of cells within the bioprocess mimics, especially for the studies on concentrated suspensions, will offer a novel means of early selection of membrane separation and other methods for cell recovery.

With the range of tests carried out, the study will present a generic evaluation of cell damage over time of operation that is envisaged to be applicable to a wide range of current and future cell therapies with varying thresholds for different cell lines. Using our USD membrane separation device facilitated the study of a range of operating conditions in a cost and time effective manner using relatively small amounts of cellular material.

Chapter 2. Materials and methods

2.1 Introduction

Changes in cell properties during exposure to various operating conditions, relevant to the use of cross-flow membrane processes operations at preparative scale, were studied. This chapter will outline the operating procedures adopted for cell handling (including cryopreservation, culture and harvesting), cell processing (including detailed operation of the device and operating conditions) as well as cell analytics (including evaluation of cell health, morphology and proliferation post-processing).

2.2 Cell lines

Three cell lines were used in this research for the development of an ultra scale-down tool.

2.2.1 HCA2 cell line

HCA2 cells (provided by Prof David Kipling, University of Cardiff, UK) are human neonatal foreskin fibroblasts and are used for skin grafting applications. These cells had previously been immortalized using an amphotropic retrovirus expressing hTERT, the catalytic protein subunit of human telomerase. The retrovirus was constructed and used for infection of the HCA2 normal human fibroblasts (Stephens et al. 2003; Wyllie et al. 2000).

2.2.2 P4E6 cell line

P4E6 cell line (provided by Onyvax Ltd, St George's Hospital, London) is one of three cell lines used in a human prostate whole-cell cancer vaccine. It is derived from an early

prostate cancer biopsy. It is a prostate carcinoma cell line (Maitland et al. 2001) immortalized by transfection of a retroviral construct (PLXSN16E6) expressing human papilloma virus (HPV) type 16 E6 gene (Halbert et al. 1992). The cell line maintains epithelial characteristics and the ability to express both prostate specific antigen (PSA) and androgen receptor (AR).

2.2.3 CTX0E03 cell line

CTX0E03 neural stem cell line (provided by ReNeuron Group plc., London) is a human clonal cell line developed to aid regeneration of human brain tissue post-stroke. It is derived by genetic modification of foetal brain tissue using a conditional immortalizing gene, c-mycER^{TAM} (Pollock et al. 2006). Incorporation of c-mycER^{TAM} gene was performed using a retroviral vector pLNCX-2 encoding for the c-mycER^{TAM} gene (Pollock et al. 2006). Cell proliferation takes place only in the presence of 4-hydroxy-tamoxifen (4-OHT) and, upon removal of 4-OHT, the cells stop dividing. Tests on rodent models demonstrated that the use of c-mycER^{TAM} provides a necessary safeguard switch to prevent against inappropriate cell division or tumour formation (Pollock et al. 2006). The human foetal cortex was obtained from first trimester foetal human brain following normal termination and in accordance with nationally (UK and/or USA) approved ethical and legal guidelines.

2.3 Cell culture

The cell banks were tested for sterility and mycoplasma infection prior to the cell culture work. All cell handling was carried out in a class II biological safety cabinet (Walker, Derbyshire, UK) using sterile techniques.

2.3.1 Growth media

All three cell lines were grown in different complete growth media (CGM).

HCA2 cells were grown in Dulbecco's Modified Eagles Medium (DMEM, Invitrogen, Paisley, UK), supplemented with 10% (v/v) foetal calf serum (PAA Laboratories, Linz, Austria) and 2 mM of glutamine (Invitrogen, Paisley, UK). The supplemented medium will be referred to as hCGM.

P4E6 cells were grown in keratinocyte serum-free medium (Gibco-Invitrogen, Paisley, Scotland, UK) supplemented with 5µg L^{-1} of epidermal growth factor (EGF; Gibco-Invitrogen, Paisley, Scotland, UK) and 2% (v/v) foetal calf serum (FCS; PAA Laboratories, Linz, Austria). The supplemented medium will be referred to as pCGM.

CTX0E03 cells were grown in reduced modified medium which comprised DMEM:F12 (Invitrogen, Paisley, UK) supplemented with human serum albumin (HSA; 0.03% v/v; Octopharma, Manchester, UK), L-Glutamine (2 mM; Invitrogen, Paisley, UK), human transferrin (100 µg/mL; Millipore, Hertfordshire, UK), putrescine dihydrochloride (16.2 µg/mL; Sigma-Aldrich, Ayrshire, UK), human insulin (5 µg/mL; Sigma-Aldrich, Ayrshire, UK), progesterone (60 ng/mL; Sigma-Aldrich, Ayrshire, UK), sodium selenite (40 ng/mL; Sigma-Aldrich, Ayrshire, UK), basic fibroblast growth factor (bFGF; 10 ng/mL; Invitrogen, Paisley, Scotland, UK) and EGF (20 ng/mL; Sigma-Aldrich, Ayrshire, UK). This medium formulation was referred to as cCGM. Before use for cell culture, 4-hydroxy-tamoxifen (4-OHT; Sigma-Aldrich, Ayrshire, UK) was added to the cCGM (referred to as cCGM:4-OHT) to a final concentration of 100 nM.

2.3.2 Cryopreservation of cell lines

HCA2 cell line*:* A cell bank for future expansion was created in-house by collaborative efforts within our group. It consisted of frozen aliquots of 1 mL containing $5x10^6$ cells in freezing medium (foetal calf serum, FCS; Thermo Fisher Scientific, Northumberland, UK) supplemented with 10% (v/v) dimethyl sulfoxide (DMSO; Sigma-Aldrich, Ayrshire, UK) and stored in liquid nitrogen. HCA2 cells were cultured between passages 11 and 25 counted from frozen state (passage 11). The minimum seeding density was approximately $2x10^4$ cells cm^{-2}.

P4E6 cell line: A cell bank for future expansion was created by Onyvax, consisting of frozen aliquots of 1 mL containing $5x10^6$ cells in freezing medium as described for HCA2 cell line. P4E6 cells were used between passages 51 and 60 counted from frozen state (passage 50). The minimum seeding density was approximately $4x10^4$ cells cm^{-2}.

CTX0E03 cell line: A cell bank, from an aliquot provided by ReNeuron, was derived in-house by Dr Kate Lawrence, consisting of frozen aliquots of 1 mL containing $5x10^6$ cells in freezing medium (cCGM, supplemented with 10% (v/v) DMSO; Sigma-Aldrich, Ayrshire, UK) and stored in liquid nitrogen. CTX0E03 cells were used between passages 24 and 37 counted from frozen stage (passage 24), in accordance with ReNeuron manufacturing protocol. The minimum seeding density used was approximately $2x10^4$ cells cm^{-2}.

2.3.3 Revival of cell lines

A cell line was revived from frozen state by placing one aliquot of cells in a 37°C waterbath for 2 minutes, then slowly transferring the defrosted sample into a 15 mL centrifuge tube and adding 9 mL of the cell's appropriate CGM. The removal of the freezing medium was facilitated by centrifugal spin (Thermo, Strasbourg, France) for 5 minutes at 500 x g. The cells were then resuspended in 18 mL of appropriate CGM and transferred to a T75 tissue culture flask (Cellstar, Greiner Bio-One, Germany). The flasks were kept in an incubator (Sanyo, Osaka, Japan) maintained at a controlled gas environment (5% CO_2, 95% air) and temperature (37°C).

2.3.4 Cell preparation for recovery studies

Cell line specific culture protocols are described in this section. It also includes information for the three cell lines such as the average diameter of the cells in suspension or days taken to reach confluency. The protocols outlined in this section describe cell culture in T175 flasks; Table 2.1 shows the volumes needed for wash buffer, detachment enzyme and CGM for all flasks used in this study (i.e. T75, T175 and triple flasks).

2.3.4.1 HCA2 and P4E6 cell lines

Cells were passaged when 70-80% confluency, as assessed by light microscopy inspection, was reached. To dissociate the cells from the T175 tissue culture flask (Cellstar, Greiner Bio-One, Germany), the spent medium was aspirated, cells were washed with 15 mL of Dulbecco's Phosphate Buffered Saline (DPBS; Sigma-Aldrich, Ayrshire, UK) and enzymatically detached using 5 mL TrypLE^{TM} Select (Invitrogen,

Flask type	Area for cell culture (cm^2)	DPBS	TrypLE™ Select	CGM
		Volume (mL)		
T75	75	7	3	18
T175	175	15	5	42
Triple flask	525	40	25	110

Table 2.1: Volumes used of reagents for different sizes of cell culture flasks. Minimum seeding densities for HCA2 and CTX0E03 was approximately $2x10^4$ cells cm^{-2} and $4x10^6$ cells cm^{-2} for P4E6 cell line.

Paisley, UK) for 4-8 minutes at 37°C. To quench the enzyme, an equal volume of appropriate CGM was introduced into the flask. The cells were then transferred to a 15 mL centrifuge tube and centrifuged (Thermo, Strasbourg, France) for 3 minutes at 500 x g at 21±1°C. The supernatant was removed by aspiration and the pellet was loosened from the tube wall by gently flicking the centrifuge tube. The cells were subsequently manually resuspended in 42 mL of appropriate CGM using a Pipetboy (IBS, Integra Biosciences, Zizers, Switzerland), counted, transferred into a new tissue culture flask at a cell density determined by the desired split and placed in the incubator to allow proliferation. A 1 in 6 split and 1 in 4 for HCA2 and P4E6 respectively, take approximately 4 days to reach 70-80% confluency, as assessed by light microscopy inspection.

2.3.4.2 CTX0E03 cell line

Prior to seeding of the cells, each cell culture flask was pre-treated with 15 mL of laminin (10 µg/mL; AMS Biotechnology) in DMEM:F12 (Invitrogen, Paisley, UK) and placed in the incubator (Sanyo, Osaka, Japan) at 5% CO_2, 95% air and 37°C for at least one hour. The addition of laminin provides a coated membrane component to assist cell attachment, growth and proliferation. Prior to cell inoculation, the laminin solution was removed by aspiration and the flasks washed with DMEM:F12.

Cells were passaged when 70-80% confluency, as assessed by light microscopy inspection, was reached. To dissociate the cells, the spent medium was removed by aspiration and the cells were washed with 15 mL of Hanks' balanced salt solution (HBSS; Sigma-Aldrich, Ayrshire, UK). The cells were then enzymatically detached

using 5 mL TrypZean (Lonza, Slough, UK), for 5 minutes at 37°C. To quench the enzyme, an equal volume of defined trypsin inhibitor (DTI; Invitrogen, Paisley, UK) supplemented with a final concentration of 20 units per mL of benzonase (Benz; Merck, Nottingham, UK) was introduced into the flask. The cells were then centrifuged (Thermo, Strasbourg, France) for 5 minutes at 800 x g, at 21±1°C. The supernatant was aspirated off and the pellet was loosened from the tube wall by gently flicking the centrifuge tube. The cells were subsequently resuspended in cCGM:4OHT, counted, re-seeded at varying cell densities depending on the desired split and placed in the incubator to allow proliferation. A 1 in 2 split takes approximately 4 days to reach 70-80% confluency, as assessed by light microscopy inspection.

2.4 Membrane separation rotating disc shear device

2.4.1 Technical details

The rotating disc shear device used (Figure 2.1) is similar to the one described by Ma et al. (2010) and was built by the Rapid Design and Fabrication Facility (RDFF) at UCL. It consists of a sealed Perspex chamber of internal diameter of 21 mm and a fixed total volume of 1.7 mL. The chamber had a centrally mounted conical disc, 15 mm in diameter with a 4º conical cross-section, with an accompanying shaft assembly fabricated in stainless steel (Figure 2.1). The shaft was fitted to a high speed motor with a feedback loop (Outrunner Motor, 920Kv Park 400, Champaign, Illinois, USA) driven by a portable power-pack also built by the RDFF. The rotating disc can be set to run at fixed speeds of 6,000 ± 50, 8,000 ± 50 and 10,000 ± 100 rpm.

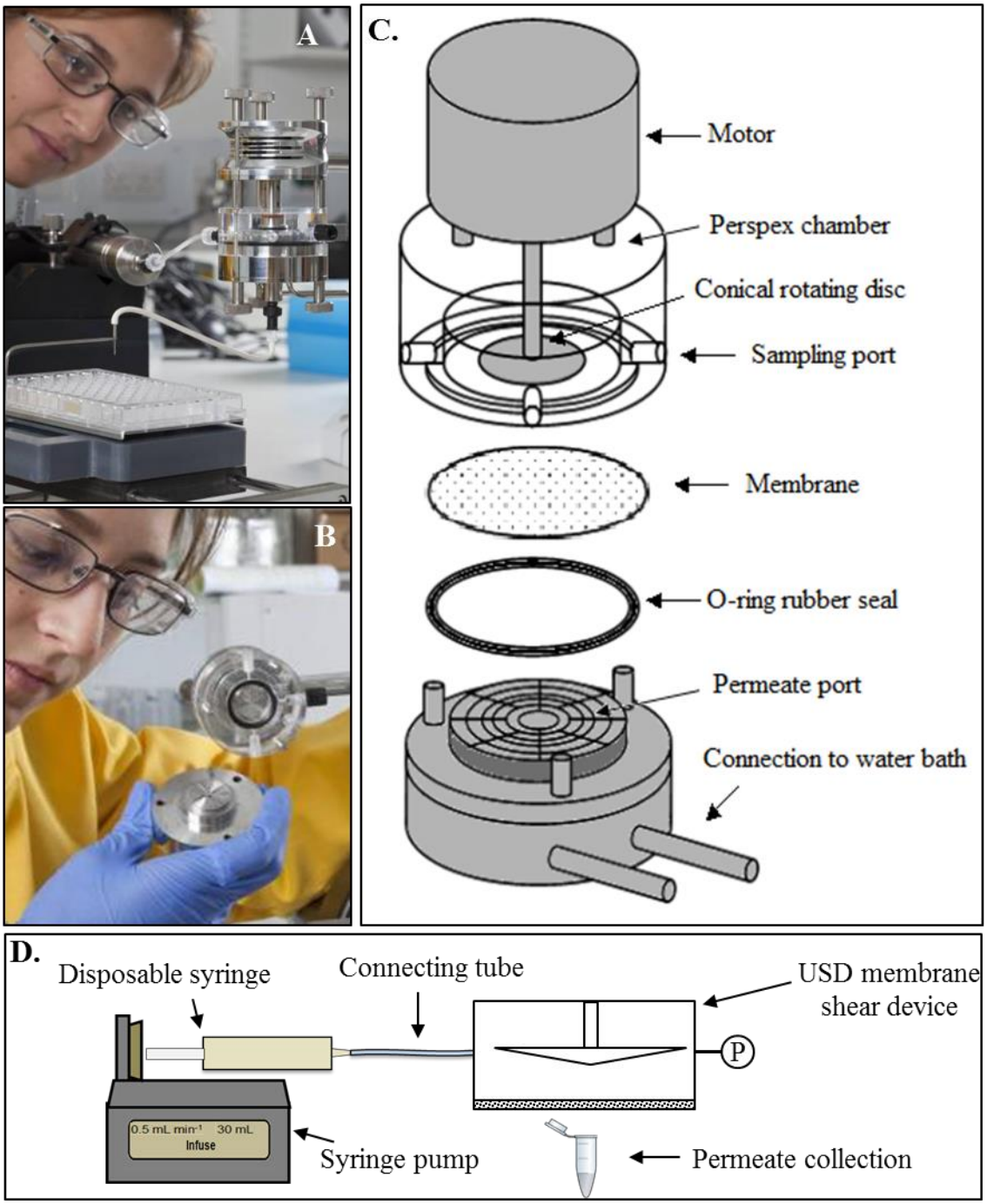

Figure 2.1: Image of the ultra scale-down membrane filtration device set-up. (A) Attached to a syringe pump and (B) inside of the chamber, (C) schematic representation of the device and (D) schematic representation of full set-up of the device, including pressure measurement and syringe pump.

A 25 mm diameter polyvinylidene fluoride Durapore® membrane (Millipore, Hertfordshire, UK) with an area of 4.91 cm^2 and 0.65 µm pore size, was mounted between the bottom of the shear cell and an O-ring seal of 25 mm outer diameter that sits on the permeate port (Figure 2.1.C). Due to the width of the O-ring, the effective area of the membrane is 3.64 cm^2. The gap between the membrane and the rotating tip was designed at 1 mm (Figure 2.2.A). Three ports were drilled into the upper half of the chamber to allow for filling, sampling, emptying the device as well as measurement of the chamber pressure.

A correlation for the surface averaged shear rate as a function of the speed of the rotating disc, was developed by Ma et al. (2010) using CFD simulations and were used in this study:

$$\gamma = 2.12 \times 10^{-6} \mu^{-1.375} \omega^{1.5} \qquad \text{Equation 2.1}$$

where 'γ' is the shear rate (s^{-1}), 'μ' is the viscosity of the fluid (Pa s) and 'ω' is the rotational speed of the disc (revolutions per minute, rpm). Assuming a viscosity like that of water at 21±1°C, the averaged shear rates for the three fixed rotating disc speeds are of 13,000 s^{-1}, 20,000 s^{-1} and 28,000 s^{-1} respectively. As was explained in section 1.5.1, the maximum shear rate is experienced at the edges of the rotating disc (Figure 1.3). For this study, maximum shear rate values will be reported instead of average ones for the two disc speeds and varying viscosities investigated. These values were obtained from Figure 1.4, also in section 1.5.1 and are summarized in the table below it.

An inline pressure sensor can be fitted into one of the sampling ports and operates within the 0-7 bar range (±0.07 bar; 40PC100G2A, Honeywell Sensors and Control,

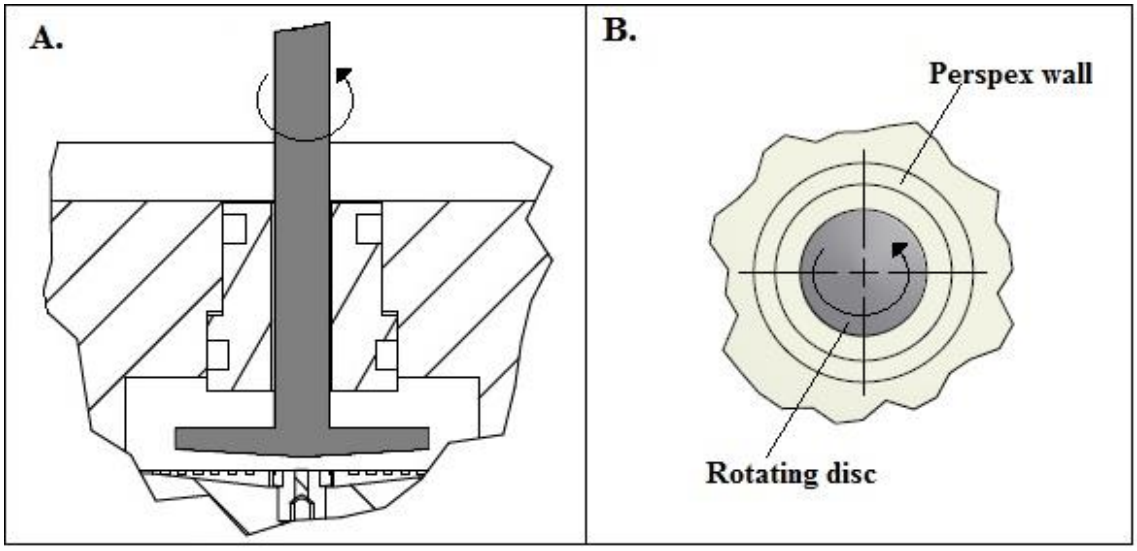

Figure 2.2: Cross-sectional view of the chamber from (A) the side and view of (B) the inside of the chamber from below.

Golden Valley, USA) and was built by the RDFF. This pressure device was composed of an amplified pressure gauge sensor (RS Components Ltd, Northants, UK) connected to a multifunction data acquisition device (National Instruments Corporation Ltd, Berkshire, UK) and powered by a power-pack also built by the RDFF. The pressure readings acquired were logged using LabVIEW software (National Instruments Corporation Ltd, Berkshire, UK) and were in the form of mV at 1 second intervals. The pressure device was calibrated in collaboration with Alex Chatel using the ÄKTA Crossflow system (GE Healthcare, Uppsala, Sweden) as a reference (Figure 2.3).

This was done by running water through a 50 kDa membrane filter at different fluxes while recording the readings from the pressure sensor as well as the ÄKTA Cross-flow system. A correlation was then established (R^2=1.00) to convert the reading from mV to bar given by:

$$p = 1.676\ (mV) + 1.380 \qquad \text{Equation 2.2}$$

where 'p' is pressure (in bar) and 'mV' is the voltage reading (in mV) from the custom pressure sensor. Accurate monitoring of the resultant absolute pressure in the chamber was possible. The transmembrane pressure ('TMP') was then calculated using the following equation:

$$TMP = p_R - p_P \qquad \text{Equation 2.3}$$

where 'p_R' is the pressure in the retentate and 'p_P' is the pressure in the permeate (bar). The pressure in the permeate is atmospheric pressure, therefore $TMP = p_R$.

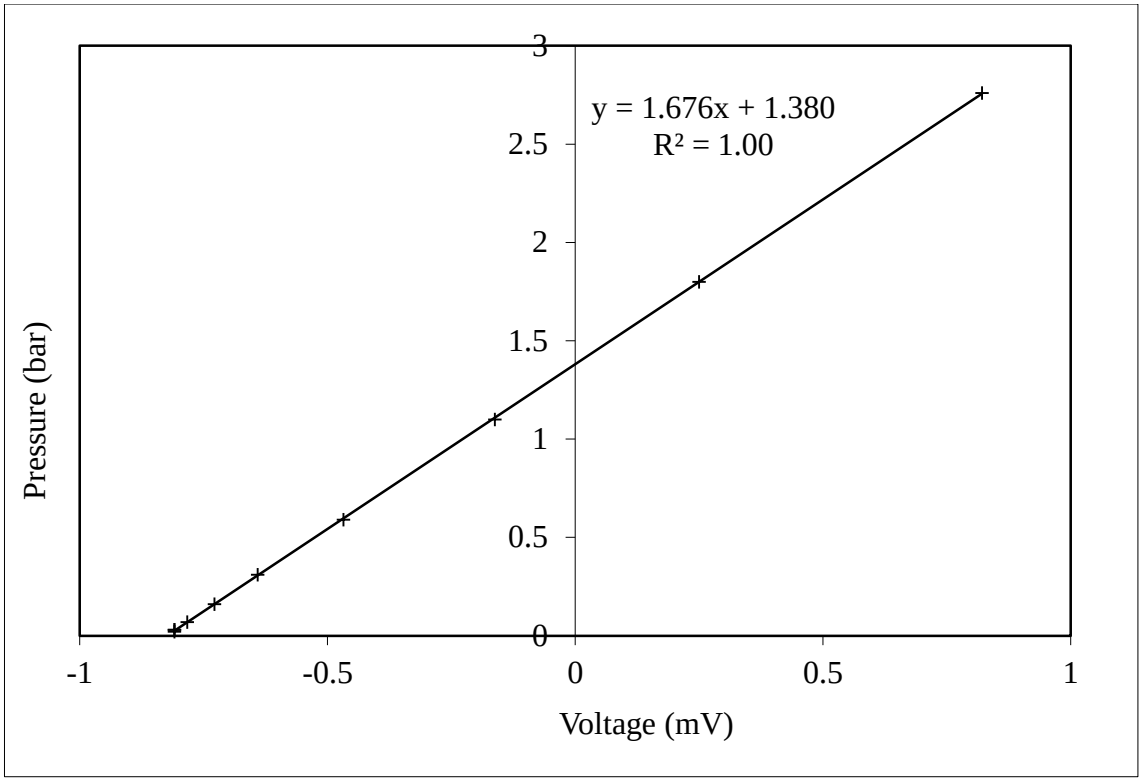

Figure 2.3: Calibration curve correlation obtained for the pressure sensor built by the RDFF by using the built-in pressure sensor in the ÄKTA cross-flow system. The equation obtained (R2= 1.00) was $p = 1.676(mV) + 1.380$, where 'p' is pressure and 'mV' the reading from the pressure sensor built by the RDFF.

A 100 mL disposable syringe driven by a Harvard syringe pump PHD 4400 (Harvard Apparatus Ltd, Kent, UK) was connected to the USD membrane device and was used to feed the buffer (diafiltration mode) into the device at an accurate and fixed flow rate ('Q') of 0.5 mL min^{-1} flow rate (equivalent membrane flux rate of 82 LMH.

2.4.2 Operation of the device

5 mL of cell suspension at the desired concentration ($1x10^6$ cells mL^{-1} to $100x10^6$ cells mL^{-1}) was prepared for each experiment. After placing a membrane into the USD device, as described in section 2.4.1, it was then filled with cell suspension using a 5 mL plastic syringe. The chamber was filled with 1.7 mL of cell suspension taking special care to ensure any air bubbles could escape by keeping another port open. The chamber was then sealed by closing the open port (taking care not to introduce any air) and connected to the syringe pump. All experiments were carried out in constant flux mode and pressure was monitored throughout. The permeate was collected every 5 minutes and the retentate was collected from the chamber using a clean syringe once the experiment finished. The 5 mL plastic syringe used to fill the device was discarded after emptying the remaining 3.3 mL of unused cellular suspension in a microfuge tube. This is the non-sheared control for the duration of the experiment (referred to as control).

Following processing in the USD membrane device, analysis such as membrane integrity by trypan blue exclusion dye exclusion and LDH protein release, for the cellular suspension fed into the device (referred to as '$R(0)$'), the control ('$C(60)$' and the retentate ('$R(60)$') were carried out. Everything was maintained at 21 ± 1 ºC except for the feed and permeate samples collected for LDH analysis which were held on ice.

2.4.2.1 Mode of operation

Diafiltration mode was used to operate the device and is detailed below (Figure 2.4). A typical diafiltration run consisted of filling the device as previously described. The cell suspension was then sheared in the USD device for 60 minutes and maintained at 21±1ºC while flushing with CGM at a fixed flow rate of 0.5 mL min^{-1} (82 LMH) as seen in Figure 2.4.A. The permeate was collected at 5 minute intervals and immediately placed on ice ready for subsequent LDH analysis.

2.5 Cell analysis

In this study, two main techniques were used to assess cell damage; automated haemocytometer and LDH assay. The automated haemocytometer is based on a trypan blue exclusion dye technique which provides a measure of cell size, total and viable cell concentrations and percentage viability based on membrane integrity. The LDH assay is a technique that measures the amount of LDH present in the supernatant and allows calculation of the number of intact cells lost due to processing by measuring the number of whole cells in the feed, retentate and control samples.

Both measurements complement each other; for instance, if a proportion of cells were fully lysed during processing, the automated haemocytometer would not be able to account for those missing cells but LDH would. On the other hand, LDH would not be able to distinguish non-viable cells from completely lysed, but trypan blue exclusion would.

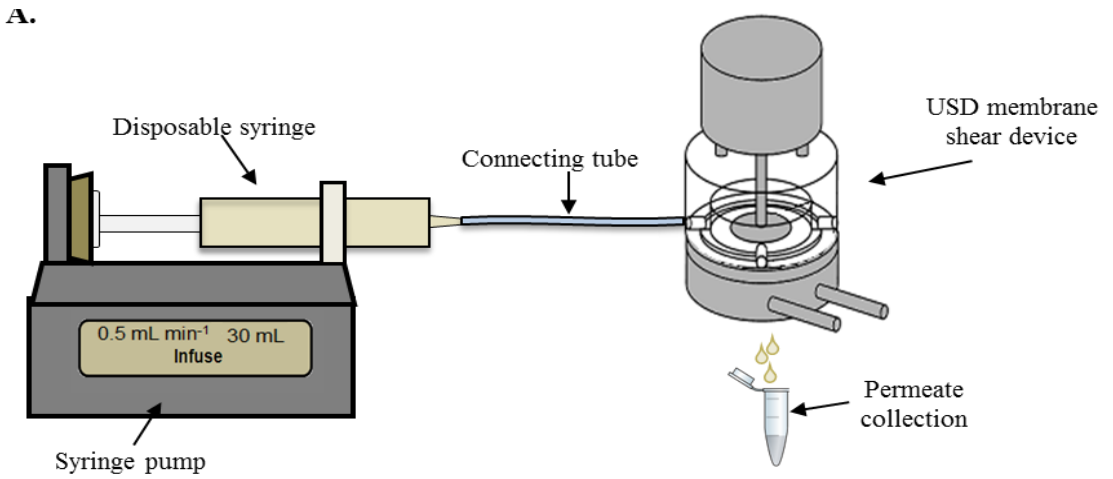

Figure 2.4: Schematic representation of the experimental set-up. The USD membrane device was fed the cellular suspension and then connected to a syringe pump that pumps CGM only in a diafiltration mode.

2.5.1 Membrane integrity, concentration and size

Membrane integrity, viable and total cell concentrations and size distributions were measured in quadruplicate, using the trypan blue exclusion method carried out in an automated system (Vi-CELL XR™, Beckman Coulter, Fullerton, CA, USA).

Cell sizing is carried out by using video imaging through a quartz flow cell. The range of detection of concentration of the Vi-Cell XR™ is between $1x10^4$ and $5x10^7$ cells mL^{-1}, therefore samples were diluted with DPBS accordingly to ensure the concentration of the sample was within range. In order to achieve statistically significant counts, the device takes fifty images per sample (each image being 10 µL of the total sample, therefore taking a minimum of 100 cells per count). Analytical settings, such as cell size in suspension and declustering degree, for each cell type were optimized within the lab in collaboration with Dr Kate Lawrence and Mr Longster.

2.5.2 Cell damage

Applying mechanical or chemical stresses on cells can lead to damage or injury which can cause cell death (Carmen et al. 2012; Chisti 2001; Goergen et al. 1993). Cell death can be manifested by the loss of membrane integrity and the subsequent uncontrolled release of cytoplasmic products into the supernatant, by a change in the rate of proliferation or through "cell suicide", expressed by changes in morphology and expression of proteins (referred to as "programmed cell death") prior to loss of membrane integrity.

Cell damage analysis assay by LDH release was used for the majority of the experiments. Cell growth and proliferation and programmed cell death assay (FLICA® assay) were used in specific experiments to gain a more in-depth insight into the effect of processing (see Chapter 3, section 3.3.4).

2.5.2.1 Cell damage analysis by LDH release

LDH is a stable cytosolic enzyme that is released upon cell lysis. LDH was measured using a colourimetric assay (CytoTox-96® Non-Radioactive Cytotoxicity Assay, Promega UK, Southampton, UK) that quantitatively measures LDH released in the supernatant by using a 30 minute coupled enzymatic assay which converts a tetrazolium salt (INT) into a red formazan product. The amount of product formed is proportional to the amount of LDH as seen from the reaction below:

$$\text{NAD}^+ + \text{lactate} \xrightarrow{\text{LDH}} \text{pyruvate} + \text{NADH}$$

$$\text{NADH} + \text{INT} \xrightarrow{\text{Diaphorase}} \text{NAD}^+ + \text{formazan (red)}$$

The assay was carried out as indicated by the protocol provided by manufacturer and detailed below.

Once the retentate was collected from the USD membrane separation device after operation, cells were aliquoted at a range of 10,000 to 20,000 cells per well in 100 µL of CGM into eight wells of a 96-well round-bottom plate (Nalgene Nunc International,

New York, USA). The same was done for the non-sheared control sample and the feed sample (placed on ice at the start of the experiment). A total of 10 µl of lysis solution (9% (v/v) Triton® X-100) was added to four wells for each sample, in order to measure the "total LDH release" (i.e. maximum release from sample). A total of 10 µl of CGM was added to the remaining four wells for each sample to correct for volume, these wells were used to measure the "external LDH release" (i.e. release from non-viable and already lysed cells). The permeate samples that were collected at 5 minute intervals, on ice, were plated in four wells at 50-100 µL per well. CGM was added to correct for the volume difference bringing all wells to a total volume of 110 µl. The plate was then incubated for 45 minutes in a humidified chamber (37°C, 5% CO_2) and subsequently centrifuged at 250 x g for 4 minutes. 50 µl of the supernatants were transferred from all wells to a fresh 96-well flat-bottom enzymatic assay plate (Nalgene Nunc International, New York, USA). The Assay Buffer (contents not disclosed by Promega) was thawed in a waterbath, protected from light and 12 mL was added to a bottle of Substrate Mix (contents not disclosed), referred to as reconstituted Substrate Mix. 50 µl of the reconstituted Substrate Mix was added to each well of the plate. The plate was incubated at 21 ± 1ºC and protected from light for 30 minutes. Lastly, 50 µl of Stop Solution (1 M acetic acid) was added to each well and absorbance was recorded at 490 nm (reference wavelength 690 nm if one needed). Results were read within one hour after the addition of Stop Solution.

The assay was previously optimized for all cell lines producing standard curves for cell numbers varying from 5,000 to 40,000 to assess the linearity range of the assay (refer to Chapter 3, section 3.4 Optimizing lactate dehydrogenase assay). To obtain a reliable

signal the number of cells per well was kept between 10,000 and 20,000. Four intra assay replicates were performed on each single sample obtained from processing and a background control was run for each experiment.

2.5.2.2 Cell growth and proliferation analysis for HCA2 cell line

For in-depth analysis of the growth, proliferation and morphology of cell populations, both processed and control samples were cultured and counted every 24 hours post seeding, for 76 hours.

Cells were processed at $25x10^7$ cells mL^{-1} under low and high disc speeds and Vi-CELL XR™ counts were carried out post-processing. 6 well plates were seeded with $2x10^5$ viable cells per well for each sample (processed and control for both experiments) and incubated for 72 hrs at 37ºC, 5% CO_2.

Cell counts using Vi-Cell XR™, as well as light microscopy imaging of the wells (Eclipse TE2000-U, microscope camera DS-Fi1, Nikon, Japan) were carried out every 24 hours to monitor the attachment, cell number proliferation and morphological changes, if any. Growth curves and rate constants were established and morphological analysis was carried out using an image analysis software (see section 2.5.3 Image processing - morphology).

2.5.2.3 Cell death by apoptosis for HCA2 cell line

Detection of cell death by apoptosis in whole cells can be identified by measuring the activity of caspase. Cell death analysis was conducted using the CaspaTag™ Pan-Caspase In Situ assay kit, Fluorescein (Millipore, Watford, UK) for the HCA2 cell line

only. The assay consists of a membrane-permeant, fluorescent labelled inhibitor of caspase (FLICA®) which bonds covalently to the activated caspase enzymes. FLICA® reagents are cell permeable and non-cytotoxic markers and once they enter the cell, they covalently bind to active caspase (Ekert et al. 1999).

The cell suspensions were processed in the USD membrane separation device (as described in section 2.4.2 Operation of the device) and the processed samples were held for 2 hours post-processing to allow increase of expression of apoptotic markers if any. Cells were then adjusted to $5x10^6$ total cells in 300 µL of hCGM using Vi-CELL XR™ data retrieved for each processed sample. The lyophilized FLICA® reagent supplied was reconstituted with 50 µL of DMSO and mixed until completely dissolved. 7 µL of 30X FLICA® reagent were added to the samples and subsequently flicked to mix. The sample tubes were covered in tin foil to protect them from light and incubated for 1 hour in a 37ºC, 5% CO_2 incubator, gently agitating the tubes twice during the incubation time to resuspend settled cells. The wash buffer, supplied as a 10X concentrate was diluted to create a 1X solution by using deionised water. 2 mL of 1X wash buffer was added to each tube and gently mixed before samples were centrifuged for 5 minutes at 400 x g. The supernatant was removed and cell pellets were loosened from the tube. A further wash step using 1 mL of 1X wash buffer was carried out. The cell samples were finally resuspended in 300 µL of 1X wash buffer and 1.5 µL of propidium iodide (PI) was added to each tube. A wash step was performed using 500 µL of DPBS and spun as previously described. The supernatant was removed and the cells were resuspended in mounting medium (VECTASHIELD® Mounting Media, Vector Laboratories, Peterborough, UK) containing 4',6-diamidino-2-phenylindole

(DAPI). 10 µL of each sample were placed on microscope slides and covered with a cover slip.

An apoptotic control was carried out by adding an inducer of apoptosis to growing HCA2 cells. A stock of 1 mM staurosporine (STA; Sigma-Aldrich, Ayrshire, UK) solution in DMSO stored at -20ºC was diluted in hCGM to create the 10 µM and 20 µM working concentrations. The hCGM was replaced by 5 mL of hCGM with added working STA and incubated for ~ 6 hrs at 37ºC, 5% CO_2. The cells were subsequently harvested using the enzymatic detachment method as previously described (section 2.3.4.1 HCA2 and P4E6 cell lines), immediately prior to application of the staining procedure as described above for the processed samples.

Images were collected using fluorescent microscope (Okolab enclosed microscope camera DS-Fi1, Nikon, Japan). FLICA® emission was measured at 518 nm, PI emission at 620 nm and DAPI emission at 460 nm.

2.5.3 Image processing - morphology

Software for image processing was developed using MATLAB Image Processing Toolbox (MathWorks, Cambridge, UK) by Nicolas Jaccard in the Biochemical Engineering Department at UCL.

Image analysis enables rules to be set to classify cells depending on their morphological characteristics. This can be especially important post-processing when the cells might change morphology due to the exposure to harsh operating conditions (Kretzmer and Schügerl 1991).

The image processing algorithms implemented using the script created by Nicolas Jaccard, operates in three steps. Firstly, it detect the objects on the image; then it corrects and allocates each object detected into a category, using rules based on decision flow chart shown in Figure 2.5; lastly, it outputs the results in an excel file.

Figure 2.6.A shows an example of a raw image as obtained from Vi-CELL XR™ and Figure 2.6.B an output from the script after classifying the cells based on morphology. Counts provided by the image processing algorithms were compared against manual counts to verify the accuracy of the software.

2.5.4 Rheology studies

Rheology studies were carried out using a cup-and-bob rheometer (LVDV-II+, Brookfield, MA, USA). Both the control and the processed samples were exposed to shear rates ranging from 37.5 s^{-1} to 1,500 s^{-1} in seven increments in both increasing and decreasing sweeps. The viscometer was allowed to complete 5 revolutions at each speed before taking a measurement. The temperature was maintained at 21 ± 1°C using a waterbath and a peristaltic recirculation pump. Two spindles were used depending on the apparent viscosity of the sample, CP-40 (cone angle 0.8°C and sample volume 0.5 mL) and CP-42 (cone angle 1.565° and sample volume 1 mL). Both spindles used were calibrated using both water and low viscosity (~5 mPa s) silicone oil standard (RT5, Cannon Instrument Company, PA, USA). The measurement error was found to be less than 4%.

Step 1: Identify dead cells (stain positive for TB). Dead cells are circled in red (○).

Step 2: Identify debris based on the following rules:

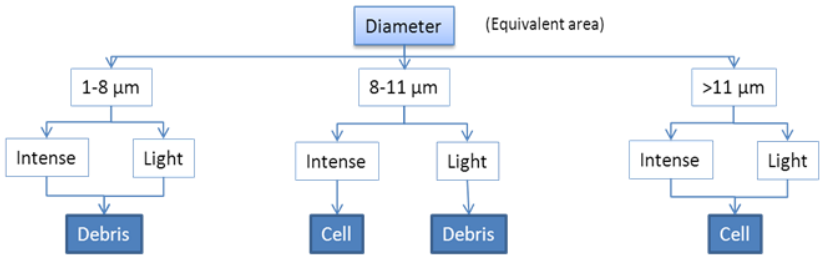

Debris are circled in yellow (○).

Step 3: Take forward only viable cells and distinguish cell type into categories – round, extremely and partially elongated.

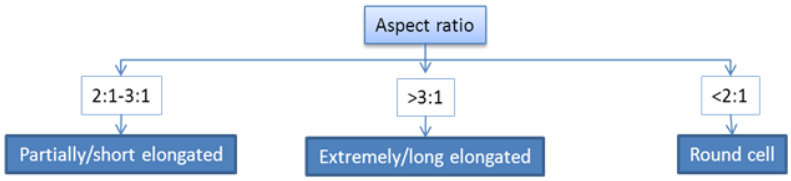

Short elongated are circled in blue (○), long elongated are circled in purple (○) and round viable are circled in green (○).

Figure 2.5: Decision flow chart used by the image processing algorithms implemented using MATLAB Image Processing Toolbox (MathWorks, Cambridge, UK) to categorize cells by morphology.

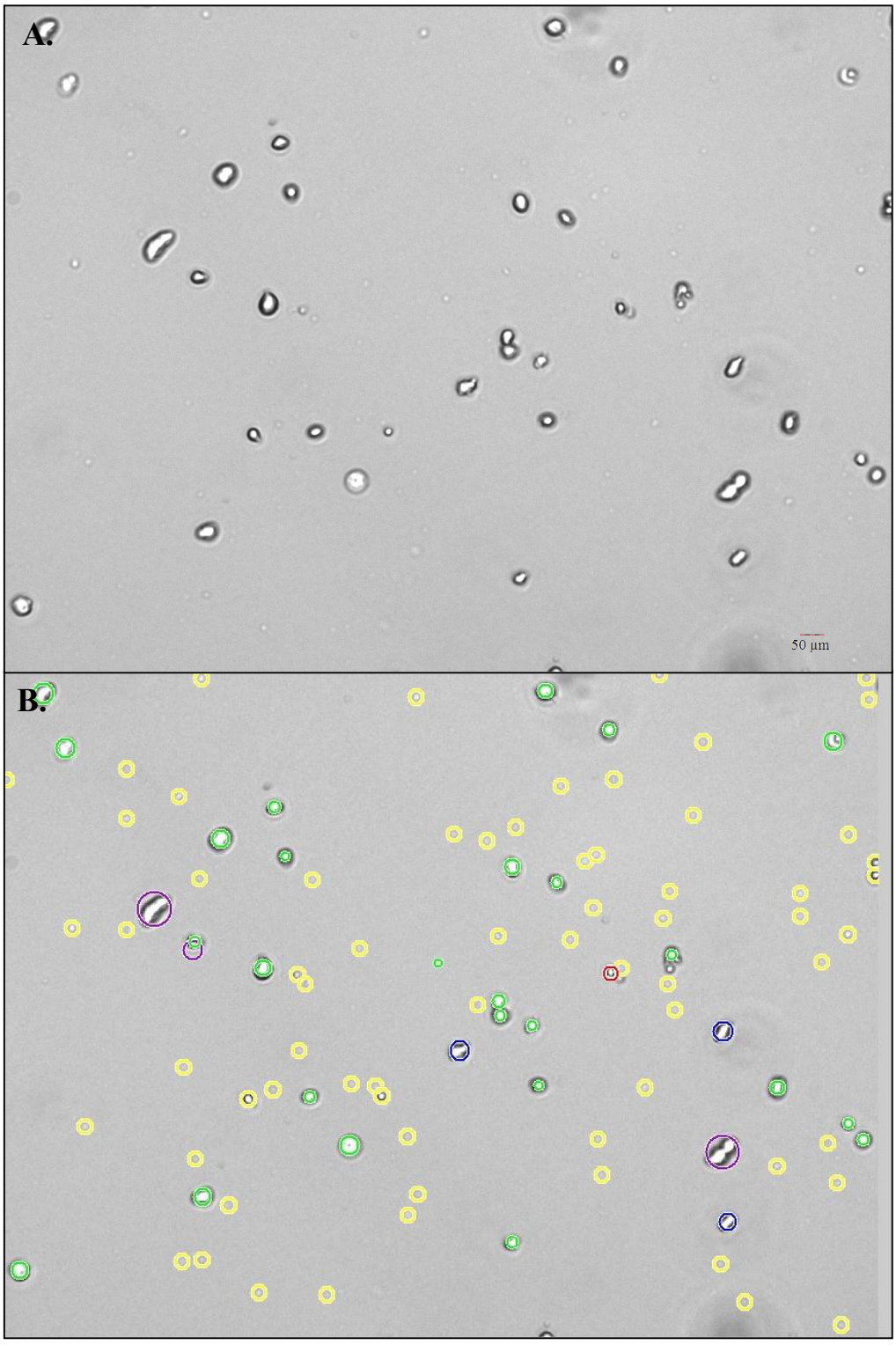

Figure 2.6: Sample image obtained of cellular suspension after processing. (A) ViCell XR™ raw image and (B) script created by Nicolas Jaccard using MATLAB Image Processing Toolbox (MathWorks, Cambridge, UK). See Figure 2.5 for explanation of object identification.

2.6 Transmission of LDH using the HCA2 cell line

Knowledge on transmission was used to develop an understanding of retention of LDH in the USD membrane separation device which was then followed by a confirmation of the observed phenomena with an empirical study of transmission during usage of the membrane and modeling of the retentate during operation. All experiments in this section were carried out using the USD membrane separation device in diafiltration mode, connected to the syringe pump that flushed hCGM for 60 minutes (although some specified shorter times of operations), at a disc speed of 10,000 rpm at a 0.5 mL min^{-1} rate. All of these parameters potentially impact on the transmission of LDH.

2.6.1 Mass balancing of LDH during processing

This section outlines the equations and assumptions used to determine the concentration of soluble LDH present in the retentate of the USD membrane separation device based on measurements of the permeate (output stream) and hence the determination of the total soluble LDH released during processing.

Figure 2.7 shows the block diagram for the experimental set-up. From left to right, a buffer feed, '*F*', is supplied to the USD membrane separation device at a constant flow rate, '*Q*'. The permeate stream, '*P*', exiting the USD membrane separation device ('Block USD device') is pooled over 5-minute intervals, where '*i*' denotes the interval number, '*i*' = 1 to 12. The average concentration of extracellular LDH present in the retentate for any given time interval ('Δt_i') is estimated using:

$$[R]_{LDH_{EXT}}(\Delta t_i) = \frac{[P]_{LDH}(\Delta t_i)}{T(t)} \qquad \text{Equation 2.4}$$

Figure 2.5: Block diagram for the experimental set-up used to derive the amount of soluble LDH present during 'Δt_i'.

where '$T(t)$' is the LDH transmission at time 't' and '$[P]_{LDH}(\Delta t_i)$' is the measured concentration of LDH present in the permeate collected over interval 'Δt_i' and subscript '$_{EXT}$' refers to extracellular component. The transmission measured is at the end of the run, '$t = t_F$':

$$T(t_F) = \frac{[P]_{LDH}(t_F)}{[R]_{LDH\_EXT}(t_F)} \qquad \text{Equation 2.5}$$

where '$[P]_{LDH}(t_F)$' is the concentration of extracellular LDH present in the permeate collected over the period '$t_F - 1\ \text{min}$' to 't_F' and '$[R]_{LDH_{EXT}}(t_F)$' is the measured concentration of extracellular LDH in the retentate. Assuming '$T(t)$' is constant and equal to '$T(t_F)$' throughout the experiment, the average concentration of extracellular LDH present in the retentate for any given time interval is given by:

$$[R]_{LDH_{EXT}}(\Delta t_i) = \frac{[P]_{LDH}(\Delta t_i)}{T(t_F)} \qquad \text{Equation 2.6}$$

The total amount, 'A', of extracellular LDH present in the system given in Figure 2.7 after any interval 'Δt_i' is:

$$\therefore A_{LDH_{EXT}}(\Delta t_i) = V_R \times [R]_{LDH_{EXT}}(\Delta t_i) + \sum_{i=1}^{i} Q \times \Delta t_i \times [P]_{LDH}(\Delta t_i) \qquad \text{Equation 2.7}$$

or from Eq 2.6:

$$A_{LDH_{EXT}}(\Delta t_i) = V_R \times \frac{[P]_{LDH}(\Delta t_i)}{T(t_F)} + \sum_{i=1}^{i} Q \times \Delta t_i \times [P]_{LDH}(\Delta t_i) \qquad \text{Equation 2.8}$$

where 'V_R' is the volume of retentate (fixed). Lastly, the amount of intracellular LDH present in the retentate after any given time interval 'Δt_i', is given by:

$$R_{LDH_{INT}}(\Delta t_i) = V_R \times [R]_{LDH_{INT}}(0) - A_{LDH_{EXT}}(\Delta t_i) \qquad \text{Equation 2.9}$$

where '$[R]_{LDH_{INT}}(0)$' is the concentration of LDH present in the intact cells in the retentate at '$t = 0$' (and is given by '$[R]_{LDH_{INT}}(0) = [R]_{LDH_{TOT}}(0) - [R]_{LDH_{EXT}}(0)$').

All of the membrane studies to test the effect of disc speed, cell concentration and cell ageing were carried out over a period 't_F' = 60 min. To test the assumption that '$T(t)$' is constant and equal to '$T(t_F = 60)$' (i.e. the membrane is not changing its transmission characteristics) experiments were carried out for varying values of 't_F' and '$T(t_F)$' recorded in each case.

The raw data for these experiments are given in Table B and Figure 2.8. An average transmission coefficient of 0.80 was recorded for 't_F' values ranging from 15 to 60 min with no significant trend noted with varying 't_F'.

Lastly, Figure 2.9 shows the transmission coefficients obtained during the last minute of a 60 min operation for varying concentrations of intact cells fed into the USD membrane separation device as measured by trypan blue exclusion and analyzed by ViCell XR™. Three repeats were carried out at 6 different concentrations of intact cells fed. Figure 2.9 shows an average of the three repeats at each concentration, showing by the use of x-errors bars, the range of concentrations of intact cells fed that each averaged point covers. It appears that after the first two low concentration points which lie around transmission coefficient of 0.80, a plateau at around 0.87 transmission coefficient seems to occur when going to higher concentrations of intact cells fed.

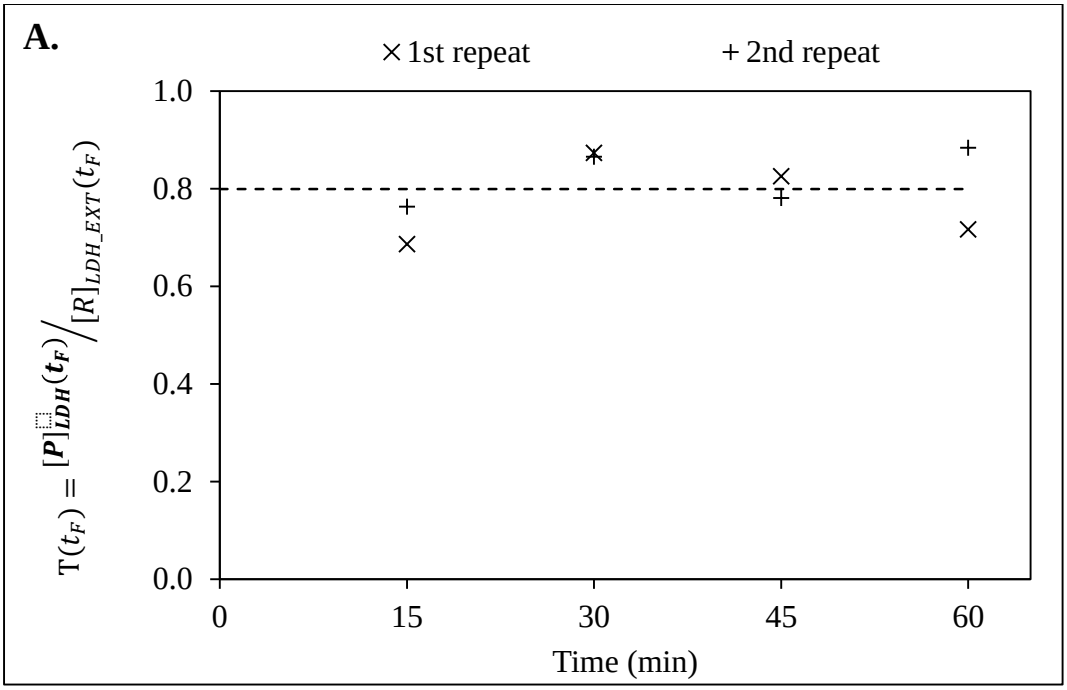

B.

	't' (min)	**'$[P]_{LDH}(t_F)$'** µU mL^{-1}	**'$[R]_{LDH_{EXT}}(t_F)$'** µU mL^{-1}	**'$T(t_F)$'**
1st repeat (×)	15	0.38 ± 0.03	0.56 ± 0.03	0.69
	30	0.30 ± 0.01	0.34 ± 0.01	0.87
	45	0.33 ± 0.06	0.39 ± 0.08	0.83
	60	0.60 ± 0.01	0.84 ± 0.06	0.72
2nd repeat (+)	15	0.26 ± 0.02	0.34 ±0.14	0.76
	30	0.35 ± 0.07	0.41 ± 0.02	0.87
	45	0.44 ± 0.09	0.56 ± 0.02	0.78
	60	0.74 ± 0.01	0.84 ± 0.02	0.88

Figure 2.6: Effect of processing time, 't_F', on the measured transmission of LDH. Two repeats of four experiments carried out for set times, 't_F' showing (A) transmission coefficient ('$T(t_F)$') as a function of 't_F'. Dashed line is for mean of '$T(t_F = 60)$' values. Table (B) shows the raw data (n = 2) for each of the four separate experiments and both repeats which were carried out under the same operating conditions with two separately prepared cell suspensions ('Q'= 0.5 mL min^{-1}, 'V_R'= 1.7 mL, 'N'= 10,000 rpm, '$[R]_{TB\_TOT}(0)$'= 2.0×10^6 cells mL^{-1}).

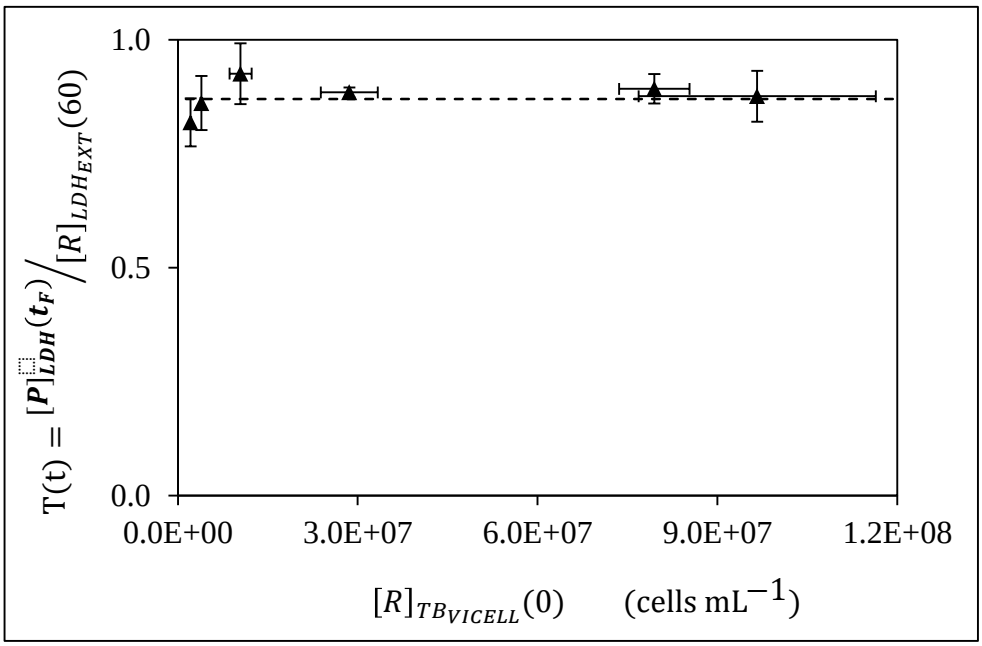

Figure 2.7: Transmission coefficient ('$T(60)$') based on the last minute of '$[P]_{LDH}(t_F')$' over the '$[R]_{LDH_{EXT}}(60)$' for HCA2 cell line with varying numbers of intact cells fed mL^{-1} into the USD membrane separation device. Dashed line shows an average of 0.87 which appears to be independent of intact cells fed concentration ('$[R]_{TB_{VICELL}}(0)$'). Error bars show ± 1 s.d. (n = 3).

Chapter 3. The impact of processing on loss of intact cells

3.1 Introduction

With cell-based therapies, careful bioprocessing of cell populations is of the utmost importance because the cells are the product (Mason and Hoare 2006). It is therefore important to ensure that cell homeostasis is not disrupted and this can be achieved by, for example, preventing increases in necrotic or apoptotic populations, avoiding changes in morphology (Fernandez-Pol 1978) or changes in growth, metabolism or surface proteins (Lee et al. 2009). However, different cell lines have different characteristics, different resistances to shear forces (Acosta-Martinez et al. 2010) and varying mechanical strengths (Stamenovic 2008) making bioprocessing complex and cell line specific.

In addition, current processing techniques suffer from drawbacks when applied to cell manufacturing. For example, most cell-based therapies to date use batch centrifugation for washing, buffer exchange and concentration of the cellular suspension. However, centrifugation has proven to be a difficult step to operate while maintaining sterility (Mason and Hoare 2006). With the current processing set-up, processing large volumes of cells require multiple rounds of centrifugation with several operators, becoming not only operator dependent but very time consuming (Pattasseril et al. 2013). Therefore if these therapies are to be commercialized at an industrial scale, the processing bottlenecks will shift to the downstream steps and will need to be addressed (Pattasseril et al. 2013; Rowley et al. 2012b). The industry faces major challenges according to Pattasseril et al. (2013). One of these challenges is to have the capacity downstream to manufacture and process large volumes of cells in suspension (100 to 1,000 litres)

whilst achieving high cell concentration and high percentage viability within acceptable limits. Current potential alternatives to batch centrifugation include continuous flow centrifugation systems such as kSep from KBI Biopharma or tangential flow filtration (TFF) units such as Uniflex from GE Healthcare. These can potentially allow for more contained and less labour-intensive processing than is achieved using batch centrifugation (Pattasseril et al. 2013).

TFF has been studied for many years. However, due to the complexity of this processing step, to translate findings from large-scale clarification of mammalian cell cultures (Roach et al. 2008) to the production of cells for therapy, a number of operating parameters will need to be optimized. Ultra scale-down (USD) tools might offer a cost-effective solution for the need to study large numbers of operating variables. USD devices allow for the investigation of several manufacturing hydrodynamic environments (McCoy et al. 2009; McCoy et al. 2010; McQueen et al. 1987; Zoro et al. 2009) and geometries (Acosta-Martinez et al. 2010) using relatively small amounts of process material. In this way, the throughput of the experimental phase is significantly increased in an efficient manner making USD tools suitable for rapid screening of manufacturing processes and identifying potential areas of damage. The USD membrane separation device in particular allows for the investigation of the effect of altering independently parameters such as shear rate and flux rate.

This chapter investigates the use of the USD membrane separation device to create and populate a design space by identifying bioprocessing conditions associated with the wash and buffer exchange steps within the filtration process. Mapping relevant

operating conditions such as shear rate (disc speed), cell ageing and cell concentration (and hence also viscosity) will help identify the sources of stress and resulting product quality loss. It is important to bear in mind that the USD membrane separation device is not a direct mimic of a full-scale TFF system, but rather facilitates the assessment of the impact of processing at full-scale using scalable parameters.

All experiments presented in this chapter were carried out using the diafiltration set-up, with hCGM being pumped into the system for 60 minutes at a flow rate of 0.5 mL min^{-1} (≈ 82 LMH). The disc speed was set to either 6,000 rpm ('γ' = 44,000 s^{-1}) or 10,000 rpm ('γ' = 116,000 s^{-1}) and the concentration of the feed material was ~2x10^6 cells mL^{-1}. The cells that are referred to as "fresh" cells, essentially had zero hours hold prior to processing. Future changes will address different cell concentrations and ages.

3.2 Calculations

Due to the need to collect material for analysis over a period of 'Δt', it is necessary to record performance as an average over a particular time interval, 'Δt_i'. One method of characterizing the effect of any operating condition is to monitor the proportion, 'ω', of intracellular LDH remaining versus time:

$$\omega(\Delta t_i) = \frac{R_{LDH_{INT}}(\Delta t_i)}{R_{LDH_{INT}}(0)} \qquad \text{Equation 3.1}$$

where '$R_{LDH_{INT}}(\Delta t_i)$' is a caclulated average amount of intracellular LDH (that of intact cells) remaining in the retentate in the USD membrane separation device over the interval 'Δt_i' and '$R_{LDH_{INT}}(0)$' is the calculated amount of intracellular LDH present in

the USD membrane separation device at the start of the experiment (i.e. in the retentate at '$t = 0$'):

$$R_{LDH_{INT}}(0) = R_{LDH_{TOT}}(0) - R_{LDH_{EXT}}(0) \qquad \text{Equation 3.2}$$

where '$R_{LDH_{TOT}}(0)$' and '$R_{LDH_{EXT}}(0)$' are the measured total and external amounts of LDH present in the USD membrane separation device at the start of the experiment, at '$t = 0$ min'.

The following relationships depend on the assumption that the total amount of LDH is the system (retentate and permeate) remains constant throughout the duration of the membrane shear study. For any particular interval, 'Δt_i', '$R_{LDH_{INT}}(\Delta t_i)$' is given by:

$$R_{LDH_{INT}}(\Delta t_i) = R_{LDH_{INT}}(0) - (\sum_{i=1}^{i} P_{LDH}(\Delta t_i) + R_{LDH_{EXT}}(\Delta t_i)) \qquad \text{Equation 3.3}$$

where '$\sum_{i=1}^{i} P_{LDH}(\Delta t_i)$' is the sum of the amounts of LDH recorded in the permeate stream collected from the start of the experiment to the end of interval 'Δt_i' and '$R_{LDH_{EXT}}(\Delta t_i)$' is the calculated average amount of extracellular LDH present in the retentate during interval 'Δt_i'.

The concentration '$[R]_{LDH\_EXT}(\Delta t_i)$' is given by:

$$[R]_{LDH_{EXT}}(\Delta t_i) = \frac{[P]_{LDH}(\Delta t_i)}{T(t_F)} \qquad \text{Equation 3.4}$$

where '$[P]_{LDH}(\Delta t_i)$' is the concentration of extracellular LDH measured in the permeate collected over interval 'Δt_i' and '$T(t_F)$' is the transmission of LDH as measured from the retentate and permeate concentrations of LDH at the end of the

experiment. Therefore the average amount of extracellular LDH present in the retentate over interval 'Δt_i' is given by:

$$R_{LDH_{EXT}}(\Delta t_i) = \frac{[P]_{LDH}(\Delta t_i)}{T(t_F)} \times V_P \qquad \text{Equation 3.5}$$

where 'V_P' is the permeate volume over interval 'Δt_i' (equal to '$Q \times \Delta t_i$'). Hence from equation 3.3 and 3.5:

$$R_{LDH_{INT}}(\Delta t_i) = R_{LDH_{INT}}(0) - \sum_{i=1}^{i} P_{LDH}(\Delta t_i) - \left(\frac{[P]_{LDH}(\Delta t_i)}{T(t_F)} \times V_P\right) \qquad \text{Equation 3.6}$$

Using values measured experimentally, equation 3.6 becomes:

$$R_{LDH_{INT}}(\Delta t_i) = [R]_{LDH_{INT}}(0) \times V_R - \sum_{i=1}^{i}([P]_{LDH}(\Delta t_i) \times Q \times \Delta t_i) - \left(\frac{V_P \times [P]_{LDH}(\Delta t_i)}{T(t_F)}\right)$$

Equation 3.7

where 'V_R' is the volume of the retentate, hence:

$$\omega(\Delta t_i) = \frac{[R]_{LDH_{INT}}(0) \times V_R - \sum_{i=1}^{i}([P]_{LDH}(\Delta t_i) \times Q \times \Delta t_i) - \left(\frac{V_P \times [P]_{LDH}(\Delta t_i)}{T(t_F)}\right)}{[R]_{LDH_{INT}}(0) \times V_R} \qquad \text{Equation 3.8}$$

This parameter is calculated at 5-minute intervals using the LDH readings from the permeate. Therefore the decrease of intracellular amount of LDH in the USD membrane separation device as a proportion of the initial amount of intracellular LDH can be investigated over time.

3.3 Effect of disc speed (shear rate) on HCA2 fibroblasts

The effect of low and high disc speeds 6,000 and 10,000 rpm (or shear rates of 44,000 and 116,000 s^{-1} respectively) on cell damage on the HCA2 cell line was assessed by the

release of LDH, by evaluation of cell membrane integrity (trypan blue exclusion) and by generation of post-processing growth curves and measurement of apoptotic markers.

3.3.1 Physical impact as measured by LDH release

Five repeats at each of the two disc speeds using freshly harvested cells each time were carried out on different occasions. The raw data and calculations for an example run at high disc speed will be used to demonstrate how the figures and tables for the LDH data for each repeat were generated. For all other runs the raw data is included in Appendix A.1.

The LDH data for the first study at high disc speed is given in Tables 3.1, 3.2 and 3.3. Table 3.1.A gives the average concentration and amount of extracellular LDH in the permeate collected over 5-minute intervals and over the final minute of operation ('t_F'). The amount is based on the concentration measured and the volume collected. The concentration of total and extracellular LDH was measured for each of (a) the retentate pre-processing (i.e. starting point, '$[R](0)$'), (b) control (i.e. non-sheared sample, '$[C](60)$') held at 21 ± 1ºC in a centrifuge tube concurrently for the duration of the experiment and (c) retentate post-processing (i.e. end point, '$[R](60)$') samples and the results are given in Table 3.1.B.

The amounts of total, extracellular and intracellular LDH for each of (a) the retentate pre-processing ('$R(0)$'), (b) control ('$C(60)$') and (c) retentate post-processing ('$R(60)$') samples were evaluated using the measured concentrations and are given in Table 3.2.A along with (d) the total LDH measured in the permeate (from Table 3.1.A).

A.

Time 'Δt_i' (min)	'$[P]_{LDH}(\Delta t_i)$' (μU mL^{-1}; n = 4)	$P_{LDH}(\Delta t_i) = [P]_{LDH}(\Delta t_i) \times Q \times \Delta t_i$' (μU)
0	0	0
0-5	0.76 ± 0.037	1.91 ± 0.092
5-10	0.52 ± 0.061	1.29 ± 0.153
10-15	0.33 ± 0.024	0.82 ± 0.061
15-20	0.11 ± 0.023	0.27 ± 0.058
20-25	0.10 ± 0.015	0.26 ± 0.038
25-30	0.07 ± 0.025	0.17 ± 0.062
30-35	0.20 ± 0.012	0.50 ± 0.031
35-40	0.09 ± 0.012	0.22 ± 0.030
40-45	0.04 ± 0.007	0.09 ± 0.017
45-50	0.12 ± 0.027	0.31 ± 0.067
50-55	0.26 ± 0.004	0.64 ± 0.011
55-59	0.23 ± 0.026	0.47 ± 0.052
59-60	0.26 ± 0.008	0.13 ± 0.004
'$\sum_{i=1}^{i} P_{LDH}(\Delta t_i)$'		7.08 ± 0.230

B.

	[LDH] μU mL^{-1} ± 1 s.d. (n = 4)		
	Disc speed	10,000 rpm	
Process stream	**Notation**	**Total ('LDH_TOT')**	**Extracellular ('LDH_EXT')**
Pre-processing	'$[R](0)$'	14.18 ± 0.93	0.65 ± 0.18
Control	'$[C](60)$'	14.68 ± 0.32	1.01 ± 0.15
Post-processing	'$[R](60)$'	9.39 ± 0.24	0.32 ± 0.09

Table 3.1: Tables (A) and (B) show the raw LDH data for the first study at high disc speed ('*N*' = 10,000 rpm, '*Q*' = 0.5 mL min^{-1}, 'V_R' = 1.7 mL, '$[R]_{TB_{TOT}}(0)$' = 2.05×10^6 cells mL^{-1}). Values reported to 2 decimal places (n = 4).

A.

		LDH µU ± 1 s.d. (n = 4)		
	Disc speed	**10,000 rpm**		
Process stream	**Notation**	**Total (‘LDH_TOT’)**	**Extracellular (‘LDH_EXT’)**	**Predicted internal (‘LDH_INT’)**
Pre-processing	(a) ‘$R(0) = [R](0) \times V_R$’	**24.10 ± 1.58**	1.11 ± 0.3	22.98 ± 1.61
Control	(b) ‘$C(t_F) = [C](60) \times V_R$’	**24.96 ± 0.55**	1.73 ± 0.26	23.23 ± 0.61
Post-processing	(c) ‘$R(t_F) = [R](60) \times V_R$’	15.97 ± 0.4	0.54 ± 0.16	15.43 ± 0.43
Permeate	(d) ‘$\sum_{i=1}^{i} P_{LDH}(\Delta t_i)$’	7.08 ± 0.12		
Post-processing + Permeate	(c) + (d) ‘$[R](60) \times V_R + \sum_{i=1}^{i}([P]_{LDH}(\Delta t_i) \times Q \times \Delta t_i)$’	**23.05 ± 0.19**	7.62 ± 0.19	15.43 ± 0.43

B.

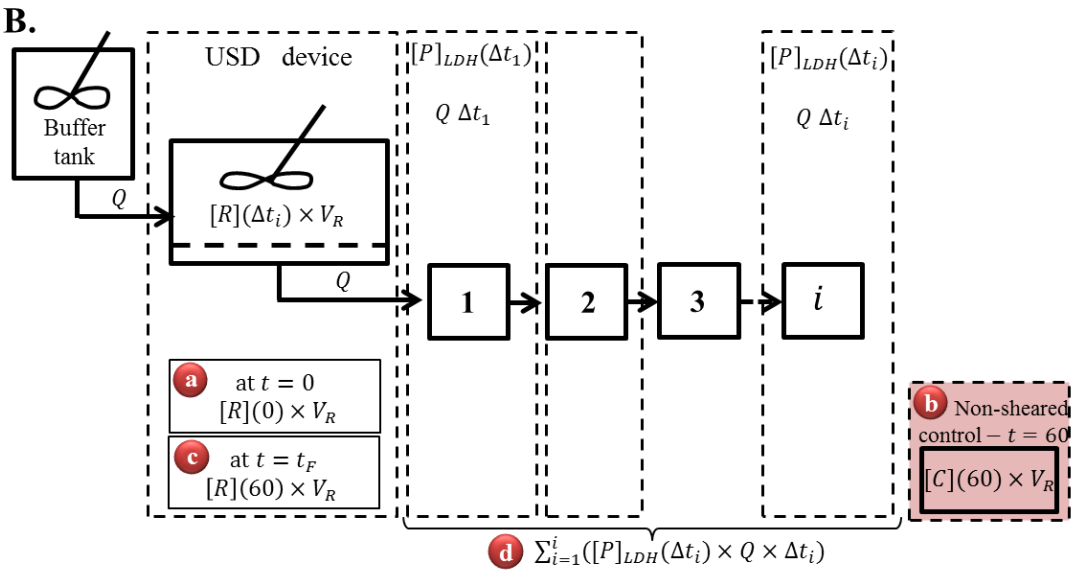

Table 3.2: Table (A) shows the amount of LDH calculated for each stream (‘*N*’ = 10,000 rpm, ‘*Q*’ = 0.5 mL min^{-1}, ‘V_R’ = 1.7 mL, ‘$[R]_{TB_{TOT}}(0)$’ = 2.05×10^6 cells mL^{-1}). Box diagram (B) of the USD membrane separation device showing process streams. Values reported to 2 decimal places (n = 4).

A.

[LDH] μU mL^{-1} ± 1 s.d. (n = 4)	
$[\boldsymbol{P}]_{\boldsymbol{LDH}}(\boldsymbol{t_F})$ **(measured)**	0.26 ± 0.01
$[\boldsymbol{R}]_{\boldsymbol{LDH_{EXT}}}(\boldsymbol{60})$**(measured)**	0.32 ± 0.09
$\boldsymbol{T(t_F) = [P]_{LDH}(60)/[R]_{LDH_{EXT}}(60)}$	0.80

B.

Time '$\Delta \boldsymbol{t_i}$' (min)	'$\boldsymbol{R_{LDH_{EXT}}(\Delta t_i) = \frac{V_R \times [P]_{LDH}(\Delta t_i)}{T(t_F)}}$, **(μU)**	'$\boldsymbol{R_{LDH_{INT}}(\Delta t_i) = R_{LDH_{INT}}(\Delta t_{i-1}) - R_{LDH_{EXT}}(\Delta t_i)}$' **(μU)**	'$\omega(\Delta t_i)$'
0	0.00	22.98	1.00
0-5	1.61	21.37	0.93
5-10	1.09	20.28	0.88
10-15	0.70	19.58	0.85
15-20	0.23	19.35	0.84
20-25	0.22	19.13	0.83
25-30	0.15	18.99	0.83
30-35	0.42	18.57	0.81
35-40	0.19	18.38	0.80
40-45	0.08	18.30	0.80
45-50	0.26	18.04	0.78
50-55	0.54	17.50	0.76
55-60	0.40	17.10	0.74

Table 3.3: Concentrations of soluble LDH measured in the retentate and permeate streams. Table (A) shows the concentration of soluble LDH measured at 't_F' for the retentate and the permeate used to calculate the transmission. Table (B) shows the average amounts of extracellular LDH predicted in the retentate, '$R_{LDH_{EXT}}(\Delta t_i)$', the average amount of intracellular LDH remaining in the retentate, '$R_{LDH_{INT}}(\Delta t_i)$', and the proportion of intracellular LDH remaining, '$\omega(\Delta t_i)$', in the USD membrane separation device over each of the 5-minute intervals. Values rounded to 2 decimal places (n = 4).

The total amount of LDH present after processing in (c) the retentate and (d) the permeate is also given in Table 3.2.A. A box diagram of the USD membrane separation device and process streams is shown in Table 3.2.B and aims to aid the interpretation of the mass balance by outlining the process streams (labelled (a) to (d)). Important information may be acquired from the interpretation of this mass balance and is outlined below.

For example, there is no significant difference in the total LDH present in the retentate pre-processing ('$R_{LDH_{TOT}}(0)$', labelled 'a') and the non-sheared control held for 60 minutes ('$C(60)$', labelled 'b'). This is in agreement with previous studies which have reported LDH in serum to be stable for at least three days at room temperature (Berger and Tietz 1976) and confirms that there should not be any loss of LDH activity by merely holding the sample without processing.

Moreover, there is good agreement in the amount of total LDH in the retentate stream pre-processing ('$R_{LDH_{TOT}}(0)$', labelled 'a' in the diagram) and that after processing by the sum of the two output process streams; retentate post-processing ('$R_{LDH_{TOT}}(60)$', labelled 'c') and permeate ('$\sum_{i=1}^{i} P_{LDH}(\Delta t_i)$', labelled 'd'). Therefore, all of the LDH mass is accounted for.

Using the data in Tables 3.1.A and 3.1.B, '$T(t_F)$', '$R_{LDH_{INT}}(\Delta t_i)$' and '$\omega(\Delta t_i)$' values were calculated and are given in Tables 3.3.A and 3.3.B. Table 3.3.A shows the concentration of extracellular LDH present in the permeate collected over the last minute of processing, ' $[P]_{LDH}(t_F)$ ' obtained from Table 3.1.A, to be

0.26 ± 0.002 μU mL^{-1}. This value is in agreement with the concentrations of LDH measured in the permeate stream during the last 10 minutes of operation, which vary from 0.23 to 0.26 μU mL^{-1}. Moreover, the standard error for the concentration of extracellular LDH in the retentate post-processing ('$[R]_{LDH_{EXT}}(60)$' = 0.32 ± 0.09 μU mL^{-1}, Table 3.2.A) gives confidence of the accuracy of this value as an estimate of the population mean. The transmission coefficient is heavily depends on both '$[P]_{LDH}(t_F)$' and '$[R]_{LDH_{EXT}}(60)$' so the above considerations are relevant to gain confidence on the value for the transmission coefficient. The value obtained which will be used to model the entire run, also shown in Table 3.3.A, is 0.80 ± 0.04. As will be discussed later, this value is in agreement with the those obtained for the four remaining runs.

The impact of disc speed on retention of intact cells as measured by remaining intracellular LDH is shown by plots of '$\omega(\Delta t_i)$' with time in Figure 3.1 (where the information given in Table 3.3.B is shown in Figure 3.1.C).

Each plot in Figure 3.1 shows both low and high disc speeds. Each of the four trends shown in Figures 3.1.A and 3.1.B are for a different cell harvest. For each of Figures 3.1.C, 3.1.D and 3.1.E the trends shown for the two disc speeds are from the same cell harvest. As will be seen, even though there is variability at high disc speed, all repeats fall within one standard deviation. However, this was not the case at low disc speed, where Figure 3.1.B is evidently an outlier. Analyzing the raw data (Appendix A1) for this particular repeat, it was seen that the measured amounts of LDH in the permeate stream were unusually high compared to the other repeats. The amount of LDH

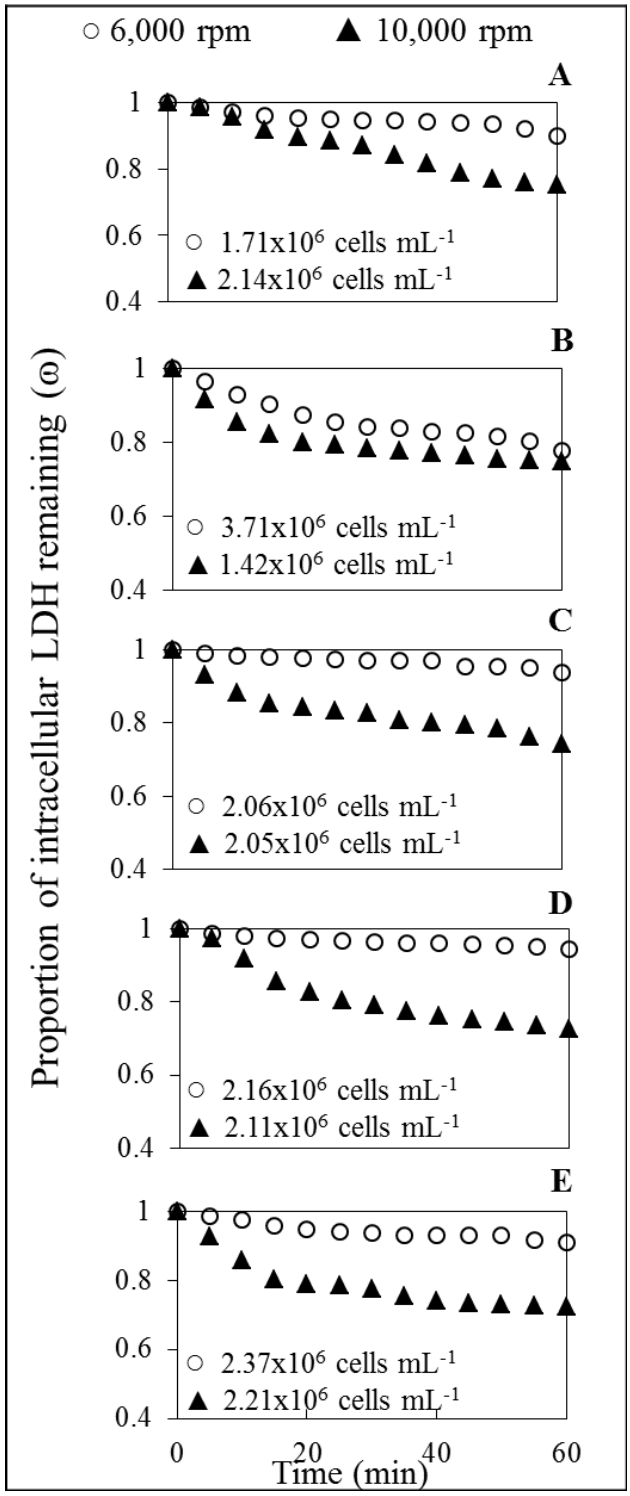

Figure 3.1: Membrane processing of feed (0 hour cell ageing) HCA2 cells – effect on cell damage as measured by LDH at low (○) and high (▲) disc speeds of 6,000 and 10,000 rpm ('γ' = 44,000 s^{-1} and 116,000 s^{-1} respectively). Figures (A) to (E) are five repeats of the same conditions. Data shown in Table 3.3.B is plotted in figure 3.1.C (n = 4).

collected in the permeate at low disc for the second repeat was 6.56 µU whereas the average of the remaining four repeats was 1.32 ± 0.25 µU. This is due to the higher concentration of total cells measured at the start of the experiment ($3.71x10^6$ cells mL^{-1} as measured by trypan blue exclusion) compared to an average of ~$2.0x10^6$ total cells mL^{-1} for the remaining runs. Therefore, Figure 3.1.B ('*N*' = 6,000 rpm only) was set aside for separate analysis (see Chapter 5) from all other runs presented in Figure 3.1.

Tables 3.4.A and 3.4.B summarize some of the key performance data for the two sets of runs for low and high disc speeds respectively. Column 2 presents the measured transmission of LDH through the membrane at the end of each of the 60 minute shear runs. These are the transmission values that are used for calculations. The mean value for LDH transmission is significantly lower at the low disc speed (0.78 ± 0.02 compared with 0.88 ± 0.04) probably due to the lower shear rate over the membrane surface.

Column 3 examines the stability of LDH over the period of the membrane study for each run. On average for both cases, the cells might be considered stable for the length of the run. Even though run B, low disc speed (Table 3.4.A), showed several anomalies, it was decided to retain the results and assess later how best these are interpreted.

Column 4 examines the total amount of LDH (extracellular and intracellular) measured - i.e. permeate plus retentate – and it is compared with total LDH at the start of the experiment. This helps to check whether all LDH is recovered (none is stuck to membrane) and none is lost through denaturation. For both low and high disc speed there is a small, but not statistically significant, loss of ~4-7% of LDH which might be trapped in the membrane or may fall within experimental error.

Column 5 is a second measure of accountability for LDH, comparing the total in the retentate and permeate to the control cells for the duration of the experiment. Again for high disc speed there is a small, but not statistically significant, loss of ~5% of LDH. For low disc speed, due the outlier Run B, the loss would be ~13% but excluding this outlier there is a ~9% loss which was not found to be statistically significant.

Overall, it can be seen from Tables 3.4.A and 3.4.B that the averages are representative of the runs. The average values of the repeats were used to produce Figure 3.2 to analyze the impact of low and high disc speed on cell damage as measured by LDH release. Overall, observing the LDH results in Figure 3.2.A, the proportion of intracellular LDH remaining in the USD membrane separation device throughout operation decreased ~8% at a low disc speed and ~30% at a high disc speed. This finding suggests that increasing the speed of the disc, causes more damage to the cellular population being processed.

From Figure 3.2, Tables B and C, show the amount of total, external and internal LDH in each of the process streams for both low and high disc speeds. Mass balances for both disc speeds show that the amount of total LDH in the non-sheared controls held at 21 ± 1^{o}C in a centrifuge tube concurrently for the duration of the experiment did not decrease. This leads to the conclusion that the changes seen at the two disc speeds can be fully attributed to processing conditions. Moreover, for both disc speeds (ignoring Run B at low disc speed) there is a small (~5%) and insignificant decrease in the total mass of LDH collected in the permeate plus the total amount collected in the retentate post-processing compared to pre-processing as was shown from Tables 3.4.A and 3.4.B.

A.	**6,000 rpm ± 1 s.e. (j = 5; n = 4)**			
1. **Run ('j')**	**2.** **'$T(t_F)$'**	**3.** **'b/a'**	**4.** **'$(c+d)/a$'**	**5.** **'$(c+d)/b$'**
A	0.82 ± 0.07	1.08 ± 0.03	1.00 ± 0.02	0.88 ± 0.02
B	*0.75 ± 0.06*	*1.69 ± 0.08*	*1.14 ± 0.05*	*0.69 ± 0.01*
C	0.84 ± 0.04	0.98 ± 0.04	0.82 ± 0.03	0.85 ± 0.03
D	0.73 ± 0.07	1.04 ± 0.04	1.01 ± 0.02	0.98 ± 0.02
E	0.74 ± 0.09	0.92 ± 0.09	0.87 ± 0.07	0.95 ± 0.05
Average	**0.78 ± 0.02**	**1.01 ± 0.14**	**0.93 ± 0.06**	**0.91 ± 0.05**

B.	**10,000 rpm ± 1 s.e. (j = 5; n = 4)**			
A	0.88 ± 0.08	1.11 ± 0.05	1.03 ± 0.04	0.93 ± 0.04
B	0.91 ± 0.04	0.82 ± 0.01	0.81 ± 0.01	1.00 ± 0.02
C	0.80 ± 0.04	1.01 ± 0.08	0.96 ± 0.06	0.92 ± 0.02
D	0.78 ± 0.06	1.17 ± 0.12	0.95 ± 0.09	0.78 ± 0.02
E	1.02 ± 0.06	0.96 ± 0.03	1.06 ± 0.04	1.10 ± 0.02
Average	**0.88 ± 0.04**	**1.01 ± 0.06**	**0.96 ± 0.04**	**0.95 ± 0.05**

C.

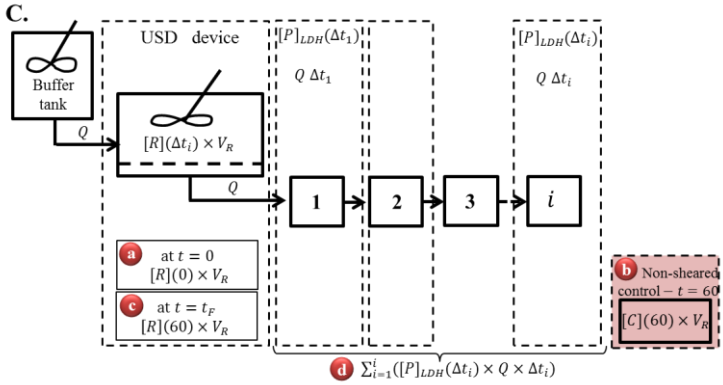

Table 3.4: Membrane processing of feed (0 hour cell ageing) HCA2 cells – effect of disc speed on cell damage. (A) 6,000 and (B) 10,000 rpm cell damage as recorded by release of LDH. From left to right columns show; (1) run; (2) transmission coefficient; (3) ratio of intracellular LDH in the control to the intracellular LDH pre-processing in the retentate to evaluate stability of LDH in the cells without processing (where 1 equals to no loss in LDH activity); (4) ratio of the sum of the total LDH in the retentate post-processing and permeate streams to the total LDH in the retentate pre-processing, to evaluate the mass balance agreement (where 1 equals to complete agreement, i.e. all LDH mass is accounted for); (5) ratio of the sum of the total LDH in the retentate post-processing and permeate streams to the total LDH in the control, to evaluate the mass balance agreement assuming the processed cells change as with control. Run B for 6,000 rpm, shown in red in table A, was considered as an outlier due to an unusually high initial cell concentration with respect to the other runs.

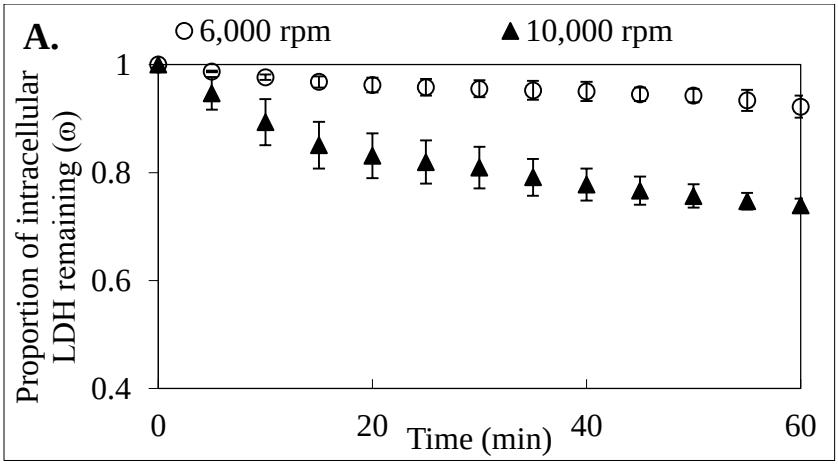

B.

	LDH µU ± 1 s.e. (j = 5; n = 4)			
	Disc speed	**6,000 rpm**		
Sample	**Notation**	**Total ('LDH_TOT')**	**Extracellular ('LDH_EXT')**	**Predicted internal ('LDH_INT')**
Pre-processing	(a) '$R(0) = [R](0) \times V_R$'	**23.92 ± 2.96**	0.76 ± 0.11	23.16 ± 2.89
Control	(b) '$C(60) = [C](60) \times V_R$'	**23.91 ± 2.50**	0.79 ± 0.21	23.12 ± 2.70
Post-processing	(c) '$R(60) = [R](60) \times V_R$'	20.03 ± 2.94	0.41 ± 0.09	19.62 ± 2.93
Permeate	(d) '$\sum_{i=1}^{i} P_{LDH}(\Delta t_i)$'	2.02 ± 0.27		
Post-processing + Permeate	(c) + (d) '$[R](60) \times V_R + \sum_{i=1}^{i}([P]_{LDH}(\Delta t_i) \times Q \times \Delta t_i)$'	**22.05 ± 2.95**	2.43 ± 0.35	19.62 ± 2.93

C.

	Disc speed	**10,000 rpm**		
Sample	**Notation**	**Total ('LDH_TOT')**	**Extracellular ('LDH_EXT')**	**Predicted Internal ('LDH_INT')**
Pre-processing	(a) '$R(0) = [R](0) \times V_R$'	**25.09 ± 0.91**	0.73 ± 0.14	24.36 ± 1.03
Control	(b) '$C(60) = [C](60) \times V_R$'	**25.73 ± 1.78**	1.06 ± 0.33	24.68 ± 1.75
Post-processing	(c) '$R(60) = [R](60) \times V_R$'	15.70 ± 1.08	0.62 ± 0.23	15.08 ± 1.05
Permeate	(d) '$\sum_{i=1}^{i} P_{LDH}(\Delta t_i)$'	8.37 ± 0.49		
Post-processing + Permeate	(c) + (d) '$[R](60) \times V_R + \sum_{i=1}^{i}([P]_{LDH}(\Delta t_i) \times Q \times \Delta t_i)$'	**24.07 ± 1.17**	8.99 ± 0.65	15.08 ± 1.05

Figure 3.2: Membrane processing of feed (0 hour cell ageing) HCA2 cells – effect of disc speed on cell damage. Recorded by (A) release of LDH. Tables (B) and (C) show mean LDH data for all streams including both external and total measurements at 6,000 and 10,000 rpm ('γ' = 44,000 and 116,000 s^{-1} respectively). A non-sheared control held in a centrifuge tube concurrently, 21 ± 1ºC, for the duration of the experiment was used to measure LDH pre and post-processing. Figure (A) shows the proportion of intracellular LDH remaining ('ω', Eq 3.8), for 6,000 rpm (○) and 10,000 rpm (▲) at a concentration of 2.1×10^6 total cells mL^{-1}. High disc speed resulted in a ~30% reduction of viable cells as measured by release of LDH. Data shown are mean values ± 1 s.e. (j = 5; n = 4).

3.3.2 Physical impact as measured by trypan blue exclusion

Plots in Figure 3.3 show the trypan blue data for the five repeats at both disc speeds, with the concentration of total and viable cells on the left-hand side (column A) and the percentage viability on the right-hand side (column B). The average values for concentrations and percentage viabilities for all repeats were calculated. Values that fall outside one standard deviation from the mean were evaluated and if considered to be outliers these were not used to produce the plots in Figures 3.4 and 3.5. For example, it is evident that the second repeat at low disc speed plotted in Figure 3.3.A.2, is an outlier since the concentration is considerably higher, almost double, than for all other repeats (note the y-axis in Figure 3.3.A.2 is the only one that shows 0 to 6 x 10^6 cells mL^{-1} compared to 0 to 3 x 10^6 cells mL^{-1} for all other repeats). This may explain the unusually high amount of LDH previously measured in the permeate and shown in Figure 3.1.B, reinforcing the experiment can indeed be considered an outlier. Even though this repeat will be excluded for the analysis of the effect of low disc speed on cell damage investigated in this section, it will be taken into consideration when examining the effect of cell concentration on cell damage.

The plots shown in Figures 3.4 and 3.5 were used to analyze the impact of low and a high disc speed on cell damage as measured by trypan blue exclusion. From the results in Figure 3.4, it appears that at a high disc speed there is a significant ~25% ($p = 0.003$) decrease in the population of viable cells compared to no decrease at a low disc speed. Analysis of Figure 3.5 shows that a high disc speed resulted in a significant ~10% ($p = 0.001$) drop in percentage viability post-processing compared to no drop in percentage viability at a low disc speed.

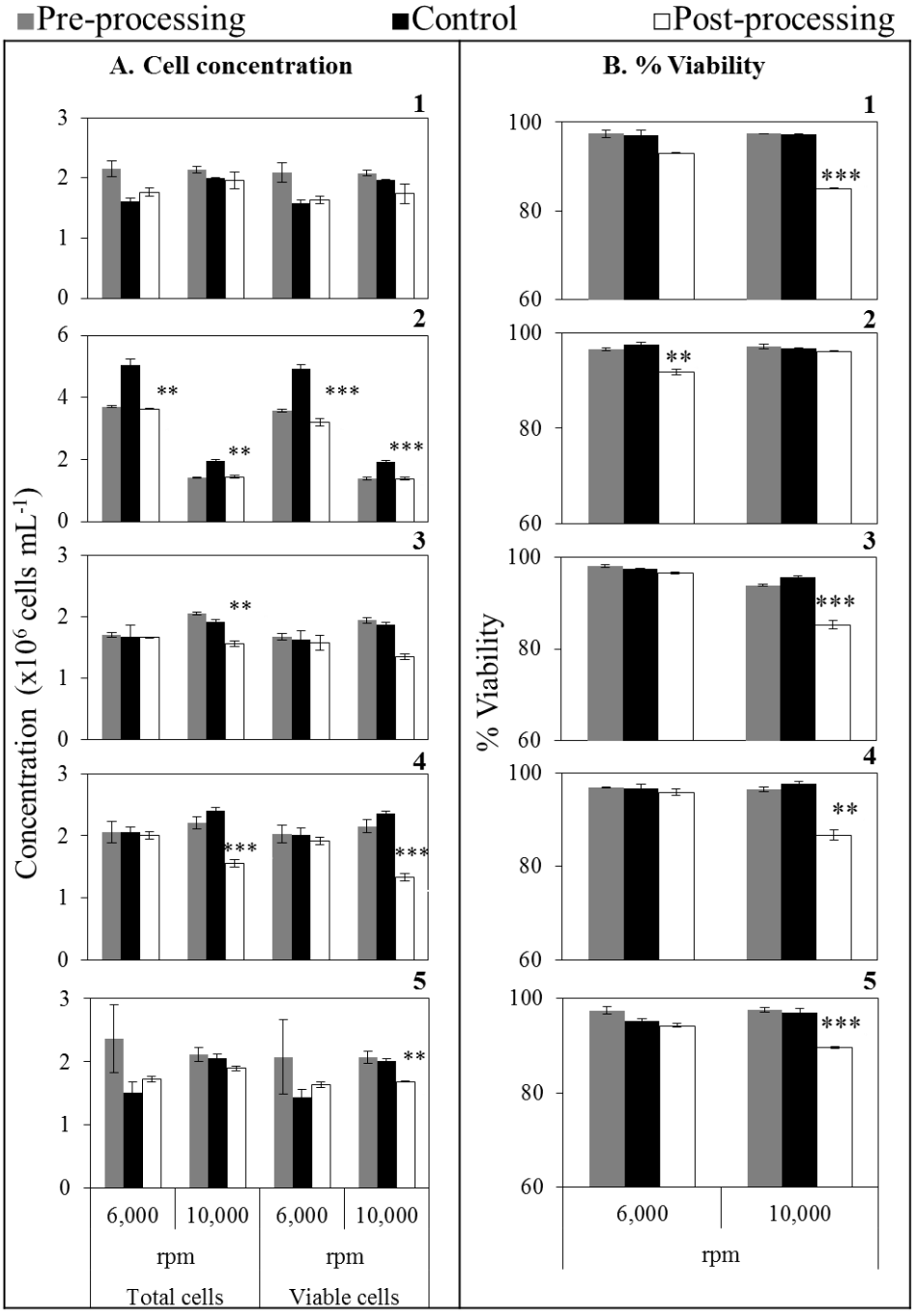

Figure 3.3: Membrane processing of feed (0 hour cell ageing) HCA2 cells – effect of low and high disc speeds ('*N*' = 6,000 and 10,000 rpm) on cell damage shown by total and viable cell concentrations pre and post-processing (column A) and percentage viability (column B) of the cellular suspension as recorded by trypan blue exclusion. (1) to (5) are five repeats. Error bars show ± 1 s.d. and significant changes between non-sheared control and post-processing (*p<0.5, **p<0.01, ***p<0.001; n = 4).

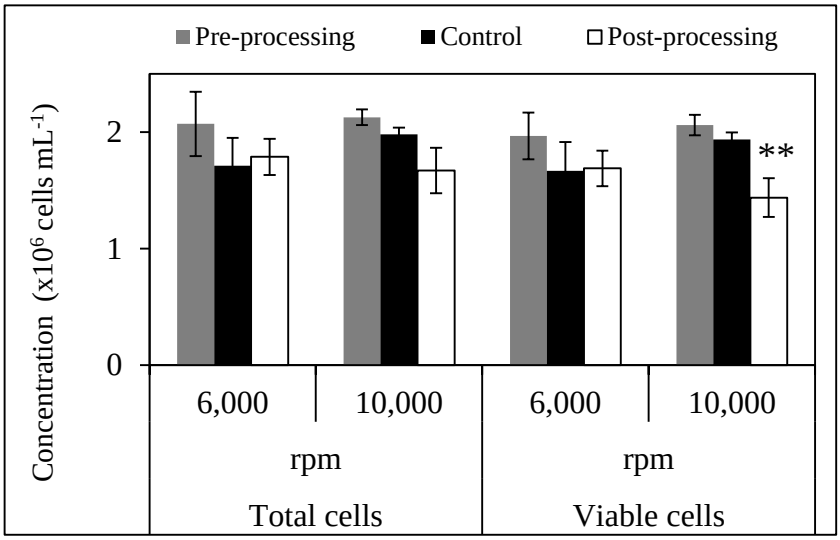

Figure 3.4: Membrane processing of feed (0 hour cell ageing) HCA2 cells – effect of disc speed on cell damage shown by total and viable cell concentrations pre and post-processing of the cellular suspension as recorded by trypan blue exclusion. Table below shows mean of raw data determined by trypan blue exclusion for concentration of total and viable cells. A non-sheared control held in a centrifuge tube concurrently, 21 ± 1ºC, for the duration of the experiment was used to measure trypan blue pre and post-processing for both 6,000 and 10,000 rpm ('γ' = 44,000 and 116,000 s^{-1} respectively). Trypan blue exclusion indicates that processing at high disc speed, resulted in a ~25% reduction of viable cells. Low drop was observed in the viable cell concentration post-processing at a low disc speed. Significant changes between non-sheared control and post-processing (*p<0.5, **p<0.01, ***p<0.001). Data shown are mean values ± 1 s.d. (j = 5; n = 4).

	Concentration (x10^6 cells mL^{-1}) ± 1 s.d. (j = 5; n = 4)					
	Total cells ('$_{TB\_TOT}$')			**Viable cells ('$_{TB\_VC}$')**		
Disc speed (rpm)	**Pre-processing**	**Control**	**Post-processing**	**Pre-processing**	**Control**	**Post-processing**
6,000	2.07 ± 0.28	1.71 ± 0.24	1.79 ± 0.15	1.97 ± 0.20	1.67 ± 0.25	1.69 ± 0.15
10,000	2.13 ± 0.07	1.98 ± 0.06	1.67 ± 0.19	2.06 ± 0.09	1.94 ± 0.06	1.44 ± 0.17

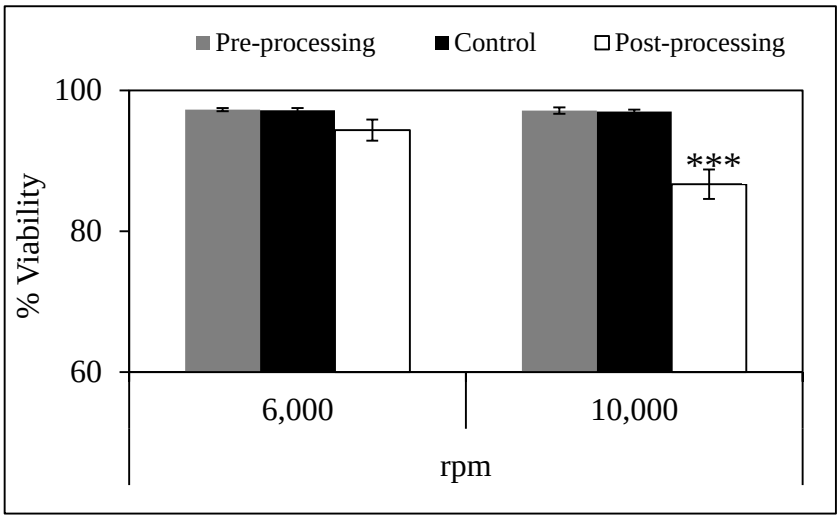

Figure 3.5: Membrane processing of feed (0 hour cell ageing) HCA2 cells – effect of disc speed on (A) percentage viability of the cellular suspension as recorded by trypan blue exclusion. Table (B) shows mean of raw data determined by trypan blue exclusion for percentage viability. A non-sheared control held in a centrifuge tube concurrently, 21 ± 1ºC, for the duration of the experiment was used to measure trypan blue exclusion pre and post-processing for both 6,000 and 10,000 rpm ('γ' = 44,000 and 116,000 s^{-1} respectively). Trypan blue exclusion indicates that processing at high disc speed, resulted in a ~10% drop in percentage viability post-membrane processing. Low drop was observed in percentage viability at a low disc speed. Significant changes between non-sheared control and post-processing (*p<0.5, **p<0.01, ***p<0.001). Data shown are mean values ± 1 s.d. (j = 5; n = 4).

	% ± 1 s.d. (j = 5; n = 4)		
	% Viability		
Disc speed (rpm)	**Pre-processing**	**Control**	**Post-processing**
6,000	97.3 ± 0.2	97.2 ± 0.3	94.4 ± 1.5
10,000	97.2 ± 0.5	97.0 ± 0.3	86.7 ± 2.1

3.3.3 Average rate constants for cell damage

To further understand and characterize the effect of each disc speed on cell damage, as measured by trypan blue and LDH, the average rate constants were calculated. The rate constant for any first order process is a numerical value that relates the rate at which a specific reaction takes place (in this case the "reaction" is cell damage) to the concentration of reactants (in this case intact cells fed). Therefore, analysis of the data indicates that cell damage could be described as a first order process with respect to the concentration of intact cells fed to the USD membrane separation. Chapter 5, Section 5.2 explains the reasoning for the assumptions made and outlines the calculations carried out to obtain the rate constants. However, in this section these calculations will not be shown because new terminology will be introduced in the next chapters that will form the basis of the calculations of the rate constants. The values obtained for each disc speed and method of assessment will however be discussed.

As measured by LDH release, high disc speed leads to a rate constant of $0.30 \pm 0.15\ h^{-1}$ compared to $0.06 \pm 0.02\ h^{-1}$ for low disc speed. For cell damage measured by trypan blue exclusion (loss of membrane integrity), high disc speed yielded a rate constant of $0.15 \pm 0.07\ h^{-1}$ compared to $0.03 \pm 0.01\ h^{-1}$ for low disc speed. These values suggest that cell damage occurs five times faster at high disc speed than at low disc speed, suggesting the rate constant is strongly dependent on the magnitude of disc speed. It also appears that LDH release is twice more sensitive to cell damage than trypan blue exclusion. Lappalainen et al. (1994) also observed differences between the sensitivity of LDH release and trypan blue exclusion assays. They concluded that LDH release appears to be a more sensitive indicator of earlier damage to the cell membrane than

trypan blue exclusion, which stains only dead cells. It may be that LDH can be released before the membrane lesions are produced and therefore can serve as an indication of earlier cytotoxicity. In fact, Diederichs et al. (1979) investigated the mechanism of release of LDH from isolated skeletal muscle and concluded that cell swelling, which is typical of necrotic cells, prior to membrane damage was connected with an increased LDH permeability.

Apart from the physical impact that disc speed appears to have on the cellular suspension, these processing conditions might have triggered biological responses such as programmed cell death (apoptosis) or might have compromised the metabolic activity of the cells in such a way that they cannot re-grow once plated after processing. The next sub-sections investigate the morphology of the cells pre-processing, immediately after processing and after a 2-hour hold post-processing as well as growth curves post-shear and finally apoptotic markers.

3.3.4 Cell morphology, growth and apoptosis analysis

It has been widely reported that changes in the rate at which cells grow, physical appearance and morphology can occur after the cells are exposed to stresses (Al-Rubeai et al. 1995; Kretzmer and Schügerl 1991) and can serve as indicators of the state of cell health (Agashi et al. 2009; Kretzmer and Schügerl 1991). For instance, both programmed cell death pathways, necrosis and apoptosis, can be indicated by specific morphological changes as was explained in Chapter 1, Section 1.6.3. Using these processed cells to inoculate further cultures can provide an insight into a different impact of a particular processing condition upon the cell population.

For all experiments presented in this section, HCA2 cell line was used. The USD membrane separation device was set-up in diafiltration mode, with hCGM being pumped into the system for 60 minutes at a flow rate of 0.5 mL min^{-1} (≈ 82 LMH). The disc speed was set to low (‘*N’* = 6,000 rpm) and high (‘*N*’ = 10,000 rpm) and the concentration of total cells of the feed material was ~25x10^6 cells mL^{-1} and only fresh cells were used, i.e. no pre-processing hold time.

After processing, cell populations were counted and split into two samples; one sample was held for 2 hours at 21 ± 1ºC and then re-counted and the other sample was seeded into tissue culture plates at a fixed seeding density of 2x10^4 viable cells per well. The seeded cells were cultured for a period of 72 hours. Light microscopy images of the attached cells were taken every 24 hours to observe if there were any morphological changes during culture and the cells were then detached to carry out trypan blue counts, also every 24 hours. For all the counts carried out in the automated haemocytometer, the samples were re-analysed using the Matlab script to classify the cells into cell populations based on morphology.

3.3.4.1 Cell morphology analysis

Within this section, the morphology and physical appearance of cells post-processing was investigated. Morphological analysis was carried out on the cellular suspension immediately post-processing and 2 hours post-processing. Further observations were carried out on the inoculated post-processed cells, in culture (attached) and in suspension (immediately after detachment). Nonetheless, categorizing the state of cell health on physical appearance alone would not be sufficient. The next sections will

therefore complement this analysis with the evaluation of growth profiles and apoptotic markers.

Examples of the type of images obtained from the automated haemocytometer are given in Figure 3.6. For both low and high disc speeds (Figures 3.6.1 and 3.6.2 respectively) three time points are shown; pre-processed samples (images labelled A), immediately post-processing (labelled B) and 2 hours hold post-processing (labelled C), all at 21±1ºC.

From Figures 3.6.1.A and 3.6.2.A, pre-processed samples for both low and high disc speeds, it can be seen that most cells are round viable cells with sharply defined outer edges or clearly non-viable as stained positive for trypan blue exclusion. However, the appearance of elongated and 'blebby' cells is observed immediately post-processing (Figures 3.6.1.B and 3.6.2.B). 'Blebs' are membrane bound protrusions from the plasma membrane caused by weakness in the actin cytoskeleton which helps maintain cellular structure (Kumar et al. 2007). Literature reveals that 'blebbing' is a dynamic process and can resolve itself once the actin cytoskeleton is restored (Kumar et al. 2007) and in fact, images C, after 2 hours hold post-processing, reveal that a large portion of the 'blebs' have disappeared and there are lower numbers of elongated cells. This trend seems to be more evident at high disc speed (Figure 3.6.2) than at low disc speed (Figure 3.6.1).

These morphological characteristics identified were used as building blocks to define the different cell types for the Matlab script. Figure 3.6.D shows some examples for each of the cell types identified for image processing using the Matlab

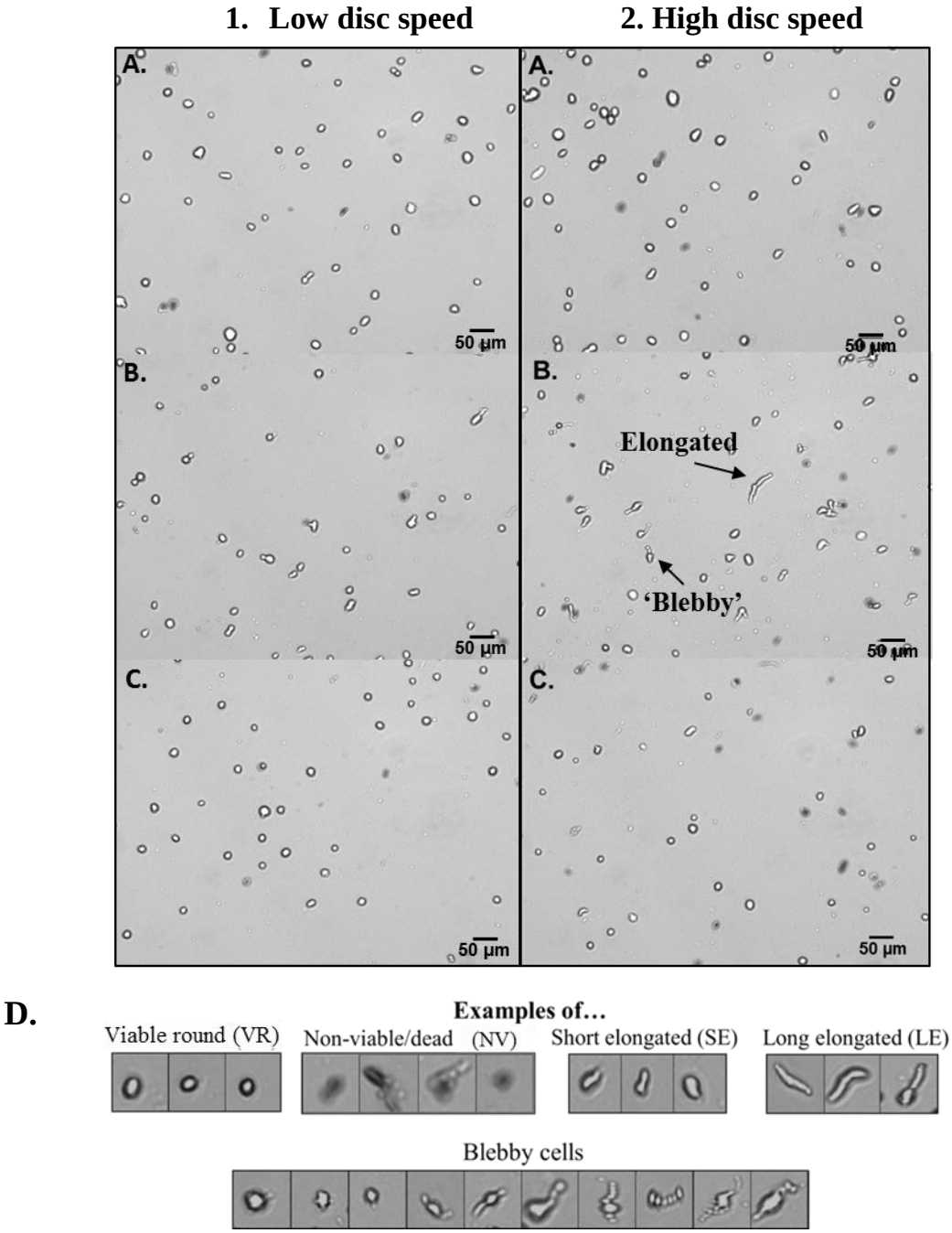

Figure 3.6: (1) Low and (2) high disc speeds ('*N*' = 6,000 and 10,000 rpm respectively) images of (A) pre-processing; (B) post-processing and (C) 2 hours hold post-processing. (D) Shows examples of HCA2 images from the cell image library created to facilitate the identification of cell phenotype in a given image. The cell library was constructed from images selected for each designated categroy. Each category was assigned paramteters (such as aspect ratio and intensity) and these were then used as rules for identification purposes for the Matlab script.

script. The cells were classified into short elongated (SE), long elongated (LE), viable round (VR), non-viable (NV) and debris (DEBRIS). For example, parameters such as aspect ratio were used to classify cells into round, short or long elongated cells; intensity was used to identify dead and alive and area was used to identify debris from cells. Originally, a degree of 'blebbing' for each cell type was going to be included as an added characteristic to each cell population. However, the implementation and incorporation of this parameter proved to be unreliable. The images from the automated haemocytometer were analyzed using the Matlab script and the proportions for each of the cell populations at the three given time points (pre-processing, immediately post-processing and 2 hour hold post-processing) are shown in Figures 3.7.A and 3.7.B (low and high disc speeds respectively).

At high disc speed in Figure 3.7.B, there is an increase in the proportion of dead cells and a reduction in the proportion of viable round cells immediately post-processing that remained the same after 2 hours hold. At both low and high disc speeds in Figures 3.7.A and 3.7.B respectively, there is an increase in the proportion of both short and long elongated cells immediately post-processing that appears to return to pre-processed levels after the 2 hour hold. The apparent trend previously appreciated in Figure 3.6 is in agreement with the quantitative data in Figures 3.7. Therefore elongation may be a temporary change of morphology, at least whilst in suspension.

The morphology of the HCA2 cells was also investigated post-processing during attachment to the surface of a tissue culture well plate and the images obtained by light microscopy every 24 hours are shown in Figure 3.8. Apart from the evident difference

in number of cells at the same time points between sheared and non-sheared samples (which is discussed in more detail in the following section), there appears to be no change in morphology or in extent of alignment. This implies that shearing the cells for a prolonged time did not cause a permanent change in morphology after inoculation post-processing and did not cause a directional growth, which reinforces that the elongation was indeed a temporary change. Finally, the cells were detached for trypan blue exclusion measurement at the 24 hour points, analyzed in suspension and the proportion of each cell population is given in Figure 3.9. Both of the sheared samples show comparable proportions of cell populations to the non-sheared controls.

3.3.4.2 Growth profiles and specific growth rate constants post-processing

As active participants in their environment, cells continually adjust their structure and function to accommodate changing extracellular stimuli. If the extracellular stresses are aggressive or prolonged enough, cells can lose their normal homeostasis that encompasses a range of physiologic parameters. Compromising cell homeostasis can therefore impact cell division. For successful cell division, a chain of events must be completed in an orderly and unidirectional manner. Changes in the rate of cell growth and doubling times can de-regulate this crucial chain of events (Kumar et al. 2007) and therefore serve as indicators of poor cell health or cell injury post-processing (Al-Rubeai et al. 1995; Veraitch et al. 2008). A way to monitor how fast cells are dividing is by calculating the specific growth rate constant:

$$\frac{dR_{IC}(t)}{dt} = k \times R_{IC}(t) \qquad \text{Equation 3.9}$$

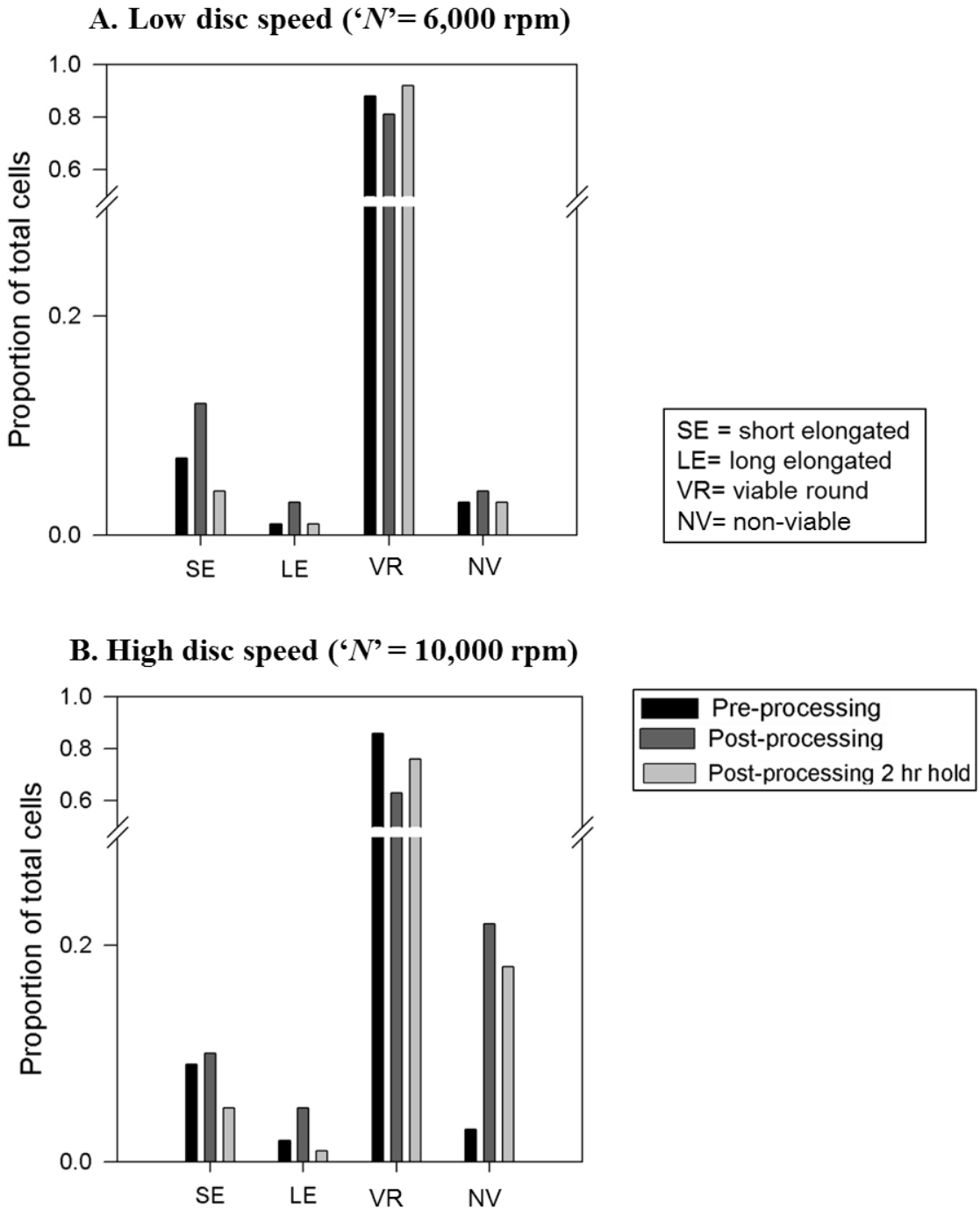

Figure 3.7: Effect of disc speed on cell morphology after shear and after shear plus hold (software for image processing developed using Matlab Image Processing Toolbox (MathWorks, Cambridge, UK) by Nicolas Jaccard in the Biochemical Engineering Department at UCL). The cell categories correspond to libraries created for the Matlab script (Figure 3.6.D). The proportion of each cell type or population was compared to the total cells in the sample for pre-processing (■), immediately post-processing (■) and 2 hours hold post-processing (■).

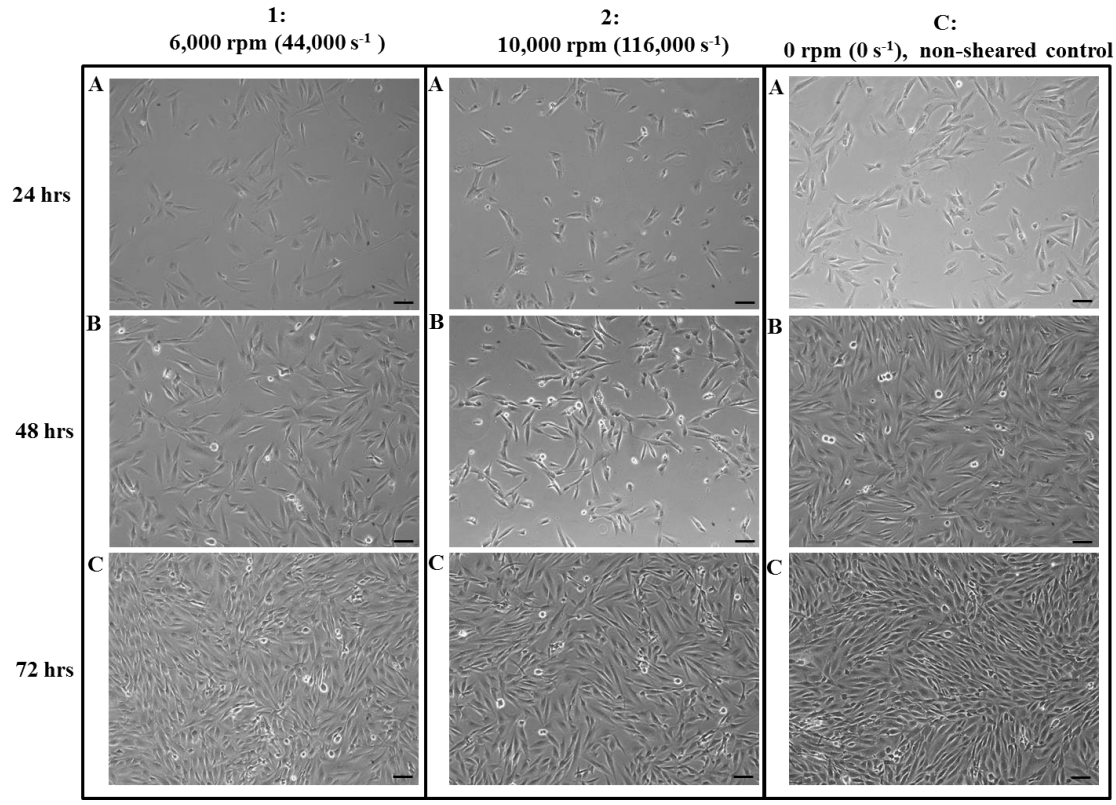

Figure 3.8: Phase contrast of HCA2 cells in culture after (A) low disc speed ('*N*' = 6,000 rpm, 'γ' = 44,000 s^{-1}), (B) high disc speed ('*N*' = 10,000 rpm, 'γ' = 116,000 s^{-1}) and (C) non-sheared control. Control cell populations were cultured in parallel with populations subjected to varying disc speeds. These images show snapshot of cells in culture for (1) 24 hours, (2) 48 hours and (3) 72 hours. The black bar scale represents 50 µm.

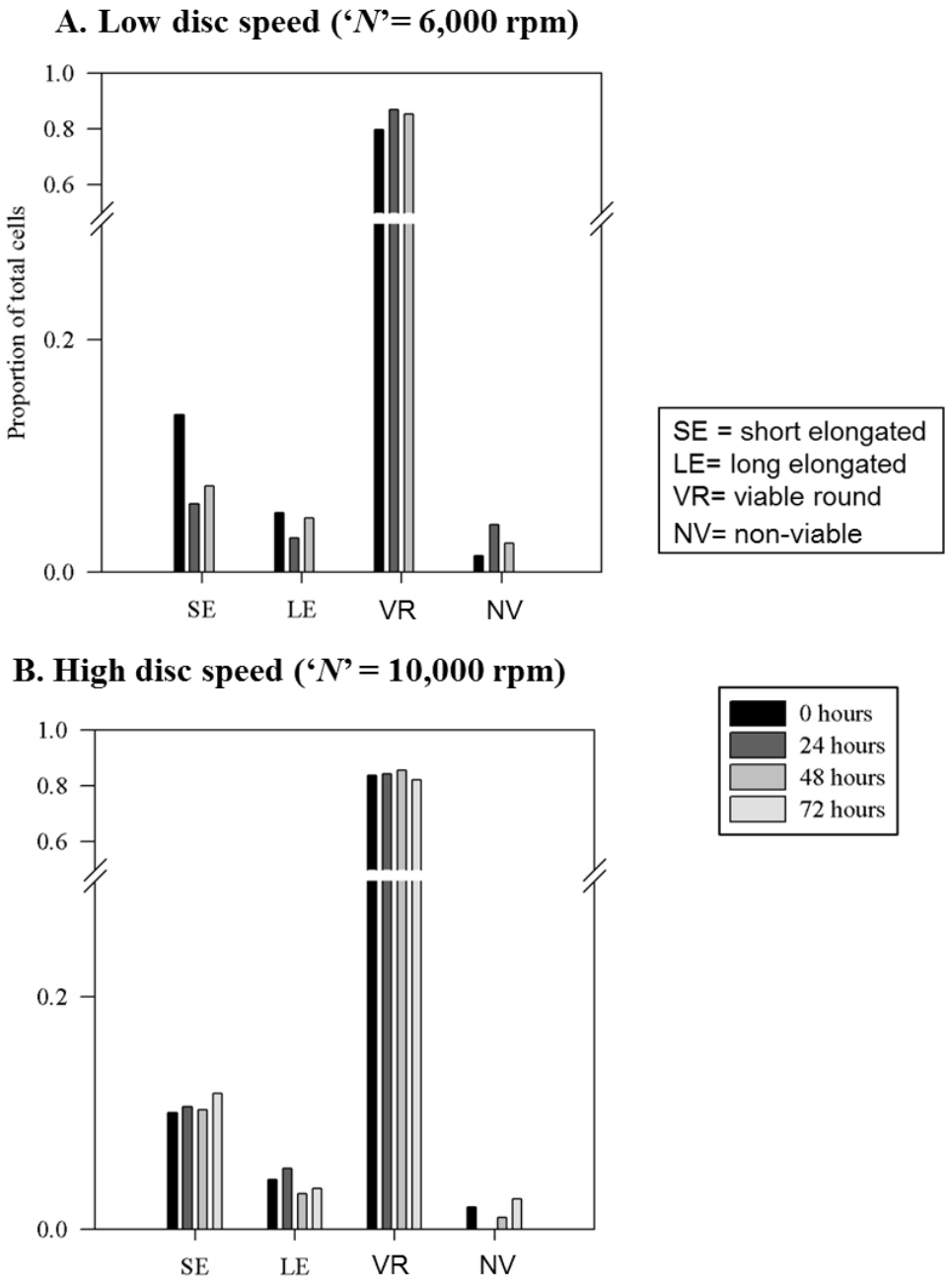

Figure 3.9: Effect of growth time point post-shear on cell morphology. Software for image processing developed using Matlab Image Processing Toolbox (MathWorks, Cambridge, UK) by Nicolas Jaccard in the Biochemical Engineering Department at UCL. The cell categories correspond to libraries created for the Matlab script (Figure 3.6.D). The proportion of each cell type or population was compared to the total cells in the sample for 24 hours after seeding (■), 48 hours after seeding (■) and 72 hours after seeding (■).

where *'k'* is the specific growth rate constant (h^{-1}), *'$R_{IC}(t)$'* is the number of intact cells in the retenate at time 't'. Integrating between the limits of 0 to 't' and '$R_{IC}(0)$' which is the number of intact cells at the start (i.e. 't = 0 min') to *'$R_{IC}(t)$'* gives:

$$k = \frac{2.303}{t} \times log\left(\frac{R_{IC}(t)}{R_{IC}(0)}\right) \qquad \text{Equation 3.10}$$

Because cell growth rates can vary as a result of several factors, ranging from the cell concentration at inoculation, to the physiochemical and physical environment, all variables used to study cell growth rate were maintained constant. In this section of the study, the growth curves and specific growth rate constants of processed cell populations were investigated to help gauge the impact of disc speed. This allows identification of any harmful or irreversible changes to the cell population otherwise undetected by analysis using LDH release and trypan blue exclusion.

Each data point shown in this section is the mean of three replicates. The HCA2 cell line was processed using the USD membrane separation device in diafiltration mode, with hCGM being pumped into the system for 60 minutes at a flow rate of 0.5 mL min^{-1} ('Q' ~82 LMH), i.e. ~18 diafiltration volumes. The disc speeds of 6,000 rpm and 10,000 rpm were used and the concentration of the feed material was fixed at ~$25x10^6$ cells mL^{-1} with essentially no hold time prior to processing. After processing in the USD membrane device, cell populations were counted and cells seeded onto tissue culture plates at a fixed density of ~$2x10^5$ viable cells per well (i.e. $4.28x10^4$ viable cells per cm^2). Light microscopy images and trypan blue counts were recorded every 24 hours and over a period of 72 hours after processing.

By inspection of this preliminary set of results shown in Figure 3.10.A, even though cells were exposed to processing for a prolonged period of time, they can still grow and proliferate. There is some suggestion of slower initial growth for both processed samples and lower overall growth for the processed sample at high speed compared with the control. However the results are preliminary and therefore not significant and it appears processed cells can grow similarly to unprocessed cells.

3.3.4.3 Biological impact post-processing by cell death analysis

Identifying potentially damaging operations and parameters can help minimize cell loss and maintain quality of the product to ensure efficacy and economic viability. It has been established that bioprocessing steps can expose the cells to severe stresses which can cause severe abnormalities and cell injury resulting in cell death (Agashi et al. 2009; Al-Rubeai et al. 1995; Augenstein et al. 1971; Born et al. 1992; Chisti 2001; Hu et al. 2011). In fact, the images from previous sections have shown that processing may cause 'blebbing' which has been reported to be a characteristic of cell death (Kumar et al. 2007).

Cell death biological assays can identify the two primary types of death; apoptosis and necrosis which are different in their morphology, mechanisms and roles in the programmed cell death pathways (Dive et al. 1992). The biological assay used in this study was based on a cytometric technique (Dive et al. 1992) used for detection and categorization of both the mode and phase of programmed cell death. The biological assay is based on Fluorochrome-labeled inhibitors of caspases (FLICA). These inhibitors have proven to provide the means for a convenient, sensitive and reliable way

of measuring caspase activation – a key molecule in the apoptotic mechanism and induction of apoptosis (Darzynkiewicz and Pozarowski 2007; Smolewski et al. 2002). Even though the caspase sub-type involved may vary from one tissue to another, caspase-3 is known as a universal caspase which functions in almost all tissues and is an indicator that the cell is committed to irreversible cell death processes. Therefore assays that work on the activation of caspase-3 correlate well with the results obtained by FLICA reagents used in this study (Darzynkiewicz and Pozarowski 2007; Smolewski et al. 2002). By using these markers in conjunction with propidium iodide (PI - cell membrane integrity marker), the cell population can be segregated into four different categories (see Table 3.5). Cells which are live will be negative for both PI and FLICA; early apoptotic cells will show apoptotic related activity but no loss of membrane integrity, therefore will stain negative for PI but positive for FLICA; late apoptotic cells will show both apoptotic related activity as well as loss of membrane integrity, staining positive for both PI and FLICA; and necrotic cells will stain positive for PI but negative for FLICA, suggesting that no apoptotic processes were induced prior to loss of membrane integrity.

This section attempts to identify if there is any degree of induction of programmed cell death for the HCA2 cell line, following the exposure to low and high disc speeds. The sheared samples were held on the bench at 21 ± 1ºC for 2 hours post-processing prior to the staining, to allow increased expression of apoptotic markers if any were present. The non-sheared control samples were also held on the bench at 21 ± 1ºC for the duration of the experiment, including the 2 hours hold post-processing and prior to the staining, to ensure these cells truly represent controls for the sheared samples.

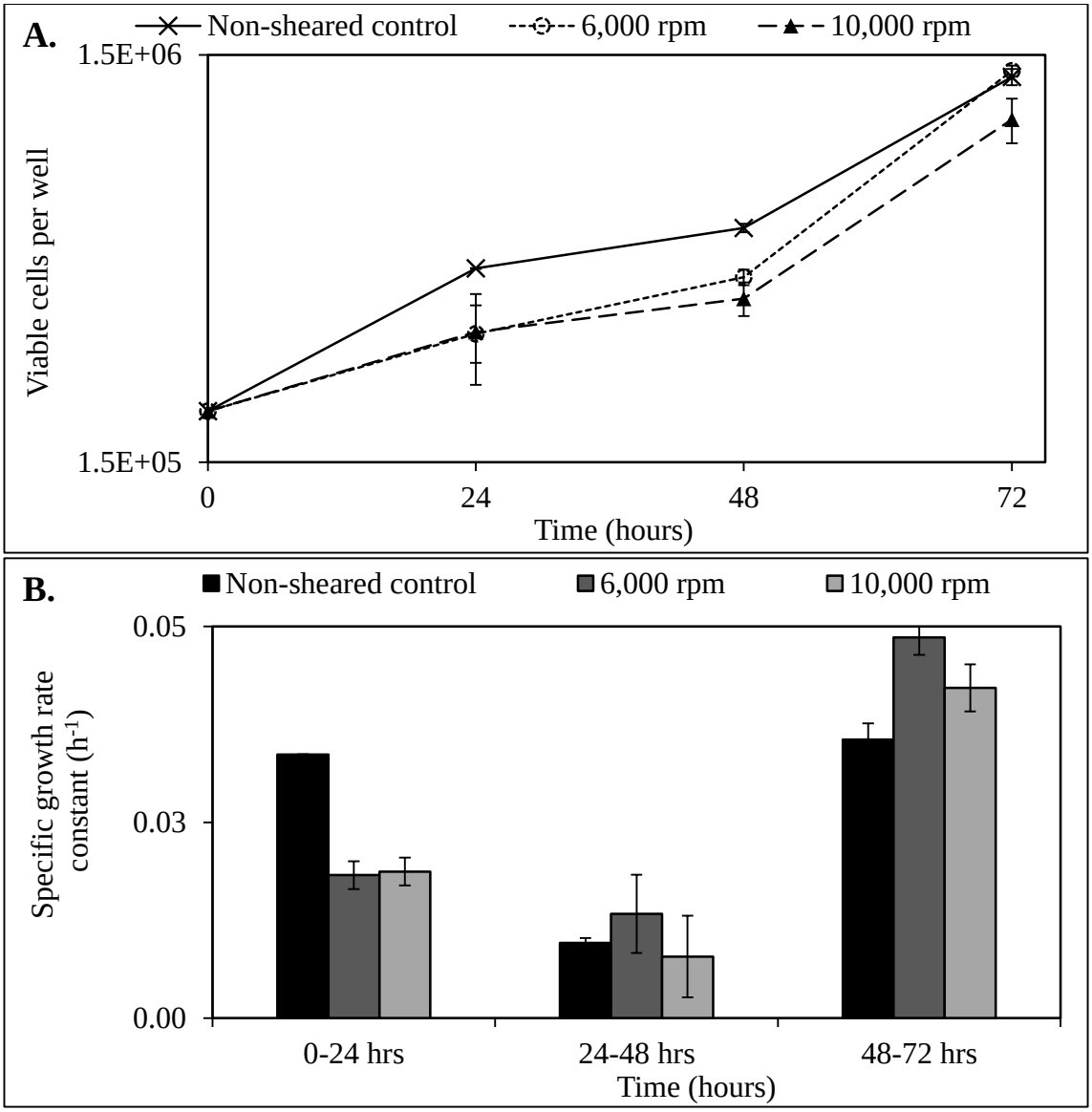

Figure 3.10: (A) Cell growth analysis of HCA2 cells following low (6,000 rpm, ○) and high (10,000 rpm, ▲) disc speeds ('γ' = 44,000 s^{-1} and 116,000 s^{-1} respectively) as well as non-sheared control (×). (B) Specific growth rate constants, Eq 3.10, calculated every 24 hours for the growth curves shown in (A) for non-sheared control (■), low (■) and high (■) disc speeds. Cells were inoculated after processing at $2x10^5$ viable cells per well and trypan blue exclusion counts performed every 24 hours. It appears that cells exposed to low and high disc speeds can grow post-processing although there is some evidence of a longer lag phase than non-sheared control by observation of the growth profiles and the specific growth rates. Specific growth rates for all three samples appear to be of similar magnitudes by the 48-72 hour time point. Data shown are mean values ± 1 s.d. (j = 3; n= 4).

Category	Description	FLICA	PI
Live	Fully functional cell without loss in membrane integrity or apoptotic related activity.	N	N
Early apoptotic	Apoptotic related activity but no loss of membrane integrity.	P	N
Late apoptotic	Apoptotic related activity and loss in membrane integrity.	P	P
Necrotic	Apoptotic processes were not initiated prior to loss in membrane integrity.	N	P

Table 3.5: The assay allows the segregation of the cell population into four different categories by staining a combination of positive (P) and negative (N) for FLICA and PI dyes. The categories identified are live, early apoptotic, late apoptotic and necrotic cells.

For Figures 3.11 to 3.14, image A refers to a normal light microscopy image of the cells; image B shows a DAPI stain that stains intact and non-intact cells containing DNA in blue; image C shows the caspase-3 expressing cells in green; and image D shows a PI stain which stains in red accessible DNA, i.e. those cells with only a damaged outer membrane.

Figure 3.11 shows the non-sheared controls for low and high disc speeds. As expected, there appears to be no induction of apoptosis (Figure 3.11.C) as well as no evident loss of membrane integrity (Figure 3.11.D). For the post-processing sample at low disc speed, the images displayed in Figure 3.12 show no induction of apoptosis in Figure 3.12.C and no loss of membrane integrity in Figure 3.12.D. This appears to indicate promising results at low disc speed in terms of processing, where low levels of cell damage were measured by both LDH release and trypan blue exclusion (as shown in sections 3.3.1 and 3.3.2) as well as low induction of apoptosis.

However, for the post-processed sample at high disc speed a degree of early apoptosis was observed (Figures 3.13.C and 3.14.C). Moreover, both early apoptotic and late apoptotic cell populations were observed for the post-processed sample in the bottom half of Figures 3.14.C and 3.14.D respectively. It was a common occurrence to see late apoptotic cell populations stick together in clumps as seen in Figure 3.14 possibly due to the release of DNA (from cell fragmentation). On top of this, the process and time taken to do the staining could explain the appearance of late apoptotic populations within the data gathered.

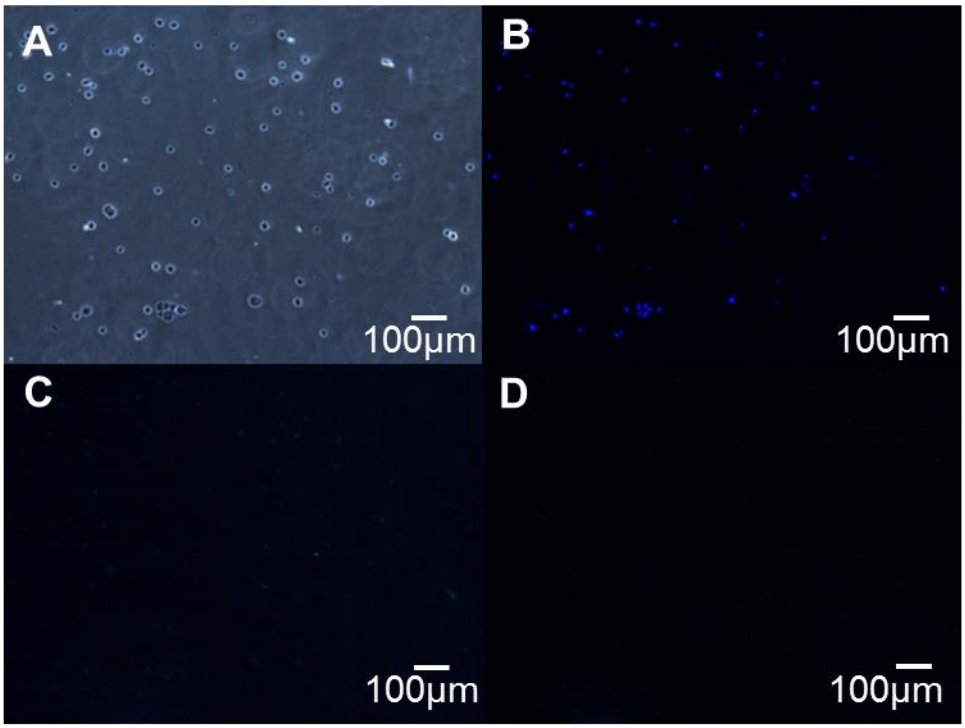

Figure 3.11: Fluorescent microscopy of CaspaTag™ Pan-Caspase staining for non-processed controls (A to D). Holding the cellular suspension on the bench at 21 ± 1ºC for the duration of the experiment, including the 2 hours hold post-processing, does not induce apoptosis (no positive FLICA staining in images C) or lead to loss of membrane integrity (no positive PI staining in images D). Enhanced images shown.

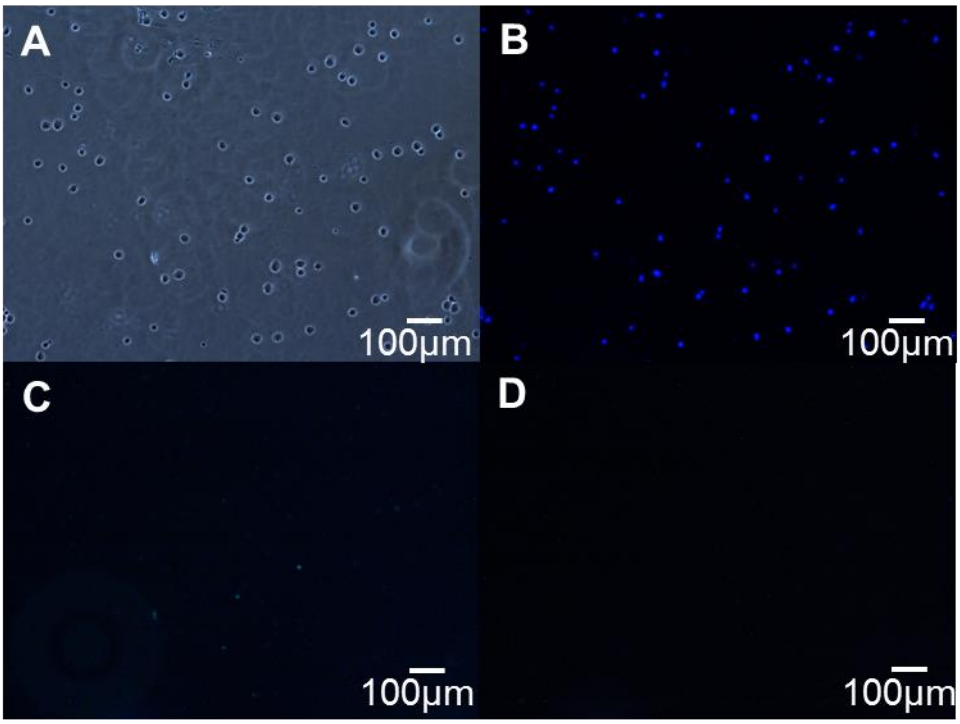

Figure 3.12: Fluorescent microscopy of CaspaTag™ Pan-Caspase staining for post-processed retentate sample at low disc speed ('*N*' = 6,000 rpm). No induction of apoptosis (C) and no loss of membrane integrity (D) are seen post-processing at low disc speed. Images shown are enhanced images.

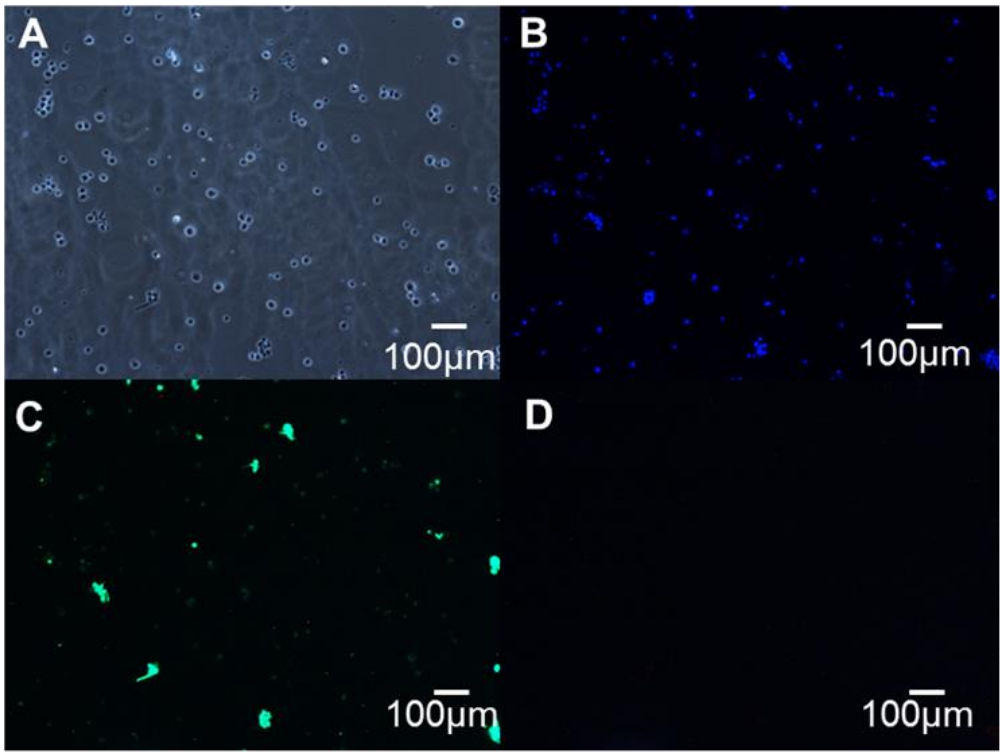

Figure 3.13: Fluorescent microscopy of CaspaTag™ Pan-Caspase staining for post-processed retentate sample at high disc speed ('*N*' = 10,000 rpm). At high disc speed early apoptotic populations are induced post-processing (images C and D respectively). Enhanced images shown.

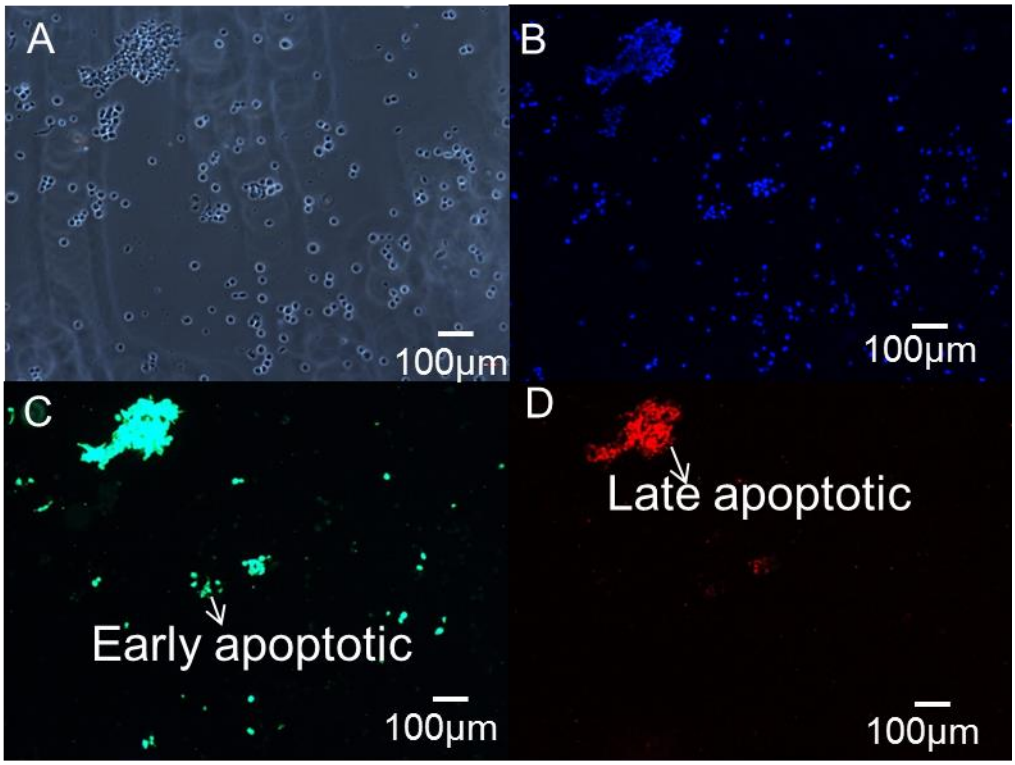

Figure 3.14: Fluorescent microscopy of CaspaTag™ Pan-Caspase staining for post-processed retentate sample at high disc speed ('*N*' = 10,000 rpm). At high disc speed late apoptotic populations are also induced post-processing (images C and D respectively). Enhanced images shown.

This observation also poses a question regarding previous post-processing growth profiles in section 3.3.4.2. If some of the cells are committed to death but remain undetected via the trypan blue technique, this suggest that the trypan blue data used to determine the process volume used to seed the well cultures based on number of viable cells, may require adjustment prior to the inoculation of cell populations. If this is the case, it may explain the fact that after 24 hours there are less number of viable cells observed at high disc speed as some have undergone apoptosis. It may also mean that at high disc speed, the possibly longer lag phase previously (Figure 3.10.A and 3.10.B) observed may be justified by the rate of cell loss of "viable" cells, as stained by trypan blue, due to apoptosis. Literature reveals that the rate of cell proliferation within any population of cells depends on three parameters; the rate of cell division, the fraction of cells within the population undergoing cell division (growth fraction) and the rate of cell loss from the population due to terminal differentiation or cell death (Kumar et al. 2007). It might be that the fraction of viable cells undergoing cell division is lower as a result of exposure to high disc speed.

3.4 Effect of cell age on HCA2 fibroblasts

Cell age (also referred to as pre-process hold time) is often encountered during processing when harvesting large quantities of cells. Cell age prior to processing might have a negative impact on cell quality affecting the percentage viability and the robustness of the cellular suspension. It has been shown (Section 3.3) that processing fresh HCA2 cells (i.e. no pre-process hold time) at a low disc speed ('N' = 6,000 rpm) leads to a small but significant level of cell damage as measured by both LDH release

and by trypan blue uptake (Figures 3.2 and 3.4 respectively). An investigation was carried out on the effect of cell age of 24 hours, on cell response to processing.

3.4.1 Physical impact as measured by LDH release

Five runs for each of fresh cells (aged 0 hours) and cells aged for 24 hours were carried out and the breakdown of each one is shown in Tables 3.6.A and 3.6.B. The results presented in Table 3.6.A are the same as those presented in Table 3.4.A and are reproduced for convenience. These tables summarize some of the key performance data for the two sets of runs. Each run, A to E, depends on preparation of a new batch of cells. Each time, enough cells were prepared to run one experiment with fresh cells and another one with cells aged for 24 hours at $21 \pm 1^{\circ}C$. Despite a constant method of preparation used, there will inherently be some variation between batches.

Column 2 presents the measured transmission of LDH through the membrane at the end of each of the 60 minutes shear runs. These are the transmission values that are used for calculations. The mean values for LDH transmission for both fresh cells and aged for 24 hours were 0.78 ± 0.02 and 0.78 ± 0.07 respectively. The similar mean values are probably due to the fact that both conditions have the same shear rate.

Column 3 examines the stability of LDH over the period of the membrane study for each run. On average for both cases, the cells might be considered stable for the length of the run. Ageing of the cells for 24 hours was held the same way and conditions as the control during the membrane study and showed no loss of LDH compared to fresh cells.

Column 4 examines the total amount of LDH (extracellular and intracellular) measured - i.e. permeate plus retentate – and it is compared with total LDH at the start of the experiment. This helps to check whether all LDH is recovered (none is stuck to membrane) and none is lost through denaturation. For both aged and fresh cells there is a small, but not statistically significant, loss of ~7% of LDH which might be trapped in the membrane.

Finally, column 5 is a second measure of accountability for LDH comparing the total in the retentate and permeate to the control cells for the duration of the experiment. For fresh cells there is a small (~9%), but not statistically significant, loss of LDH and there was no loss showed for aged cells.

Overall, it can be seen from Tables 3.6.A and 3.6.B that the averages are representative of the runs. Therefore, the average values of the repeats were used to produce Figure 3.15.A. This figure shows the proportion of intracellular LDH remaining with time. This proportion decreased by ~8% for fresh cells and by ~15% for cells aged for 24 hours. These results suggest that by prolonging the cell ageing period, the cells appear to be twice as susceptible to damage during processing than fresh cells.

From Figure 3.15, Tables B and C show the amount of total, extracellular and internal LDH in each of the process streams for 0 and 24 hours cell ageing respectively. The mass balances for both conditions show that the amount of total LDH in the non-sheared controls held at 21 ± 1ºC in a centrifuge tube for the duration of the experiment, did not decrease. As with the disc speed investigation, any changes seen can therefore be fully attributed to processing conditions.

A.	**0 hours cell age ± 1 s.e. (j = 5; n = 4)**			
1. **Run (‘j’)**	**2.** **‘$T(t_F)$’**	**3.** **‘b/a’**	**4.** **‘$(c+d)/a$’**	**5.** **‘$(c+d)/b$’**
A	0.82 ± 0.07	1.08 ± 0.03	1.00 ± 0.02	0.88 ± 0.02
B	*0.75 ± 0.06*	*1.69 ± 0.08*	*1.14 ± 0.05*	*0.69 ± 0.01*
C	0.84 ± 0.04	0.98 ± 0.04	0.82 ± 0.03	0.85 ± 0.03
D	0.73 ± 0.07	1.04 ± 0.04	1.01 ± 0.02	0.98 ± 0.02
E	0.74 ± 0.09	0.92 ± 0.09	0.87 ± 0.07	0.95 ± 0.05
Average	**0.78 ± 0.02**	**1.01 ± 0.14**	**0.93 ± 0.06**	**0.91 ± 0.05**

B.	**24 hours cell age ± 1 s.e. (j = 5; n = 4)**			
A	1.03 ± 0.04	0.92 ± 0.02	0.84 ± 0.01	0.92 ± 0.02
B	0.85 ± 0.08	0.91 ± 0.09	0.88 ± 0.05	0.98 ± 0.08
C	0.68 ± 0.05	0.80 ± 0.09	0.97 ± 0.05	1.21 ± 0.04
D	0.62 ± 0.04	0.88 ± 0.10	0.96 ± 0.10	1.10 ± 0.05
E	0.71 ± 0.05	1.28 ± 0.12	1.00 ± 0.08	0.78 ± 0.03
Average	**0.78 ± 0.07**	**0.96 ± 0.08**	**0.93 ± 0.03**	**1.00 ± 0.07**

C.

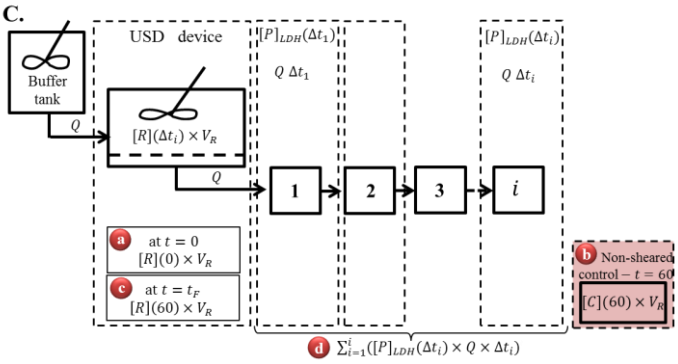

Table 3.6: Membrane processing of feed (‘N’ = 6,000 rpm, ‘γ’ = 44,000 s^{-1}) HCA2 cells – effect of (A) 0 and (B) 24 hours cell age on cell damage as recorded by release of LDH. To note results presented in Table 3.6.A are as presented in Table 3.4.A. Box diagram (C) of the USD membrane separation device showing process streams. From left to right columns show; (1) run; (2) transmission coefficient; (3) ratio of intracellular LDH in the control to the intracellular LDH pre-processing in the retentate to evaluate stability of LDH in the cells without processing (where 1 equals to no loss in LDH activity); (4) ratio of the sum of the total LDH in the retentate post-processing and permeate streams to the total LDH in the retentate pre-processing, to evaluate the mass balance agreement (where 1 equals to all LDH mass is accounted for); (5) ratio of the sum of the total LDH in the retentate post-processing and permeate streams to the total LDH in the control, to evaluate the mass balance agreement assuming the processed cells change as with control. Run B for 0 hour cell ageing, shown in red in table A, was considered as an outlier due to an unusually high initial cell concentration with respect to the other runs (j = 5; n = 4).

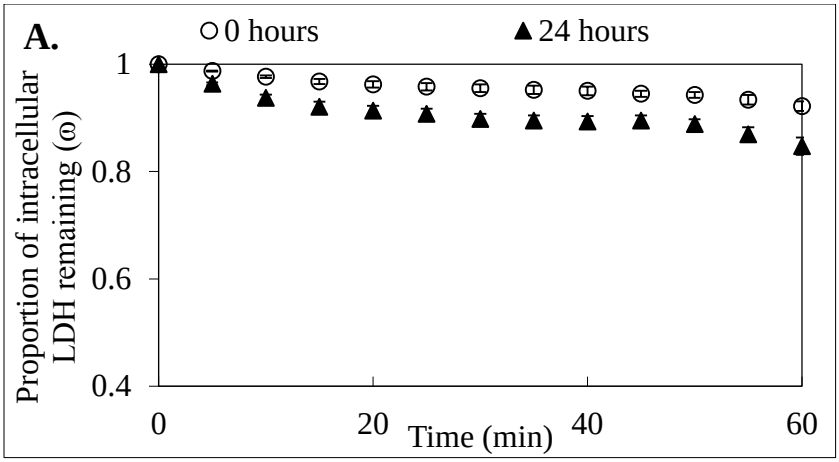

B.

	LDH µU ± 1 s.e. (j = 5; n =4)			
	Cell age (hrs)	**0**		
Sample	**Notation**	**Total ('LDH_TOT')**	**Extracellular ('LDH_EXT')**	**Predicted internal ('LDH_INT')**
Pre-processing	(a) '$R(0) = [R](0) \times V_R$'	**23.92 ± 2.96**	0.76 ± 0.11	23.16 ± 2.89
Control	(b) '$C(60) = [C](60) \times V_R$'	**23.91 ± 2.50**	0.79 ± 0.21	23.12 ± 2.70
Post-processing	(c) '$R(60) = [R](60) \times V_R$'	20.03 ± 2.94	0.41 ± 0.09	19.62 ± 2.93
Permeate	(d) '$\sum_{i=1}^{i} P_{LDH}(\Delta t_i)$'	2.02 ± 0.27		
Post-processing + Permeate	(c) + (d) '$[R](60) \times V_R + \sum_{i=1}^{i}([P]_{LDH}(\Delta t_i) \times Q \times \Delta t_i)$'	**22.05 ± 2.95**	2.43 ± 0.35	19.62 ± 2.93

C.

	Cell age (hrs)	**24**		
Sample	**Notation**	**Total ('LDH_TOT')**	**Extracellular ('LDH_EXT')**	**Predicted internal ('LDH_INT')**
Pre-processing	(a) '$R(0) = [R](0) \times V_R$'	**24.66 ± 0.89**	0.94 ± 0.18	23.72 ± 0.77
Control	(b) '$C(60) = [C](60) \times V_R$'	**23.42 ± 1.66**	1.13 ± 0.23	22.29 ± 1.47
Post-processing	(c) '$R(60) = [R](60) \times V_R$'	18.82 ± 1.02	0.78 ± 0.12	18.04 ± 0.95
Permeate	(d) '$\sum_{i=1}^{i} P_{LDH}(\Delta t_i)$'	4.19 ± 0.42		
Post-processing + Permeate	(c) + (d) '$[R](60) \times V_R + \sum_{i=1}^{i}([P]_{LDH}(\Delta t_i) \times Q \times \Delta t_i)$'	**23.01 ± 1.19**	4.97 ± 0.51	18.04 ± 0.95

Figure 3.15: Membrane processing of feed ('N' = 6,000 rpm, 'γ' = 44,000 s^{-1}) HCA2 cells – effect of cell ageing on cell damage as recorded by (A) release of LDH. Tables (B) and (C) show the mean LDH data for all streams including both external and total measurements. To note results presented in Figure 3.15 (Table B) are as presented in Figure 3.2 (Table B). A non-sheared control held in a centrifuge tube concurrently, 21 ± 1°C, for the duration of the experiment was used to measure LDH pre and post-processing. Figure (A) shows proportion of intracellular LDH remaining ('ω', Eq 3.8), for 0 hours (○) and 24 hours (▲) at a concentration of ~2.0x10^6 cells mL^{-1}. LDH release suggests that the cells are twice as weak, as reflected by damage during membrane processing, after 24 hours of cell ageing. Data shown are mean values ± 1 s.e. (j = 5; n = 4).

It also appears that for both fresh cells and cells aged for 24 hours, the total amount of LDH in the retentate pre-processing is ~5% less than the total amount of LDH collected post-processing in both the retentate and in the permeate. However, this does lie within experimental error and is not statistically significant as previously shown in Tables 3.6.A and 3.6.B.

3.4.2 Physical impact as measured by trypan blue exclusion

The plots shown in Figures 3.16 and 3.17 were used to analyze the impact of cell age on cell damage as measured by trypan blue exclusion. The results presented for the fresh cells (i.e. 0 hours cell ageing) in Figures 3.16 and 3.17 are the same as those presented in Figures 3.4 and 3.5 for low disc speed ('N' = 6,000 rpm) and are reproduced for convenience. Figure 3.16 shows the concentration of total and viable cells for the pre-processing, control and post-processing samples for fresh cells and cells aged for 24 hours. There is no major difference between the two conditions investigated and no evident decrease of the population of viable or total cells after processing.

Figure 3.17 shows the percentage viability for pre-processing, control and post-processing samples for both fresh cells and cells aged for 24 hours. Analysis of this figure shows that cell age has no major impact on the drop of the percentage viability. It was expected that by ageing the cells for 24 hours (i.e. holding the cells at 21 ± 1ºC without processing) a lower percentage viability would be observed due to the fact that the cellular suspension was not held at optimum conditions.

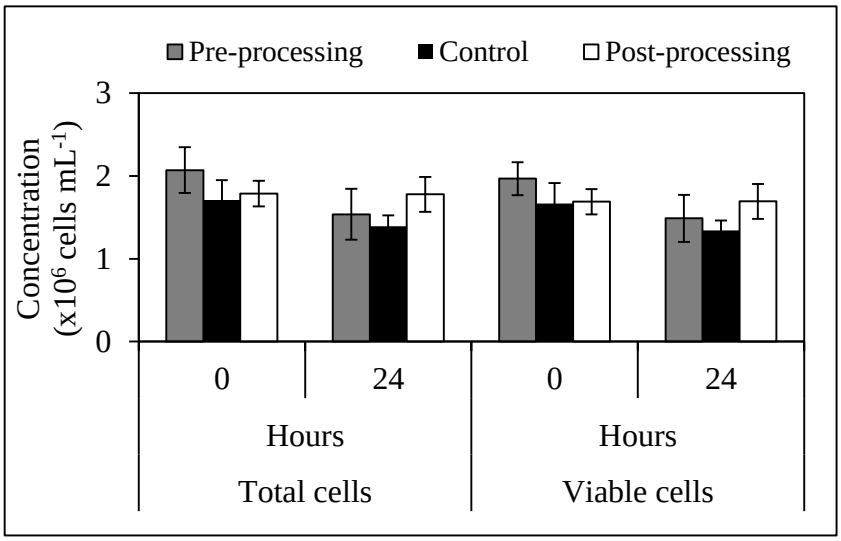

Figure 3.16: Membrane processing of feed ('*N*' = 6,000 rpm, 'γ' = 44,000 s^{-1}) HCA2 cells – effect of cell ageing on cell damage as shown by total and viable cell concentrations pre and post-processing. Table below shows mean of raw data determined by trypan blue exclusion for concentration of total and viable cells for pre and post-processing as well as a non-sheared control. To note results for fresh cells presented in this figure are as presented in Figure 3.4 for low disc speed. A non-sheared control held in a centrifuge tube concurrently, 21 ± 1ºC, for the duration of the experiment was used to measure trypan blue pre and post-processing for 0 and 24 hours cell ageing. Trypan blue exclusion indicates that there is no evident drop in concentration of total or viable cells after processing at a 0 and 24 hours cell ageing. Data shown are mean values ± 1 s.d. (j = 5; n = 4).

	Concentration (x10^6 cells mL^{-1}) ± 1 s.d. (j = 5; n = 4)					
	Total cells ('$_{TB\_TOT}$')			**Viable cells ('$_{TB\_VC}$')**		
Cell ageing (hours)	**Pre-processing**	**Control**	**Post-processing**	**Pre-processing**	**Control**	**Post-processing**
0	2.07 ± 0.28	1.71 ± 0.24	1.79 ± 0.15	1.97 ± 0.20	1.67 ± 0.25	1.69 ± 0.15
24	1.54 ± 0.31	1.39 ± 0.13	1.78 ± 0.21	1.49 ± 0.28	1.34 ± 0.12	1.69 ± 0.21

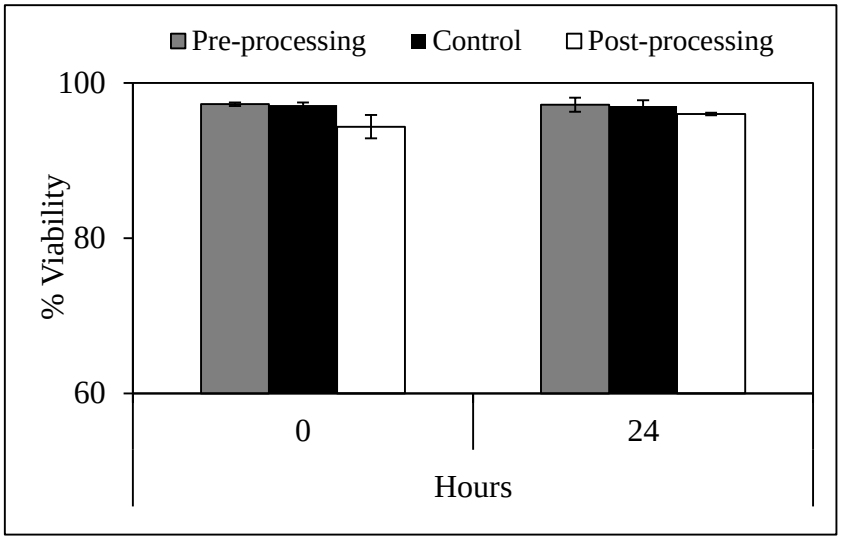

Figure 3.17: Membrane processing of feed ('*N*' = 6,000 rpm, 'γ' = 44,000 s^{-1}) HCA2 cells – effect of cell ageing on the percentage viability of cellular suspension as recorded by trypan blue exclusion. Table below shows mean of raw data determined by trypan blue exclusion for percentage viability. To note results for fresh cells presented in this figure are as presented in Figure 3.5 for low disc speed. A non-sheared control held in a centrifuge tube concurrently, 21 ± 1ºC, for the duration of the experiment was used to measure trypan blue pre and post-processing for 0 and 24 hours cell ageing. Trypan blue exclusion indicates that there is no significant drop in percentage viability after processing at a 0 and 24 hours cell ageing. Data shown are mean values ± 1 s.d. (j = 5; n = 4).

	% ± 1 s.d. (j = 5; n = 4)		
	% Viability		
Cell ageing (hrs)	**Pre-processing**	**Control**	**Post-processing**
0	97.3 ± 0.2	97.2 ± 0.3	94.4 ± 1.5
24	97.2 ± 0.9	97.0 ± 0.8	96.0 ± 0.2

3.5 Effect of cell concentration on HCA2 fibroblasts

As part of downstream processing operations, key requirements such as achieving a broad range of cell concentrations should be considered (Pattasseril et al. 2013). These concentrations could range from 1-2x10^6 cells mL^{-1} to 100x10^6 cells mL^{-1} (Pattasseril et al. 2013). This high concentration factor will have an impact on the properties of the cellular suspension, such as an increase in the viscosity. The change in fluid properties will therefore have an effect on key processing parameters such as shear stress or shear rate and these will vary according to the mathematical relationship previously described in Chapter 1, section 1.5.

Ma et al. (2010) developed a specific CFD model for the USD membrane separation device to determine the relationship between fluid viscosity and rotating speed and the resultant shear rate. From these values, the average shear stress may be estimated as the product of shear rate and viscosity. This simulation was run and adapted by Dr. Spyridon Gerontas at varying disc speeds and viscosities. He found that increasing the viscosity of the suspension decreased the average shear rate for a fixed rotating speed in the USD device. This is presumably due to the decreased recirculation rate or pumping effect of the rotating disc.

In this section, the HCA2 cell lines were processed at fixed high disc speed ('N' = 10,000 rpm), using fresh cells and two concentrations; high cell concentration of ~50 x 10^6 cells mL^{-1} which translates to a shear stress of 176 Pa ($\mu \approx 2.03$ mPa s) and shear rate of 88,000 s^{-1}; and low cell concentration of approximately 2.0 x 10^6 cells

mL^{-1} which translates to a shear stress of 116 Pa ($\mu \approx 1.02$ mPa s) and shear rate of 116,000 s^{-1}.

3.5.1 Physical impact as measured by LDH release

As with the disc speed and cell age experiments, five runs for each low and high cell concentration were carried out and the breakdown of each one is shown in Tables 3.7.A and 3.7.B. The results presented in Table 3.7.A are the same as those presented in Table 3.4.B and are reproduced for convenience. These tables summarize some of the key performance data for the two sets of runs. Each run, A to E, depends on preparation of a new batch of cells. Despite a constant method of preparation used, there will inherently be some variation between batches.

Column 2 presents the measured transmission of LDH through the membrane at the end of each of the 60 minutes shear runs. These are the transmission values that are used for calculations. The mean value for LDH transmission is significantly lower at the higher cell concentration (0.77 ± 0.04 compared with 0.88 ± 0.04) probably due to the lower shear rate over the membrane surface or due to the greater level of membrane fouling species. The average transmission value at high cell concentration and high disc speed is similar to the average transmission value at low cell concentration and low disc speed of 0.78 ± 0.02, which might be a reflection of the similarity in the average shear rates (11,000 s^{-1} and 13,000 s^{-1} respectively).

Column 3 examines the stability of LDH over the period of the membrane study for each run. On average for both cases, the cells might be considered stable for the length of the run. There were two anomalies; Run C for the high cell concentration (Table

3.7.B) and, to a lesser extent, Run D for low cell concentration (Table 3.7.A). Both these runs have slightly higher values of the LDH in the control than that in the retentate pre-processing. However, overall, the averages for low and high cell concentrations were 1.01 ± 0.06 and 0.97 ± 0.06 respectively concluding that the cells might be considered as stable for both cases.

Column 4 examines the total amount of LDH (extracellular and intracellular) measured - i.e. permeate plus retentate – and it is compared with total LDH at the start of the experiment. This helps to check whether all LDH is recovered (none is stuck to membrane) and none is lost through denaturation. For low cell concentration there is a small, but not statistically significant, loss of ~4% of LDH which might be trapped in the membrane or may fall within experimental error. For high cell concentration, there is no loss of LDH.

Finally, column 5 is a second measure of accountability for LDH, comparing the total in the retentate and permeate to the control cells for the duration of the experiment. Again for low cell concentrations there is a small, but not statistically significant, loss of ~5% of LDH and no loss for high cell concentration.

Overall, it can be seen from Tables 3.7.A and 3.7.B that the averages are representative of the runs. Therefore, the average values of the repeats were used to produce Figure 3.18.A. This figure shows the proportion of intracellular LDH remaining with time. The trends seen in this figure show that at a high cell concentration, more cells are damaged than at a low concentration. However, the proportion of intracellular LDH remaining has decreased ~26 ± 1.7% for low cell concentration and ~19 ± 6.1% for high cell

A.	**Low concentration ± 1 s.e. (j = 5; n = 4)**			
1. **Run (‘j’)**	**2.** **‘$T(t_F)$’**	**3.** **‘b/a’**	**4.** **‘$(c+d)/a$’**	**5.** **‘$(c+d)/b$’**
A	0.88 ± 0.08	1.11 ± 0.05	1.03 ± 0.04	0.93 ± 0.04
B	0.91 ± 0.04	0.82 ± 0.01	0.81 ± 0.01	1.00 ± 0.02
C	0.80 ± 0.04	1.01 ± 0.08	0.96 ± 0.06	0.92 ± 0.02
D	0.78 ± 0.06	1.17 ± 0.12	0.95 ± 0.09	0.78 ± 0.02
E	1.02 ± 0.06	0.96 ± 0.03	1.06 ± 0.04	1.10 ± 0.02
Average	**0.88 ± 0.04**	**1.01 ± 0.06**	**0.96 ± 0.04**	**0.95 ± 0.05**

B.	**High concentration ± 1 s.e. (j = 5; n = 4)**			
A	0.65 ± 0.06	0.84 ± 0.04	1.11 ± 0.03	1.34 ± 0.05
B	0.80 ± 0.03	0.95 ± 0.04	1.10 ± 0.02	1.15 ± 0.04
C	0.85 ± 0.07	1.21 ± 0.09	1.03 ± 0.08	0.84 ± 0.03
D	0.83 ± 0.09	0.87 ± 0.07	0.86 ± 0.06	0.96 ± 0.05
E	0.71 ± 0.07	0.99 ± 0.05	0.89 ± 0.04	0.89 ± 0.01
Average	**0.77 ± 0.04**	**0.97 ± 0.06**	**1.00 ± 0.05**	**1.04 ± 0.09**

C.

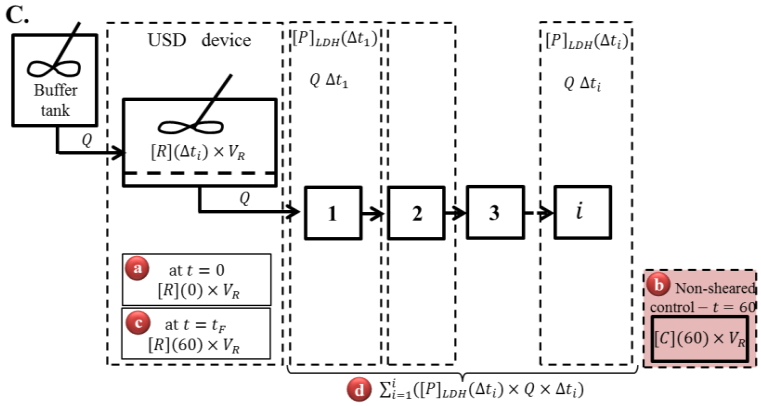

Table 3.7: Membrane processing of feed (‘*N*’ = 10,000 rpm) HCA2 cells – effect of (A) low and (B) high cell concentration on cell damage as recorded by release of LDH. To note results presented in Table 3.7.A are as presented in Table 3.4.B. From left to right columns show; (1) run; (2) transmission coefficient; (3) ratio of intracellular LDH in the control to the intracellular LDH pre-processing in the retentate to evaluate stability of LDH in the cells without processing (where 1 equals to no loss in LDH activity); (4) ratio of the sum of the total LDH in the retentate post-processing and permeate streams to the total LDH in the retentate pre-processing, to evaluate the mass balance agreement (where 1 equals to complete agreement, i.e. all LDH mass is accounted for); (5) ratio of the sum of the total LDH in the retentate post-processing and permeate streams to the total LDH in the control, to evaluate the mass balance agreement assuming the processed cells change as with control.

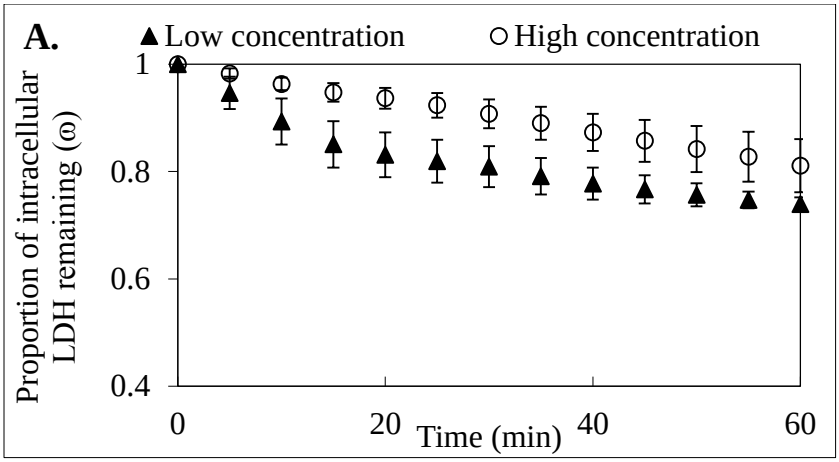

B.

	LDH µU ± 1 s.e. (j = 5; n = 4)			
	Cell concentration	Low concentration		
Sample	**Notation**	**Measured total (‘LDH_TOT’)**	**Measured external (‘LDH_EXT’)**	**Predicted internal (‘LDH_INT’)**
Pre-processing	(a) ‘$R(0) = [R](0) \times V_R$’	**25.09 ± 0.91**	0.73 ± 0.14	24.36 ± 1.03
Control	(b) ‘$C(60) = [C](60) \times V_R$’	**25.73 ± 1.78**	1.06 ± 0.33	24.68 ± 1.75
Post-processing	(c) ‘$R(60) = [R](60) \times V_R$’	15.70 ± 1.08	0.62 ± 0.23	15.08 ± 1.05
Permeate	(d) ‘$\sum_{i=1}^{i} P_{LDH}(\Delta t_i)$’	8.37 ± 0.49		
Post-processing + Permeate	(c) + (d) ‘$[R](60) \times V_R + \sum_{i=1}^{i}([P]_{LDH}(\Delta t_i) \times Q \times \Delta t_i)$’	**24.07 ± 1.17**	8.99 ± 0.65	15.08 ± 1.05

C.

	Cell concentration	High concentration		
Sample	**Notation**	**Measured total (‘LDH_TOT’)**	**Measured external (‘LDH_EXT’)**	**Predicted internal (‘LDH_INT’)**
Pre-processing	(a) ‘$R(0) = [R](0) \times V_R$’	**572.9 ± 33.0**	20.4 ± 4.5	552.5 ± 34.2
Control	(b) ‘$C(60) = [C](60) \times V_R$’	**564.0 ± 50.4**	26.3 ± 6.5	537.7 ± 44.5
Post-processing	(c) ‘$R(60) = [R](60) \times V_R$’	439.7 ± 22.0	12.1 ± 1.4	427.6 ± 22.9
Permeate	(d) ‘$\sum_{i=1}^{i} P_{LDH}(\Delta t_i)$’	111.9 ± 17.5		
Post-processing + Permeate	(c) + (d) ‘$[R](60) \times V_R + \sum_{i=1}^{i}([P]_{LDH}(\Delta t_i) \times Q \times \Delta t_i)$’	**551.6 ± 5.2**	124.0 ± 18.3	427.6 ± 22.9

Figure 3.18: Membrane processing of feed (0 hours cell ageing, ‘*N*’ = 10,000 rpm) HCA2 cells – effect of cell concentration on cell damage as recorded by (A) release of LDH. Tables (B) and (C) show the mean LDH data for all streams including both external and total measurements. To note results presented in Figure 3.18 (Table B) are as presented in Figure 3.2 (Table C). A non-sheared control held in a centrifuge tube concurrently, at 21 ± 1 ºC, for the duration of the experiment was used to measure LDH before and after processing. Figure (A) shows the proportion of intracellular LDH remaining (‘ω’, Eq 3.8), for low (~2x10^6 cells mL^{-1}, ○) and high (~50x10^6 cells mL^{-1}, ▲) concentrations. LDH release indicates that after processing the same proportion of intact cells remain after processing at both concentrations. Data shown are mean values ± 1 s.e. (j = 5; n = 4).

concentration. Taking into consideration the experimental errors, the values obtained for the decrease for both cell concentrations overlap. Therefore even though more cells are damaged at high cell concentration, the proportion of intact cells remaining in the USD device appears to be relatively constant and independent of cell concentration.

From Figure 3.18.A, it can be also seen that even though the final proportion of intact cells remaining in the USD device appears to be the same for both concentrations, the profiles of decrease are dissimilar. On the one hand, high cell concentration follows a constant decrease of ~2 ± 0.2% every five minutes. On the other hand, low cell concentration has two different slopes of release of LDH into the permeate stream. During the first 15 minutes of processing, ~15% of the intracellular LDH is collected in the permeate. For the remaining 45 minutes of operation there is a ~1 ± 0.4% decrease in intracellular LDH every 5 minutes of operation.

From Figure 3.18, Tables B and C show the amount of total, extracellular and internal LDH in each of the process streams for low and high cell concentration respectively. The results in Figure 3.18, Table B are the same as those presented in Figure 3.2, Table A. The mass balances for both conditions show that the amount of total LDH in the non-sheared controls held at 21 ± 1ºC in a centrifuge tube for the duration of the experiment, did not decrease. As with the disc speed and cell age investigations, any changes seen can therefore be fully attributed to processing conditions.

It also appears that for both low and high cell concentrations the total amount of LDH in the retentate pre-processing is in good agreement with the total amount of LDH

collected post-processing in both the retentate and in the permeate, as was also previously shown from Tables 3.7.A and 3.7.B.

3.5.2 Physical impact as measured by trypan blue exclusion

The plots shown in Figures 3.19 and 3.20 were used to analyze the impact of a low and a high cell concentration on cell damage as measured by trypan blue exclusion. The results presented for low cell concentration in Figures 3.19 and 3.20 are the same as those presented in Figures 3.4 and 3.5 for high disc speed ('N' = 10,000 rpm) and are reproduced for convenience. Figure 3.19 shows the concentration of total and viable cells for pre-processing, control and post-processing samples for low cell concentration (Figure 3.19.A) and high cell concentration (Figure 3.19.B). At low cell concentration there is a ~15% ($p = 0.051$) decrease in the population of total cells and lower decrease of ~8% ($p = 0.167$) at high cell concentration. There is also a ~25% decrease in the population of viable cells ($p = 0.003$) at low cell concentration and a lower decrease of ~8% ($p = 0.159$) at high cell concentration. The only significant change ($p < 0.01$) noted is the ~25% decrease in the concentration of viable cells at low cell concentration.

Figure 3.20 shows the percentage viability for pre-processing, control and post-processing samples for both cell concentrations. Analysis of this figure shows that low cell concentration resulted in a significant ~10% ($p = 0.001$) drop in percentage viability post-processing compared to a minimal and not significant drop ~1% in percentage viability at high cell concentration. Therefore, these results suggest that operating at low cell concentration resulted in a generally poorer quality (lower percentage viability) cellular suspension post-processing as measured by trypan blue

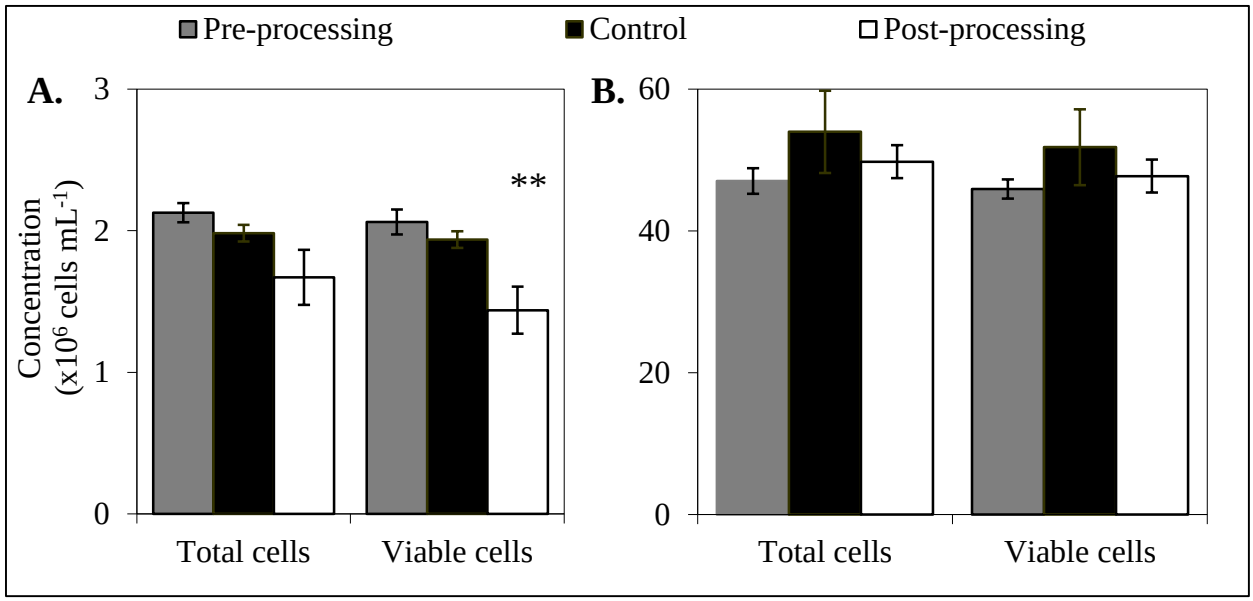

Figure 3.19: Membrane processing of feed ('*N*' = 10,000 rpm) HCA2 cells – effect of cell concentration on cell damage shown by total and viable cell concentrations pre and post-processing of the cellular suspension as recorded by trypan blue exclusion. Table below shows mean of raw data determined by trypan blue exclusion for concentration of total and viable cells. A non-sheared control held in a centrifuge tube concurrently, 21 ± 1ºC, for the duration of the experiment was used to measure trypan blue pre and post-processing for both low and high cell concentration. To note results for low cell concentration presented in this figure are as presented in Figure 3.4 for high disc speed. Trypan blue exclusion indicates that processing at low cell concentration resulted in ~25% reduction of viable cells compared to ~8% at high cell concentration. Significant changes between non-sheared control and post-processing (*p<0.5, **p<0.01, ***p<0.001). Data shown are mean values ± 1 s.d. (j = 5; n = 4).

	Concentration ($x10^6$ cells mL^{-1}) ± 1 s.d. (j = 5; n = 4)					
	Total cells			Viable cells		
Concentration	Control	Pre-processing	Post-processing	Control	Pre-processing	Post-processing
Low	1.98 ± 0.06	2.13 ± 0.07	1.67 ± 0.19	1.94 ± 0.06	2.06 ± 0.09	1.44 ± 0.17
High	54.0 ± 5.8	47.1 ± 1.8	49.8 ± 2.3	51.8 ± 5.3	45.9 ± 1.4	47.8 ± 2.3

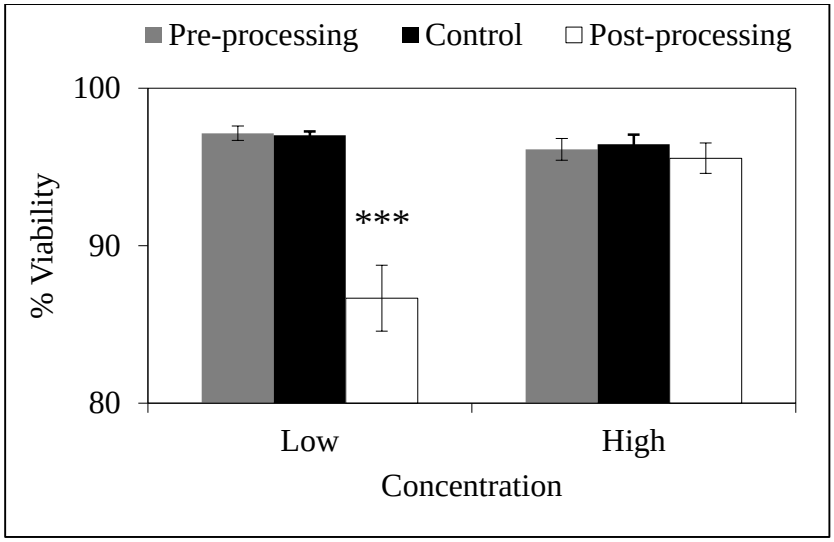

Figure 3.20: Membrane processing of feed ('*N*' = 10,000 rpm) HCA2 cells – effect of cell concentration on percentage viability of cellular suspension as determined by trypan blue exclusion. The figure shows percentage viability before and after membrane processing as determined by trypan blue exclusion. Table below shows mean of raw data determined by trypan blue exclusion for percentage viability. To note results for low cell concentration presented in this figure are as presented in Figure 3.5 for high disc speed. Trypan blue exclusion indicates that at low cell concentration there is a ~10% drop in percentage viability after membrane processing compared to no drop after processing at a higher cell concentration. Data shown are mean values ± 1 s.d. (*p<0.5, **p<0.01, ***p<0.001; j = 5; n = 4).

	% ± 1 s.d. (j = 5; n = 4)		
	% Viability		
Concentration	**Control**	**Pre-processing**	**Post-processing**
Low	97.0 ± 0.3	97.1 ± 0.5	86.7 ± 2.1
High	96.5 ± 0.6	96.1 ± 0.7	95.6 ± 1.0

exclusion. The loss of viable cells is due largely to loss of membrane integrity but there is some evidence also for cell destruction (i.e. the proportion of viable cells lost is bigger than the loss of viability).

3.6 Chapter discussion

Having processed the human fibroblast cell line under different operating conditions using the USD membrane separation device, this chapter established a level of understanding concerning the type of processing stresses that lead to cell death. The design space investigated in this chapter for various bioprocessing factors such as (i) disc speed, (ii) cell age and (iii) cell concentration (viscosity) assess extreme processing conditions with the aim of identifying a window of operation for the production and recovery of high quality human cells.

For the first condition investigated, i.e. disc speed (shear rate), both physical and biological characterization of the cells were carried out. Investigation confirmed that the decrease in the proportion of intracellular LDH remaining in the USD membrane separation device throughout operation was higher at high disc speed than at low disc (~30% compared to ~8%). Trypan blue exclusion also revealed a higher decrease in the population of viable cells at high disc speed than at low disc speed (~25% compared to no drop). Moreover, high disc speed resulted in a significant drop of ~10% in percentage viability post-processing compared to no drop at a low disc speed. Rate constants for cell damage were calculated to further assess the impact of disc speed on cell damage as measured by the two analytical techniques described. Both techniques

indicated that damage at higher disc speeds occurs five times faster than at low disc speed. Moreover, LDH release is twice as sensitive as trypan blue exclusion data.

Preliminary studies were also performed to evaluate CQAs including morphology, growth profiles and specific growth rates as well as cell death induction. Morphological analysis of cells in suspension revealed the appearance of elongated and 'blebby' cells immediately post-processing, most of which disappear after a 2 hour hold. The observed trend was more apparent when operating at high disc speed than at low disc speed. Literature reveals that 'blebbing' can be indicative of programmed cell death but can also can resolve itself once the actin cytoskeleton is restored (Kumar et al. 2007). Assessment of the growth curves indicated that both processed samples retained the ability to grow and proliferate after being exposed to shear for 60 minutes. Both displayed very similar profiles over the course of the initial 48 hours of the study, exhibiting a lower rate of growth when compared to the non-processed control. However, by the 72 hour time point, the sample processed at low disc speed proliferated at the same rate as the non-sheared control sample, which was not the case for the sample processed at high disc speed. The information gathered serves as an indication that differences in growth rates exist between samples sheared at varying disc speeds although a larger sample and more testing would be required in order to draw firm conclusions. Cell death analysis confirmed increased damage at higher shear rate by the appearance of apoptotic and necrotic cell populations. It is therefore evident that, overall, all findings indicate that harsher operating conditions not only caused more damage to the cellular population being processed but also resulted in a generally poorer quality (lower percentage viability) cellular suspension post-processing. Although

trypan blue exclusion is a rapid and powerful technique, it does not offer the same level of detail as the cell death assay which can offer useful insight into the quality of cells post-processing.

The second operating condition investigated was cell age prior to processing, i.e. processing of fresh cells versus cells held for 24 hours. On the one hand, LDH data indicated that ageing the cells led to an overall weaker cellular population, twice as susceptible to shear forces during processing (~15% compared to ~8%). On the other hand, trypan blue data indicated that both fresh cells and those aged for 24 hours have comparable results with a small (< 2%) and insignificant drop in cell viability. The difference may be due to the difference in sensitivity of both measurements and the small magnitudes of damage measured.

The third and final parameter investigated in this chapter was low and high cell concentrations (~$2x10^6$ and ~$50x10^6$ cells mL^{-1}). At low concentration there is ~25% cell loss as recorded both by LDH release and loss of viable cells as measured by trypan blue exclusion. The majority of this loss is most likely due to loss of membrane integrity but there is some evidence to suggest that a proportion of the loss may be due to total cell destruction. At high concentration there is ~17% cell loss as recorded by LDH release but losses as measured by cell counts (total or viable) appear to be significantly less (maximum ~10%). However, when considering the errors measured for LDH release, a constant proportion of cells appear to have been recovered at both concentrations. It should however be noted that the absolute level of damage recorded is

significantly more at higher cell concentration (i.e. the total cells lost as opposed to the proportion of cells lost).

The findings of the investigation of the processing variables using the HCA2 cell line led to the desire to gain more understanding on the translation to other clinically relevant cell lines. The following chapter will utilize the analytical techniques developed in this chapter for the evaluation of neural stem cells and prostate carcinoma cells.

Chapter 4. The physical impact of processing on loss of intact cells for CTX0E03 and P4E6 cell lines

4.1 Introduction

Understanding and defining the mechanical properties of various candidate cell lines may facilitate the design of robust bioprocessing steps, allowing not only the generation of cells of reproducible quality and efficacy, but also rejecting inappropriate cell candidates prior to the clinical manufacturing stage (Acosta-Martinez et al. 2010). USD tools may be used at early discovery stage to gain an indication of the properties of different cell lines (Acosta-Martinez et al. 2010; Delahaye 2013).

The methods developed with the human fibroblast candidates are evaluated for two other whole cell therapies; a neural stem cell line (CTX0E03) and one of three cell lines in a prostate cancer whole cell therapy (P4E6 cell line). The CTX0E03 cell line, currently undergoing Phase II clinical trials for the treatment of debilitated stroke victims, was kindly provided by ReNeuron Group plc. The P4E6 cell line is a prostate carcinoma cell line derived from an early prostate cancer biopsy and was kindly provided by Onyvax Ltd. The effect on cell damage of the same three processing parameters as previously studied (disc speed, cell ageing and cell concentration) is investigated in this chapter for the two cell lines above described. For the CTX0E03 cell line, both LDH and trypan blue measurements are shown. For P4E6 cell line, only trypan blue analysis is given. This is because the experiments carried out with the P4E6 cells were prior to the ones with the HCA2 cells used to develop and optimize the LDH measurements and therefore the LDH data collected for P4E6 cell line is considered insufficient for analysis (no transmission measurements available).

4.2 Effect of disc speed on CTX0E03 and P4E6 cell lines

The impact of low and high disc speeds (6,000 and 10,000 rpm respectively) using CTX0E03 and P4E6 cell lines was investigated in a similar fashion to HCA2 cell line. However, unlike the five runs carried out for the HCA2 cell line, for each of the CTX0E03 and P4E6 cell lines three repeats for each condition were carried out.

4.2.1 Physical impact as measured by LDH release

Tables 4.1.A and 4.1.B summarize some of the key performance data for the two sets of runs for low and high disc speeds respectively. Each run, A to C, was from a new batch of cells prepared using the same method.

Column 2 presents the measured transmission of LDH through the membrane at the end of each of the 60 minutes shear runs. These are the transmission values that are used for calculations. The mean value for LDH transmission is significantly lower at the low disc speed (0.78 ± 0.03 compared with 0.87 ± 0.04) probably due to the lower shear rate over the membrane surface. These values are similar to the transmission values measured with the HCA2 cells at low and high disc speeds (0.78 ± 0.02 and 0.88 ± 0.04 respectively; Table 3.4).

Column 3 demonstrates the stability of LDH over the period of the membrane study for each run. For both low and high disc speed there is a small and probably insignificant drop of ~3 and ~8% respectively. Hence, the cells are considered stable for the length of the run (as for HCA2 fibroblasts, Table 3.4).

Column 4 shows the total amount of LDH (extracellular and intracellular) measured - i.e. permeate plus retentate – and it is compared with total LDH at the start of the experiment. This helps to check whether all LDH is recovered (none is stuck to membrane) and none is lost through denaturation. For both disc speeds there is a small, but not statistically significant, loss of LDH (~2% and ~6% respectively) which might be trapped in the membrane.

Finally, column 5 is a second measure of accountability for LDH comparing the total in the retentate and permeate to the control cells for the duration of the experiment. In this case for both disc speeds there is no loss of LDH, averaging 1.02 ± 0.10 and 1.02 ± 0.06 for low and high disc speed respectively.

Overall, it can be seen from Tables 4.1.A and 4.1.B that the averages are representative of the runs. The average values of the repeats were used to produce Figure 4.1 to analyze the impact of low and high disc speed on cell damage as measured by LDH release for the CTX0E03 cell line. Processing at low and high disc speeds caused a decrease of ~50 – 60% after 60 minutes in each case. These results suggest that CTX0E03 cells are more shear sensitive than HCA2 cells. In Chapter 3 Section 3.3, it was shown that for the HCA2 fibroblasts the proportion of intracellular LDH remaining with time decreased ~8% at a low disc speed and by ~30% at a high disc speed.

Moreover, these findings also suggest that the damage caused to this particular cell line is mainly dependent on the experience of being exposed to shear forces and the time of exposure and less so by the magnitude of the shear forces. Previous studies conducted by Acosta-Martinez (2011) somehow reinforce CTX0E03 cells being damaged mainly by

A.	**6,000 rpm ± 1 s.e. (j = 3; n = 4)**			
1. **Run (‘j’)**	**2.** **‘$T(t_F)$’**	**3.** **‘b/a’**	**4.** **‘$(c+d)/a$’**	**5.** **‘$(c+d)/b$’**
A	0.77 ± 0.03	1.11 ± 0.01	1.17 ± 0.02	1.05 ± 0.02
B	0.73 ± 0.10	1.02 ± 0.02	0.85 ± 0.03	0.83 ± 0.03
C	0.84 ± 0.07	0.80 ± 0.01	0.94 ± 0.01	1.17 ± 0.01
Average	**0.78 ± 0.03**	**0.97 ± 0.09**	**0.98 ± 0.10**	**1.02 ± 0.10**

B.	**10,000 rpm ± 1 s.e. (j = 3; n = 4)**			
A	0.92 ± 0.03	0.82 ± 0.02	0.88 ± 0.01	1.07 ± 0.01
B	0.88 ± 0.05	0.99 ± 0.02	1.08 ± 6.43	1.09 ± 0.00
C	0.79 ± 0.12	0.96 ± 0.02	0.86 ± 0.01	0.89 ± 0.01
Average	**0.87 ± 0.04**	**0.92 ± 0.05**	**0.94 ± 0.07**	**1.02 ± 0.06**

C.

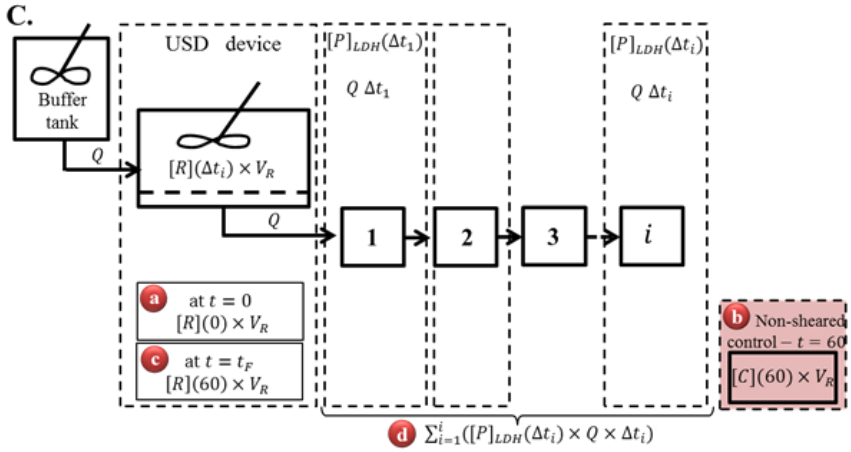

Table 4.1: Membrane processing of feed (0 hour cell ageing) CTX0E03 cells – effect of (A) 6,000 and (B) 10,000 rpm on cell damage as recorded by release of LDH. (C) Shows a box diagram of the USD membrane separation device including all process streams. From left to right columns show; (1) run; (2) transmission coefficient; (3) ratio of internal LDH in the control to the internal LDH pre-processing in the retentate to evaluate stability of LDH in the cells without processing (where 1 equals to no loss in LDH activity); (4) ratio of the sum of the total LDH in the retentate post-processing and permeate streams to the total LDH in the retentate pre-processing, to evaluate the mass balance agreement (where 1 equals to complete agreement, i.e. all LDH mass is accounted for); (5) ratio of the sum of the total LDH in the retentate post-processing and permeate streams to the total LDH in the control, to evaluate the mass balance agreement assuming the processed cells change as with control (j = 3; n = 4).

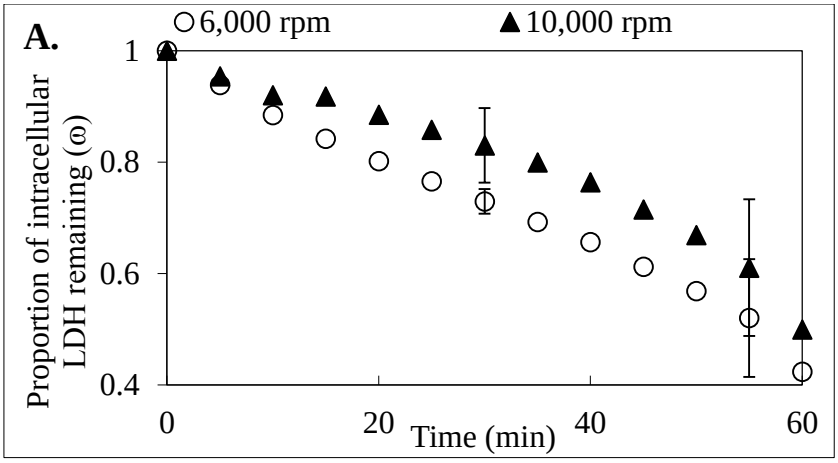

B.

	LDH µU ± 1 s.e. (j = 3; n = 4)			
	Disc speed	**6,000 rpm**		
Sample	**Notation**	**Total ('*LDH_TOT*')**	**Extracellular ('*LDH_EXT*')**	**Predicted internal ('*LDH_INT*')**
Pre-processing	(a) '$R(0) = [R](0) \times V_R$'	**17.16 ± 0.97**	1.26 ± 0.22	15.89 ± 0.75
Control	(b) '$C(60) = [C](60) \times V_R$'	**16.60 ± 1.20**	1.12 ± 0.38	15.48 ± 1.36
Post-processing	(c) '$R(60) = [R](60) \times V_R$'	6.99 ± 1.72	0.88 ± 0.21	6.11 ± 1.92
Permeate	(d) '$\sum_{i=1}^{i} P_{LDH}(\Delta t_i)$'	9.70 ± 1.11		
Post-processing + Permeate	(c) + (d) '$[R](60) \times V_R + \sum_{i=1}^{i}([P]_{LDH}(\Delta t_i) \times Q \times \Delta t_i)$'	**16.69 ± 0.68**	10.58 ± 1.32	6.11 ± 1.92

C.

	Disc speed	**10,000 rpm**		
Sample	**Notation**	**Total ('*LDH_TOT*')**	**Extracellular ('*LDH_EXT*')**	**Predicted internal ('*LDH_INT*')**
Pre-processing	(a) '$R(0) = [R](0) \times V_R$'	**12.96 ± 1.03**	0.91 ± 0.37	12.05 ± 0.66
Control	(b) '$C(60) = [C](60) \times V_R$'	**12.06 ± 1.50**	0.95 ± 0.41	11.12 ± 1.24
Post-processing	(c) '$R(60) = [R](60) \times V_R$'	4.44 ± 0.48	1.01 ± 0.40	3.43 ± 0.73
Permeate	(d) '$\sum_{i=1}^{i} P_{LDH}(\Delta t_i)$'	7.71 ± 1.16		
Post-processing + Permeate	(c) + (d) '$[R](60) \times V_R + \sum_{i=1}^{i}([P]_{LDH}(\Delta t_i) \times Q \times \Delta t_i)$'	**12.15 ± 1.24**	8.72 ± 1.54	3.43 ± 0.73

Figure 4.1: Membrane processing of feed (0 hour cell ageing) CTX0E03 cells – effect of disc speed on (A) cell damage as recorded by release of LDH. Tables (B) and (C) show mean LDH data for all streams including both external and total measurements at 6,000 rpm and 10,000 rpm ('γ' = 44,000 and 116,000 s^{-1} respectively). A non-sheared control held in a centrifuge tube concurrently, 21± 1ºC, for the duration of the experiment was used to measure LDH pre and post-processing. Figure (A) shows the proportion of intracellular LDH remaining ('ω', Eq 3.8), for 6,000 rpm (○) and 10,000 rpm (▲) at a concentration of ~1.5x10^6 total cells mL^{-1}. Both disc speeds resulted in a ~50-60 % reduction of viable cells as measured by LDH release. Data shown are mean values ±1s.e. (j=3;n=4).

exposure to shear forces rather than by the magnitude of these forces. His studies describe a controlled flow through an USD capillary device where cells are exposed to several defined hydrodynamic stresses. He concluded that the variable with the largest impact on the final cell integrity of the CTX0E03 population was the number of passes through a capillary device. For other cell lines in his study (prostate cancer OnyCap23 and P4E6 cell lines), flow rate and length of the capillary had had the largest impact on cell integrity. For Acosta-Martinez (2011), this finding suggested that CTX0E03 cells were therefore mainly affected by the experience of being exposed to an elongational stress event and less so by the time spent inside the capillary or the magnitude of this stress.

From Figure 4.1, Tables B and C show the average values for the three runs of the amount of total, extracellular and internal LDH in each of the process streams for low and high disc speeds respectively. For both disc speed conditions, the mass balances show that the amount of total LDH in the non-sheared controls held at 21 ± 1ºC in a centrifuge tube for the duration of the experiment, within experimental error can be considered as stable (low disc speed shows ~6% loss of LDH which is not statistically significant and can be attributed to experimental error).

Moreover, for both disc speeds the total mass of LDH collected in the permeate plus the total amount collected in the retentate post-processing is in agreement with the total amount pre-processing as was shown from Tables 4.1.A and 4.1.B.

4.2.2 Physical impact as measured by trypan blue exclusion

The plots in this section show the impact of low and high disc speed on cell damage as measured by trypan blue exclusion for CTX0E03 (Figures 4.2 and 4.3) and P4E6 (Figures 4.4 and 4.5) cell lines.

Figure 4.2 shows the average concentration of total and viable CTX0E03 cells as measured by trypan blue exclusion for the three repeats at each of both disc speeds. Analysis of this figure shows that there is a significant decrease in the population of viable cells of ~42% ($p = 0.002$) at a low disc speed and ~47% ($p = 0.001$) at high disc speed. Figure 4.3 shows the percentage viability of CTX0E03 cells for pre-processing, control and post-processing samples for both disc speeds. From this figure it can be seen that there is a significant drop in the percentage viability at both low and high disc speeds of ~17% ($p = 0.01$) and ~14% ($p = 0.001$) respectively. Therefore, these results suggest that comparable amounts of cell damage were observed at both disc speeds.

Processing for 60 minutes caused in both cases a high proportion of viable cells lost as well as a generally poor quality (low percentage viability of ~76%) cellular suspension post-processing. At both disc speeds there is ~50% cell loss as recorded both by LDH release and loss of viable cells. The loss of viable cells is due largely to loss of membrane integrity but there is some evidence for both cell destruction (i.e. the proportion of viable cells lost is bigger than the loss of viability).

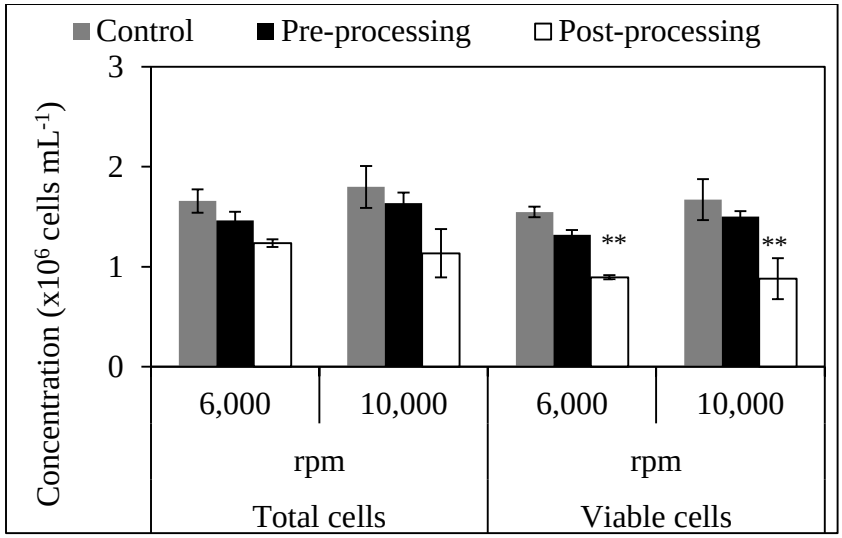

Figure 4.2: Membrane processing of feed (0 hour cell ageing) CTX0E03 cells – effect of disc speed on cell damage shown by total and viable cell concentrations pre and post-processing of the cellular suspension as recorded by trypan blue exclusion. Table below shows mean of raw data determined by trypan blue exclusion for concentration of total and viable cells. A non-sheared control held in a centrifuge tube concurrently, 21 ± 1ºC, for the duration of the experiment was used to measure trypan blue pre and post-processing for both 6,000 and 10,000 rpm ('γ' = 44,000 and 116,000 s^{-1} respectively). Trypan blue exclusion indicates that processing at both low and high disc speed resulted in ~50% reduction of viable cells. Significant changes between non-sheared control and post-processing (*p<0.5, **p<0.01, ***p<0.001). Data shown are mean values ± 1 s.d. (j = 3; n =4).

	Concentration (x10^6 cells mL^{-1}) ± 1 s.d. (j = 3; n =4)					
	Total cells ('$_{TB\_TOT}$')			**Viable cells ('$_{TB\_VC}$')**		
Disc speed (rpm)	**Pre-processing**	**Control**	**Post-processing**	**Pre-processing**	**Control**	**Post-processing**
6,000	1.46 ± 0.09	1.66 ± 0.12	1.24 ± 0.04	1.32 ± 0.05	1.55 ± 0.05	0.90 ± 0.02
10,000	1.64 ± 0.10	1.80 ± 0.21	1.14 ± 0.24	1.50 ± 0.06	1.67 ± 0.15	0.88 ± 0.14

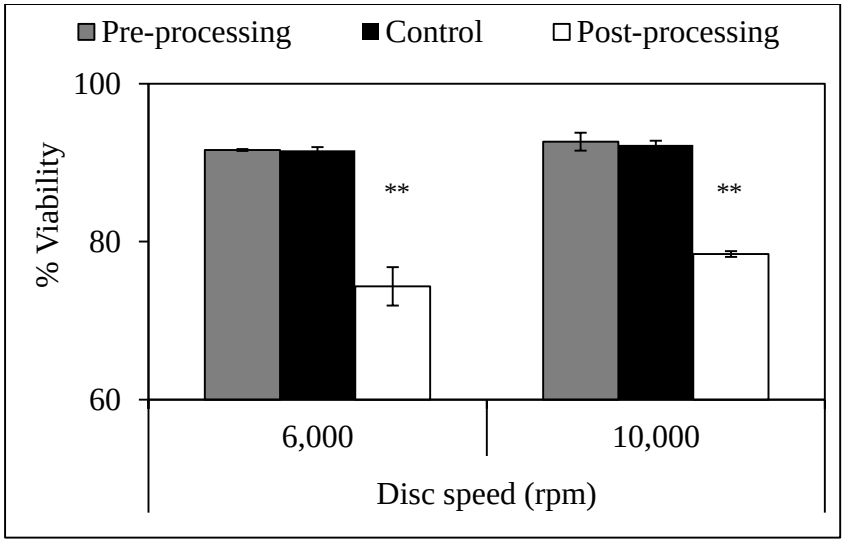

Figure 4.3: Membrane processing of feed (0 hour cell ageing) CTX0E03 cells – effect of disc speed on percentage viability of the cellular suspension as recorded by trypan blue exclusion. Table below shows mean of raw data determined by trypan blue exclusion for percentage viability. A non-sheared control held in a centrifuge tube concurrently, 21 ± 1ºC, for the duration of the experiment was used to measure trypan blue pre and post-processing for both 6,000 and 10,000 rpm ('γ' = 44,000 and 116,000 s^{-1} respectively). Trypan blue exclusion indicates that processing resulted in a significant drop in percentage viability compared to the pre-processed sample, both at low disc speed (~17% drop, p = 0.01) and high disc speed (~14% drop, p = 0.001). Significant changes between non-sheared control and post-processing (*p<0.5, **p<0.01, ***p<0.001). Data shown are mean values ± 1 s.d. (j = 3; n = 4).

	% ± 1 s.d. (j = 3; n = 4)		
	% Viability		
Disc speed (rpm)	**Pre-processing**	**Control**	**Post-processing**
6,000	91.6 ± 0.1	91.6 ± 0.4	74.3 ± 2.4
10,000	92.6 ± 1.1	92.2 ± 0.5	78.4 ± 0.4

Figure 4.4 shows the average concentration of P4E6 total and viable cells as measured by trypan blue exclusion for the three repeats at each of both disc speeds. At low disc speed there is a significant decrease in the population of viable cells of ~18% ($p = 0.001$) and ~41% ($p = 4.05x10^{-5}$) at high disc speed. Moreover, from Figure 4.5 which shows the percentage viability as measured by trypan blue exclusion, there is a non-significant drop in the percentage viability of ~1% ($p = 0.263$) at low disc speed and a low, yet significant, ~3% ($p = 0.008$) drop at high disc speed.

Therefore, these results indicate that harsher operating conditions resulted mainly in a higher proportion of cells lysed after 60 minutes of operation and to a lesser extent in a drop in percentage viability of the cellular suspension post-processing. However, unlike for the HCA2 cell line, significant cell damage for P4E6 cells was also observed at low disc speed, indicating P4E6 cells are more shear sensitive than HCA2 fibroblasts but less than CTX0E03.

4.3 Effect of cell age on CTX0E03 and P4E6 cell lines

The impact of cell age, using fresh cells and cells aged for 24 hours, on the two cell lines (CTX0E03 and P4E6) was investigated in a similar fashion to HCA2 cell line. Three repeats for each condition were carried out for each cell line.

For the CTX0E03 cell line, both LDH release and trypan blue exclusion measurements will be shown, whereas for P4E6 cell line, only trypan blue analysis will be given. This is because the experiments carried out with the P4E6 cells were completed before the protocol for balancing using LDH analysis had been established.

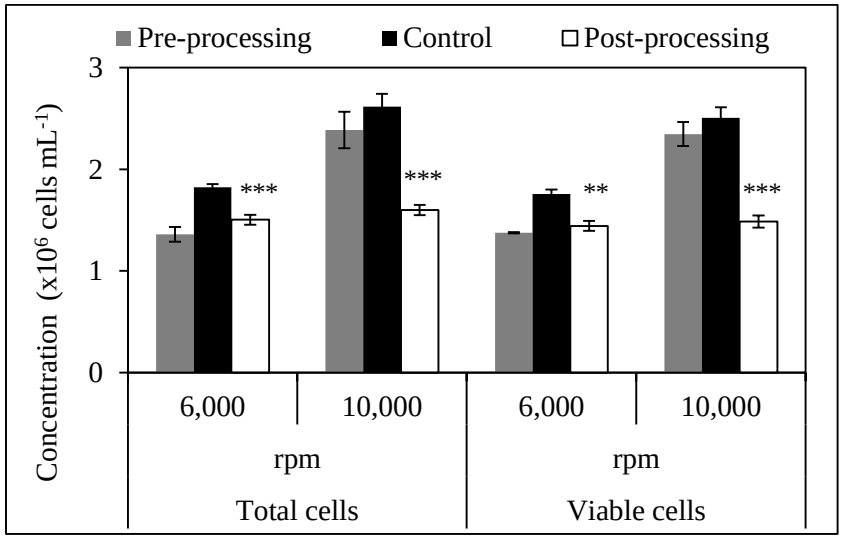

Figure 4.4: Membrane processing of feed (0 hour cell ageing) P4E6 cells – effect of disc speed on cell damage shown by total and viable cell concentrations pre and post-processing of the cellular suspension as recorded by trypan blue exclusion. Table below shows mean of raw data determined by trypan blue exclusion for concentration of total and viable cells. A non-sheared control held in a centrifuge tube concurrently, 21 ± 1ºC, for the duration of the experiment was used to measure trypan blue pre and post-processing for both 6,000 and 10,000 rpm ('γ' = 44,000 and 116,000 s^{-1} respectively). Trypan blue exclusion indicates that processing at low disc speed resulted in ~18% reduction of viable cells whereas high disc speed resulted in a ~41% reduction of viable cells. Significant changes between non-sheared control and post-processing (*p<0.5,p<0.01, ***p<0.001). Data shown are mean values ± 1 s.d. (j = 3; n = 4).**

	Concentration ($x10^6$ cells mL^{-1}) ± 1 s.d. (j = 3; n = 4)					
	Total cells			Viable cells		
Disc speed (rpm)	**Pre-processing**	**Control**	**Post-processing**	**Pre-processing**	**Control**	**Post-processing**
6,000	1.36 ± 0.07	1.82 ± 0.03	1.50 ± 0.05	1.38 ± 0.01	1.76 ± 0.05	1.44 ± 0.05
10,000	2.39 ± 0.18	2.62 ± 0.13	1.60 ± 0.05	2.35 ± 0.12	2.51 ± 0.11	1.49 ± 0.06

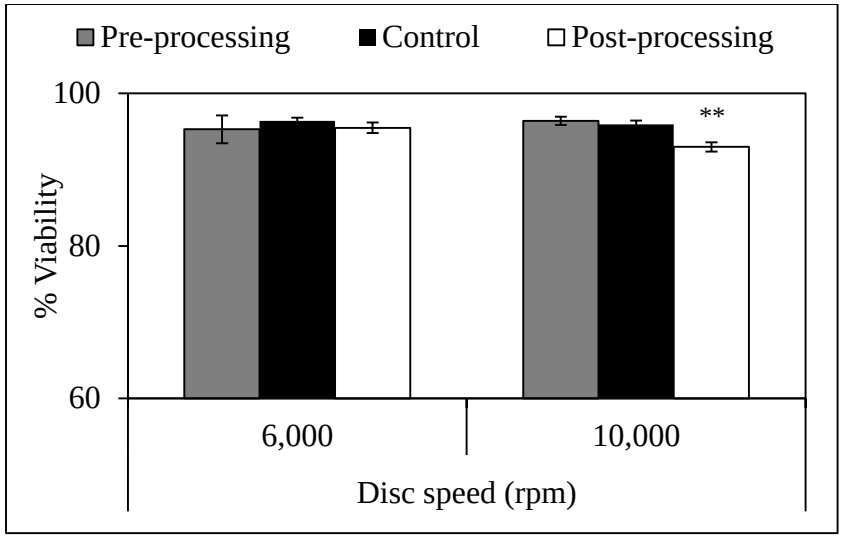

Figure 4.5: Membrane processing of feed (0 hour cell ageing) P4E6 cells – effect of disc speed on percentage viability of the cellular suspension as recorded by trypan blue exclusion. Table below shows mean of raw data determined by trypan blue exclusion for percentage viability. A non-sheared control held in a centrifuge tube concurrently, 21 ± 1ºC, for the duration of the experiment was used to measure trypan blue pre and post-processing for both 6,000 and 10,000 rpm ('γ' = 44,000 and 116,000 s^{-1} respectively). Trypan blue exclusion indicates that processing resulted in a small but significant drop in percentage viability at high disc speed (~3% drop, p = 0.008) and a low but not significant change at low disc speed (~1%). Significant changes between non-sheared control and post-processing (*p<0.5, **p<0.01, ***p<0.001). Data shown are mean values ± 1 s.d. (j = 3; n = 4).

	% ± 1 s.d. (j = 3; n = 4)		
	% Viability		
Disc speeds (rpm)	**Pre-processing**	**Control**	**Post-processing**
6,000	95.3 ± 1.8	96.4 ± 0.4	95.5 ± 0.7
10,000	96.4 ± 0.6	96.0 ± 0.5	93.0 ± 0.6

4.3.1 Physical impact as measured by LDH release

Tables 4.2.A and 4.2.B summarize the key performance data for the runs for fresh cells (aged 0 hours) and cells aged for 24 hours. The results presented in Table 4.2.A are the same as those presented in Table 4.1.A and are reproduced for convenience. Each run, A to C, was from a new batch of cells prepared using the same method. For each cell preparation, enough cells were prepared to run two experiments, one with fresh cells and another with cells aged for 24 hours at 21 ± 1˚C.

Column 2 presents the measured transmission of LDH through the membrane at the end of each of the 60 minutes shear runs. These are the transmission values that are used for calculations. An average value of 0.78 ± 0.03 transmission is observed when using fresh cells and 0.93 ± 0.03 for cells aged for 24 hours.

Column 3 examines the stability of LDH over the period of the membrane study for each run. For both 0 and 24 hours cell ageing cases, there is a small and probably insignificant drop (~3% and ~6% respectively). Hence, the cells are considered as stable for the duration of the experiment (as for HCA2 fibroblasts Table 3.6).

Column 4 examines the total amount of LDH (extracellular and intracellular) measured - i.e. permeate plus retentate – and it is compared with total LDH at the start of the experiment. This helps to check whether all LDH is recovered (none is stuck to membrane) and none is lost through denaturation. For fresh cells there is no loss of LDH with an average value of 0.98 ± 0.10 whereas for cells aged for 24 hours, there is a

significant loss of ~12% ($p = 0.009$) of LDH which might be due to entrapment in the membrane.

Finally, column 5 is a second measure of accountability for LDH comparing the total in the retentate and permeate to the control cells for the duration of the experiment. For the aged cells there is a small, but not statistically significant, loss of LDH of ~6% and there was no loss showed for fresh cells.

Overall, it can be seen from Tables 4.2.A and 4.2.B that the averages are representative of the runs. Therefore, the average values of the repeats were used to produce Figure 4.6.A together with Tables B and C. The results in Figure 4.6, Table A are the same as those presented in Figure 4.1, Table A. Ageing over 24 hours was held the same way and under the same conditions as the control during the membrane study. This resulted in a ~12% ($p = 0.033$) loss of stability from total LDH in the control at 0 hours to the same control at 24 hours (Figure 4.6, 16.60 ± 1.20 from Table B to 14.62 ± 1.73 from Table C). However, by statistical analysis, this loss is classified as not significant.

Figure 4.6 shows the proportion of intracellular LDH remaining with time for the CTX0E03 cell line. From this figure, both 0 and 24 hours cell age caused a decrease of ~50 – 60% after 60 minutes of processing. These findings suggests that the damage caused to this particular cell line is dependent on the experience of being exposed to shear forces and the time of exposure and less so by cell ageing or pre-processing hold times. Previous studies conducted by Delahaye (2013) reinforce this finding. He investigated the effect of resuspension method after centrifugation on percentage loss of intact CTX0E03 cells with pre-process hold times of 5 and 120 minutes. His findings suggest

A.	0 hours ± 1 s.e. (j = 3; n = 4)			
1. Run (‘j’)	2. ‘$T(t_F)$’	3. ‘b/a’	4. ‘$(c+d)/a$’	5. ‘$(c+d)/b$’
A	0.77 ± 0.03	1.11 ± 0.01	1.17 ± 0.02	1.05 ± 0.02
B	0.73 ± 0.10	1.02 ± 0.02	0.85 ± 0.03	0.83 ± 0.03
C	0.84 ± 0.07	0.80 ± 0.01	0.94 ± 0.01	1.17 ± 0.01
Average	**0.78 ± 0.03**	**0.97 ± 0.09**	**0.98 ± 0.10**	**1.02 ± 0.10**

B.	24 hours ± 1 s.e. (j = 3; n = 4)			
A	0.88 ± 0.02	0.82 ± 0.02	0.84 ± 0.03	1.02 ± 0.03
B	0.98 ± 0.12	0.97 ± 0.01	0.89 ± 0.02	0.91 ± 0.02
C	0.94 ± 0.11	1.03 ± 0.02	0.91 ± 0.03	0.88 ± 0.03
Average	**0.93 ± 0.03**	**0.94 ± 0.06**	**0.88 ± 0.02**	**0.94 ± 0.04**

C.

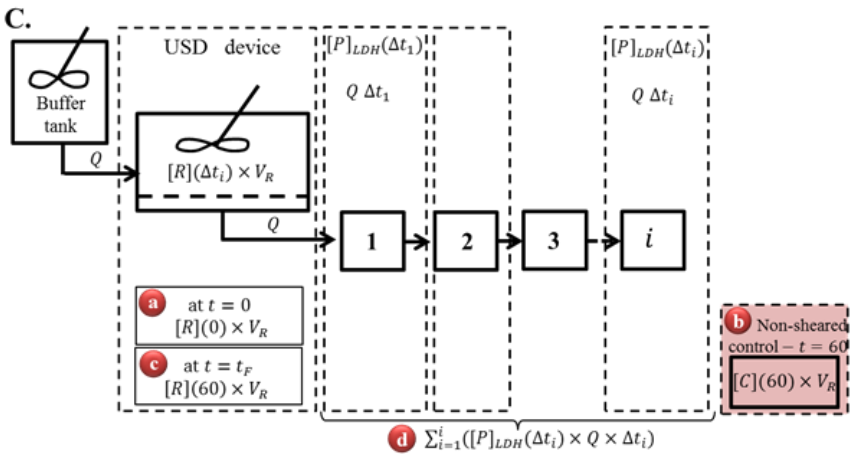

Table 4.2: Membrane processing of feed (‘N’ = 6,000 rpm, ‘γ’ = 44,000 s^{-1}) CTX0E03 cells – effect of (A) 0 and (B) 24 hours cell age on cell damage as recorded by release of LDH. To note results presented in Table 4.2.A are as presented in Table 4.1.A. Box diagram (C) of the USD membrane separation device shows process streams. From left to right columns show; (1) run; (2) transmission coefficient; (3) ratio of internal LDH in the control to the internal LDH pre-processing in the retentate to evaluate stability of LDH in the cells without processing (where 1 equals to no loss in LDH activity); (4) ratio of the sum of the total LDH in the retentate post-processing and permeate streams to the total LDH in the retentate pre-processing, to evaluate the mass balance agreement (where 1 equals to complete agreement, i.e. all LDH mass is accounted for); (5) ratio of the sum of the total LDH in the retentate post-processing and permeate streams to the total LDH in the control, to evaluate the mass balance agreement assuming the processed cells change as with control (j = 3; n = 4).

A.

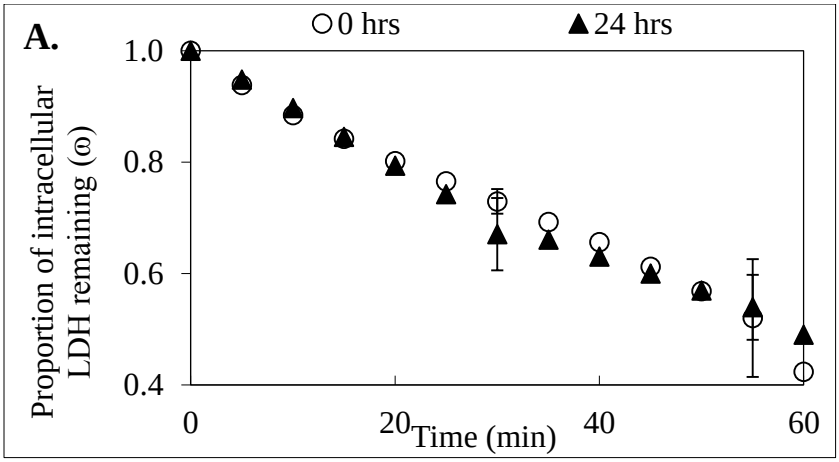

B.

	LDH µU ± 1 s.e. (j = 3; n = 4)			
	Cell ageing (hrs)	**0**		
Sample	**Notation**	**Total ('LDH_TOT')**	**External ('LDH_EXT')**	**Predicted internal ('LDH_INT')**
Pre-processing	(a) '$R(0) = [R](0) \times V_R$'	**17.16 ± 0.97**	1.26 ± 0.22	15.89 ± 0.75
Control	(b) '$C(60) = [C](60) \times V_R$'	**16.60 ± 1.20**	1.12 ± 0.38	15.48 ± 1.36
Post-processing	(c) '$R(60) = [R](60) \times V_R$'	6.99 ± 1.72	0.88 ± 0.21	6.11 ± 1.92
Permeate	(d) '$\sum_{i=1}^{i} P_{LDH}(\Delta t_i)$'	9.70 ± 1.11		
Post-processing + Permeate	(c) + (d) '$[R](60) \times V_R + \sum_{i=1}^{i}([P]_{LDH}(\Delta t_i) \times Q \times \Delta t_i)$'	**16.69 ± 0.68**	10.58 ± 1.32	6.11 ± 1.92

C.

	Cell ageing (hrs)	24		
Sample	**Notation**	**Total ('LDH_TOT')**	**External ('LDH_EXT')**	**Predicted internal ('LDH_INT')**
Pre-processing	(a) '$R(0) = [R](0) \times V_R$'	**15.43 ± 0.95**	1.60 ± 0.20	13.83 ± 0.78
Control	(b) '$C(60) = [C](60) \times V_R$'	**14.62 ± 1.73**	1.87 ± 0.41	12.75 ± 1.55
Post-processing	(c) '$R(60) = [R](60) \times V_R$'	4.47 ± 0.41	0.86 ± 0.10	3.60 ± 0.33
Permeate	(d) '$\sum_{i=1}^{i} P_{LDH}(\Delta t_i)$'	9.08 ± 1.30		
Post-processing + Permeate	(c) + (d) '$[R](60) \times V_R + \sum_{i=1}^{i}([P]_{LDH}(\Delta t_i) \times Q \times \Delta t_i)$'	**13.55 ± 1.08**	9.95 ± 1.28	3.60 ± 0.33

Figure 4.6: Membrane processing of feed ('*N*' = 6,000 rpm, 'γ' = 44,000 s^{-1}) CTX0E03 cells – effect of cell ageing on (A) cell damage as recorded by release of LDH. Tables (B) and (C) show mean LDH data for all streams including both external and total measurements at 0 and 24 hours cell age respectively. To note results presented in Figure 4.6 (Table B) are as presented in Figure 4.1 (Table B). A non-sheared control held in a centrifuge tube concurrently, 21 ± 1ºC, for the duration of the experiment was used to measure LDH pre and post-processing. Figure (A) shows the proportion of intracellular LDH remaining ('ω', Eq 3.8), for 0 (○) and 24 (▲) hours at ~1.5x10^6 cells mL^{-1}. Both conditions resulted in a ~50 - 60 % reduction of viable cells as measured by release of LDH. Data shown are mean values ± 1 s.e. (j = 3; n = 4).

that applying a constant shear environment using automatic resuspension caused equivalent loss independent of pre-process hold times.

From Figure 4.6, Tables B and C show the average values for the three runs of the amount of total, extracellular and internal LDH in each of the process streams for 0 and 24 hours cell age respectively. The mass balances show that the amount of total LDH in the non-sheared controls held at 21 ± 1ºC in a centrifuge tube for the duration of the experiment, did not decrease for either fresh cells or aged cells. However, the total amount of LDH in the retentate pre-processing decreased by ~3% for fresh cells and ~12% for aged cells for 24 hours as was shown from Tables 4.2.

4.3.2 Physical impact as measured by trypan blue exclusion

The plots in this section show the impact of 0 and 24 hours cell age on cell damage as measured by trypan blue exclusion for the CTX0E03 (Figures 4.7 and 4.8) and P4E6 (Figures 4.9 and 4.10) cell lines. The results presented for the fresh cells (i.e. 0 hours cell ageing) for the CTX0E03 cell line in Figures 4.7 and 4.8 are the same as those presented in Figures 4.2 and 4.3 for low disc speed (‘N’ = 6,000 rpm) and are reproduced for convenience. The results presented for the fresh cells (i.e. 0 hours cell ageing) for the P4E6 cell line in Figures 4.9 and 4.10 are the same as those presented in Figures 4.4 and 4.5 for low disc speed (‘N’ = 6,000 rpm) and are reproduced for convenience.

Figure 4.7 shows the average concentration of total and viable CTX0E03 cells as measured by trypan blue exclusion for the three repeats at each of both conditions.

Analysis of this figure shows that there is a significant decrease in the population of viable cells for both fresh cells and cells aged for 24 hours (~42% with $p = 0.002$ and ~57% with $p = 0.006$ respectively). Figure 4.8 shows the percentage viability of CTX0E03 cells for pre-processing, control and post-processing samples for both conditions. There is a significant drop in the percentage viability at both 0 and 24 hours cell ageing of ~17% ($p = 0.005$) and ~23% ($p = 0.001$) respectively is observed. These results suggest that 24 hours cell ageing has led to higher amounts of cell damage and slightly worse quality of cells (lower percentage viability) post-processing.

Figure 4.9 shows the average concentration of total and viable P4E6 cells as measured by trypan blue exclusion for the three repeats at each of both cell age conditions. Analysis of this figure shows that there is a significant decrease in the population of viable cells of ~18% ($p = 0.001$) at 0 hours cell ageing and probably insignificant ~5% ($p = 0.103$) decrease at 24 hours cell ageing. However, when comparing the concentration of total and viable cells from 0 to 24 hours for both the control and the pre-processed samples, there is an evident and statistically significant drop from 0 to 24 hours for all samples. For example, the viable cell concentration for the control decreases by ~16% ($p = 0.005$) from 0 to 24 hours. Similarly, the total cell concentrations for the controls from 0 to 24 hours cell ageing decreases by ~22% ($p = 0.003$). It may be that by holding the cellular suspension for 24 hours, a weaker population of cells was eradicated prior to processing and after 24 hours hold. This weaker population may have been the one damaged during processing at 0 hours cell ageing, which would explain no cell damage after processing for the 24 hours cell age.

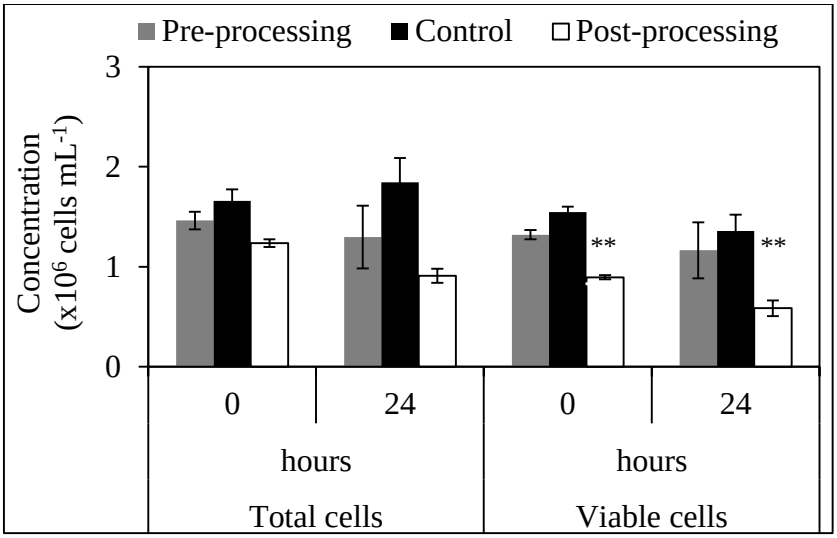

Figure 4.7: Membrane processing of feed ('*N*' = 6,000 rpm, 'γ' = 44,000 s^{-1}) CTX0E03 cells – effect of cell age on cell damage as shown by total and viable cell concentrations pre and post-processing. Table below shows mean of raw data determined by trypan blue exclusion for concentration of total and viable cells for pre and post-processing as well as a non-sheared control. To note results for 0 hours cell age (fresh cells) presented in this figure are as presented in Figure 4.2 for low disc speed. A non-sheared control held in a centrifuge tube concurrently, 21 ± 1ºC, for the duration of the experiment was used to measure trypan blue exclusion pre and post-processing for 0 and 24 hours cell age. Trypan blue exclusion indicates that there is a significant drop in the concentration of viable cells after processing at both a 0 and 24 hours cell ageing of ~42% (p = 0.002) and ~57% (p = 0.006) respectively. Significant changes between non-sheared control and post-processing (*p<0.5, **p<0.01, ***p<0.001). Data shown are mean values ± 1 s.d. (j = 3; n = 4).

	Concentration ($x10^6$ cells mL^{-1}) ± 1 s.d. (j = 3; n = 4)					
	Total cells ('TB_TOT')			**Viable cells ('TB_VC')**		
Cell ageing (hrs)	**Pre-processing**	**Control**	**Post-processing**	**Pre-processing**	**Control**	**Post-processing**
0	1.46 ± 0.09	1.66 ± 0.12	1.24 ± 0.04	1.32 ± 0.05	1.55 ± 0.05	0.90 ± 0.02
24	1.30 ± 0.31	1.85 ± 0.24	0.91 ± 0.07	1.17 ± 0.28	1.36 ± 0.23	0.59 ± 0.11

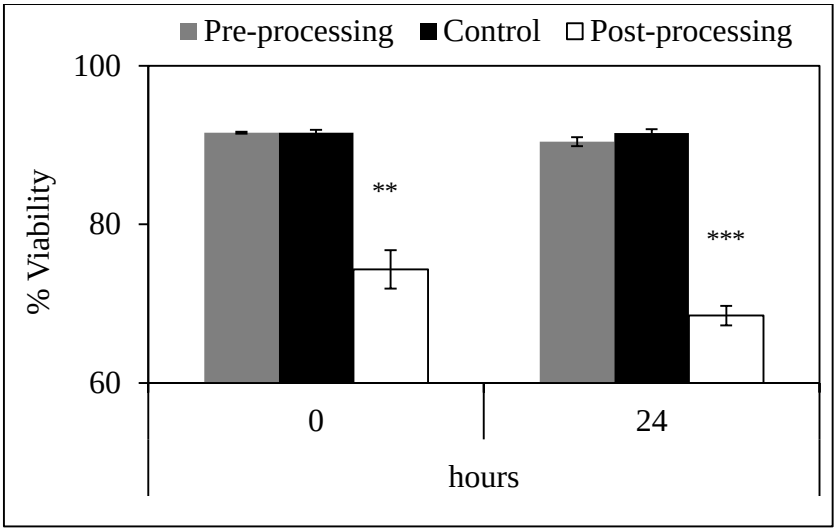

Figure 4.8: Membrane processing of feed ('*N*' = 6,000 rpm, 'γ' = 44,000 s^{-1}) CTX0E03 cells – effect of cell age on the percentage viability of cellular suspension as recorded by trypan blue exclusion. Table below shows mean of raw data determined by trypan blue exclusion for percentage viability. To note results for 0 hours cell ageing (fresh cells) presented in this figure are as presented in Figure 4.3 for low disc speed. A non-sheared control held in a centrifuge tube concurrently, 21 ± 1ºC, for the duration of the experiment was used to measure trypan blue pre and post-processing for 0 and 24 hours cell ageing. Trypan blue exclusion shows a drop in percentage viability post-processing for both fresh cells and cells aged for 24 hours. Significant changes between non-sheared control and post-processing (*p<0.5, **p<0.01, ***p<0.001). Data shown are mean values ± 1 s.d. (j = 3; n = 4).

	% ± 1 s.d.		
	% Viability (j = 3; n = 4)		
Cell ageing (hrs)	**Pre-processing**	**Control**	**Post-processing**
0	91.6 ± 0.1	91.6 ± 0.4	74.3 ± 2.4
24	90.5 ± 0.6	91.5 ± 0.5	68.5 ± 1.2

Therefore, the overall effect of ageing the cells prior to processing yielded the equal amounts of damage as for fresh cells.

Figure 4.10 shows the percentage viability for both conditions. There is no significant drop in the percentage viability for either 0 hours (~1% with $p = 0.131$) or 24 hours (~1% with $p = 0.050$) cell age.

4.4 Effect of cell concentration on CTX0E03 and P4E6 cell lines

The impact of low and high cell concentrations (fresh cells, 'N' = 10,000 rpm) using CTX0E03 and P4E6 cell lines was investigated in a similar fashion to HCA2 cell line. As with the previous sections, both LDH release and trypan blue exclusion measurements will be shown for CTX0E03 cells and only trypan blue analysis for P4E6 cells. For both cell lines, the viscosity was assumed to be the same as that measured for equivalent concentrations for the HCA2 fibroblast. This was based on the fact that when in suspension, all three cell lines have the same mean cell diameter of ~15 μm and hence the solids volume fraction will be the same for the same cell density.

For the CTX0E03 cells, three runs were carried out at low cell concentration (~1.50×10^6 viable cells mL^{-1}) and two runs at high cell concentration (~29.8×10^6 viable cells mL^{-1}). For the P4E6 cells, three runs were carried out at low cell concentration (~2.35×10^6 viable cells mL^{-1}) and high cell concentration (~36.6×10^6 viable cells mL^{-1}).

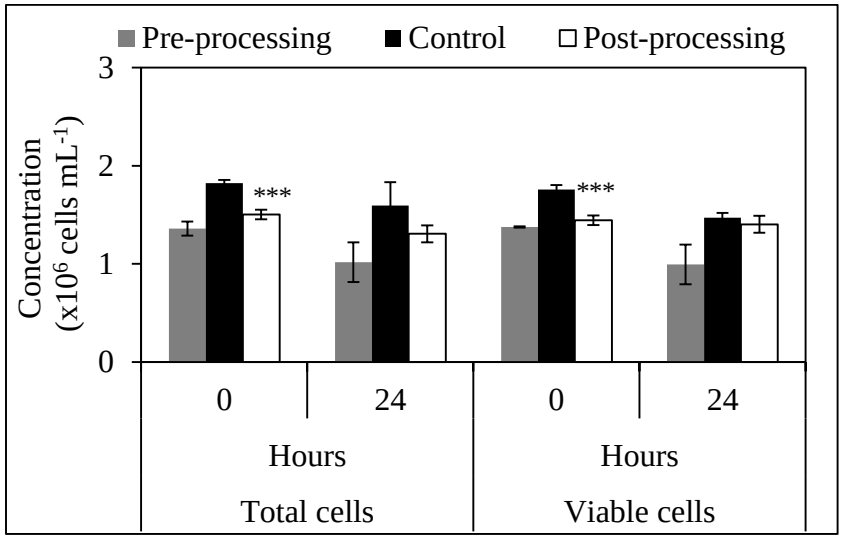

Figure 4.9: Membrane processing of feed ('*N*' = 6,000 rpm, 'γ' = 44,000 s^{-1}) P4E6 cells – effect of cell age on cell damage as shown by total and viable cell concentrations pre and post-processing. Table below shows mean of raw data determined by trypan blue exclusion for concentration of total and viable cells for pre and post-processing as well as a non-sheared control. To note results for 0 hours cell ageing presented in this figure are as presented in Figure 4.4 for low disc speed. A non-sheared control held in a centrifuge tube concurrently, 21 ± 1ºC, for the duration of the experiment was used to measure trypan blue pre and post-processing for 0 and 24 hours cell ageing. Trypan blue exclusion indicates that there is a significant drop of ~18% (p = 0.001) in the viable population at 0 hours cell ageing. Small drop in concentration of total or viable cells after processing with 24 hours cell ageing (~5%), although significant from 0 hours to end of processing (~21%). Significant changes between non-sheared control and post-processing (*p<0.5, **p<0.01, ***p<0.001). Data shown are mean values ± 1 s.d. (j = 3; n = 4).

	Concentration (x10^6 cells mL^{-1}) ± 1 s.d. (j = 3; n = 4)					
	Total cells ('TB_TOT')			**Viable cells ('TB_VC')**		
Cell ageing (hrs)	**Pre-processing**	**Control**	**Post-processing**	**Pre-processing**	**Control**	**Post-processing**
0	1.36 ± 0.07	1.82 ± 0.03	1.50 ± 0.05	1.38 ± 0.01	1.76 ± 0.05	1.44 ± 0.05
24	1.02 ± 0.20	1.60 ± 0.24	1.31 ± 0.09	1.00 ± 0.20	1.47 ± 0.05	1.40 ± 0.09

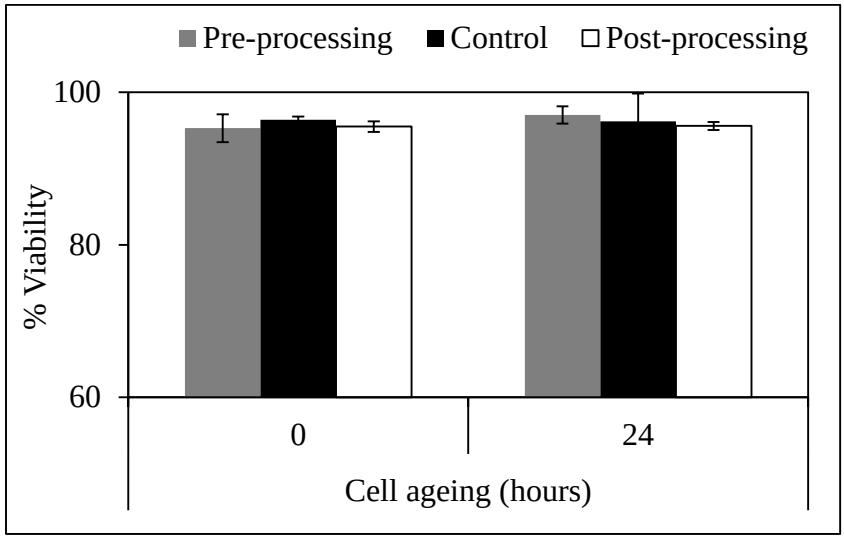

Figure 4.10: Membrane processing of feed ('*N*' = 6,000 rpm, 'γ' = 44,000 s^{-1}) P4E6 cells – effect of cell ageing on the percentage viability of cellular suspension as recorded by trypan blue exclusion. Table below shows mean of raw data determined by trypan blue exclusion for percentage viability. To note results for 0 hours cell age (fresh cells) presented in this figure are as presented in Figure 4.5 for low disc speed. A non-sheared control held in a centrifuge tube concurrently, 21 ± 1ºC, for the duration of the experiment was used to measure trypan blue pre and post-processing for 0 and 24 hours cell ageing. Trypan blue exclusion indicates that there is no significant drop in percentage viability after processing at a 0 and 24 hours cell ageing. Significant changes between non-sheared control and post-processing (*p<0.5, **p<0.01, ***p<0.001). Data shown are mean values ± 1 s.d. (j = 3; n = 4).

	% ± 1 s.d. (j = 3; n = 4)		
	% Viability		
Cell ageing (hrs)	**Pre-processing**	**Control**	**Post-processing**
0	95.3 ± 1.8	96.4 ± 0.4	95.5 ± 0.7
24	97.0 ± 1.1	96.2 ± 3.7	95.6 ± 0.5

4.4.1 Physical impact as measured by LDH release

Tables 4.3.A and 4.3.B summarize key performance data for the two sets of runs for the CTX0E03 cell line. The results presented in Table 4.3.A are the same as those presented in Table 4.1.B and are reproduced for convenience. Table 4.3.B presents the key performance data for high cell concentration. In both cases, each run, A to C and A to B respectively, was from a new batch of cells prepared using the same method.

Column 2 presents the measured transmission of LDH through the membrane at the end of each of the 60 minutes shear runs. These are the transmission values that are used for calculations. The mean value for LDH transmission is lower at the high cell concentration (0.75 ± 0.04 compared with 0.87 ± 0.04) probably due to the lower shear rate over the membrane surface or due to the greater level of membrane fouling species. The average transmission value at high cell concentration ('*N*' = 10,000 rpm) is similar to the average transmission value at low cell concentration and low disc speed ('*N*' = 6,000 rpm) of 0.78 ± 0.03. This might be a reflection of the similarity of the average shear rates (14,000 s^{-1} and 13,000 s^{-1} respectively, based on the viscosity measurements for the HCA2 cells at $30x10^6$ and $2x10^6$ cells mL^{-1} of $1.64x10^{-3}$ and $1.02x10^{-3}$ Pa s respectively).

Column 3 examines the stability of LDH over the period of the membrane study for each run. For low concentration there is a small (~ 8%) but probably insignificant drop ($p = 0.325$) and there is essentially no drop for high cell concentration (~1% decrease with $p = 0.474$). Hence for both cases, the LDH levels are considered stable for the length of the run.

Column 4 examines the total amount of LDH (extracellular and intracellular) measured - i.e. permeate plus retentate – and it is compared with total LDH at the start of the experiment. This helps to check whether all LDH is recovered (e.g. none is stuck to membrane) and none is lost through denaturation. For both low and high cell concentration there is a small, but not statistically significant, loss of ~5 - 6% ($p = 0.321$ and $p = 0.375$ respectively) of LDH which might be due to entrapment in the membrane or may fall within experimental error.

Finally, column 5 is a second measure of accountability for LDH comparing the total in the retentate and permeate to the control cells for the duration of the experiment. For low cell concentrations there is no loss and for high cell concentration there is a small but probably insignificant loss of LDH (~4% with $p = 0.380$).

Overall, it can be seen from Tables 4.3.A and 4.3.B that the averages are representative of the runs. The average values of the repeats were used to produce Figure 4.11 to analyze the impact of low and high cell concentration on cell damage as measured by LDH release for the CTX0E03 cell line. The results in Figure 4.11 (Table B) are the same as those presented in Figure 4.1 (Table C). The trends in this figure show that at a high cell concentration, more cells are damaged than at a low concentration. However, the proportion of intracellular LDH remaining has decreased ~50 ± 10.5% for low cell concentration and ~22 ± 8.8% for high cell concentration. Unlike with the HCA2 cells, taking into consideration the experimental errors, the values obtained for the decrease for both cell concentrations do not overlap. Therefore the proportion of intact cells

A.	**Low cell concentration ± 1 s.e. (j = 3; n = 4)**			
1. **Run ('j')**	**2.** **'$T(t_F)$'**	**3.** **'b/a'**	**4.** **'$(c+d)/a$'**	**5.** **'$(c+d)/b$'**
A	0.92 ± 0.03	0.82 ± 0.02	0.88 ± 0.01	1.07 ± 0.01
B	0.88 ± 0.05	0.99 ± 0.02	1.08 ± 6.43	1.09 ± 0.00
C	0.79 ± 0.12	0.96 ± 0.02	0.86 ± 0.01	0.89 ± 0.01
Average	**0.87 ± 0.04**	**0.92 ± 0.05**	**0.94 ± 0.07**	**1.02 ± 0.06**

B.	**High cell concentration ± 1 s.e. (j = 2; n = 4)**			
A	0.80 ± 0.02	1.02 ± 0.08	0.97 ± 0.05	0.95 ± 0.05
B	0.71 ± 0.09	0.96 ± 0.02	0.94 ± 0.01	0.97 ± 0.01
Average	**0.75 ± 0.04**	**0.99 ± 0.03**	**0.95 ± 0.01**	**0.96 ± 0.01**

C.

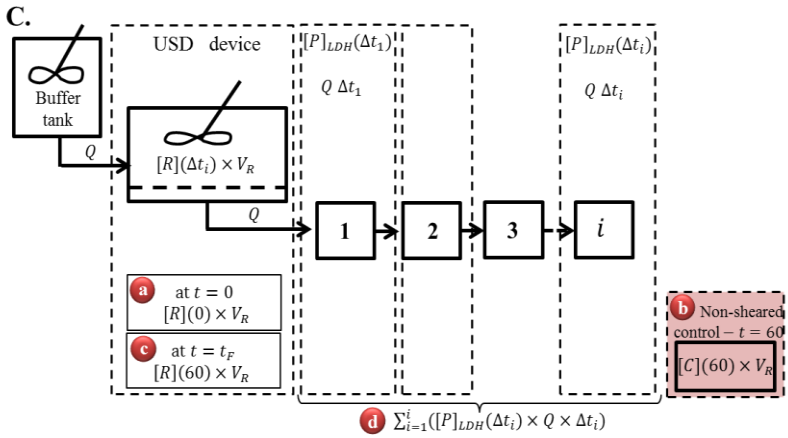

Table 4.3: Membrane processing of feed ('*N*' = 10,000 rpm) CTX0E03 cells – effect of (A) low and (B) high cell concentration on cell damage as recorded by release of LDH. To note results presented in Table 4.3.A are as presented in Table 4.1.B. Box diagram (C) of the USD membrane separation device showing process streams. From left to right columns show; (1) run; (2) transmission coefficient; (3) ratio of internal LDH in the control to the internal LDH pre-processing in the retentate to evaluate stability of LDH in the cells without processing (where 1 equals to no loss in LDH activity); (4) ratio of the sum of the total LDH in the retentate post-processing and permeate streams to the total LDH in the retentate pre-processing, to evaluate the mass balance agreement (where 1 equals to complete agreement, i.e. all LDH mass is accounted for); (5) ratio of the sum of the total LDH in the retentate post-processing and permeate streams to the total LDH in the control, to evaluate the mass balance agreement assuming the processed cells change as with control.

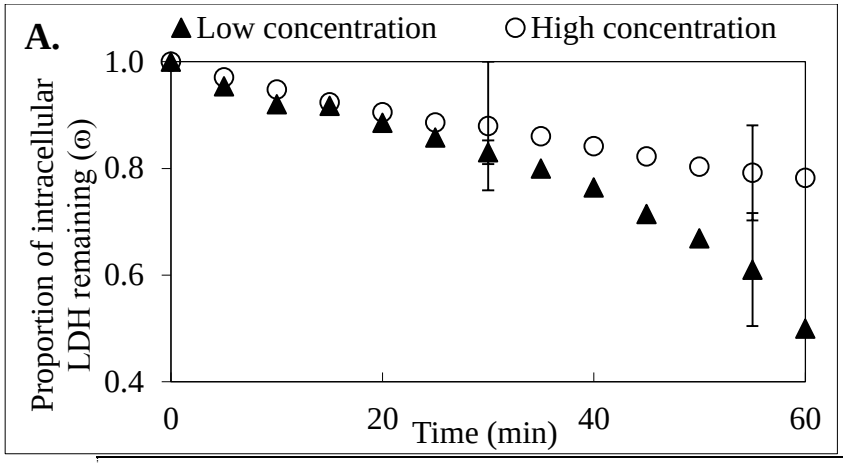

B.

Sample	Notation	LDH µU ± 1 s.d. (j = 3; n = 4) Cell concentration 2x10⁶ cells mL⁻¹ Measured total (‘LDH_TOT’)	Measured external (‘LDH_EXT’)	Predicted internal (‘LDH_INT’)
Pre-processing	(a) ‘$R(0) = [R](0) \times V_R$’	**12.96 ± 1.03**	0.91 ± 0.37	12.05 ± 0.66
Control	(b) ‘$C(60) = [C](60) \times V_R$’	**12.06 ± 1.50**	0.95 ± 0.41	11.12 ± 1.24
Post-processing	(c) ‘$R(60) = [R](60) \times V_R$’	4.44 ± 0.48	1.01 ± 0.40	3.43 ± 0.73
Permeate	(d) ‘$\sum_{i=1}^{i} P_{LDH}(\Delta t_i)$’	7.71 ± 1.16		
Post-processing + Permeate	(c) + (d) ‘$[R](60) \times V_R + \sum_{i=1}^{i}([P]_{LDH}(\Delta t_i) \times Q \times \Delta t_i)$’	**12.15 ± 1.24**	8.72 ± 1.54	3.43 ± 0.73

C.

Sample	Notation	Cell concentration 30x10⁶ cells mL⁻¹ (j = 2; n = 4) Measured total (‘LDH_TOT’)	Measured external (‘LDH_EXT’)	Predicted internal (‘LDH_INT’)
Pre-processing	(a) ‘$R(0) = [R](0) \times V_R$’	**270.4 ± 22.9**	7.2 ± 0.3	263.2 ± 23.2
Control	(b) ‘$C(60) = [C](60) \times V_R$’	**267.8 ± 16.5**	5.3 ± 0.6	262.5 ± 17.1
Post-processing	(c) ‘$R(60) = [R](60) \times V_R$’	183.7 ± 25.2	3.6 ± 0.1	180.2 ± 25.1
Permeate	(d) ‘$\sum_{i=1}^{i} P_{LDH}(\Delta t_i)$’	57.2 ± 6.7		
Post-processing + Permeate	(c) + (d) ‘$[R](60) \times V_R + \sum_{i=1}^{i}([P]_{LDH}(\Delta t_i) \times Q \times \Delta t_i)$’	**241.0 ± 31.9**	60.8 ± 6.8	180.2 ± 25.1

Figure 4.11: Membrane processing of feed (0 hours cell ageing, ‘*N*’ = 10,000 rpm) CTX0E03 cells – effect of cell concentration on cell damage as recorded by (A) release of LDH. Tables (B) and (C) show mean LDH data for all streams including both external and total measurements. To note results presented in Figure 4.11 (Table B) are as presented in Figure 4.1 (Table C). A non-sheared control held in a centrifuge tube concurrently, 21 ± 1ºC, for the duration of the experiment was used to measure LDH before and after processing. Figure (A) shows the proportion of intracellular LDH remaining (‘*ω*’, Eq 3.8), for low (~1.50 x 10^6 cells mL^{-1}, ○) and high (~29.77 x 10^6 cells mL^{-1},▲) concentrations. LDH release indicates that after membrane processing at higher concentration, less proportional damage is seen, suggesting that a higher cell concentration has a protective effect on cells. Data shown are mean values ± 1 s.d. (j = 3 and j = 2; n = 4).

remaining in the USD device appears to change with cell concentration for the CTX0E03 cells.

It was previously shown for this cell line that the proportion of cells damaged appeared to be independent of disc speed and therefore shear rate. This observation together with the lower proportion of LDH lost at high cell concentration suggest that there may be a protective effect with increasing concentration.

4.4.2 Physical impact as measured by trypan blue exclusion

The plots in this section show the impact of low and high cell concentration on cell damage as measured by trypan blue exclusion for CTX0E03 (Figures 4.12 and 4.13) and P4E6 (Figures 4.14 and 4.15) cell lines. The results presented low cell concentration for the CTX0E03 cell line in Figures 4.12 and 4.13 are the same as those presented in Figures 4.2 and 4.3 for high disc speed ('N' = 10,000 rpm) and are reproduced for convenience. The results presented for low cell concentration for the P4E6 cell line in Figures 4.14 and 4.15 are the same as those presented in Figures 4.4 and 4.5 for high disc speed ('N' = 10,000 rpm) and are reproduced for convenience.

Figure 4.12 shows the concentration of total and viable cells for pre-processing, control and post-processing samples for low cell concentration (Figure 4.12.A) and high cell concentration (Figure 4.12.B). At low cell concentration there is a ~37% ($p = 0.099$) decrease in the population of total cells and lower decrease of ~31% ($p = 0.023$) at high cell concentration. There is also a ~47% ($p = 0.061$) decrease in the population of viable cells at low cell concentration and a lower decrease of ~36% ($p = 0.043$) at high cell

concentration. Even though none of these decreases is statistically significant, it is evident that there is a decrease for both conditions and both cell populations.

Figure 4.13 shows the percentage viability for pre-processing, control and post-processing samples for both cell concentrations. Analysis of this figure shows that low cell concentration resulted in a significant ~14% ($p = 0.001$) drop in percentage viability post-processing compared to an insignificant ~5% ($p = 0.333$) drop in percentage viability at high cell concentration. Therefore, these results suggest that operating at low cell concentration resulted in a generally poorer quality (lower percentage viability) cellular suspension post-processing as measured by trypan blue exclusion.

At low cell concentration there is ~50% cell loss as recorded by both LDH release and loss of viable cells as measured by trypan blue exclusion. This loss is probably due to a combination of loss of membrane integrity and total cell destruction.

Figure 4.14 shows the same plots but focusing on the P4E6 cell line. At low cell concentration there is a ~39% ($p = 0.099$) decrease in the population of total cells and a decrease of ~60% ($p = 1.7 \times 10^{-5}$) at high cell concentration. There is also a significant decrease in the population of viable cells at both low and high cell concentrations (~41% with $p = 4.1 \times 10^{-5}$ and ~75% with $p = 0.001$ respectively), more so at higher cell concentration.

Figure 4.15 shows the percentage viability for pre-processing, control and post-processing samples for both cell concentrations. Analysis of this figure shows that

operating at both low and high cell concentration resulted in significant drops in the percentage viability. The drop at low cell concentration was small compared to that at high cell concentration (~3% with $p = 0.005$ and ~35% with $p = 2.0 \times 10^{-5}$ respectively). Therefore, unlike the CTX0E03, these results suggest that operating at high cell concentration resulted in a generally poorer quality (lower percentage viability) cellular suspension post-processing as measured by trypan blue exclusion.

4.5 Chapter discussion

The USD membrane separation methods and analytical techniques developed for the HCA2 cell line in Chapter 3 were evaluated for a prostate carcinoma cell line (P4E6) and a neural stem cell line (CTX0E03). The findings for these two clinically relevant cell lines aid in the characterization of the physical impact of USD membrane separation as well as in understanding the cell line specificity of bioprocessing. The variables investigated were the same as those presented in Chapter 3; disc speed, cell age and cell concentration (viscosity). The assessment of the impact of processing conditions on cell damage was measured by LDH release (for the CTX0E03 cell line only) and by trypan blue exclusion (for both cell lines).

4.5.1 CTX0E03 discussion

Assessment of the impact of disc speed on cell damage for the CTX0E03 cell line was measured by the release of LDH and trypan blue exclusion. LDH release showed similar trends and amounts of damage for both low and high disc speed (~50 – 60% damage). Trypan blue exclusion also revealed similar decrease in the population of viable cells for both conditions (~40 – 50% decrease). The variability for the CTX0E03

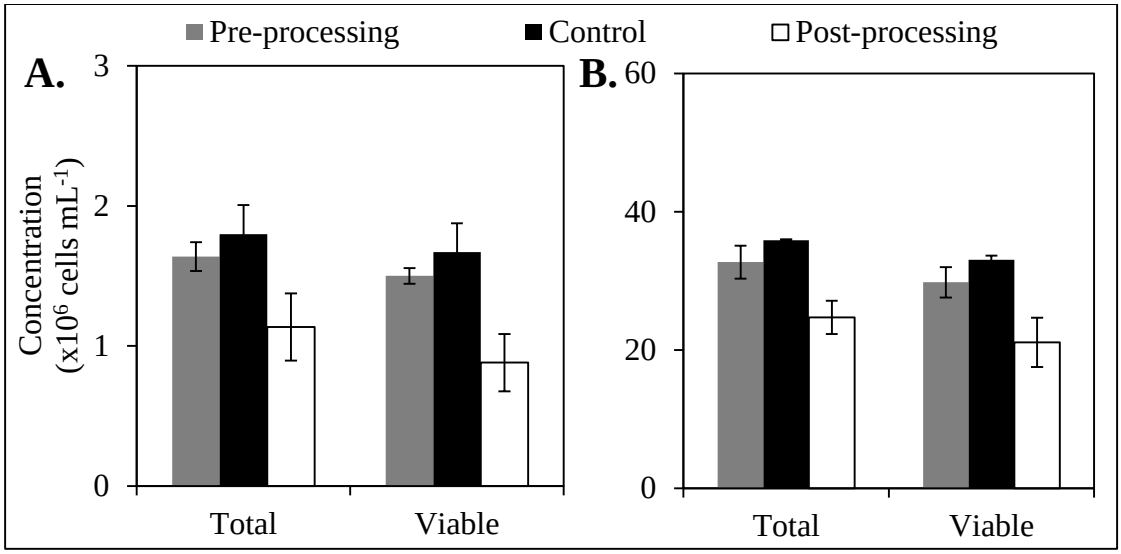

Figure 4.12: Membrane processing of feed ('*N*' = 10,000 rpm) CTX0E03 cells – effect of cell concentration on cell damage shown by total and viable cell concentrations pre and post-processing of the cellular suspension as recorded by trypan blue exclusion. Table below shows mean of raw data determined by trypan blue exclusion for concentration of total and viable cells. To note results for low cell concentration presented in this figure are as presented in Figure 4.2 for high disc speed. A non-sheared control held in a centrifuge tube concurrently, 21 ± 1ºC, for the duration of the experiment was used to measure trypan blue pre and post-processing for both low and high cell concentration. Trypan blue exclusion indicates that processing at low cell concentration resulted in ~47% reduction of viable cells compared to ~36% at high cell concentration. Significant changes between non-sheared control and post-processing (*p<0.5, **p<0.01, ***p<0.001). Data shown are mean values ± 1 s.d. (j = 3 and j = 2; n = 4).

	Concentration (x10^6 cells mL^{-1}) ± 1 s.d. (j = 3 and j = 2; n = 4)		
	Total cells ('$_{TB\_TOT}$')		
Concentration	**Pre-processing**	**Control**	**Post-processing**
Low	1.64 ± 0.10	1.80 ± 0.21	1.14 ± 0.24
High	32.7 ± 2.4	35.9 ± 0.2	24.7 ± 2.4

	Viable cells ('$_{TB\_VC}$')		
Concentration	**Pre-processing**	**Control**	**Post-processing**
Low	1.50 ± 0.06	1.67 ± 0.21	0.88 ± 0.20
High	29.8 ± 2.2	33.0 ± 0.6	21.1 ± 3.6

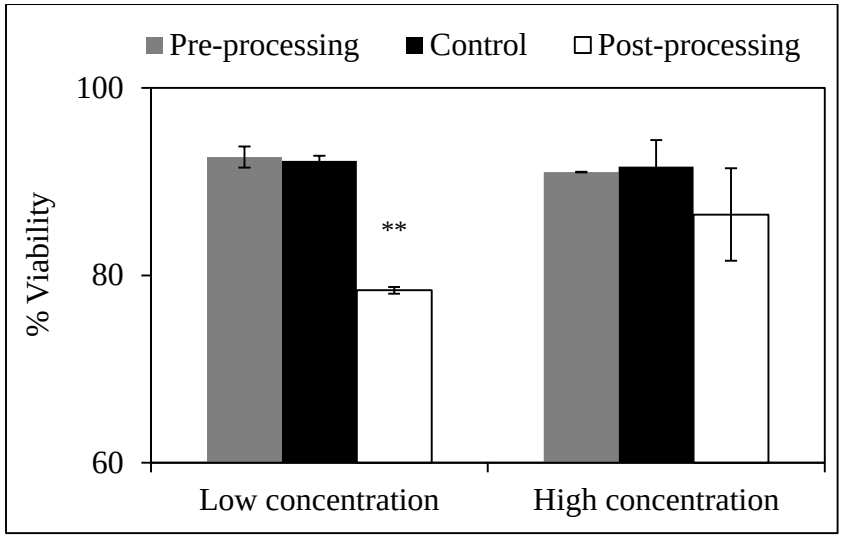

Figure 4.13: Membrane processing of feed ('*N*' = 10,000 rpm) CTX0E03 cells – effect of cell concentration on percentage viability of cellular suspension as determined by trypan blue exclusion. The figure shows percentage viability before and after membrane processing as determined by trypan blue exclusion. Table below shows mean of raw data determined by trypan blue exclusion for percentage viability. To note results for low cell concentration presented in this figure are as presented in Figure 4.3 for high disc speed. Trypan blue exclusion indicates that at low cell concentration there is a significant drop in percentage viability of ~14% (p = 0.001) after membrane processing compared to a non-significant drop of ~5% (p = 0.333) after processing at a higher cell concentration. Data shown are mean values ± 1 s.d. (j = 3 and j = 2; n = 4).

	% ± 1 s.d. (j = 3 and j = 2; n = 4)		
	% Viability		
Concentration	**Pre-processing**	**Control**	**Post-processing**
Low	92.6 ± 1.1	92.2 ± 0.5	78.4 ± 0.4
High	91.0 ± 0.04	91.6 ± 2.8	86.5 ± 5.0

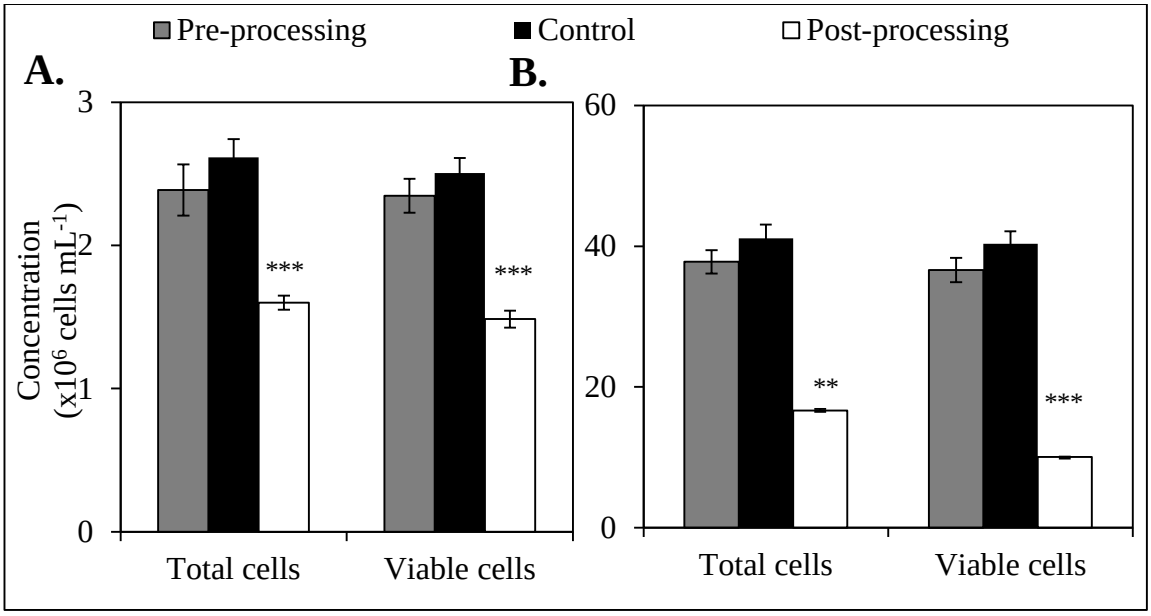

Figure 4.14: Membrane processing of feed ('*N*' = 10,000 rpm) P4E6 cells – effect of cell concentration on cell damage shown by total and viable cell concentrations pre and post-processing of the cellular suspension as recorded by trypan blue exclusion. Table below shows mean of raw data determined by trypan blue exclusion for concentration of total and viable cells. To note results for low cell concentration presented in this figure are as presented in Figure 4.4 for high disc speed. A non-sheared control held in a centrifuge tube concurrently, 21 ± 1ºC, for the duration of the experiment was used to measure trypan blue pre and post-processing for both low and high cell concentration. Trypan blue exclusion indicates that processing at low cell concentration resulted in a significant ~41% ($p = 4.1x10^{-5}$) reduction of viable cells compared to ~75% ($p = 0.001$) at high cell concentration. Significant changes between non-sheared control and post-processing (*p<0.5, **p<0.01, ***p<0.001). Data shown are mean values ± 1 s.d. (j = 3; n = 4).

	Concentration ($x10^6$ cells mL^{-1}) ± 1 s.d. (j = 3; n = 4)		
	Total cells ('TB_TOT')		
Concentration	**Pre-processing**	**Control**	**Post-processing**
Low	2.39 ± 0.18	2.62 ± 0.13	1.60 ± 0.05
High	37.8 ± 1.7	41.1 ± 2.0	16.6 ± 0.2
	Viable cells ('TB_VC')		
Concentration	**Pre-processing**	**Control**	**Post-processing**
Low	2.35 ± 0.12	2.51 ± 0.11	1.49 ± 0.06
High	36.6 ± 1.7	40.4 ± 1.8	10.0 ± 0.0

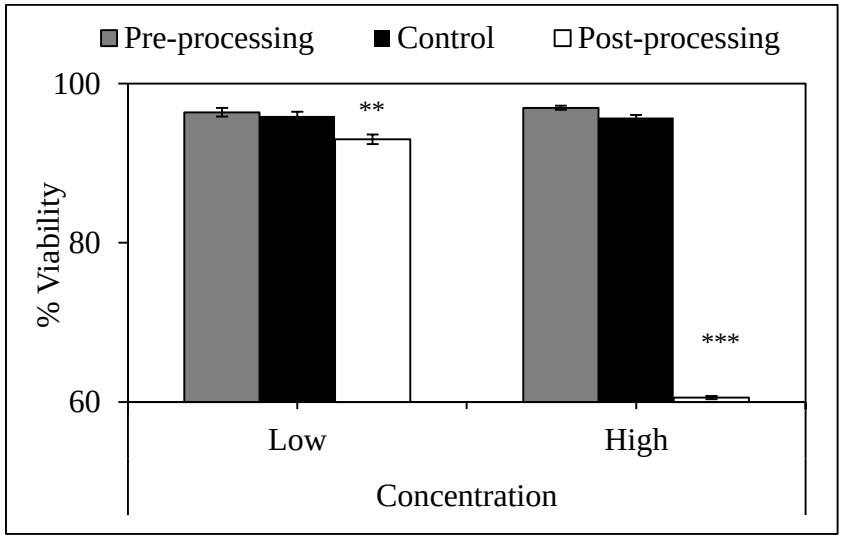

Figure 4.15: Membrane processing of feed ('*N*' = 10,000 rpm) P4E6 cells – effect of cell concentration on percentage viability of cellular suspension as determined by trypan blue exclusion. The figure shows percentage viability before and after membrane processing as determined by trypan blue exclusion. Table below shows mean of raw data determined by trypan blue exclusion for percentage viability. To note results for low cell concentration presented in this figure are as presented in Figure 4.5 for high disc speed. Trypan blue exclusion indicates that at low cell concentration there is a small but significant drop in percentage viability of ~3% (p = 0.008) after membrane processing compared to a significant drop of ~35% (p = 2.0×10^{-5}) after processing at a higher cell concentration. Significant changes between non-sheared control and post-processing (*p<0.5, **p<0.01, ***p<0.001). Data shown are mean values ± 1 s.d. (j = 3; n = 4).

	% ± 1 s.d. (j = 3; n = 4)		
	% Viability		
Concentration	**Pre-processing**	**Control**	**Post-processing**
Low	96.4 ± 0.6	96.0 ± 0.5	93.0 ± 0.6
High	97.0 ± 0.3	95.8 ± 0.3	60.6 ± 0.2

cell line appears to be higher than for the HCA2 cell line. The temperamental nature of neural stem cells means that the slightest change in cell culture conditions or handling of the cells whilst harvesting, may have a more pronounced impact on cell quality than the same change for HCA2 fibroblasts. This combined with the fact that three repeats were carried out rather than five, potentially increase the error measured. Nevertheless, it is evident from the collected data that cell damage caused to CTX0E03 cells is mainly dependent on the experience of being exposed to shear forces and the time of exposure and less so by the magnitude of the shear forces as both disc speed conditions exhibited the same proportion of intact cells lost during processing. Acosta-Martinez (2011) reached a similar conclusion after exposing the same cell line to several passes through a capillary device. He observed that the cells were mainly affected by the experience of being exposed to the elongational stress event and less so by the magnitude of the stress.

Like with the disc speed results, both fresh CTX0E03 cells and cells aged for 24 hours prior to processing exhibited equivalent cell damage profiles as measured by LDH release (~50 – 60% damage). Once again, the experience of being exposed to shear and time of exposure appear to impact more on cell damage than the variable investigated. Delahaye (2013) reported the same observation when investigating pre-centrifugation hold times of 5 and 120 minutes for the same cell line. He observed equivalent loss profiles independent of pre-process hold time. However, trypan blue exclusion dye indicated a higher loss of viable cells for the sample aged for 24 hours (~60% decrease which agrees with the value reported from the LDH release) than for the fresh sample (~40% decrease). It also recorded a drop in the percentage viability of ~20% for fresh cells and cells aged for 24 hours.

Lastly, the effect low and high cell concentration was investigated (~$1.5x10^6$ and ~$30x10^6$ cells mL^{-1} respectively). Unlike with the HCA2 cells, LDH release indicated that at high cell concentration the proportion of CTX0E03 cells damage was less than at low cell concentration (~20% compared to ~50% respectively). Trypan blue exclusion reinforces the observation that operating at low cell concentration resulted in higher loss of intact cells (~35% compared to ~50%) as well as generally a poorer quality of cellular material post-processing in terms of percentage viability (~14% decrease compared to ~5%).

4.5.2 P4E6 discussion

Cell damage for the three processing variables for the P4E6 cell line was assessed using only trypan blue exclusion. Results suggest that for low and high disc speed, these cells behave in a similar manner to HCA2 cells in terms of loss of viable cells. Like with the HCA2 fibroblasts, more cell damage was observed at high disc speed than at low disc speed (~40% compared to ~20%). However, the two cell lines differ in that P4E6 showed low drop in percentage viability for both disc speeds.

With respect to fresh P4E6 cells versus cells aged for 24 hours, there was no drop in percentage viability due to processing. Therefore, trypan blue exclusion data indicated that regardless of pre-process hold time for the P4E6 cell line, the overall quality of the cellular population after processing was unchanged. However, two other important observations must be made. First, there is a ~15% decrease in the population of viable cells merely from holding for 24 hours. Second, there is a higher decrease in the viable cell population during processing when using fresh cells compared to cells aged for 24

hours (~20% compared to ~5%). Therefore, overall the extent of damage for both conditions (including the ageing step) is the same (~20%). It may be that there is a weaker population of cells that is eradicated prior to processing by holding the cells for 24 hours. However, this is not enough information to form an informed final conclusion.

Lastly, low and high cell concentration was investigated at ~$2x10^6$ and ~$35x10^6$ cells mL^{-1} for the P4E6 cell line. Opposite to the observations drawn with the CTX0E03 cell line, P4E6 cells showed a higher decrease of the population of viable cells at high cell concentration than at low cell concentration (~75% compared to ~40%). Moreover, high cell concentration resulted in high drop of percentage viability when compared to low cell concentration (~35% compared to ~3%). Therefore unlike CTX0E03 cells, operating at high cell concentration when using P4E6 cells resulted in generally a poorer quality of the cellular suspension (in terms of percentage viability).

Overall, this chapter investigated the susceptibility of cell lines to choice of operating conditions. It was shown that different cell lines possess different thresholds leading to varying amounts of cell damage, making bioprocessing cell line specific. Where disc speed and cell age generally varied in the amount of cell damage recorded depending on the cell line investigated, remarkable findings were observed with respect to the impact of cell concentration. These findings led to the desire to gain more understanding of the effect of cell concentration within a 100-fold increment by assessment of cell damage and rheological insights, all which will be tackled in the next chapter.

Chapter 5. Effect of cell concentration on loss of intact cells during processing

5.1 Introduction

In the previous chapters, the impact of processing at low and high cell concentrations on cell damage was investigated using three different cell lines. When a cell therapy dose is thawed at clinic for administration, it is expected to have a minimum set of requirements, including a final concentration between $10x10^6$ and $100x10^6$ cells mL^{-1} with a specified number of viable cells (Brandenberger et al. 2011; Pattasseril et al. 2013). However, when cells are harvested upstream, the initial cell concentrations are generally around $1\text{-}2x10^6$ cells mL^{-1}. Therefore, the cellular suspension must be concentrated by 100-fold to achieve adequate dose for administration which will inevitably have an effect on the properties of the fluid.

This chapter aims to understand the effect of cell concentration on cell damage in more depth by investigating a range of concentrations of viable (i.e. intact) cells fed to the USD membrane separation device using the HCA2 fibroblasts.

5.2 Loss of intact cells with increasing discrete intact cells fed

The effect of discrete concentration of intact cells fed (referred to as '$[R]_{IC}$') to the USD membrane separation device on cell damage using the HCA2 cell line was assessed by the release of LDH and trypan blue exclusion. Three repeats each consisting of six different concentrations ranging from ~$1x10^6$ to ~$100x10^6$ cells mL^{-1} were carried out on different occasions. For each of the three repeats, enough cells were prepared for the six different concentrations. The operating conditions were kept the same as those

presented in Chapters 3 and 4 for the cell concentration studies (i.e. 'Q' = 0.5 mL min^{-1}, 'V_R' = 1.7 mL, 'N' = 10,000 rpm, fresh cells, 60 minutes of processing and varying shear rates and shear stress according to viscosity of the cellular suspension).

Tables 5.1 and 5.2 show the trypan blue exclusion data for the three repeats (labelled 1 to 3) at each of the six concentrations investigated (listed in decreasing order of cell concentration from A to F in column 1). Table 5.1 shows the concentrations of total cells pre-processing (i.e. fed), control and post-processing (i.e. recovered) respectively in columns 2, 3 and 4 or '$[R]_{TC_{TB}}(0)$', '$[C]_{TC_{TB}}(60)$' and '$[R]_{TC_{TB}}(60)$'. Intact cell concentrations for the three streams are shown in columns 5, 6 and 7 and referred to as '$[R]_{IC_{TB}}(0)$', '$[C]_{IC_{TB}}(60)$' and '$[R]_{IC_{TB}}(60)$' respectively. Column 8 in Table 5.1 shows the volume fractions given by:

$$\emptyset = '[R]_{TC_{TB}}(0)' \times \left(\frac{4}{3}\pi\left(\frac{d_{AV}}{2}\right)^3\right) \qquad \text{Equation 5.1}$$

where '$\emptyset$' is the volume fraction, 'd_{AV}' is the average diameter of a cell in suspension (assumed to be 15 μm for the HCA2 cell line). Assuming cells to be perfect spheres, the range of volume fractions varied from 0.002 to 0.210.

Table 5.2 shows the percentage viabilities for the pre-processing, control and post-processing samples as measured by trypan blue exclusion. The percentage viabilities of HCA2 cells upon harvest tend to lie within 90 and 95%. However, this was not the case for the second repeat, where the percentage viabilities for both pre-processing and control samples for experiments 2.A to 2.D, lied between 85 and 90%. Nevertheless, despite the lower percentage viabilities prior to processing, the

	Concentration (x10^6 cells mL^{-1})						
	Total cells			Viable cells			
1. Run	2. Pre-processing $[R]_{TC_{TB}}(0)$	3. Control $[C]_{TC_{TB}}(60)$	4. Post-processing $[R]_{TC_{TB}}(60)$	5. Pre-processing $[R]_{IC_{TB}}(0)$	6. Control $[C]_{IC_{TB}}(0)$	7. Post-processing $[R]_{IC_{TB}}(60)$	8. Volume fraction Ø
1.A	118.91	123.76	123.05	111.29	117.57	110.55	0.210
1.B	42.71	37.93	31.36	39.28	35.05	27.91	0.075
1.C	21.39	18.69	13.78	19.79	17.45	11.20	0.038
1.D	8.23	7.91	8.70	7.71	7.14	7.38	0.015
1.E	2.13	1.93	2.20	1.99	1.77	1.99	0.004
1.F	1.29	1.31	1.12	1.19	1.17	0.96	0.002
2.A	114.40	104.93	56.52	104.49	95.19	35.21	0.202
2.B	55.12	56.49	49.16	49.80	50.61	43.45	0.097
2.C	18.01	14.39	15.98	16.15	12.92	14.19	0.032
2.D	4.93	3.93	3.87	4.31	3.46	3.27	0.009
2.E	2.32	2.52	1.80	2.06	2.22	1.46	0.004
2.F	1.35	1.41	1.05	1.17	1.24	0.79	0.002
3.A	77.46	76.56	80.73	74.14	72.58	75.03	0.137
3.B	42.42	40.17	46.82	40.09	37.78	44.12	0.075
3.C	11.08	11.74	10.13	10.36	10.98	8.85	0.020
3.D	5.25	3.82	4.52	4.79	3.53	4.09	0.009
3.E	2.48	2.18	2.51	2.30	2.02	2.27	0.004
3.F	1.09	1.01	0.89	1.01	0.95	0.77	0.002

Table 5.1: Concentration of total and intact (i.e. viable) cells pre-processing, control and post-processing (i.e. recovered) as measured by trypan blue exclusion and analyzed by automated haemocytometer (ViCell XR™) software. Three repeats, each of the six starting concentrations were carried out ('*Q*' = 0.5 mL min^{-1}, 'V_R' = 1.7 mL, '*N*' = 10,000 rpm, fresh cells, 60 minutes). Volume fraction (Ø) based on the concentration of total cells fed ('$[R]_{TC_{TB}}(0)$') to the USD membrane device. Some over-counts are evident post-processing due to incorrect cell identification by the software as shown in Figure 5.1.

1. Run	%		
	% Viability		
	2. Pre-processing	3. Control	4. Post-processing
1.A	90.13	94.60	84.33
1.B	92.23	91.13	89.25
1.C	94.10	91.15	84.80
1.D	92.47	92.77	81.15
1.E	92.87	92.78	88.75
1.F	93.93	94.73	90.60
2.A	85.83	88.40	78.15
2.B	89.63	88.85	79.50
2.C	88.60	88.10	86.35
2.D	89.75	89.80	88.80
2.E	91.00	89.90	88.65
2.F	91.50	90.45	62.20
3.A	91.80	94.45	87.13
3.B	92.47	92.20	89.60
3.C	92.90	92.03	90.95
3.D	94.35	94.55	89.60
3.E	95.20	94.03	95.55
3.F	95.73	95.93	93.33

Table 5.2: Percentage viability of cells pre-processing, control and post-processing as measured by trypan blue exclusion for the three repeats at each of the six starting concentrations as shown in Table 5.1 ('Q' = 0.5 mL min^{-1}, 'V_R' = 1.7 mL, 'N' = 10,000 rpm, 0 hours cell ageing, 60 minutes). Pre-processing and control percentage viabilities for the second repeat, runs A to D, are lower than expected for HCA2 cells upon harvest. Moreover, the drop in percentage viability pre-processing to post-processing for run 2.F is considerably higher than all other runs at approximately 30%. It is presumed that an error in cell preparation must have led the second repeat to a poorer quality of cells as a starting point for the experiments.

change due to processing itself remained the same as for the other repeats. The only exception was experiment 2.F, where the pre-processing and control percentage viabilities appear to be within the expected values (90 to 95%) but the drop post-processing was ~30% (significantly higher than any other experiment). This may be due to the cells been exposed to the detachment enzyme for a prolonged time during the harvesting of the cellular suspension, compromising the quality of the harvested cells. Going forward with the analysis in this chapter, all experiments from this repeat will be considered but carefully inspected to assess whether or not they should be classified as an outlier.

Figure 5.1 shows an image obtained from the automated haemocytometer for the post-processed sample from experiment 3.A ('$[R]_{IC_{TB}}(0)$'= 77.46x10^6 cells mL^{-1}). This image was included to exemplify the method of cell identification used by the software provided with the automated haemocytometer. As can be seen, the software identifies "viable" (or "intact") and "non-viable" (or "dead") cells by placing green and red circles respectively. Figures 5.1.A and 5.1.B show the same image analyzed by the software using two different settings; "medium" and "none" declustering modes. The "declustering" option intends to help in optimization of different cell types to account for "sticky cells" and cells in clusters. From the images in Figure 5.1, it is evident that when dealing with elongated cells rather than spherical ones, counts per image can halve depending on the setting use (130 in Figure 5.1.A compared to 67 in Figure 5.1.B). For example, with the "medium" declustering option, one elongated cell is counted as multiple smaller round cells whereas with "none" declustering that same cell is counted as one big round cell. This explains why some of the experiments (1.D, 1.E,

3.A, 3.B, 3.D and 3.E) shown in Table 5.1 showed higher concentration of cells post-processing than initially fed to the device. The same problem was previously encountered in Chapter 3, Section 3.3.4 Cell morphology, growth and apoptosis analysis. In Section 3.3.4, it was identified that the software provided by manufacturer of the automated haemocytometer did not have the capabilities to recognize new cell populations and therefore could not account for the increase in the population of elongated and "blebby" cells post-processing. To over-come this issue, a Matlab script for image processing was kindly developed by Nicolas Jaccard and used to re-analyze the images provided by the automated haemocytometer. Further analysis and results on the morphology of cells using the Matlab script will be shown in Section 5.3 Cell morphology analysis.

To assess the impact on cell damage, the concentration of intact cells fed as measured by trypan blue exclusion using the software from the automated haemocytometer ('$[R]_{TC_{TBVICELL}}(0)$') is shown in Figure 5.2. '$[R]_{TC_{TBVICELL}}(0)$' was plotted against three measurements of intact cells recovered as measured by; (A) trypan blue exclusion using automated haemocytometer software, '$[R]_{IC_{TBVICELL}}(60)$'; (B) trypan blue exclusion using Matlab script, '$[R]_{IC_{TBMATLAB}}(60)$' and (C) LDH release, '$[R]_{LDH_{INT}}(60)^{*}$'. A common x-axis of '$[R]_{IC_{TBVICELL}}(0)$' was chosen to compare all three measurements as no issues were encountered with cell counting for the pre-processed samples. Due to the large range of concentrations investigated, log scales were used for the x-axis of the three plots.

A.
"Medium" declustering

Cell type	HCA2	
Dilution factor	12.0	
	Image 20	**Total**
Cell count	130	5115
Viable cells	126	4809
Viability	**96.9 %**	**94.0 %**
Total cells / ml	80.06 $\times 10^6$	63.00 $\times 10^6$
Viable cells / ml	77.60 $\times 10^6$	59.23 $\times 10^6$
Avg. diam. (microns)	12.61	12.80
Avg. circularity	0.80	0.82
Avg. background intensity	200	205
Images		50

B.
"None" declustering

Cell type	HCA2 (modified)	
Dilution factor	12.0	
	Image 20	**Total**
Cell count	67	2983
Viable cells	61	2646
Viability	**91.0 %**	**88.7 %**
Total cells / ml	41.26 $\times 10^6$	36.74 $\times 10^6$
Viable cells / ml	37.57 $\times 10^6$	32.59 $\times 10^6$
Avg. diam. (microns)	19.78	17.79
Avg. circularity	0.58	0.68
Avg. background intensity	200	205
Images		50

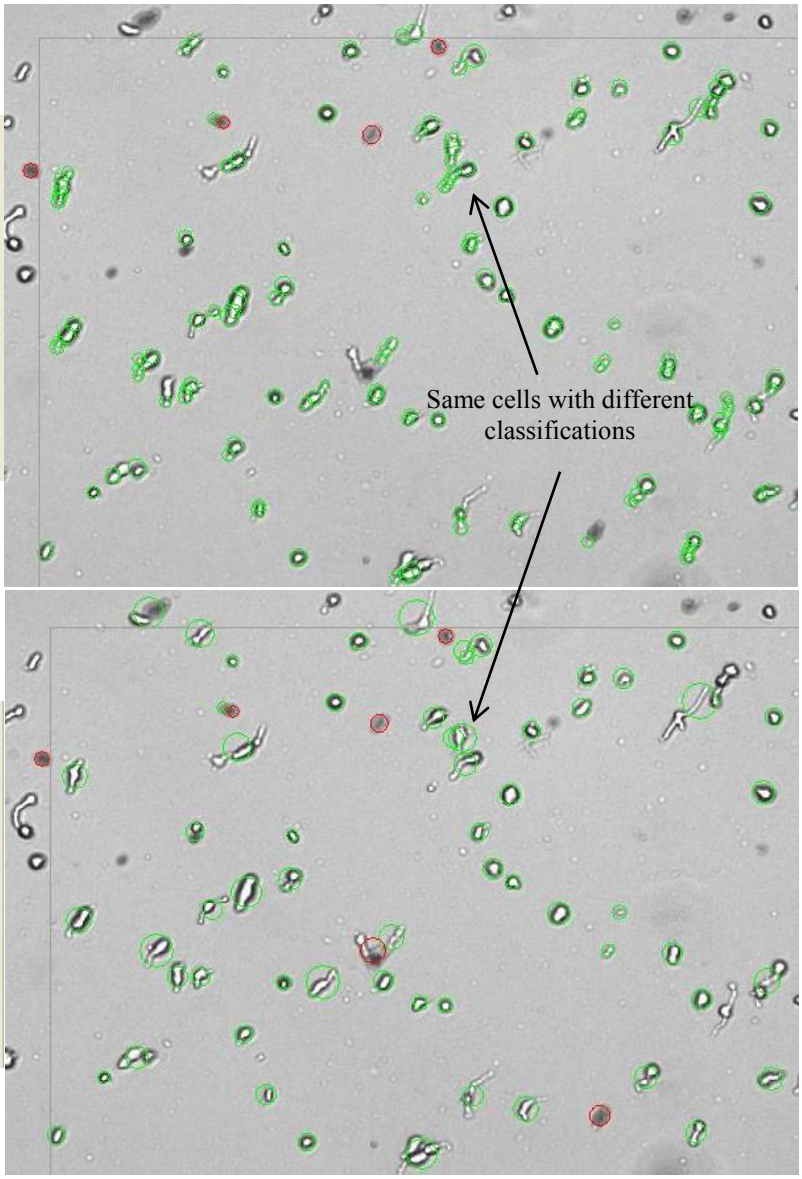

Figure 5.1: Software analysis from the automated haemocytometer using (A) "medium" and (B) "none" declustering modes for the same image for run 3.A for the HCA2 cellular suspension post-processing ('$[R]_{TC_{TBVICELL}}(0)$'= 77.46x10^6 cells mL^{-1}, 'N' = 10,000 rpm). The software places a green circle on "viable" (or "intact") cells and a red circle on "non-viable" (or "dead") cells. "Medium" declustering mode identified almost twice the number of cells as "none" declustering mode.

The concentration of intact cells recovered as measured by LDH release, '$[R]_{LDH_{INT}}(60)^{*}$', was based on the concentration of internal LDH calculated pre and post-processing:

$$[R]_{LDH_{INT}}(60)^{*} = [R]_{IC_{TBVICELL}}(0) \times \frac{[R]_{LDH_{\mathrm{INT}}}(60)}{[R]_{LDH_{\mathrm{INT}}}(0)} \qquad \text{Equation 5.2}$$

where '$[R]_{LDH_{INT}}(60)^{*}$' is the concentration of intact cells recovered (in cells mL^{-1}) as measured by LDH release, '$[R]_{IC_{TBVICELL}}(0)$' is the concentration of intact cells fed (in cells mL^{-1}) as measured by trypan blue exclusion using automated haemocytometer software, '$[R]_{LDH_{INT}}(60)$' and '$[R]_{LDH_{INT}}(0)$' are the predicted concentrations of internal LDH (in µU mL^{-1}) post-processing (i.e. in the retentate at 't = 60 min') and pre-processing (i.e. in the retentate at 't = 0 min') respectively. The predicted concentration of internal LDH is at any given time 't' is given by:

$$[R]_{LDH_{INT}}(t) = [R]_{LDH_{TOT}}(t) - [R]_{LDH_{EXT}}(t) \qquad \text{Equation 5.3}$$

where '$[R]_{LDH_{TOT}}(t)$' and '$[R]_{LDH_{EXT}}(t)$' are the measured concentrations of total and extracellular LDH (in µU mL^{-1}) in the retentate at 't' respectively.

From the three plots in Figure 5.2, it can be seen that as the concentration of intact cells fed into the USD membrane separation device increases, the concentration of cells lost during operation also increases. However, also with increasing concentration of intact cells fed, a higher concentration of intact cells post-processing is recovered. Those data points lying on the parity line (shown as dashed line) indicate that the concentration of intact cells recovered is equal to the concentration of intact cells fed. For example, the line of best fit for the experimental data in Figure 5.2.A (cell counts carried out using

the software provided by the automated haemocytometer) shows a closer fit to the parity line than Figures 5.2.B and 5.2.C. However, as was previously mentioned, over-counts post-processing were observed in several occasions using this software for analysis. Therefore, Figures 5.2.B and 5.2.C (trypan blue exclusion as analyzed by Matlab script and LDH release respectively) are the two measurements with the most confidence and also appear to have similar coefficients for the lines of best fit for the experimental data. The coefficients from these plots suggest that as the concentration of intact cells fed increases, the difference between the intact cells recovered and intact cells fed will increase. By inspection of the equations of the lines of best fit within range of concentrations studied, both Matlab analysis and LDH release expect 20% higher recovery of intact cells at low cell concentration (starting at 60% and 80% respectively). This observation suggests that the proportion of intact cells recovered to intact cells fed should decrease with increasing concentration.

Figure 5.3 shows the proportion of '$[R]_{IC}(60)$' to '$[R]_{IC_{TBVICELL}}(0)$' for (A) automated haemocytometer (ViCell XR^{TM}), (B) Matlab script and (C) LDH release. From all three plots, it appears as if the proportion of '$[R]_{IC}(60)$' to '$[R]_{IC_{TBVICELL}}(0)$' remained constant and was independent of '$[R]_{IC_{TBVICELL}}(0)$'. The data points that fall outside the upper and lower standard deviation from the average value in Figure 5.3, were considered as outliers. Most of these are the runs from the 2nd repeat with low percentage viabilities pre-processing previously identified. As was mentioned, these outliers may be due to differences in cell preparation leading to weaker cells at harvest, which is reflected in the initial percentage viabilities on Table 5.2. The average

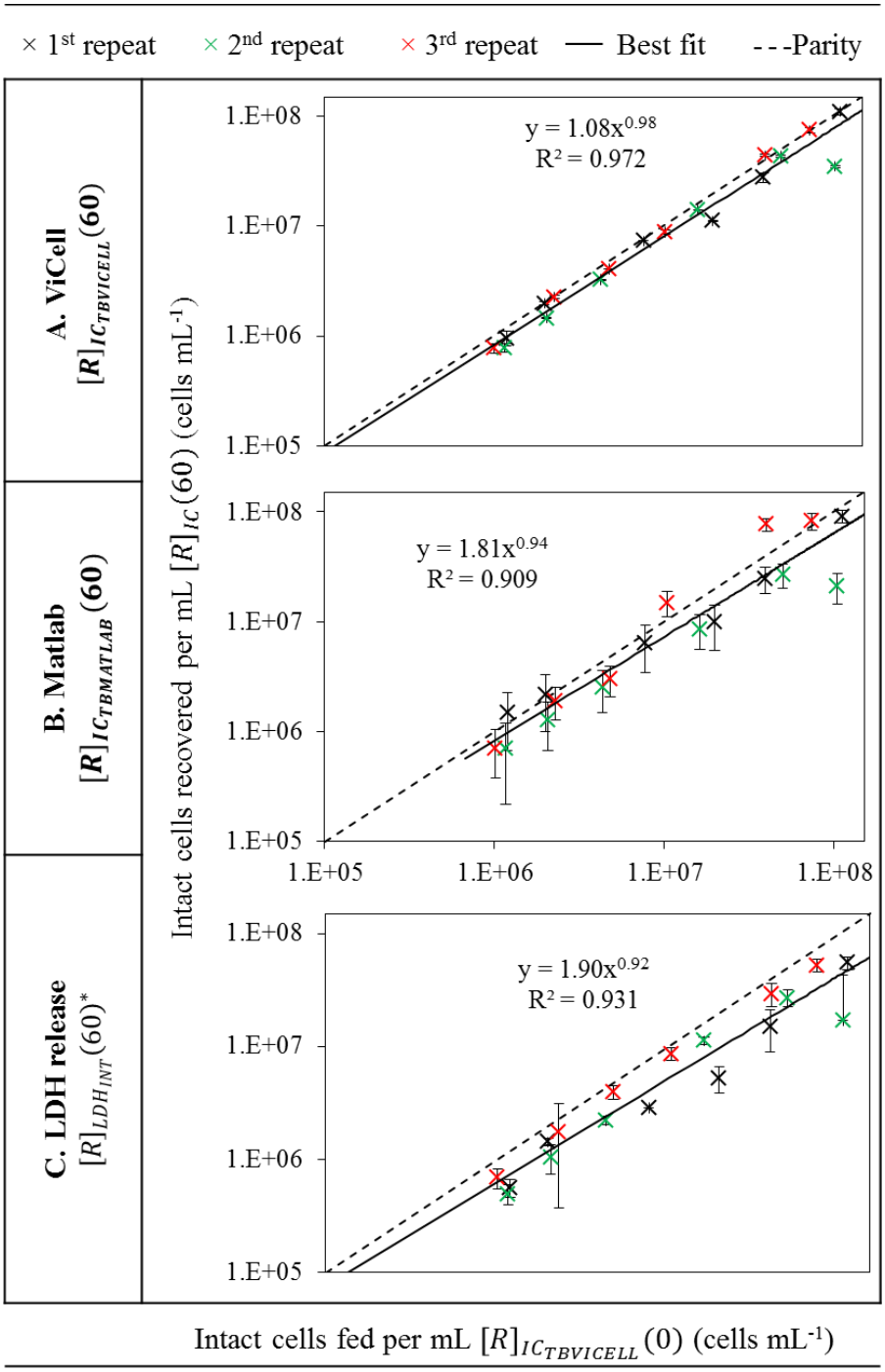

Figure 5.2: Concentration of intact cells recovered versus concentration of intact cells fed into the USD membrane separation device. Analyzed by (A) automated haemocytometer software (ViCell XR™) and (B) Matlab script and (C) LDH release. Lines of best fit for all data points as one series are shown. As '$[R]_{IC_{TBVICELL}}(0)$' increases, the concentration of cells lost during operation also increases (j = 3; n = 4).

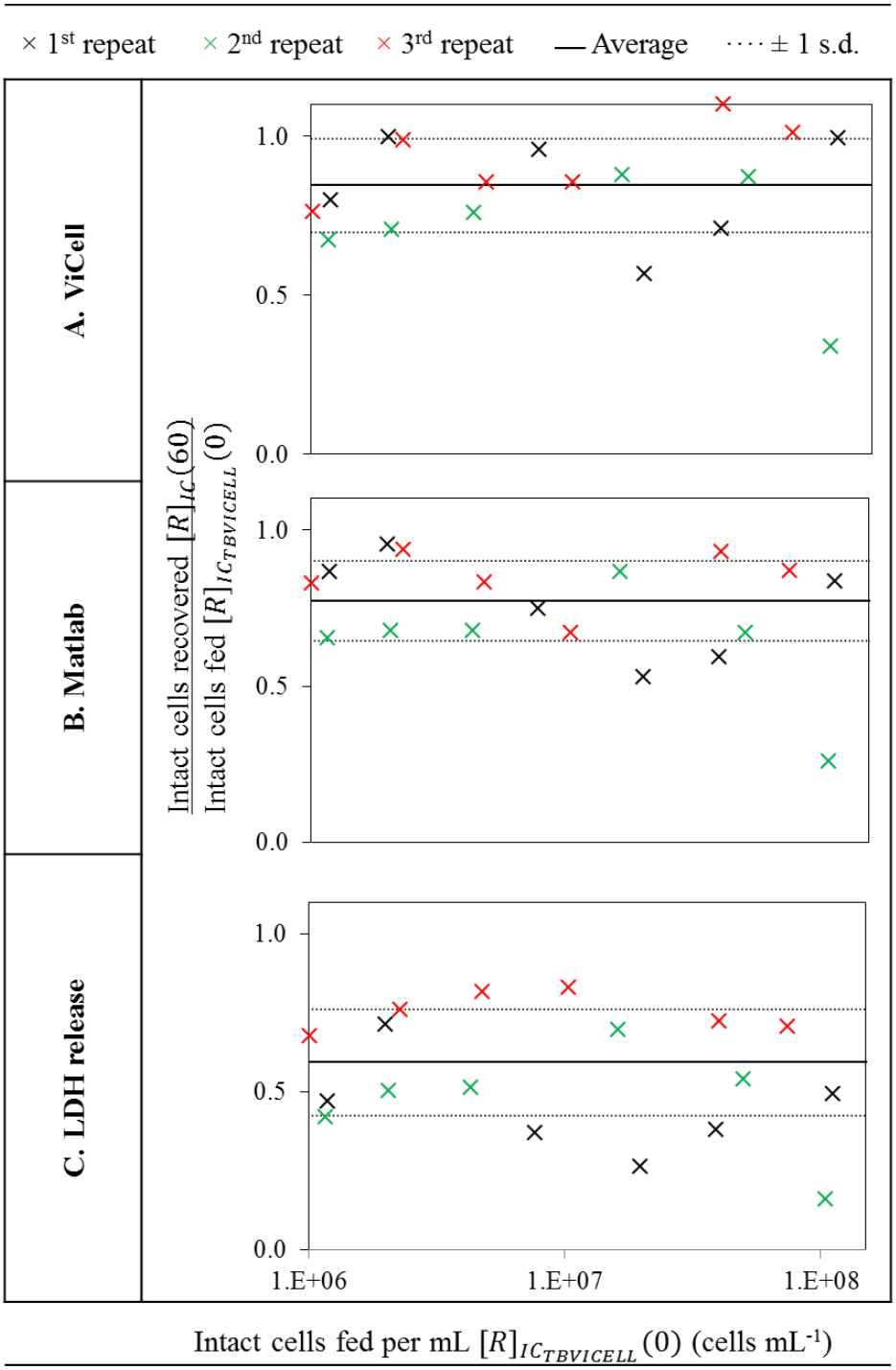

Figure 5.3: Intact cells fed versus intact cells recovered over intact cells fed. Trypan blue exclusion data analyzed by (A) automated haemocytometer software (ViCell XR™), (B) Matlab software and (C) LDH release. Proportion of cells recovered over cells fed appears to be independent of the changes in cell concentration (and therefore viscosity). Dashed lines show ± 1 s.d. (j = 3; n = 4); outliers may be due to change in cell preparation leading to weaker cells.

proportion of '$[R]_{IC}(60)$' to '$[R]_{IC_{TBVICELL}}(0)$' was 0.85 ± 0.15 for ViCell XM^{TR}, 0.77 ± 0.13 for the Matlab script and 0.60 ± 0.17 for LDH release (Figure 5.3). Due to the over-estimation post-processing seen with the ViCell XM^{TR} software, Matlab script is the analysis with most confidence out of the two trypan blue exclusion plots.

Several hypotheses were proposed as to why this proportion appears to be constant. Using CFD analysis, it was shown that there is a specific region of high shear, by the edges of the rotating disc, in the device. As the concentration of cells fed increases, the concentration of cells in this region or volume of high shear also increases, potentially leading to higher number of cells damaged. Another possibility to explain the constant proportion of cells lost with varying concentration is that there may be an age distribution of the cell population at harvest. If the proportion of older (or younger) cells are constant per flask harvested and were the ones most affected by shear, then this would explain a constant proportion of cells being damaged independent of concentration. This weaker population of cells within the cellular suspension may not be able to withstand the operating conditions due to different elasticity and mechanical properties, metabolic needs and in general physiological needs which are characteristic of different stages in the cell cycle.

5.2.1 Average rate of cell damage constants

Based on the previous findings, cell damage can be described as a first order process with respect to the concentration of cells present and the rate constant can be said to be unchanged with change in viscosity of the suspension. The average rate constant for the

60 minutes of operation for a first order process with respect to the concentration of cells present is given by:

$$\frac{d[R]_{IC}(60)}{d[R]_{IC_{VICELL}}(0)} = k[R]_{IC}(60) \qquad \text{Equation 5.4}$$

where 'k' is the average rate of cell damage over 60 minutes of operation (h^{-1}). Using equation 5.4, the average rate of damage was calculated for all three repeats and each of the six concentrations investigated (Table 5.3). Cell damage assessed on LDH release showed the fastest average rate constant of 0.29 ± 0.14 h^{-1} compared to 0.14 ± 0.08 h^{-1} for cell damage based on loss of membrane integrity as analyzed using Matlab script. The average rate of damage calculated for LDH release is almost twice as fast as the one calculated for the Matlab data. This is consistent with prior observations in Chapter 3, section 3.3.3 where the average rate constants for both low and high disc speeds as measured by LDH released were twice as fast as that measured by trypan blue exclusion.

5.2.2 Cell morphology analysis

Even though analysis of cell morphology can be a more subjective parameter than for example cell population growth rates, it may offer an inexpensive and interesting insight into the physical behaviour and appearance of individual cells at an early stage.

In Section 3.3.4.1 Cell morphology analysis in Chapter 3, examples for each of the cell types identified by the Matlab script for image processing were shown (Figure 3.6.D). Morphological characteristics such as aspect ratio and intensity were used as building blocks to define the different cell types. These included five main types or populations:

Repeat		$[R]_{TB\_VICELL}(0)$ (cells mL^{-1})	k (h^{-1}) LDH	k (h^{-1}) Matlab
1	A	1.11E+08	-0.31	-0.08
	B	3.93E+07	-0.42	-0.23
	C	1.98E+07	-0.58	-0.28
	D	7.71E+06	-0.43	-0.12
	E	1.99E+06	-0.15	-0.02
	F	1.19E+06	-0.33	-0.06
	Average		-0.37	-0.13
2	A	1.04E+08	-0.79	-0.59
	B	4.98E+07	-0.27	-0.17
	C	1.62E+07	-0.16	-0.06
	D	4.31E+06	-0.29	-0.17
	E	2.06E+06	-0.30	-0.17
	F	1.17E+06	-0.38	-0.18
	Average		-0.36	-0.22
3	A	7.41E+07	-0.15	-0.06
	B	4.01E+07	-0.14	-0.03
	C	1.04E+07	-0.08	-0.17
	D	4.79E+06	-0.09	-0.08
	E	2.30E+06	-0.12	-0.03
	F	1.01E+06	-0.17	-0.08
	Average		-0.12	-0.08
	Average		**-0.29**	**-0.14**
	±		0.14	0.08

Table 5.3: Average rate of cell damage for the three repeats investigated at each of the six concentrations of intact cells fed. Measurements include constants for LDH release and trypan blue exclusion analyzed using Matlab script.

short elongated (SE), long elongated (LE), viable round (VR), non-viable (NV) and debris (DEBRIS). In Chapter 3, it was shown that for low and high disc speeds and low cell concentration, appearance of elongated and 'blebby' cells was observed immediately post-processing. In this section, the study of cell morphology aims to provide a basic breakdown of cell appearance in suspension to draw a preliminary comparison of the pre-processed to post-processed samples for all cell concentrations.

Figure 5.4 shows the plots of the proportions for each of the cell populations compared to the total cells for both pre and post-processing samples. This figure presents an average of repeats 1 and 3, experiments A to F. The experiments carried out for the 2nd repeat were not included in Figure 5.4 due to the elevated proportions of dead cells pre-processing (previously addressed and identified as outliers). For all the experiments carried out, the pre-processing samples follow a similar profile with respect to the proportions of each cell type. For instance, irrespective of concentration, the pre-processing proportion of SE falls within 8-12%, LE between 2-5%, VR between 75-85% and NV between 5-12%. However, with the post-processing samples, different population profiles and ranges for each cell type arise. For example, levels of SE and LE appear to be higher post-processing for high concentration experiments (A to C).

Figure 5.5 summarizes the changes in proportions of each cell population for all six concentrations. It shows the ratio of the proportion of each cell population post-processing to pre-processing. The values below 1 therefore indicate a higher proportion of that specific population prior to processing, whereas values over 1 indicate an increase in the proportion of that population due to processing. The main observation

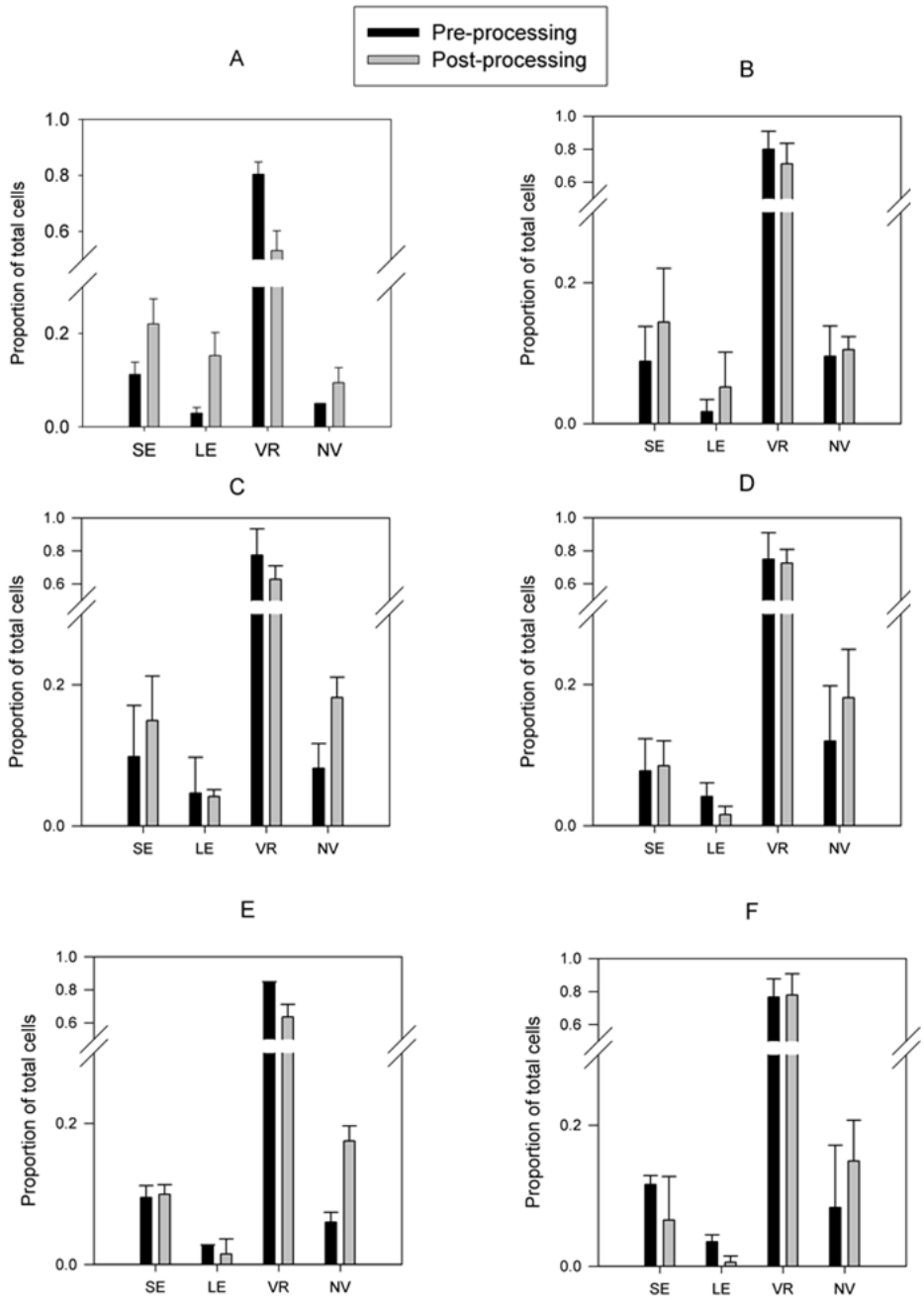

Figure 5.4: Examples of cell types identified by software for image processing developed using Matlab Image Processing Toolbox (MathWorks, Cambridge, UK). Software kindly developed by Nicolas Jaccard in the Biochemical Engineering Department at UCL. Plots A to F show decreasing concentration of intact cells fed to the USD membrane separation device. The cell categories correspond to libraries created for the Matlab script. The proportion of each cell type or population was compared to the total cells in the sample for pre-processing (■) and immediately post-processing (■) (j = 2; n = 4).

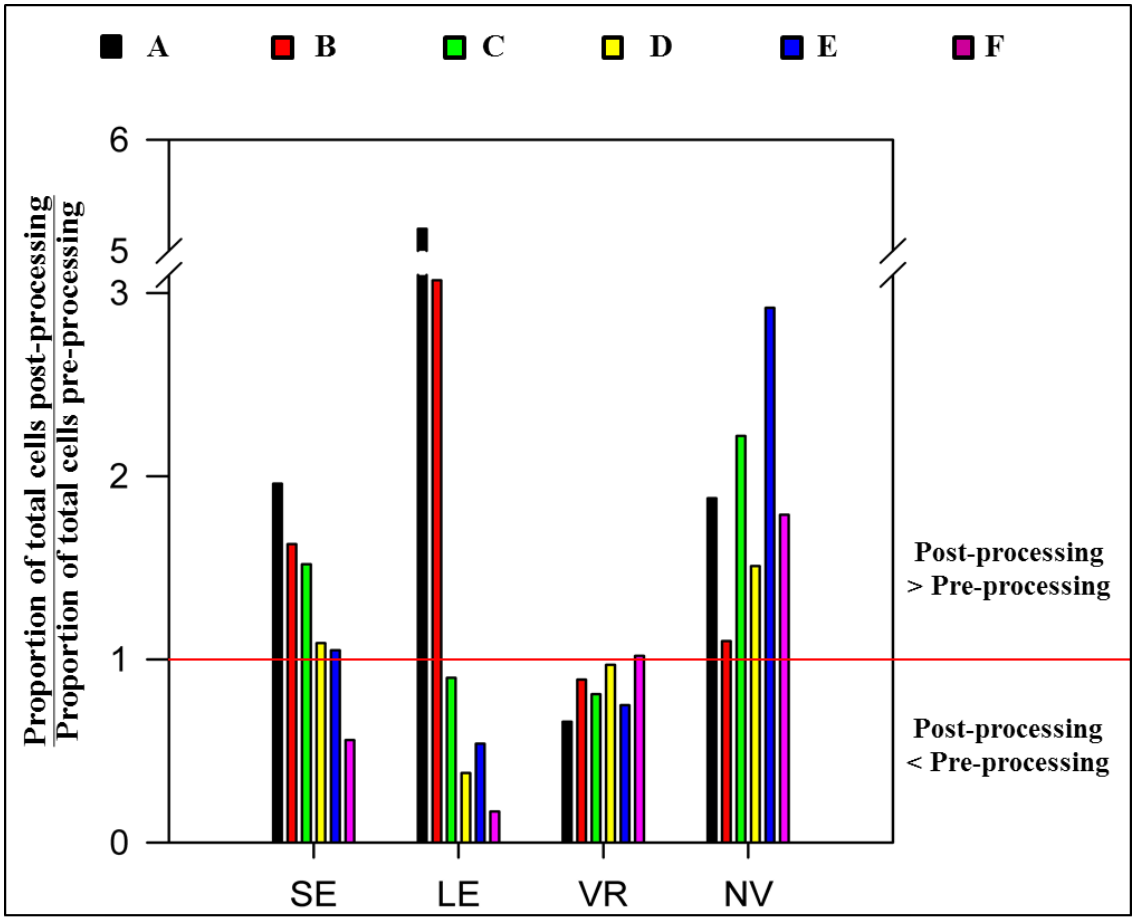

Figure 5.5: Ratio of the proportions of each cell population post-processing to pre-processing to assess the change in cell populations with varying concentrations. Runs A to F represent the six cell concentrations studied, where A is the highest cell concentration and F is the lowest one. Values below 1 represent a decrease in the proportion of a specific population post-processing and values above 1 represent an increase. For example, at the highest concentration investigated, A, the proportion of SE cells doubles from pre to post-processing and quintupled for LE.

from this plot is once again that there is an increase in the population of SE and LE cells at the highest cell concentrations.

5.3 Investigating the effect of viscosity on loss of intact cells

Preliminary studies were carried out to investigate the effect of viscosity on the loss of intact cells. A change in viscosity was achieved by one of two methods; an increase in concentration of the cellular suspension or by the addition of dextran to a low cell concentration suspension. Three repeats (‘ N ’ = 10,000 rpm, ‘ t ’ = 60 min, ‘ Q ’ = 0.5 mL min^{-1}) consisting each of three experiments (i.e. one at low cell concentration, one at high cell concentration and one at low cell concentration with added dextran) were carried out in this section.

The concentrations of total and viable (intact) cells as well as the percentage viability for the three repeats for pre-processing, post-processing and control samples are shown in Table 5.4 for all three conditions. The first condition (labelled ‘1’) was performed at low cell concentration without the addition of dextran; the second condition (labelled ‘2’) was performed at high cell concentration without the addition of dextran and the third condition (labelled ‘3’) was carried out at low cell concentration with the addition of dextran adjusted to match the viscosity of run 2. Runs 2 and 3 should therefore have comparable viscosities (hence shear stress values) whereas runs 1 and 3 should have comparable initial cell concentrations. All conditions had a non-sheared control held at 21 ± 1°C for the duration of the experiment to monitor cell quality. The addition of dextran did not lead to loss of intact cells or percentage viability as measured by the control (Table 5.4). It also shows the measured viscosity at the highest shear rate

(760 s^{-1}) for the control samples for each experiment. This was used to measure the averaged and maximum shear rates from the plots in Section 1.5.1. From the measured viscosity profiles (shown in Section 5.3.1) it is clear that after about a shear rate of 300 s^{-1}, the viscosity of the cellular suspension remains unchanged. The shear rates experienced inside the device are significantly higher than 300 s^{-1} and therefore it was assumed that the viscosity of the cellular suspension inside the USD membrane separation device would be comparable to that of the control at shear rate 760 s^{-1}.

Figure 5.6 shows the proportion of intact cells recovered to the proportion of intact cells fed for the three conditions studied as measured by (A) trypan blue exclusion data and (B) LDH release. Over-counts post-processing measured by the trypan blue exclusion data are evident from Figure 5.6.A, with values higher than 1 for the proportion of cells recovered to cells fed. Therefore no evident trend can be withdrawn from this information. However, the LDH release measurements (Figure 5.6.B) for the proportion of intact cells recovered to intact cells fed do provide some information. The low and high cell concentration experiments without added dextran yield a comparable loss, whereas the cellular suspension with added dextran yields a slightly lower proportion of recovered cells (~45% loss compared to ~35%). It appears that processing at the same concentration but higher shear stress leads to more damage observed, indicating that shear stress possibly is the cause of damage. However, these are preliminary results and more studies need to be carried out to reach a certain conclusion.

Repeat	Condition	Total cells mL^{-1} ('$[R]_{TC_{VICELL}}(0)$')	Intact cells mL^{-1} ('$[R]_{IC_{VICELL}}(0)$')	% Viability	Viscosity (mPa s)	Maximum shear rate* (s^{-1})	Maximum shear stress* (Pa)
1st	1	2.29E+06	2.15E+06	93.89	1.02	116,000	116
	2	3.79E+07	3.58E+07	94.46	1.99	88,000	176
	3	3.28E+06	3.22E+06	98.17	1.96	88,000	176
2nd	1	2.45E+06	2.39E+06	97.75	1.27	98,000	147
	2	6.54E+07	6.18E+07	94.42	2.66	79,000	237
	3	2.71E+06	2.68E+06	99.01	2.93	79,000	237
3rd	1	3.00E+06	2.87E+06	95.67	1.29	98,000	147
	2	4.84E+07	4.48E+07	92.57	2.03	88,000	176
	3	2.72E+06	2.56E+06	94.12	2.51	84,000	210

Table 5.4: Three repeats each consisting of three scenarios investigated, labelled 1 to 3, ('N' = 10,000 rpm, 't' = 60 min, 'Q' = 0.5 mL min^{-1}). Table shows the concentration of total and viable (intact) cells fed ('$[R]_{TC_{VICELL}}(0)$' and '$[R]_{IC_{VICELL}}(0)$'), percentage viability, measured viscosity to the nearest half mPa s and maximum shear rate and shear stress obtained from CFD simulation plots (Figure 1.5) using viscosity value rounded to the nearest half. For each repeat, the scenarios investigated were (1) low concentration without added dextran; (2) high concentration without added dextran and (3) low concentration with added dextran to match the viscosity of experiment 2. The viscosities shown are those of the control samples at the highest shear rate (760 s^{-1}) as measured by the rheometer (j = 3; n = 4).

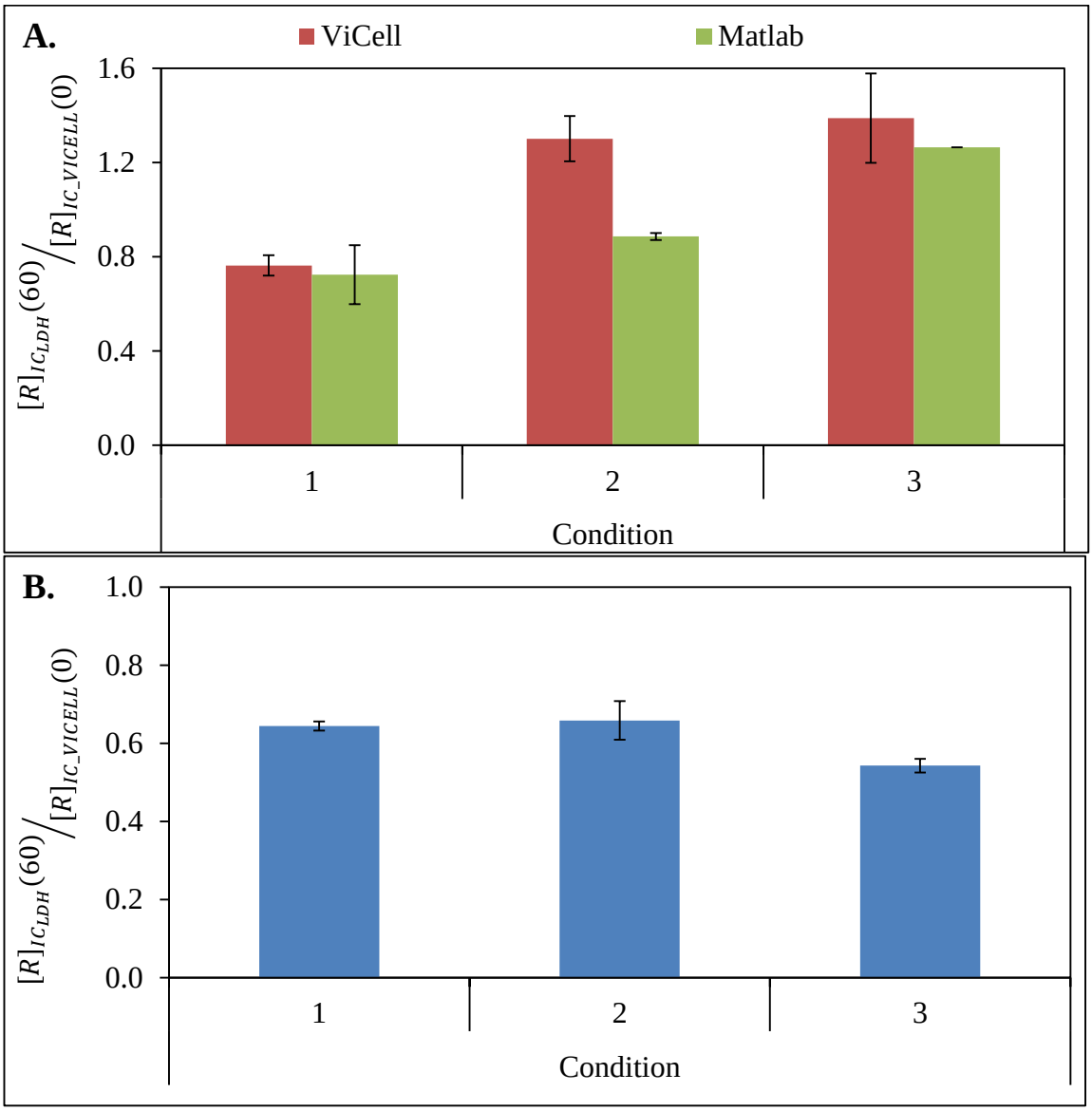

Figure 5.6: Intact cells recovered ('$[R]_{IC}(60)$') over intact cells fed ('$[R]_{IC_{VICELL}}(0)$') for (A) trypan blue exclusion as analyzed by ViCell XR™ and Matlab software and (B) as measured by LDH release for the three conditions as shown in Table 5.4. An average of the three repeats for each condition is shown. Due to over-counts for the trypan blue exclusion data there is no evident trend. However, the LDH release data suggests a comparable loss of ~35% for both low and high cell concentration without the addition of dextran and a ~45% loss for low cell concentration with added dextran. Error bars show ± 1 s.d. (j = 3; n = 4).

5.3.1 Rheological observations

Figure 5.7 shows the rheological characteristics of the cellular suspensions measured for the 2nd repeat for each of the three conditions investigated. For all three repeats, rheological profiles of the cell suspension (like the ones shown in Figure 5.7) were measured. For the purpose of analysis, only the 2nd repeat is shown given that the observations are the same for the 1st and 3rd repeat with the only difference being, the values measured for the apparent viscosity.

Figure 5.7.A shows the non-sheared control and Figure 5.7.B shows the viscosity measurements for the cellular suspension post-processing. For all conditions the apparent viscosity was measured using a single up and down shear sweep, ranging from 19 s^{-1} to 760 s^{-1}. For both control and post-processed samples, conditions 1 and 2 exhibit a pseudoplastic behavior. This means that with increasing shear rate there is a clear decrease in the apparent viscosity, which is a characteristic of a shear thinning suspension. Condition 3 (also for both control and post-processing samples), behaves more like a Newtonian fluid possibly due to the addition of dextran.

Comparing the apparent viscosities measured for the control samples (Figure 5.7.A) to the post-processing samples (Figure 5.7.B), it can be seen that both low cell concentration conditions (1 and 3) exhibit no change in the values of apparent viscosities measured. However, the high cell concentration sample (condition 2) does appear to have higher apparent viscosities throughout the range of shear rates investigated for the control sample compared to the post-processing sample. The decrease in viscosity from the control to the post-processed sample at high cell

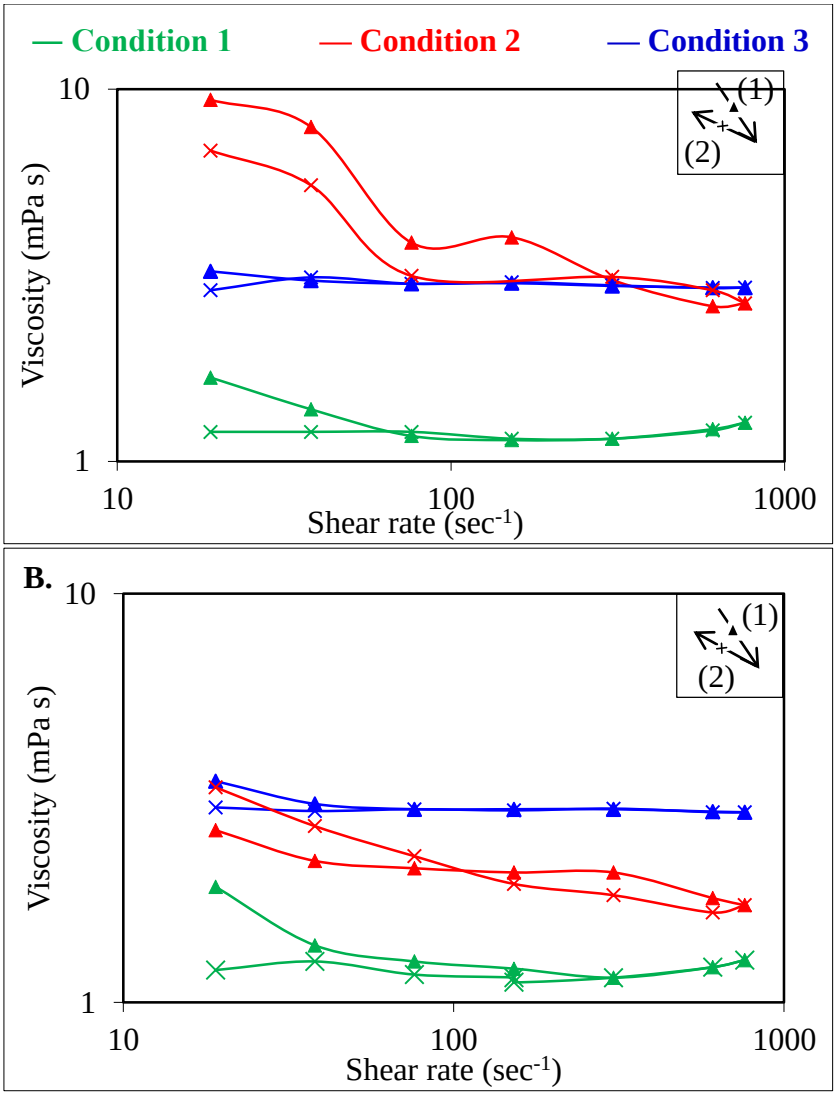

Figure 5.7: Apparent viscosity of HCA2 cell line for (A) control and (B) post-processing samples using a single up and down shear sweep as measured over a range of shear rates in a cone and plate rheometer for the 2nd repeat. Condition 1 (shown in green) has a low cell concentration of 2.39x10^6 cells mL^{-1} and no added dextran; condition 2 (shown in red) has a high cell concentration of 65.4x10^6 cells mL^{-1} with no added dextran and condition 3 (shown in blue) has a low cell concentration of 2.71x10^6 cells mL^{-1} and added dextran to match the viscosity of condition 2. Inset box: cone angular velocity (shear rate) was first stepped up (1, ▲) and then down (2, ×).

concentration could be explained by the lysis of cells leaving less number of intact cells in the USD membrane separation chamber. Release of nucleic acid material typically leads to an increase in viscosity. However, because of the constant washing of the cells with hCGM in the chamber, it may be that as cells are broken, the nucleic material is being washed out of the chamber leading to a decrease in viscosity with time as the number of cells remaining decreases.

The profiles for all three conditions and both samples (control and post-processing) do have one characteristic in common. As the shear rate increases (300 s^{-1} or more), the apparent viscosity becomes fairly constant. Therefore, it was assumed that the apparent viscosity of the cellular suspension inside the USD membrane device during processing is equivalent to the apparent viscosity measured at 760 s^{-1} of the control samples for each condition.

5.4 Chapter discussion

As part of the manufacturing of cell-based products, a concentration step of up to 100-fold may be necessary whilst maintaining CQAs. Such a large concentration change will inevitably lead to changes in the properties of the fluid which will impact the hydrodynamic conditions experienced during processing.

This chapter investigated the effect of cell concentration ranging from $1x10^6$ to $100x10^6$ cells mL^{-1} using the HCA2 fibroblasts. At a constant disc speed of 10,000 rpm and assuming a viscosity equal to that of water (~1 mPa s) for the lowest concentration (~$1x10^6$ cells mL^{-1}) investigated, the maximum shear rate experienced by the cellular

suspension is 116,000 s^{-1} (shear stress of 116 Pa). On the other hand, the lowest shear stress must happen whilst operating at the same disc speed at the highest cell concentration (~100x10^6 cells mL^{-1}). The viscosity of this cell suspension was not measured due to the amount of material needed for the analysis. However, assuming a viscosity of at least that measured for a cellular suspension of 65.4x10^6 cells mL^{-1} (~2.66 mPa s, reported in section 5.3.1) the maximum shear rate experienced in the USD membrane separation device is 79,000 s^{-1} (shear stress of 237 Pa). Despite the change in the extent of shear forces, the proportion of cells recovered post-processing was independent of initial starting cell concentration as measured by LDH release and trypan blue exclusion analyzed by both ViCell XR^{TM} and Matlab (~0.60, ~0.85 and ~0.77 respectively). This means that cell damage may be described as a first order process with respect to concentration of cells present in the USD membrane separation device. Moreover, it also indicates that the first order rate constant is unchanged with the change in viscosity of the suspension. The change in extent of shear stress is not as significant as the change in extent of shear rate indicating that cell damage may be more dependent on shear stress. However, the total cells damaged increased with increasing initial starting cell concentration.

Preliminary analysis on other CQAs such as average rate of cell damage, cell morphology and rheological properties of the cellular suspensions were investigated in this chapter. The average rates of cell damage indicated that cell damage as measured by LDH release happens almost twice as fast as the one calculated for the Matlab data, suggesting that LDH may be a more sensitive analytical technique. Following, morphological analysis of the cell population pre and post-processing revealed an

increase in the proportions of short and long elongated due to processing. This increase was found to be more evident at the three highest cell concentrations investigated. For instance, the highest cell concentration investigated shows 5 times as many long elongated cells post-processing than pre-processing. The gathered information is not sufficient to establish why the appearance of elongated cells is higher with increasing concentration. Lastly, an initial glance at the effect of viscosity on loss of intact cells and the rheological properties were carried out. Dextran was added to the cellular suspensions to mimic the viscosity increase measured by the increase in cell concentration. It appears that processing at the same concentration but higher shear stress leads to more damage observed (~45% loss compared to ~35%), indicating that shear stress possibly is the cause of damage although a larger sample and more testing would be required in order to draw firm conclusions.

Chapter 6. Final words and future work

6.1 Final words

This study was undertaken with the aim of characterizing the response of human cell lines to membrane-based processing using an ultra scale-down tool that required only small amounts of cellular material. This response was measured by assessing both the nature and the extent of the physical and, in some cases, biological changes induced within the cell populations as a response to the processing environment. Each chapter discussion summarized the key findings specific to that section. With these final words, the aim is to provide a more generic picture on the findings, what these convey and their relevance to the cell therapy bioprocessing industry.

6.1.1 Cell line comparison

Three human cell lines used for therapies were tested for cell damage using a combination of techniques developed in this thesis. A human fibroblast cell line, a neural stem cell line and a prostate cancer cell line. It appears that further studies to evaluate susceptibility to processing and the effect of process change will be needed, especially for the prostate cancer cell line which was only assessed for cell damage using trypan blue exclusion. Yet, findings suggest that the most robust cell lines to processing damage were fibroblasts followed by prostate carcinoma and neural stem cells with respectively ~0%, ~18% and ~42% damage at the lowest shear stress (~44 Pa) conditions. For cells aged for 24 hours prior to processing, trypan blue exclusion findings also suggest the same order of resistance to cell damage with ~2%, ~21% and ~57% damage for fibroblasts, prostate cancer and neural stem cells. Table 6.1 summarizes all this information and more on the cell damage figures presented in this study for the two main analytical techniques; (i) LDH release and

(ii) trypan blue exclusion. It helps to underline the importance of cell line selection at an early stage in the development of the processing strategy.

6.1.2 Kinetics of damage

The LDH release data curves give a sense of the kinetics of damage for the different operating conditions and cell lines. Due to the number of assumptions and the complexity of the calculations to account for transmission, modelling of the kinetics of damage is not ideal. However, the data curves do give a sense of the kinetics of damage. For the HCA2 fibroblasts, the data appears to show a combination of first order expressions (i.e. rate of damage is proportional to the variable investigated). Probably two fairly evident ones, with a weaker population of cells to start with (faster damage) and a more robust remaining cell population. If processing was prolonged, the second population may continue to be progressively damaged until there are no cells left in the USD membrane separation device. However, this is not a straightforward and certain observation to test due to the number of complications that this implies. Prolonged processing time may cause cell damage by the introduction of other complications such as cell ageing whilst processing or change in the processing medium properties due to release of intracellular components. High cell concentration LDH release curve for the HCA2 cells is the only curve for this cell line that exhibits a slightly different damage profile. It appears to indicate a zero order process (i.e. the rate of damage is constant). However, it may well be that high cell concentration also obeys a series of first order equations and the slope observed over the 60 minutes of operation is only the beginning of the cell damage curve at high cell concentration (i.e. the population of weaker cells that are damage begin with).

What was also evident from the kinetics of damage investigation was that LDH release appears to be more sensitive to changes in cell damage than trypan blue exclusion. Previous studies conducted by Lappalainen et al. (1994) also observed differences between the sensitivity of these two techniques. They concluded that LDH release is a more sensitive indicator of earlier damage to the cell membrane than trypan blue exclusion, which stains only dead cells. Diederichs et al. (1979) investigated the mechanism of release of LDH from isolated skeletal muscle and concluded that cell swelling, which is typical of necrotic cells, prior to membrane damage was connected with an increased LDH permeability suggesting that LDH can potentially be released prior to membrane lesions and therefore can serve as an indication of earlier cytotoxicity.

6.1.3 Relevance of this research to the cell therapy field

The recovery of human cells for therapy generally has several particular objectives e.g.:

(i) the processing of the cells without any alteration of cell functionality.

(ii) the removal of soluble growth media components, mainly macromolecular.

(iii) the preparation of suspensions of high cell concentration (especially for tissue therapy or for reduced volume administration).

(iv) the avoidance of any contamination of the cells.

These objectives are achieved with skill at bench scale using dead-end centrifugation in test tube batches. Here several repeat centrifugation stages might be required to remove sufficient soluble components but provided the cells are suspended with care then loss of functionality can be avoided and high concentrations achieved. However, while

carrying this out at small scale with skilled operators allows aseptic recovery to be achieved, translation to large scale (e.g. 10s of litres) is very challenging.

The translation to continuous centrifugation has been attempted but is so far not successful due to lack of suitable devices. The use of low-stress feed zones and low-stress discharge mechanisms is feasible but design of small-scale machines to achieve this will probably require very expensive engineering. One challenge will be the scale of translation from dead end to continuous centrifugation and while some success has been achieved, e.g. with mammalian cell recovery, there is a long way to go for cells for therapy.

The development of counter-flow centrifugation (kSep®, from KBI Biopharma Inc.) is potentially ground breaking. Here viable cells are recovered and very effective cell washing takes place in situ. Good concentration is achieved provided the suspension remains flowable. The use of single use equipment allows sterile operation to be achieved.

Understanding the tolerance of cells in a manufacturing process can have a major impact on the feasibility. Hence, adopting new and ground breaking manufacturing technology for cell therapies can have disadvantages in terms of cost of development, regulatory precedent and easily accessible pools of industrial expertise. However, in many cases, already existing technologies prove to be unsuitable and inefficient for these types of therapies leading to lengthy and costly manufacturing processes.

The way forward explored in this thesis is the use of cross flow membranes. Here several challenges are posed:

(a) the ability to flow cells repeatedly in a recycle loop (via pump, valve, membrane etc.) with no damage or change of cell functionality.

(b) the use of open membrane pores which remain un-fouled which allows soluble components to transmit through the membrane easily i.e. to avoid excessive use of diafiltration buffer. Here the flow rate needs to remain high which might contradict need to achieve (a).

(c) the use of cascades of membrane sizes to achieve high levels of cell concentration without unacceptable loss of suspension in hold up/ recycle loops.

The USD device used in this study goes some way to allowing these challenges to be addressed while still only having a limited number of cells available. Future work will require the device to be so designed such that the maximum stress at the tip of the rotating disc matches that experienced by cells in a pumped loop. At the same time the average stress over the membrane surface must match that for commercial scale membrane separators. Finally the use of syringe feeding of cells to go from low to high concentration must be matched with concentration effects at full scale. It is not likely that all of these functions can be mimicked at the same time but the relatively small scale of the device will allow multiple experiments to determine critical regimes of operation at full scale.

The USD device used in this study also goes some way in investigating another major challenge; cell line selection. The response to processing stress varied significantly with choice of cell line and of processing conditions as was previously discussed. Selection of the most robust candidates at an early stage by thorough characterization can help minimize the cost of development and manufacturing. Moreover, understanding and

quantifying the impact of process changes on cell quality at an early stage will allow validating a design space for the manufacturing scenario in order to incorporate changes without the need to go through validation again.

6.2 Future work

This study has formed the basis of a generic characterization of the susceptibility of cell lines to processing conditions which may apply during full-scale processing. A number of interesting potential avenues of research have arisen due to the wide scope of the unit operation. Three main developments could serve as a basis for future research projects.

Firstly, the impact of processing at increasing cell concentrations was investigated. However, it may be important to establish how continuous concentration of cells into the USD membrane separation device rather than discrete analysis compares in terms of cell damage. With continuous concentration, the rheological considerations become ever more complicated as the viscosity increases with cells fed but potentially decreases if cells are damaged and intracellular components are constantly washed away. Understanding the impact of constant concentration may lead to important decisions on how membrane separation should be operated (fed-batch or continuous modes).

Secondly, processing in this study was carried out in CGM which is potentially, in terms of avoiding cell damage, a relatively good buffer for the cells to be processed in. Central to membrane separation is the buffer exchange step and processing the cellular suspension in a buffer suitable for storage or administration. The buffer exchange step would focus mainly on the removal of contaminants from upstream whereas processing in a suitable buffer for administration or delivery would focus mainly on CQAs.

Forming both an operational and cost based window of operation of would not only increase process knowledge but also would aid in cost estimation.

Thirdly, the USD tool used in this study has been developed for the characterization of the response of human cell lines to membrane-based processing, using just small quantities of cells commonly available at the early discovery stage. A direct comparison to larger scale TFF systems would be paramount to the development of the tool in order to perform experiments more relevant to full-scale processing.

HCA2 cell line		**Analytical technique to assess cell damage**	
Processing condition		**LDH release**	**Trypan blue**
Disc speed (rpm)	6,000	~8%	~0%
	10,000	~30%	~25%
Cell ageing (hours)	0 (fresh)	~8%	~0%
	24	~15%	~2%
Cell concentration (cells mL^{-1})	$2x10^6$	~26%	~25%
	$50x10^6$	~19%	~8%
CTX0E03 cell line		**Analytical technique to assess cell damage**	
Processing condition		**LDH release**	**Trypan blue**
Disc speed (rpm)	6,000	~50-60%	~42%
	10,000	~50-60%	~47%
Cell ageing (hours)	0 (fresh)	~50-60%	~42%
	24	~50-60%	~57%
Cell concentration (cells mL^{-1})	$2x10^6$	~50-60%	~47%
	$50x10^6$	~20%	~36%
P4E6 cell line		**Analytical technique to assess cell damage**	
Processing condition		**LDH release**	**Trypan blue**
Disc speed (rpm)	6,000	N/A	~18%
	10,000		~41%
Cell ageing (hours)	0 (fresh)		~18%
	24		~21%
Cell concentration (cells mL^{-1})	$2x10^6$		~41%
	$50x10^6$		~75%

Table 6.1: Brief overview of the findings observed within the two main analytical techniques used to assess cell damage as measured by decrease of intact cells conducted within this study.

References

Acosta-Martinez JP. 2011. Bioprocessing of human cells for vaccines and other cell therapies. London: University College London.

Acosta-Martinez JP, Papantoniou I, Lawrence K, Ward S, Hoare M. 2010. Ultra scale down stress analysis of the bioprocessing of whole human cells as a basis for cancer vaccines. Biotechnology and Bioengineering 107(6):953-963.

Agashi K, Chau DY, Shakesheff KM. 2009. The effect of delivery via narrow-bore needles on mesenchymal cells. Regenerative Medicine 4(1):49-64.

Al-Rubeai M, Singh RP, Emery AN, Zhang Z. 1995. Cell cycle and cell size dependence of susceptibility to hydrodynamic forces. Biotechnology and Bioengineering 46(1):88-92.

Altman SA, Randers L, Rao G. 1993. Comparison of trypan blue dye exclusion and fluorometric assays for mammalian cell viability determinations. Biotechnology Progress 9(6):671-4.

Ameen C, Strehl R, Bjorquist P, Lindahl A, Hyllner J, Sartipy P. 2008. Human embryonic stem cells: current technologies and emerging industrial applications. Crit Rev Oncol Hematol 65(1):54-80.

Arora T, R G, Mercer J TP, Casais M, Feldman S, Look J, Lubiniecki T, Mezzatesta, J PS, Rosolowsky M, Rathore AS, Schenerman M, Schofield T, Sheridan S, Smock, P AS, Atkins L, McGarvey B, Meiklejohn B, Precup J, Towns J. 2009. Quality by Design for biotechnology products — Part 1 A PhRMA working group's advice on applying QbD to biotech. BioPharm International 22(11).

Augenstein DC, Sinskey AJ, Wang DI. 1971. Effect of shear on the death of two strains of mammalian tissue cells. Biotechnology and Bioengineering 13(3):409-18.

Axelsson H. 2002. Cell separation, centrifugation. Encyclopedia of Bioprocess Technology: John Wiley & Sons, Inc.

Bartel RL, Cramer C, Ledford K, Longcore A, Parrish C, Stern T, Watling S, Zeigler F. 2012. The Aastrom experience. Stem Cell Research & Therapy 3(4):26.

Bayas J-M, Costas L, Muñoz A. 2008. Cervical cancer vaccination indications, efficacy, and side effects. Gynecologic Oncology 110(3, Supplement 2):S11-S14.

Bell E, Ehrlich HP, Buttle DJ, Nakatsuji T. 1981. Living tissue formed in vitro and accepted as skin-equivalent tissue of full thickness. Science 211(4486):1052-4.

Berger S, Tietz NW. 1976. Fundamentals of clinical chemistry. Clinical Pathology.

Berthiaume F, Maguire TJ, Yarmush ML. 2011. Tissue engineering and regenerative medicine: history, progress, and challenges. Annual Review of Chemical and Biomolecular Engineering 2:403-30.

Born C, Zhang Z, Al-Rubeai M, Thomas CR. 1992. Estimation of disruption of animal cells by laminar shear stress. Biotechnology and Bioengineering 40(9):1004-10.

Brandenberger R, Burger S, Campbell A, Fong T, Lapinskas E, Rowley JA. 2011. Cell therapy bioprocessing. Integrating process and product development for the next generation of biotherapeutics. BioProcess International. Cell Therapies Technology.

Burke JF, Yannas IV, Quinby WC, Jr., Bondoc CC, Jung WK. 1981. Successful use of a physiologically acceptable artificial skin in the treatment of extensive burn injury. Annals of Surgery 194(4):413-28.

Carmen J, Burger SR, McCaman M, Rowley JA. 2012. Developing assays to address identity, potency, purity and safety: cell characterization in cell therapy process development. Regenerative Medicine 7(1):85-100.

Chandler M, Zydney A. 2004. High throughput screening for membrane process development. Membrane Science 237(1):181-188.

Chang S, Fane AG. 2002. Filtration of biomass with laboratory-scale submerged hollow fibre modules - effect of operating conditions and module configuration. Journal of chemical technology and biotechnology 77(9):1030-1038.

Chisti Y. 2001. Hydrodynamic damage to animal cells. Critical Reviews in Biotechnology 21(2):67-110.

Choumerianou DM, Dimitriou H, Kalmanti M. 2008. Stem cells: promises versus limitations. Tissue Eng Part B Rev 14(1):53-60.

Copier J, Ward S, Dalgleish A. 2007. Cell based cancer vaccines: Regulatory and commercial development. Vaccine 25 Suppl 2:B35-B46.

Darzynkiewicz Z, Pozarowski P. 2007. All that glitters is not gold: all that FLICA binds is not caspase. A caution in data interpretation-and new opportunities. Cytometry Part A 71(8):536-7.

De Loecker W, Koptelov VA, Grischenko VI, De Loecker P. 1998. Effects of cell concentration on viability and metabolic activity during cryopreservation. Cryobiology 37(2):103-9.

Delahaye M. 2013. An ultra scale-down study of recovery by centrifugation of human cells for therapy. London: University College London (UCL).

Diederichs F, Muhlhaus K, Trautschold I, Friedel R. 1979. On the mechanism of lactate dehydrogenase release from skeletal muscle in relation to the control of cell volume. Enzyme 24(6):404-15.

Diefenbach A, Jensen ER, Jamieson AM, Raulet DH. 2001. Rae1 and H60 ligands of the NKG2D receptor stimulate tumour immunity. Nature 413(6852):165-71.

Dive C, Gregory CD, Phipps DJ, Evans DL, Milner AE, Wyllie AH. 1992. Analysis and discrimination of necrosis and apoptosis (programmed cell death) by multiparameter flow cytometry. Biochimica et Biophysica Acta 1133(3):275-85.

Doran PM. 1995. Bioprocess Engineering Principles.

Ekert PG, Silke J, Vaux DL. 1999. Caspase inhibitors. Cell Death & Differentiation 6(11):1081-6.

Farge D, Labopin M, Tyndall A, Fassas A, Mancardi GL, Van Laar J, Ouyang J, Kozak T, Moore J, Kötter I and others. 2010. Autologous hematopoietic stem cell transplantation for autoimmune diseases: an observational study on 12 years' experience from the European Group for Blood and Marrow Transplantation Working Party on Autoimmune Diseases. Haematologica 95(2):284–292.

Fernandes AM, Fernandes TG, Diogo MM, da Silva CL, Henrique D, Cabral JM. 2007. Mouse embryonic stem cell expansion in a microcarrier-based stirred culture system. Biotechnology 132(2):227-36.

Fernandez-Pol JA. 1978. Morphological changes induced by picolinic acid in cultured mammalian cells. Experimental and Molecular Pathology 29:348-357.

Fuller R, Devireddy RV. 2008. The effect of two different freezing methods on the immediate post-thaw membrane integrity of adipose tissue derived stem cells. International Journal of Heat and Mass Transfer 51(23–24):5650-5654.

Ghosh R, Cui Z. 2000. Analysis of protein transport and polarization through membranes using pulsed sample injection technique. Membrane Science 175(1):75-84.

Glen KE, Workman VL, Ahmed F, Ratcliffe E, Stacey AJ, Thomas RJ. 2013. Production of erythrocytes from directly isolated or Delta1 Notch ligand expanded CD34+ hematopoietic progenitor cells: process characterization, monitoring and implications for manufacture. Cytotherapy 15(9):1106-17.

Goergen JL, Marc A, Engasser JM. 1993. Determination of cell lysis and death kinetics in continuous hybridoma cultures from the measurement of lactate dehydrogenase release. Cytotechnology 11(3):189-95.

Goldsby RA, Kindt T, Osborne BA. 2007. Kuby immunology. New York: W.H. Freeman.

Gruijl TDd, van den Eertwegh AJM, Pinedo HM, Scheper RJ. 2008. Whole-cell cancer vaccination: from autologous to allogeneic tumor- and dendritic cell-based vaccines. Cancer Immunology and Immunotherapy 57(10):1569-1577.

Haber DA, Settleman J. 2007. Cancer: drivers and passengers. Nature 446(7132):145-6.

Halbert CL, Demers GW, Galloway DA. 1992. The E6 and E7 genes of human papillomavirus type 6 have weak immortalizing activity in human epithelial cells. Virology 66(4):2125.

Halme D, Kessler D. 2006. FDA regulation of stem cell-based therapies. The New England Journal of Medicine 355(16):1730-1735.

Herold C, Reimers K, Allmeling C, Rennekampff HO, Vogt PM. 2009. A normothermic perfusion bioreactor to preserve viability of rat groin flaps extracorporally. Transplantation Proceedings 41(10):4382-8.

Hourd P, Chandra A, Medcalf N, Williams DJ. 2014a. Regulatory challenges for the manufacture and scale-out of autologous cell therapies. StemBook.

Hourd P, Ginty P, Chandra A, Williams DJ. 2014b. Manufacturing models permitting roll out/scale out of clinically led autologous cell therapies: regulatory and scientific challenges for comparability: Cytotherapy. 2014 Aug;16(8):1033-1047. doi: 10.1016/j.jcyt.2014.03.005. Epub 2014 May 20.

Hu W, Berdugo C, Chalmers JJ. 2011. The potential of hydrodynamic damage to animal cells of industrial relevance: current understanding. Cytotechnology 63(5):445-60.

Hutchinson N, Bingham N, Murrell N, Farid S, Hoare M. 2006. Shear stress analysis of mammalian cell suspensions for prediction of industrial centrifugation and its verification. Biotechnology and Bioengineering 95(3):483-91.

Kantoff PW, Higano CS, Shore ND, Berger ER, Small EJ, Penson DF, Redfern CH, Ferrari AC, Dreicer R, Sims RB and others. 2010. Sipuleucel-T immunotherapy for castration-resistant prostate cancer. The New England Journal of Medicine 363(5):411-22.

Kehoe DE, Jing D, Lock LT, Tzanakakis ES. 2010. Scalable stirred-suspension bioreactor culture of human pluripotent stem cells. Tissue Eng Part A 16(2):405-21.

Kemp P. 2006. History of regenerative medicine: looking backwards to move forwards. Regenerative medicine 1(5):653-69.

Kempner ME, Felder RA. 2002. A Review of Cell Culture Automation. Journal of the Association for Laboratory Automation 7(2):56-62.

Kirouac DC, Zandstra PW. 2008. The systematic production of cells for cell therapies. Cell Stem Cell 3(4):369-381.

Kretzmer G, Schügerl K. 1991. Response of mammalian cells to shear stress. Applied Microbiology and Biotechnology 34(5):613-616.

Kumar V, Abbas AK, Fausto N, Mitchell R, Robbins SL. 2007. Robbins basic pathology. Philadelphia, USA: Saunders/Elseiver.

Kuo J, Zhao Y, Schiro P, Ng L, Lim DW, Shelby JP, Chiu D. 2010. Deformability considerations in filtration of biological cells. Lab on a Chip 10(7):837-842.

Lapinskas E. 2010. Scaling Up Research to Commercial Manufacturing. Chemical Engineering Progress 106(11):44-49.

Lappalainen K, Jaaskelainen I, Syrjanen K, Urtti A, Syrjanen S. 1994. Comparison of cell proliferation and toxicity assays using two cationic liposomes. Pharmaceutical Research 11(8):1127-31.

Lee HJ, Choi HB, Min B, Park SR. 2009. Changes in surface markers of human mesenchymal stem cells during the chondrogenic differentiation and dedifferentiation processes in vitro. Arthritis & Rheumatism 60(8):2325-2332.

Liu L, Hartwig D, Harloff S, Herminghaus P, Wedel T, Geerling G. 2005. An optimised protocol for the production of autologous serum eyedrops. Graefe's Archive for Clinical and Experimental Ophthalmology 243(7):706-714.

Ma G. 2009. Development of ultra scale-down shear filtration system and modelling of large scale diafiltration system. London: University College London.

Ma G, Aucamp J, Gerontas S, Eardley-Patel R, Craig A, Hoare M, Zhou Y. 2010. Mimic of a large-scale diafiltration process by using ultra scale-down rotating disc filter. Biotechnology Progress 26(2):466-76.

Macchiarini P, Jungebluth P, Go T, Asnaghi MA, Rees LE, Cogan TA, Dodson A, Martorell J, Bellini S, Parnigotto PP. 2008. Clinical transplantation of a tissue-engineered airway. Lancet (London, England) 372(9655):2023-2030.

Maiorella B, Dorin G, Carion A, Harano D. 1991. Crossflow microfiltration of animal cells. Biotechnol Bioeng 37(2):121-6.

Maitland NJ, Macintosh CA, Hall J, Sharrard M, Quinn G, Lang S. 2001. In vitro models to study cellular differentiation and function in human prostate cancers. Radiation Research 155(1):133-142.

Markert. 1984. Lactate dehydrogenase, biochemistry and function of lactate dehydrogenase Cell Biochemistry and Function 2.

Mason C, Brindley DA, Culme-Seymour EJ, Davie NL. 2011. Cell therapy industry: billion dollar global business with unlimited potential. Regenerative Medicine 6(3):265-72.

Mason C, Hoare M. 2006. Regenerative medicine bioprocessing: the need to learn from the experience of other fields. Regenerative Medicine 1(5):615.

Mason C, Hoare M. 2007. Regenerative medicine bioprocessing: building a conceptual framework based on early studies. Tissue Eng 13(2):301-11.

McCoy R, Hoare M, Ward S. 2009. Ultra scale-down studies of the effect of shear on cell quality; Processing of a human cell line for cancer vaccine therapy. Biotechnology Progress 25(5):1448-58.

McCoy R, Ward S, Hoare M. 2010. Sub-population analysis of human cancer vaccine cells-ultra scale-down characterization of response to shear. Biotechnology and Bioengineering 106(4):584-597.

McNeil PL, Steinhardt RA. 2003. Plasma membrane disruption: repair, prevention, adaptation. Annual Review of Cell and Developmental Biology 19:697-731.

McQueen A, Meilhoc E, Bailey JE. 1987. Flow effects on the viability and lysis of suspended mammalian cells. Biotechnology Letters 9(12):831-836.

Nema S, Avis KE. 1993. Loss of LDH activity during membrane filtration. Parenteral Science and Technology 47(1):16-21.

Nerem RM. 2010. Regenerative medicine: the emergence of an industry. Royal Society Interface 7 Suppl 6:S771-5.

Ng YC, Berry JM, Butler M. 1996. Optimization of physical parameters for cell attachment and growth on macroporous microcarriers. Biotechnology and Bioengineering 50(6):627-35.

O'Callaghan AR, Daniels JT. 2011. Concise review: limbal epithelial stem cell therapy: controversies and challenges. Stem Cells 29(12):1923-32.

Passweg JR, Baldomero H, Bregni M, Cesaro S, Dreger P, Duarte RF, Falkenburg JH, Kroger N, Farge-Bancel D, Gaspar HB and others. 2013. Hematopoietic SCT in Europe: data and trends in 2011. Bone Marrow Transplant 48(9):1161-7.

Pattasseril J, Varadaraju H, Lock L, Rowley JA. 2013. Downstream technology landscape for large-scale therapeutic cell processing. BioProcess International. Cell Therapies Manufacturing 11:38-47.

Pegg DE. 1981. The effect of cell concentration on the recovery of human erythrocytes after freezing and thawing in the presence of glycerol. Cryobiology 18(3):221-8.

Perry RH, Green DW. 2008. Perry's chemical engineers' handbook. New York, USA: McGraw-Hill.

Pollock K, Stroemer P, Patel S, Stevanato L, Hope A, Miljan E, Dong Z, Hodges H, Price J, Sinden JD. 2006. A conditionally immortal clonal stem cell line from human cortical neuroepithelium for the treatment of ischemic stroke. Experimental Neurology 199(1):143-155.

Quante M, Wang TC. 2009. Stem cells in gastroenterology and hepatology. Nature Reviews. Gastroenterology & Hepatology 6(12):724-37.

Racher AJ, Looby D, Griffiths JB. 1990. Use of lactate dehydrogenase release to assess changes in culture viability. Cytotechnology 3(3):301-7.

Roach PCJ, Postis VLG, Deacon SE, Roach PCJ, Postis VLG, Deacon SE, Wright GSA, Ingram JC, Xia X, Roach PCJ and others. 2008. Large-scale preparation of bacterial cell membranes by tangential flow filtration. Molecular Membrane Biology 25(8):609-616.

Rowley J, Pattasseril J, Mohamed A. 2012a. High yield method and apparatus for volume reduction and washing of therapeutic cells using tangential flow filtration. Google Patents.

Rowley JA, Abraham E, Campbell A, Brandwein H, Oh S. 2012b. Meeting lot-size challenges of manufacturing adherent cells for therapy. BioProcess International. Cell Therapies Manufacturing 10:16-22.

Rowley JA, Abraham E, Campbell A, Brandwein H, Oh S. 2012c. Meeting Lot-Size Challenges of Manufacturing Adherent Cells for Therapy. BioProcess International 10(3):7.

Saris DB, Vanlauwe J, Victor J, Haspl M, Bohnsack M, Fortems Y, Vandekerckhove B, Almqvist KF, Claes T, Handelberg F and others. 2008. Characterized chondrocyte implantation results in better structural repair when treating symptomatic cartilage defects of the knee in a randomized controlled trial versus microfracture. The American journal of sports medicine 36(2):235-46.

Serra M, Brito C, Sousa MF, Jensen J, Tostoes R, Clemente J, Strehl R, Hyllner J, Carrondo MJ, Alves PM. 2010. Improving expansion of pluripotent human

embryonic stem cells in perfused bioreactors through oxygen control. Biotechnology 148(4):208-15.

Smolewski P, Grabarek J, Halicka HD, Darzynkiewicz Z. 2002. Assay of caspase activation in situ combined with probing plasma membrane integrity to detect three distinct stages of apoptosis. Immunological Methods 265(1-2):111-21.

Sowemimo-Coker SO, Andrade F, Kim A, Pesci S. 2009. A simple filtration system for red blood cell depletion and volume reduction in routine processing of human umbilical cord blood. Vox Sanguinis 96(2):138-45.

Stamenovic D. 2008. Rheological behavior of mammalian cells. Cellular and Molecular Life Sciences 65(22):3592-605.

Stephens P, Cook H, Hilton J, Jones C, Haughton M, Wyllie F, Skinner J, Harding K, Kipling D, Thomas D. 2003. An analysis of replicative senescence in dermal fibroblasts derived from chronic leg wounds predicts that telomerase therapy would fail to reverse their disease-specific cellular and proteolytic phenotype. Experimental Cell Research 283(1):22.

Tait AS, Aucamp JP, Bugeon A, Hoare M. 2009. Ultra scale-down prediction using microwell technology of the industrial scale clarification characteristics by centrifugation of mammalian cell broths. Biotechnology and Bioengineering 104(2):321-31.

Takahashi K, Tanabe K, Ohnuki M, Narita M, Ichisaka T, Tomoda K, Yamanaka S. 2007. Induction of pluripotent stem cells from adult human fibroblasts by defined factors. Cell 131(5):861-72.

Thomas ED, Buckner CD, Banaji M, Clift RA, Fefer A, Flournoy N, Goodell BW, Hickman RO, Lerner KG, Neiman PE and others. 1977. One hundred patients with acute leukemia treated by chemotherapy, total body irradiation, and allogeneic marrow transplantation. Blood 49(4):511-33.

Thomas RJ, Anderson D, Chandra A, Smith NM, Young LE, Williams D, Denning C. 2009. Automated, scalable culture of human embryonic stem cells in feeder-free conditions. Biotechnology and Bioengineering 102(6):1636-44.

Titchener-Hooker NJ, Dunnill P, Hoare M. 2008. Micro biochemical engineering to accelerate the design of industrial-scale downstream processes for biopharmaceutical proteins. Biotechnology and Bioengineering 100(3):473-487.

U.S. Food and Drug Administration. 1993. Application of current statutory authorities to human somatic cell therapy products and gene therapy products. Federal Register 58(197).

Uygun BE, Soto-Gutierrez A, Yagi H, Izamis ML, Guzzardi MA, Shulman C, Milwid J, Kobayashi N, Tilles A, Berthiaume F and others. 2010. Organ reengineering through development of a transplantable recellularized liver graft using decellularized liver matrix. Nature Medicine 16(7):814-20.

van Reis R, Zydney A. 2001. Membrane separations in biotechnology. Curr Opin Biotechnol 12(2):208-11.

Varani J, Dame M, Rediske J, Beals TF, Hillegas W. 1985. Substrate-dependent differences in growth and biological properties of fibroblasts and epithelial cells grown in microcarrier culture. Biological Standarization 13(1):67-76.

Veraitch FS, Scott R, Wong JW, Lye GJ, Mason C. 2008. The impact of manual processing on the expansion and directed differentiation of embryonic stem cells. Biotechnology and Bioengineering 99(5):1216-29.

Wagner A, Marc A, Engasser JM, Einsele A. 1992. The use of lactate dehydrogenase (LDH) release kinetics for the evaluation of death and growth of mammalian cells in perfusion reactors. Biotechnology and Bioengineering 39(3):320-6.

Wang WK. 2001. Membrane separations in biotechnology. New York, USA: Taylor & Francis.

Want AJ, Nienow AW, Hewitt CJ, Coopman K. 2012. Large-scale expansion and exploitation of pluripotent stem cells for regenerative medicine purposes: beyond the T flask. Regenerative Medicine 7(1):71-84.

Ward S, Casey D, Labarthe MC, Whelan M, Dalgleish A, Pandha H, Todryk S. 2002. Immunotherapeutic potential of whole tumour cells. Cancer Immunology and Immunotherapy 51(7):351-357.

Wendt D, Riboldi SA, Cioffi M, Martin I. 2009. Potential and bottlenecks of bioreactors in 3D cell culture and tissue manufacturing. Advanced Materials 21(32-33):3352-67.

Wlodkowic D, Telford W, Skommer J, Darzynkiewicz Z. 2011. Apoptosis and beyond: cytometry in studies of programmed cell death. Methods in Cell Biology 103:55-98.

Wolterbeek HT, van der Meer AJ. 2005. Optimization, application, and interpretation of lactate dehydrogenase measurements in microwell determination of cell number and toxicity. Assay and Drug Development Technologies 3(6):675-82.

Woods EJ. 2010. Container system for enabling commercial production of cryopreserved cell therapy products. Regenerative Medicine 5(4):659-667.

Wyllie FS, Jones CJ, Skinner JW, Haughton MF, Wallis C, Wynford Thomas D, Faragher RG, Kipling D. 2000. Telomerase prevents the accelerated cell ageing of Werner syndrome fibroblasts. Nature Genetics 24(1):16-17.

Zaborsky OR. 1995. Bioprocess engineering: now and beyond 2000. FEMS Microbiology Reviews 16(2-3):277-285.

Zoro BJ, Owen S, Drake RA, Mason C, Hoare M. 2009. Regenerative medicine bioprocessing: concentration and behavior of adherent cell suspensions and pastes. Biotechnology and Bioengineering 103(6):1236-47.

Zoro BJH, Owen S, Drake RAL, Hoare M. 2008. The impact of process stress on suspended anchorage-dependent mammalian cells as an indicator of likely challenges for regenerative medicines. Biotechnol Bioeng 99(2):468-474.